UNIVERSITY OF LEEDS

Three-stage pyrolysis-reformer-shift system for hydrogen production from waste biomass

Japhet Olatomiwa Oladipo

Submitted in accordance with the requirements for the degree of
Doctor of Philosophy as part of the integrated PhD with MSc in
Bioenergy

November 2019

Centre for Doctoral Training

School of Chemical and Process Engineering
University of Leeds

Declaration of Authorship

The candidate confirms that the work submitted is his own and that appropriate credit has been given where reference has been made to the work of others. This copy has been supplied on the understanding that it is copyright material and that no quotation from the thesis may be published without proper acknowledgement.

Acknowledgements

I want to express my deepest and sincere gratitude to God who has given me the strength and intellect to start and ultimately finish this doctorate study; it has indeed been a journey for which I am most grateful.

Prof Paul T Williams, words cannot describe how helpful you have been in providing support, guidance, wisdom, encouragement and pushing me to be the best. You have been a brilliant role model, mentor, teacher and a guardian to me, your constant supervision and input during this project have been remarkable. I appreciate you. Thank you

To Dr Anas Nahil for your assistance during the development of this research project. Your feedback and input have been invaluable for developing the methodologies and analysis used throughout the research. You have truly been a source of inspiration during this project, and I genuinely appreciate your help on the novel 3 stage reactor

I would also like to thank Ed Woodhouse, who has assisted invaluably in building, repairing and maintaining the pyrolysis equipment.

My fellow students, both from the bioenergy CDT and in my research group, have helped me more than I can explain. They have spent endless hours discussing various aspects of the project and listened to my frustrations. I am so thankful for their encouragement.

To my friends and family for bearing with me so well during the whole PhD and thesis writing process and encouraging me towards completion. Without your help, assistance and encouragement, this would have taken so much longer.

To my parents, your constant prayers and encouragement during the duration of this project have been a driving force for me, thank you so very much.

Finally, to my wife, Pamela, my deepest gratitude. Your constant encouragement during this project is much appreciated and never to be forgotten. Love you very much

This Research Project is dedicated to my wife, Pamela and Daughter Adora.

Abstract

One of the most feasible way of recycling waste materials in a sustainable way is thermal processing. There has been a few studies that investigated the steam reforming process for syngas and hydrogen production from biomass, there has also been a few studies that Investigated water gas shift reactions from biomass, but due to the limited research related to both catalytic steam reforming and water gas shift steam reforming in one process using a three stage reactor, this became the focus of this research This research has used pyrolysis of pelletised wood, followed by steam reforming reactions of the pyrolysis products to produce syngas, which is a mixture of hydrogen and carbon monoxide. This was followed by water gas shift steam reforming reactions to convert more carbon monoxide to hydrogen and, reduce the amount of carbon dioxide being produced in the experiments. A preliminary analysis was conducted in order to have a general understanding of the effects each components of biomass has on the pyrolysis gases.

A two-stage pyrolysis catalytic steam reforming reactor was used to investigate various process conditions and types of catalyst to maximize syngas and hydrogen production. A consistent average char yield of 22% was obtained and the GC/MS analysis of the product gases indicated that gas components were chiefly; CO, CO_2, H_2 and CH_4. One key finding from this two-stage fixed bed reaction systems was that H_2 increased in the N_2 atmosphere. Nickel based catalysts with different metal supports (Alumina, Zeolite, Silica, Dolomite and MCM41) were selected for the investigation of pyrolysis steam reforming of waste biomass.

Based on the review of literature, it was concluded that wet impregnation is the most efficient technique for synthesizing catalysts for thermochemical reactions. Among the catalysts tested, the 20wt% Nickel dolomite catalysts presented the highest catalytic activity resulting in a syngas production of 43 mmol syngas with no detectable carbon formation on the catalysts surface. In contrast to nickel dolomite catalyst, increased in nickel loading from 10wt% to 20wt% resulted in a steep decrease in hydrogen yield.

A three-stage pyrolysis-catalytic steam reforming water gas shift reactor was used to investigate various process conditions and types of catalyst to maximize hydrogen production. Various process parameters such as metal supports, steam to carbon ratio, reforming temperature, steam federate and catalyst to biomass ratio were tested. It was evident that third stage water gas shift reactor deficit of a catalyst was ineffective in optimizing total gas and H_2 yield. Another finding was that the use of iron and alkali earth oxide bimetallic catalysts, the optimal content of Fe and CaO in FeCaO-alumina catalysts for enhancing CO_2 absorption was found to be 10 wt. % Fe and 20 wt. % CaO. This catalyst produced the lowest CO_2 and the second highest H_2, yields representing 9.14 mmol and 45.59 mmol per gram of biomass respectively. This was also supported by the Temperature-Programmed Oxidation (TPO) results since it has the lowest weight. It was also found out that steam injection into the water gas shift reactor led to an increase in the hydrogen yield in the presence of reduced CaO-alumina catalyst, in contrast reduction in hydrogen yield was obtained in the presence of unreduced CaO-alumina catalyst.

An optimal condition of 10 wt. % CaO-alumina catalysts was the best suitable for maximizing hydrogen production because it produced the highest hydrogen yield of 51.58 mmolg^{-1} biomass. It was also found that the addition of Fe to FeCaO-alumina inhibited CO_2 absorption by the CaO but at the same time. Water gas shift reaction was promoted. The XRD result confirmed that spent CaO-alumina catalysts have good catalytic performance at high temperatures due to the presence of fewer oxidized species.

The commercial scale practice utilized in the deconstruction of biomass to char, syngas, and hydrogen gas were not compared with the laboratory scale results obtained in this research, and this was primarily owing to the current limitations in the large-scale technologies.

Overall, this research work showed that there is a promising opportunity in hydrogen production from biomass through a three-stage thermochemical process.

Table of Contents

List of Tables

List of Figures

Abbreviations

BEIS	Department for Business Energy and Industrial Strategy
BECCS	Bioenergy with carbon capture and storage
BMS	Biomass
CHNS	Carbon, hydrogen, Nitrogen and Sulphur Analysis
DEFRA	Department for Environment, Food and Rural Affairs
EFW	Energy from waste
FCC	Fluid catalytic cracking
FID	Flame ionisation detector
GC	Gas chromatography
GWP	Global warming potential
MS	Mass spectrometry
Mtoe	Million Tonnes of oil equivalent
RF	Response factor
SEM	Scanning electron microscope

TCD	Thermal conductivity detector
TPD	Temperature programmed desorption
TPO	Temperature programmed oxidation
XRD	X-ray diffraction
XRF	X-ray Fluorescence spectrometry

Chapter 1: Introduction

1.1 Global Energy Consumption

The world's primary energy consumption in the last decade has been at a record high and is rapidly growing, the highest growth rate since 2010 in total global energy demand and the emission peaked in 2018 at 2.9% and 2.0% respectively. These upward swings have been principally linked with the sprawling population, weather factors, intense industrial activities and commercial indices that necessitate more heating and cooling demands (BP, 2019).

Despite this increasing trend in energy consumption as shown in figure 1-1, according to International energy agency (IEA), about 2.8 billion people across the globe cannot access clean cooking and while 14% representing 1.1 billion people lack access to electricity (IEA, 2017).

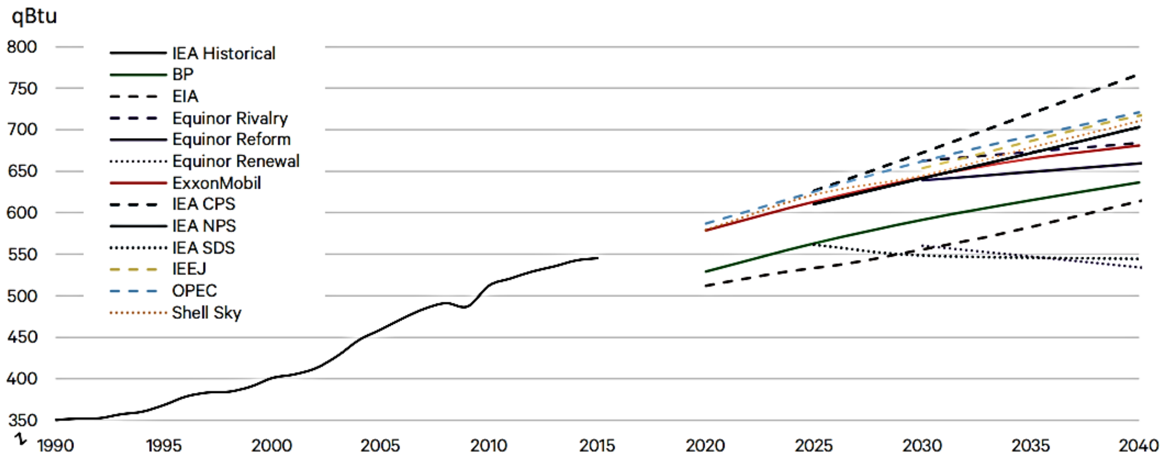

Figure 1-1: Global energy consumption growth (BP, 2019)

In the current energy mix, fossil fuel sources continue to dominate with a general rise in generation recorded in 2018. Crude oil rose by 2.2 million barrel per day, refinery production increased by 960,000 b/d, natural gas generated rose by 190 billion cubic metres (bcm), and coal production increased by 162 Mtoe representing 4.3%. The effect of this fossil growth is evident on the 2% rise in CO_2 emission levels.

In another report by the International Energy Agency (IEA) in 2016, the burning of fossil fuels for power production accounted for about 30% of the total global carbon emissions (IEA, 2016). Another cause for concern to the energy sector apart from the need to decarbonise is the depleting nature of the fossil resources.

1.2 Alternatives to Non-renewable energy fuel

The great divide between the increasing global energy demand and the request for an imminent accelerated switch to zero-carbon energy systems requires a rapid embrace of clean and sustainable fuels. Measures like complete coal-to-gas transition, utilisation of geoengineering carbon capture, use and Storage system (CCUS), among others, cannot drive the future economy because they only have good potential to cause a decline in carbon emissions but a deficit in meeting elevating energy demands. Renewable energy systems possess enormous potential for addressing sustainable energy production and emission control challenges. Solar power, hydroelectric, wind, nuclear, biomass energy systems among others have been identified as reliable renewable substitutes.

In 2018, the global total renewable energy rose by 14.5% thereby increasing the share of renewables in the world power production from 8.4% to 9.3%. Solar production contributed over 40% to the renewable growth representing 30 mtoe increase, hydroelectric power grew by 3.1%, nuclear by 2.4%, wind by 32 mtoe (IEA, 2019).

In addition to this, for all the overall renewable energy sources in Africa, biomass constitutes 90% of the total primary energy supply. Biomass energy is currently the largest world renewable energy source representing 56.5EJ (Global bioenergy statistics, 2018). World Bioenergy Association (WBA) report also showed that electricity generated from biomass (biopower) was the world's third biggest renewable electricity production source in 2016, representing 571TWh while direct heating using biomass accounted for 42.4EJ. Biofuel is also playing an enormous role, especially in the transport sector as a decarbonising substitute. For seven consecutive year until 2016, a rise from 1% to 3% in biofuel consumption was recorded in the transport sector. The IEA predicted that that bioenergy would continue as the single most significant primary source of renewable energy for next decades. The supply of biomass is broadly categorised into three key sectors namely; forestry, agriculture and waste (WBA, 2019). The broad spectrum of biomass supply feedstock is not limited to the following; municipal waste (solid and liquid), industrial waste, forest residues, wood pellets, energy crops, wood chips, charcoal, among others. It is worthy of note that converting liquid or solid wastes to energy presents an effective answer to the numerous challenges facing the world today which are employment creation, sustainable waste management systems, energy production and emission alleviation.

1.3 Waste generation and Disposal

An average person across the globe generates 740g of waste per day while the current global trend (figure 1-2) shows that an annual over 2 billion tons of municipal waste is generated, this estimate is predicted to soar rapidly to 3.40 billion tons by 2050 per year (Kaza et al. 2018). More than 33% of the municipal solid waste generated is unfriendly to the environment and human health. Metrics such as high-income levels, population and technology have a positive relationship with waste generation.

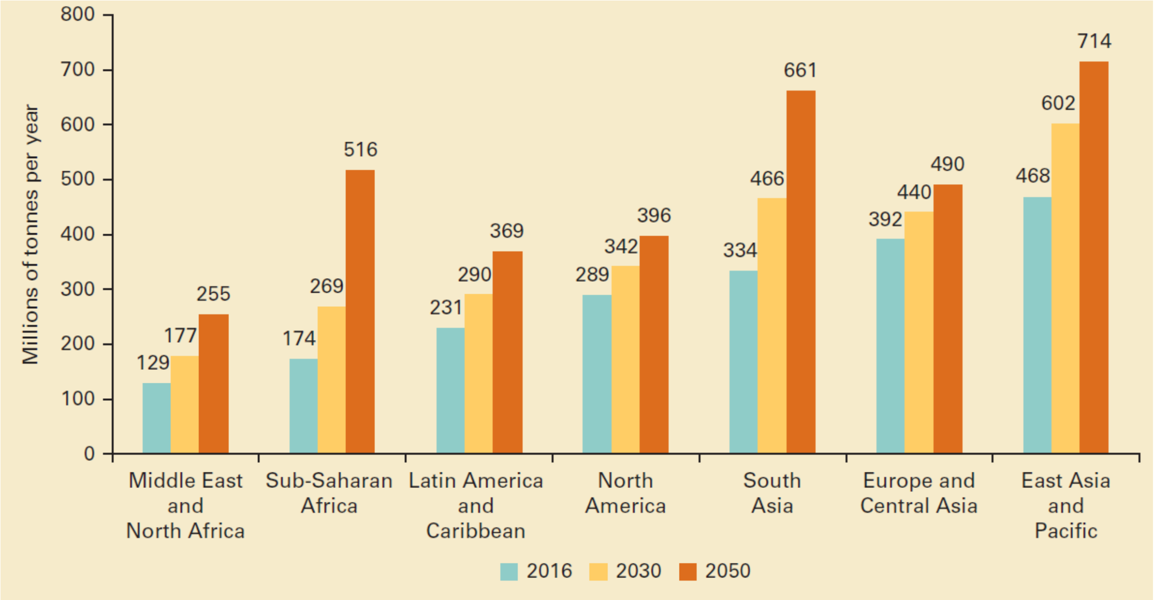

Figure 1-2: Projected waste generation, by region (millions of tonnes/year) (Source, World Bank, 2019)

The composition of waste across different countries and continents vary; this has a strong consequence on their waste management practices. Over 50% of the total wastes generated in developed countries are dry wastes comprising, metals, plastics, glass, and all kinds of paper while about 60% of wastes of produced in developing and under-developed countries are organic-based comprising of food and green wastes (World Bank, 2019). Method of disposing of these wastes without compromising the environmental standards has been the subject of discussion over the decades. About 1.5 billion metric tons of CO_2 equivalent greenhouse gas (GHG) emissions were liberated into the environment from municipal solid waste treatment in 2016. Open dumping still accounts over 90% of total wastes in low-income countries and landfilling still retains one for the largest share of global waste disposal practice as shown in figure 1-3. Although stringent measures culminating into the international standard for landfilling systems, other methods have proven more resourceful in both disposing the wastes and recovering energy from the wastes with a net-zero adverse effect on the ecosystem.

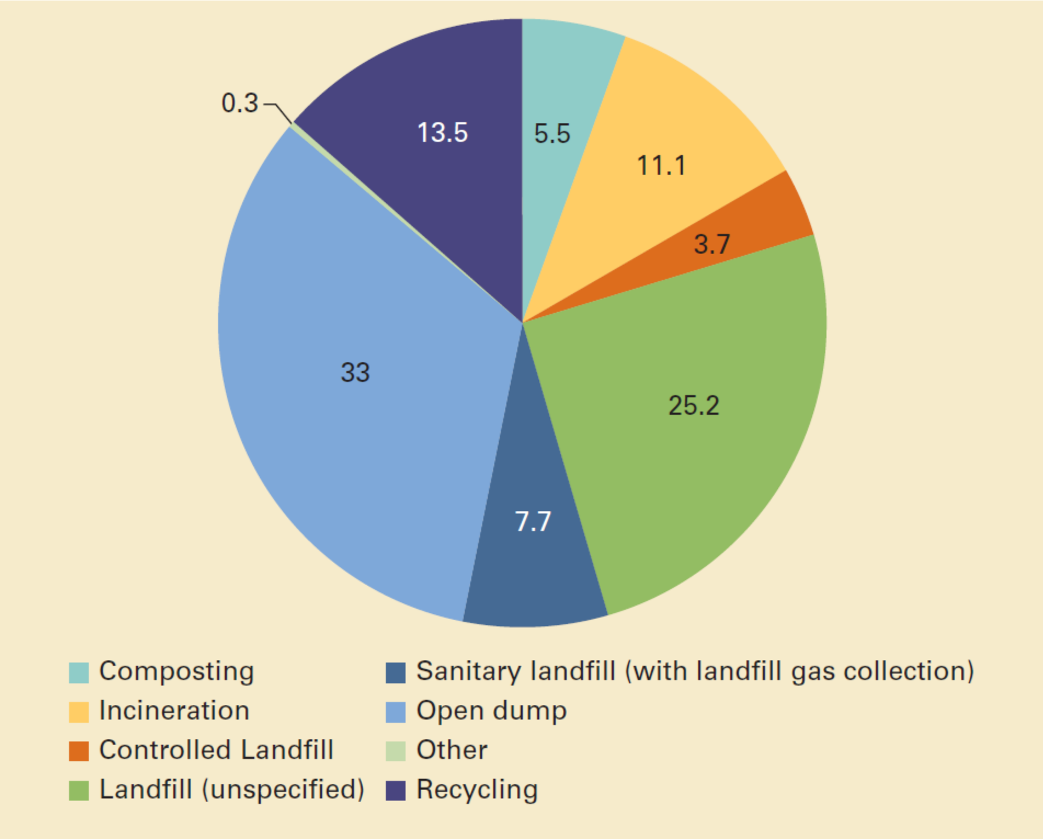

Figure 1-3: Global treatment and disposal of waste (percent) (Source: World Bank, 2019)

1.4 Energy recovery from biomass waste

The operational costs which cover collection, sorting and landfilling or incineration is posing a substantial challenge to many countries; hence, low-income countries have difficulties in financing waste management systems. However, a rising level of attention and effort is presently tailored to the transformation of wastes to use chemical and products to justify the capital investment in waste management. Thermochemical, biochemical and physicochemical techniques have significant potential to produce commercial products with wide industrial applications from waste conversion (Voloshin et al. 2016; Aro et al. 2016). In the thermochemical transformation processes, the organic matter is deconstructed thermally to generate fuel oil, syngas or heat energy, through incineration, pyrolysis, gasification, steam reforming and water gas shift processes. From the pyrolysis or gasification of organic wastes, the residual carbonaceous materials such as char and activated carbon are effective substitutes to the costly commercial activated carbons, and they have been employed in mitigating several environmental challenges. More so, these waste-derived carbons have been utilized as high-performance anode for ion batteries (Hong et al.; 2014; Zhang et al 2014), supercapacitor applications (Su et al 2018; Deng et al 2016, Wang et al 2017, Gao et al 2017), in the adsorption of heavy metals and organic pollutants (Giri et al 2012, Budinova et al 2009, Ahluwalia et al 2007, Li et al 2013, Tiwari et al 2011, Anastopoulos et al 2019) , tar cracking and gas pollutants removal (Guo et al 2019, Saleem et al 2019, Hai et al 2019).Wastes are also being considered as feedstock for the generation of the cheap adsorbent. The net effect of this techno-waste disposal system is a gross decline in the costs of waste disposal. Other economic products from wastes include methane, syngas, and hydrogen (Shayan et al. 2018, Arregi et al. 2018). These products gases are a good source of modern energy. The numerous energy recovery from wastes techniques are briefly discussed below:

- **Anaerobic digestion**: Anaerobic digesters are used to bio-decompose the organic matter such as lignocellulosic biomass in the presence of enzymes and microbes to produce biogas; chiefly methane and carbon dioxide which have viable combustible properties for energy generation, a residual and digested sludge which has wide application as a soil conditioner, ethanol and biomethane are also (Azman et al. 2015, Sawatdeenarunat et al. 2015, Ranganathan et al. 2017, Gouveia and Passarinho 2017).
- **Incineration**: Incineration is a thermochemical method that entails the burning of biomass to generate heat; the heat generated is afterwards converted to energy. Combustion has been applied to municipal solid waste (MSW), but issues related to the emission of toxic chemicals (NOx, SO2, dioxins, furan among others) have limited its application. However, research is ongoing in the area of avoiding or transforming the pollutant (Hicks et al. 2017, Zhao et al. 2018).
- **Co-pyrolysis with coal:** Another area of growing interest in the combustion of the mixture of coal and biomass (especially the MSW) to generated syngas for the turbine (Zhou et al. 2016a, Guo et al. 2018). It is predicted that in no distant time the co-combustion (either co-gasification or co-pyrolysis) of goal and biomass will proffer solution energy crunch as it will generate high efficiency, least operational cost and risk technique for producing clean energy (Kijo-Kleczkowska et al. 2016. The net calorific value of product gases obtained from this process is very high (Zhou et al. 2016b).

1.5 Thermochemical conversion technologies

Due to the environmental concerns associated with incineration, other thermochemical processes such as gasification, pyrolysis and steam reforming are gaining acceptance in the energy sector as possible sustainable options for transforming waste into economic products depending on the technique and the process conditions.

1.5.1 Gasification

This technique is used to produce gaseous intermediates or precursors in the thermal decomposition of biomass in the present of gasifying agents like air, oxygen, steam, among others. One main advantage of gasification is that it optimises the yield of gaseous products at the expense of the liquid and solid phases (Brown, 2019). As shown in table 1-1, there are several types of gasification and products mix depending on the process parameters.

1.5.2 Pyrolysis

Pyrolysis involves thermal degradation of biomass into three phases of products in the absence of oxygen; these phases include; gas, liquid (tars and oils) and solid (mainly char) (Brown, 2019). The pyrolytic yields depend principally on the pyrolysis operating conditions which are not limited to the temperature, heating rates, and residence time. These parameters can be manipulated to obtain the desired final products. As shown in table 1-1, pyrolysis is classified into fast pyrolysis, slow pyrolysis, vacuum pyrolysis, among others, based on their heating rates and temperatures applied.

Table 1-1: Summary of the different thermochemical techniques for biomass transformation (Patel et al. 2016)

Conversion technology	**Process condition**	**Reactor types**	**Product Yield**		
Pyrolysis Technique			Liquid (wt%)	Gas (wt%)	Solid (wt%)
Fast Pyrolysis	Atmospheric pressure, small particle size (< 3mm), short residence time (0.5-2s), moderate temperature (400-5500C) in the absence of oxygen	Fixed bed reactor, Tubular reactor, Bubbling fluidised bed reactor, Circulating fluidised bed reactor	65-75	13-25	12-19

Slow pyrolysis	Low heating rate, moderate temperature (350-7500C), atmospheric pressure, the long residence time in the absence of oxygen	Ablative Pyrolyzer, Rotating Cones reactor, Auger reactor, Cyclone reactor	30-50	15-30	30-60
Intermediate Pyrolysis	Moderate temperature (<5000C), moderate vapour residence time (4-10s) and atmospheric pressure		45-55	25-35	15-25
Flash Pyrolysis	Rapid heating (<0.5s), very small particle sizes (<0.5mm), temperature (400-10000C)		60-70	10-15	15-32
Vacuum Pyrolysis	Moderate temperature (300-5000C), pressure below atmospheric (<50kPa)		45-60	17-27	19-27
Ablative Pyrolysis	Moderate temperature (450 - 6000C), atmospheric pressure, particle size < 3.5mm		60-80	6-10	12-20
Gasification Technique					
Hydrothermal gasification	Moderate to high temperature (600-12000C), presence/absence of catalyst, small particle size desirable, gasifying agent	Fixed bed, moving bed, fluidized bed and entrained flow gasifier	1-2.6 (m3 gas/kg biomass):		
Combustion	Maximum temperature: 740-13000C, Air mass flow: 0.1-0.5 kg/m2.s	Fixed bed, fluidised bed, circulating bed and entrained flow bed combustor	Power and heat		

Liquefaction Technique					
Hydrothermal/thermochemical liquefaction	Temperature: moderate to high (250-5500C), pressure: 5-25 MPa, solvent type, heating rate: 5-1400C/min	Parr high pressure reactor	60-75	15-20	8-20
Carbonization	Temperature: low to high: (400-12000C), heating rate: 4-5 0C	Stainless steel container inside a furnace	--	--	20-35
Co-firing	%wt of biomass: 5 -20	Boiler	Power and heat		

Among the end products obtained from these thermochemical processes, hydrogen gas has received sheer favour for energy purpose both for electricity generation and transportation reasons. In addition to this, hydrogen fuel is considered as the cleanest because the by-product of its combustion only produces water vapour (Sinigaglia et al. 2017, Łukajtis et al. 2018) and because of this, it is widely utilized in refining processes, as a chemical reactant and for metal refining, fuel in automotive applications, fuel cells for electricity, among others (Arrehi et al. 2018). The numerous benefits derived from hydrogen fuel gave rise to the term “hydrogen economy”, that is the future energy system being driven by hydrogen gas (Ball et al. 2015, Moliner et al. 2016). This has stimulated the need to optimise hydrogen yield in the thermochemical conversion systems. Other techniques have been attached to pyrolysis as a way of enhancing hydrogen yields; this includes; steam reforming and water gas shift process. The amount of hydrogen produced from these methods also hinges on the process conditions. Suitable process conditions are therefore the interest of every researcher.

1.6 Aims

This project aims to investigate the thermochemical conversion of biomass (wood pellets) for the generation of hydrogen gas through pyrolysis, catalytic steam reforming and water gas shift processes in a fluidised bed reactor. Suitable conditions for optimal hydrogen yield was chiefly focused on which include; catalyst composition and steam flow rate.

1.7 Objectives

- To determine the suitable catalyst in a two-stage Pyrolysis-catalytic steam reforming of Biomass
- To determine the effects of different Nickel loadings on total gas and hydrogen production
- To determine the effects of oxide support on Nickel catalyst in a two-stage reactor on total gas and hydrogen production
- To determine the suitable catalyst for optimum hydrogen production from the three-stage process
- To assess the effect of nickel loading on hydrogen yield from the three-stage process
- The influence of steam ratio on H_2 production from pyrolysis, catalytic steam reforming and water gas shift process
- To determine the effect of adding reduced 10% nickel supported on alumina in the catalytic steam reforming stage with no catalyst at the water gas shift stage was investigated to determine the influence on hydrogen production.
- To determine the influence of adding CaO at states (reduced or unreduced) and different metal loadings to enhance water gas shift reaction performance.
- To determine the quality of the reacted catalysts by subjecting them to different characterisation techniques; Temperature Programmed Oxidation and X-ray diffraction (XRD) to investigate the type and extent of carbon depositions on the reacted catalysts.

1.8 References

Ahluwalia, S. S., & Goyal, D. (2007). Microbial and plant-derived biomass for removal of heavy metals from wastewater. Bioresource Technology, 98(12), 2243-2257.

Anastopoulos, I., Robalds, A., Tran, H. N., Mitrogiannis, D., Giannakoudakis, D. A., Hosseini-Bandegharaei, A., & Dotto, G. L. (2019). Removal of heavy metals by leaves-derived biosorbents. Environmental Chemistry Letters, 17(2), 755-766.

Aro, E. M. (2016). From first-generation biofuels to advanced solar biofuels. Ambio, 45(1), 24-31.

Arregi, A., Amutio, M., Lopez, G., Bilbao, J., & Olazar, M. (2018). Evaluation of thermochemical routes for hydrogen production from biomass: A review. Energy conversion and management, 165, 696-719.

Azman, S., Khadem, A. F., Van Lier, J. B., Zeeman, G., & Plugge, C. M. (2015). Presence and role of anaerobic hydrolytic microbes in the conversion of lignocellulosic biomass for biogas production. Critical Reviews in Environmental Science and Technology, 45(23), 2523-2564.

Ball, M., & Weeda, M. (2015). The hydrogen economy–vision or reality?. International Journal of Hydrogen Energy, 40(25), 7903-7919.

Brown, R. C. (Ed.). (2019). Thermochemical processing of biomass: conversion into fuels, chemicals and power. John Wiley & Sons.

Budinova, T., Savova, D., Tsyntsarski, B., Ania, C. O., Cabal, B., Parra, J. B., & Petrov, N. (2009). Biomass waste-derived activated carbon for the removal of arsenic and manganese ions from aqueous solutions. Applied Surface Science, 255(8), 4650-4657.

BP Statistical Review of World Energy, 2019. Pureprint Group Limited, UK, ISO 14001. Available at: www.bp.com/energyoutlook

Deng, J., Li, M., & Wang, Y. (2016). Biomass-derived carbon: synthesis and applications in energy storage and conversion. Green Chemistry, 18(18), 4824-4854.

Gao, Z., Zhang, Y., Song, N., & Li, X. (2017). Biomass-derived renewable carbon materials for electrochemical energy storage. Materials Research Letters, 5(2), 69-88.

Giri, A. K., Patel, R., & Mandal, S. (2012). Removal of Cr (VI) from aqueous solution by Eichhornia crassipes root biomass-derived activated carbon. Chemical Engineering Journal, 185, 71-81.

Gouveia, L., & Passarinho, P. C. (2017). Biomass conversion technologies: biological/biochemical conversion of biomass. In Biorefineries (pp. 99-111). Springer, Cham.

Guo, F., & Zhong, Z. (2018). Optimisation of the co-combustion of coal and composite biomass pellets. Journal of cleaner production, 185, 399-407.

Guo, F., Peng, K., Liang, S., Jia, X., Jiang, X., & Qian, L. (2019). Evaluation of the catalytic performance of different activated biochar catalysts for the removal of tar from biomass pyrolysis. Fuel, 258, 116204.

Hai, A., Bharath, G., Babu, K. R., Taher, H., Naushad, M., & Banat, F. (2019). Date seeds biomass-derived activated carbon for efficient removal of NaCl from the saline solution. Process Safety and Environmental Protection.

Hicks, K. O., Chavda, S., Santoianni, J., & Gorodetsky, A. (2017). U.S. Patent No. 9,669,248. Washington, DC: U.S. Patent and Trademark Office.

Hong, K. L., Qie, L., Zeng, R., Yi, Z. Q., Zhang, W., Wang, D., ... & Huang, Y. H. (2014). Biomass-derived hard carbon used as a high-performance anode material for sodium-ion batteries. Journal of Materials Chemistry A, 2(32), 12733-12738.

IEA, 2016. International Energy Access Outlook 2016. Energy access database, International Energy Agency. Available at: https://www.eia.gov/outlooks/ieo/pdf/0484(2016).pdf

IEA, 2017. Energy Access Outlook 2017. Energy access database, International Energy Agency. Available at: https://www.iea.org/energyaccess/database/

Kaza, Silpa; Yao, Lisa C.; Bhada-Tata, Perinaz; Van Woerden, Frank. 2018. What a Waste 2.0: A Global Snapshot of Solid Waste Management to 2050. Urban Development. Washington, DC: World Bank. Available at: https://openknowledge.worldbank.org/handle/10986/30317 License: CC BY 3.0 IGO

Kijo-Kleczkowska, A., Środa, K., Kosowska-Golachowska, M., Musiał, T., & Wolski, K. (2016). Experimental research of sewage sludge with coal and biomass co-combustion, in pellet form. Waste management, 53, 165-181.

Li, M., Liu, Q., Guo, L., Zhang, Y., Lou, Z., Wang, Y., & Qian, G. (2013). Cu (II) removal from aqueous solution by Spartina alterniflora derived biochar. Bioresource technology, 141, 83-88.

Łukajtis, R., Hołowacz, I., Kucharska, K., Glinka, M., Rybarczyk, P., Przyjazny, A., & Kamiński, M. (2018). Hydrogen production from biomass using dark fermentation. Renewable and Sustainable Energy Reviews, 91, 665-694.

Moliner, R., Lázaro, M. J., & Suelves, I. (2016). Analysis of the strategies for bridging the gap towards the Hydrogen Economy. International journal of hydrogen energy, 41(43), 19500-19508.

Patel, M., Zhang, X., & Kumar, A. (2016). Techno-economic and life cycle assessment on lignocellulosic biomass thermochemical conversion technologies: A review. Renewable and Sustainable Energy Reviews, 53, 1486-1499.

Ranganathan, A., Smith, O. P., Youssef, N. H., Struchtemeyer, C. G., Atiyeh, H. K., & Elshahed, M. S. (2017). Utilising anaerobic fungi for two-stage sugar extraction and biofuel production from lignocellulosic biomass. Frontiers in microbiology, 8, 635.

Saleem, F., Harris, J., Zhang, K., & Harvey, A. (2019). Non-thermal plasma as a promising route for the removal of tar from the product gas of biomass gasification-A critical review. Chemical Engineering Journal, 122761.

Sawatdeenarunat, C., Surendra, K. C., Takara, D., Oechsner, H., & Khanal, S. K. (2015). Anaerobic digestion of lignocellulosic biomass: challenges and opportunities. Bioresource technology, 178, 178-186.

Shayan, E., Zare, V., & Mirzaee, I. J. E. C. (2018). Hydrogen production from biomass gasification; a theoretical comparison of using different gasification agents. Energy conversion and management, 159, 30-41.

Sinigaglia, T., Lewiski, F., Martins, M. E. S., & Siluk, J. C. M. (2017). Production, storage, fuel stations of hydrogen and its utilisation in the automotive applications-a review. International journal of hydrogen energy, 42(39), 24597-24611.

Su, X. L., Chen, J. R., Zheng, G. P., Yang, J. H., Guan, X. X., Liu, P., & Zheng, X. C. (2018). Three-dimensional porous activated carbon derived from loofah sponge biomass for supercapacitor applications. Applied Surface Science, 436, 327-336.

Tiwari, D. (2011). Biomass-derived materials in the remediation of heavy metal contaminated water: removal of cadmium (II) and copper (II) from aqueous solutions. Water Environment Research, 83(9), 874-881.

Voloshin, R. A., Rodionova, M. V., Zharmukhamedov, S. K., Veziroglu, T. N., & Allakhverdiev, S. I. (2016). Biofuel production from plant and algal biomass. International journal of hydrogen energy, 41(39), 17257-17273.

Wang, J., Nie, P., Ding, B., Dong, S., Hao, X., Dou, H., & Zhang, X. (2017). Biomass-derived carbon for energy storage devices. Journal of Materials Chemistry A, 5(6), 2411-2428.

WBA Global Bioenergy Statistics 2018 Summary Report. World Bioenergy Association. Available at: https://worldbioenergy.org/uploads/181017%20WBA%20GBS%202018_Summary_hq.pdf

World Bank. 2019. Access to electricity (% of the population). Available at: https://data.worldbank.org/indicator/eg.elc.accs.zs

Zhang, J., Xiang, J., Dong, Z., Liu, Y., Wu, Y., Xu, C., & Du, G. (2014). Biomass-derived activated carbon with 3D connected architecture for rechargeable lithium− sulfur batteries. Electrochimica Acta, 116, 146-151.

Zhao, Y., Ren, Q., & Na, Y. (2018). Phosphorus Transformation from Municipal Sewage Sludge Incineration with Biomass: Formation of Apatite Phosphorus with High Bioavailability. Energy & fuels, 32(10), 10951-10955.

Zhou, C., Liu, G., Wang, X., & Qi, C. (2016). Co-combustion of bituminous coal and biomass fuel blends: thermochemical characterization, potential utilization and environmental advantage. Bioresource technology, 218, 418-427.

Zhou, C., Liu, G., Wang, X., Qi, C., & Hu, Y. (2016). Combustion characteristics and arsenic retention during the co-combustion of agricultural biomass and bituminous coal. Bioresource technology, 214, 218-224.

Chapter 2: Literature Review

2.1 Waste and Biomass Resources

The EU Waste Framework Directive defines 'waste' as: "Any substance or objects the holder discards, intends to discard or is required to discard" (European Directive 2006/12/EC) [EC, 2009]. The UK Waste Strategy defines 'waste' as being "ubiquitous material which appears in several waste streams, including construction and demolition of waste, agricultural waste, municipal waste, bulky household waste, packaging waste and other commercial and industrial waste."

While the UK bioenergy strategy defines waste as use of-end-life materials for energy can be optimum use of biomass, where it maximises carbon and cost-effectiveness, and where it is consistent with the waste hierarchy (REA, 2018). Due to changes in the law and legislations [Grosso et al. 2010; Burnley, 2001; Price, 2001; EC, 2009; EC, 1999], landfilling is no longer a viable option for the disposal of waste produced. The report (REA, 2018) produced by the government has highlighted the tremendous potential waste biomass (especially wood) has in the production of electricity, heat and transport.

Waste has increased exponentially due to population, low production efficiency and economic growth. The amount of waste generated in the European Union (EU) in 2016 was 2.54 billion tonnes per year.

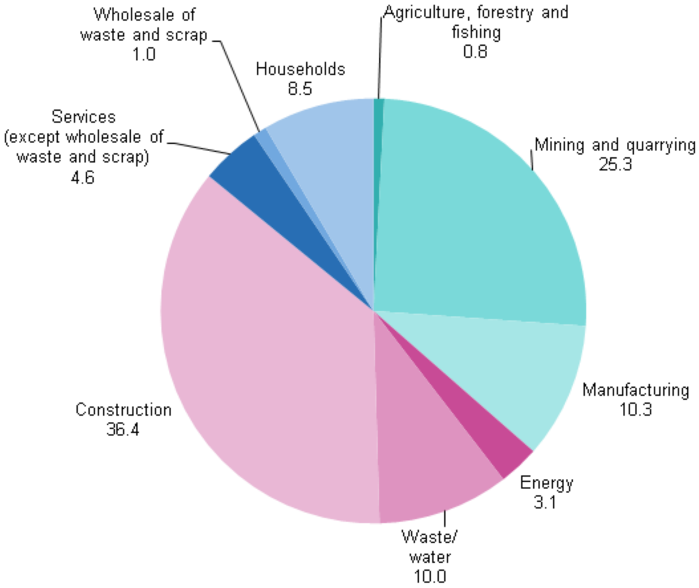

Figure 2-1: Waste generation in EU-28, 2016 by economic activities and households [EC, 2019]

The amount of waste produced in 2012 was 2.5 billion tonnes per year, as seen in figure 2-1. Generally, the trend of waste produced in the European Union (EU) appears to be on the increase, according to the European Environment Agency (EEA). [EC, 2019] In the United Kingdom, 222.9 million tonnes of waste was produced in 2016 as seen in figure 2-2 while 241.1 million tonnes of waste was produced in 2012 [EC, 2019]

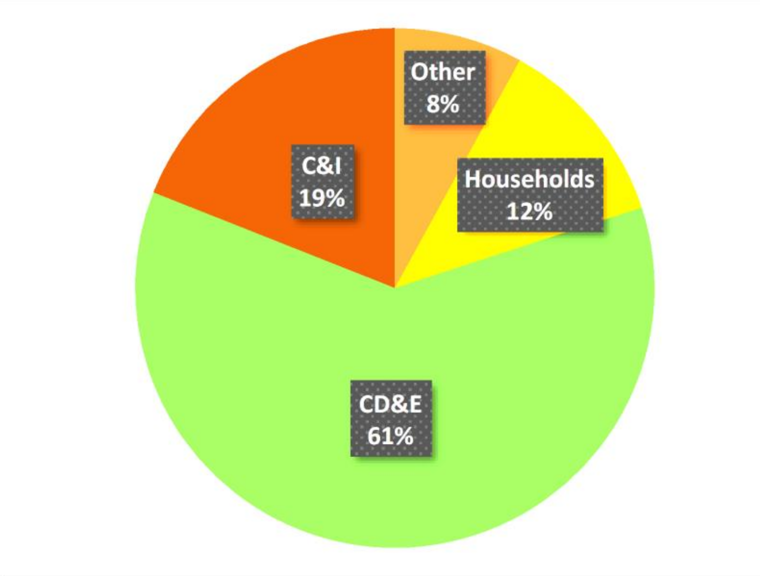

CD&E means Construction, demolition and excavation while Commercial and Industrial (C&I)

Figure 2-2: Waste generation split by waste material, UK 2016 [DEFRA, 2019]

24.4 per cent of the total waste produced in the UK, which is approximately 52.3 million tonnes still ends up in landfill in the year 2016 representing the second most used waste treatment system. This 52.3 million tonnes of waste can be used to generate power and energy instead of being put to landfill. [DEFRA, 2019] Consistent with DEFRA and WRAP [Brown and Kearley, 2009; DEFRA, 2012; WRAP, 2009], there are six (6) core sources of waste wood resources in the UK which are depicted in figure 2-3, namely;

- Construction
- Demolition
- Industrial
- Municipal
- Packaging
- Remodelling

Figure 2-3: Sources of Post-Consumer Wood Waste [WRAP, 2009]

Household waste is referred to as municipal waste; municipal waste includes fencing, decking, pallets, furniture, garden waste. Municipal wastes are usually collected by the local council or household waste recycling centres.

Construction and demolition waste can vary a great deal due to its compositions, according to a report by Defra [DEFRA, 2015; Consulting, 2011], approximately 2.3 million tonne of waste wood is produced from the construction and demolition stream every year as seen in figure 2-4 below. Construction and demolition waste usually contain a mix of not just wood waste; these mixes can include anything from nails, screws to tilings, reinforcing bars and rubbles. It is essential to pre-sort construction and demolition waste to isolate just the waste wood.

Commercial and industrial wastes are primarily generated from the production of industrial and commercial products such as furniture, joinery, utility poles and packaging as seen in figure 2-4 below.

2.2 Wastes Hierarchy

According to Article 4 of the European Waste Framework [Jamasb and Nepal, 2010; Costa et al. 2010; Grosso et al. 2010], the least favoured option for waste management is the disposal of waste either through landfill and or incineration without energy recovery. The most favoured choice for waste management is the prevention of waste through the utilisation of less material either in the design stage, the manufacturing stage and the utilisation stage of the product.

The waste strategy for England 2010 [Strategy, 2000] has estimated that 13000Gwh of electricity can be generated from 10 million tonnes of waste wood. 5.75 million Tonnes of carbon dioxide emissions can be saved from 10 million tonnes of waste wood produced [Strategy, 2000]. To address the energy challenges and reduce the greenhouse gases produced in the UK, the UK Government released a report [Dti, 2007] which enumerated strategies to address the energy challenges and reduce the greenhouse gases produced. This report also led to the release of the UK Bioenergy strategy [DECC, 2012], in this report "Waste: use of-end-life materials for energy can be an optimum use of biomass, where it maximises carbon and cost effectiveness, and where it is consistent with the waste hierarchy;" was identified as a resource that can be utilised.

Current waste disposal methods in no particular order include biological recycling, chemical recycling, mechanical recycling, landfilling, anaerobic digestion, pyrolysis, gasification and incineration without energy recovery.

Due to change in legislation such as the European landfill directive [Burnley, 2001; Price, 2001 landfilling is no longer a viable option for the disposal of waste; currently 70 million tonnes of waste still ends up in the landfill according to DEFRA [DEFRA, 2015]. Alternative sources for the disposal of waste are needed to meet 35% of 1995 levels by 2020.

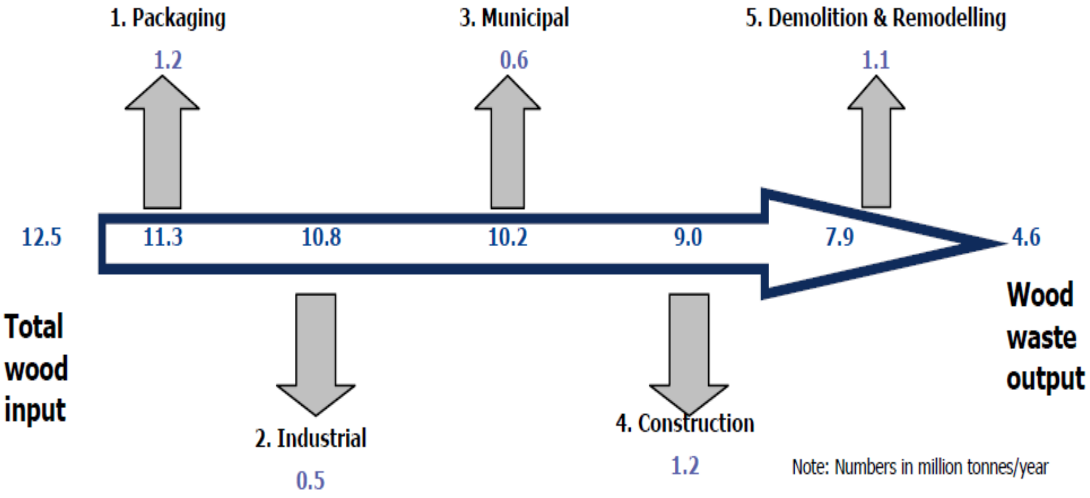

Figure 2-4: Wood Waste Flow in 2007 (arrows indicate the volume of wood waste from each stream)

2.3 Biomass and its constituents

Biomass consists of organic matter which can be converted into bioenergy through different processes. There are a great variety of feedstocks that can be utilised as biomass which include energy crops, food waste, forest and wood residues, short rotation forests, crop residues, municipal solid waste and animal wastes.

Biomass has been widely used to produce solid fuels, like wood pellets or briquettes, but also liquid fuels, such as biodiesel, ethanol or methanol and gaseous fuels, like syn-gas, biogas and hydrogen. All of them can be used at the same time to provide heat, electricity and transport fuels through many pathways (International Energy Agency, 2007). Recently biomass has received increased attention for its many advantages, which include meeting energy requirements, energy generation in different forms (power and heat), CO_2 neutral and land restoration (Balat & Kirtay, 2010). Concerning the transport sector, biomass offers an attractive solution to replace conventional liquid fuels, which currently supply almost 100% of transport fuels and achieve decarbonisation of transport fuels, by producing biofuels like biodiesel, bioethanol, biogas and even hydrogen. One of the biggest challenges in using biomass for biofuel production is to prove the overall sustainability of the process (IEA Bioenergy, 2011).

Solid biomass is composed of three main constituents which are cellulose, hemicellulose and lignin. Other components are holocellulose, lignocellulose, extractives (resins, glycerol, waxes, terpenes, steroids and fats) and minerals (major and minor essential elements). Cellulose represents the most abundant part of biomass (40-50% dry weight), it offers a “skeleton” fibril encircled by hemicellulose and lignin. Hemicellulose provides strength to the cell wall, and it is usually 20-30% of the dry weight of biomass. Lignin is the hardest part, typically 10-30% of the dry weight of biomass (Collard and Blin, 2014).

2.4 Thermal treatment of Biomass waste

Due to changes in legislation and climatic changes, energy from waste has become a viable option. Energy from biomass, in particular, is becoming very attractive due to its versatile nature. Biomass is now being used for heat generation, for electricity and transportation fuel. Figure 2-5 shows the different possible conversion routes to produce bioenergy from a wide range of biomass feedstocks.

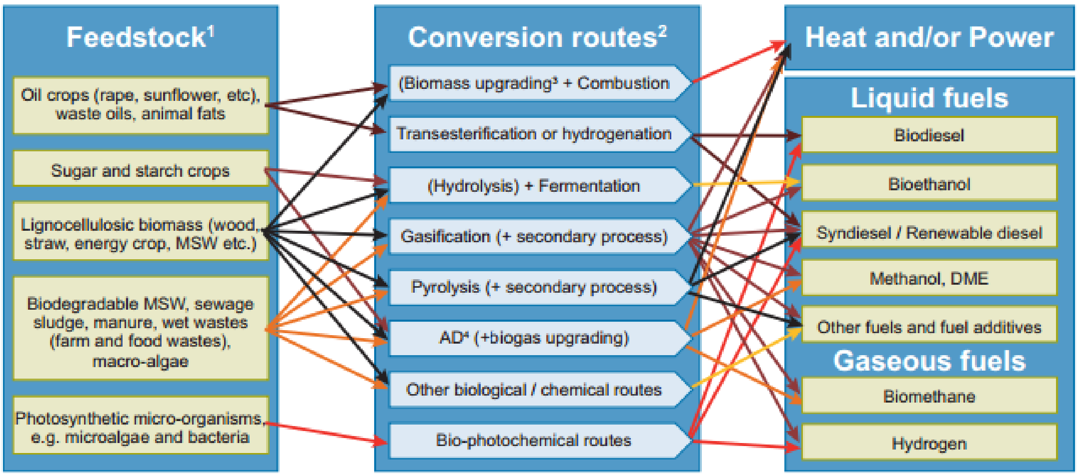

[1] Parts of each feedstock, e.g. crop residues, could also be used in other routes

[2] Each route also gives co-products

[3] Biomass upgrading includes any one of the densification processes (pelletisation, pyrolysis, torrefaction, etc.)

[4] AD = Anaerobic Digestion

Figure 2-5: Biomass Conversion Routes [DFT and DEFRA, 2012]

Some conversion routes are well known and straightforward like combustion of biomass, anaerobic digestion, gasification, pyrolysis, thermal oxidation, thermal cracking, while some are not so common such as plasma arc, and waste to fuel [Waste to energy, 2010].

As shown in figure 2-5, pyrolysis and gasification are standard conversion techniques used to deconstruct biomass feedstocks to derive alternative fuels. Pyrolysis, also known as thermolysis/cracking is the thermal conversion or chemical degradation of waste material or organic material in the absence of oxygen [Mohan et al. 2006]. The waste material or organic material decomposes because the chemical bonds responsible for the formation of the organic materials are broken down into three phases, synthetic gas, liquid/oil and solid char. Pyrolysis is an endothermic reaction, therefore, requires a heat supply. During the liberation of the volatile matter, significant weight loss of the waste material occurs followed by the decomposition of the char (Blanco et al., 2012, Cortright et al., 2010; Aigner et al., 2009; Cornelissen et al., 2008). According to Al-Salem et al. (2009), a clean high calorific fuel gas of approximately 30MJ/m^3 can be produced using the advanced pyrolysis process.

There are three major pyrolysis methods; the first is slow pyrolysis, it utilises a slow heating rate, and a higher yield of biochar is produced. The second method is fast pyrolysis, which utilises a high heating rate and favours a higher liquid yield from the product stream. The third pyrolysis method is a bridge between fast and slow pyrolysis (Bizkarra et al., 2017). According to Greenhalf, et al. (2012) a significant difference in the oil composition was observed when fast and slow pyrolysis was carried out.

There are a number of experimental parameters that can affect the yield of the product from the pyrolysis-gasification of biomass waste. These factors include but are not limited to reaction agents, presence of reactive gases, absence of reactive gases, catalyst type, feedstock chemical composition, pressure, temperature, heating rate, reactor type and other factors. Various researchers have conducted extensive research into pyrolysis of biomass [Greenhalf, et al. 2012; Fagbemi et al. 2001; Karagoz, 2009; Parparita et al., 2014; Yanik et al. 2013, Cornelissen et al., 2008; Fahmi, et al. 2008; Greenhalf et al., 2013; Zhang, et al. 2007].

2.4.1 Pyrolysis of Biomass

During the relatively simple technique used in the pyrolysis stage, organic material is heated in the absence of air or inert atmosphere. This, in turn, leads to the constituents of the biomass (cellulose, hemicelluloses and lignin) being broken down into three separate fractions: condensed vapours (bio-oil), solid fraction (char) and non-condensable gases (Ronsse et al., 2012, Arregi, et al., 2018). The amounts in which each of these fractions are produced can be manipulated by varying the heating rate and the temperature at which it is taking place (Collard et al., 2014). Similarly, according to Biskarra, et al. (2017) the reactions involved in the pyrolysis of biomass are very complex and are affected by many factors. The reactions are divided into primary reactions, which break the cellulose, hemicellulose, and lignin in the biomass and secondary reactions which are cross-reactions from the primary reaction products and unpyrolyzed biomass. The general reaction for biomass pyrolysis is given in equation 2.1 below (Ni, et al., 2006):

$$Biomass + heat \rightarrow H_2 + CO + CH_4 + other\ products \qquad 2.1$$

For any pyrolysis, the general steps are defined in Figure 2-6. Once the biomass has been broken down, the process gases can be used in the production of syngas, hydrogen and other fuels.

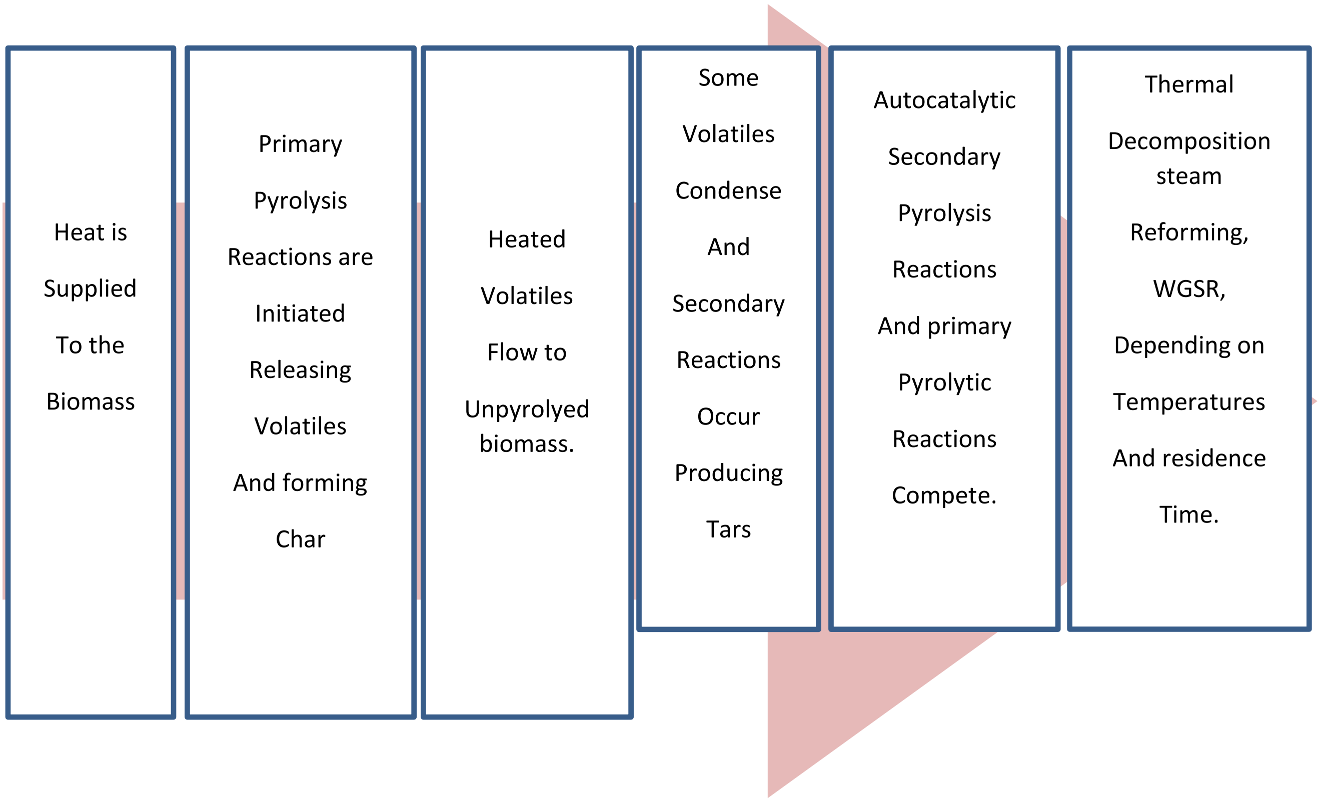

Figure 2-6:Biomass Pyrolysis process steps (Bizkarra et al., 2017).

In general, the slow (or conventional) pyrolysis looks for solid product yield (char) maximisation while the fast pyrolysis is commonly used when higher liquid product yields are desired (Saleh, 2018). Saleh (2018) studied both slow and fast pyrolysis in biomass for syngas production and found that the fast pyrolysis produced less syngas than conventional pyrolysis. However, in the slow pyrolysis, there were more mass losses than in the fast pyrolysis.

In addition to slow and fast pyrolysis, Demirbas (2009) discusses other pyrolysis methods, which are indicated in Table 2-1, and are applied depending on the desired product - whether it's char, bio-oil and gas, and in some cases chemicals.

Table 2-1: *Pyrolysis methods with their conditions, adapted from Demirbas (2009)*

Method	**Residence (Time)**	**Temperature (K)**	**Heating rate**	**Products**
Carbonation	Days	675	Very low	Charcoal
Slow	5-30 mins	875	Low	Oil, gas, char
Fast	0.5-5 s	925	Very high	Bio-oil
Flash-liquid[a]	<1 s	<925	High	Bio-oil

Flash-gas[b]	<1 s	<925	High	Chemicals, gas
Hydro-pyrolysis[c]	<10 s	<775	High	Bio-oil
Methano-pyrolysis[d]	<10 s	<775	High	Chemicals
Ultra pyrolysis[e]	<0.5 s	1,275	Very high	Chemicals, gas
Vacuum pyrolysis	2-30 s	675	Medium	Bio-oil

[a] Liquid from flash pyrolysis

[b] Gas from flash pyrolysis

[c] In the presence of water

[d] In the presence of methanol

[e] High degradation rate

Pyrolysis feedstocks and methods have different yields in their products. At the same time, these yields have a high dependence on the heating rate, the residence time, the particle size and the temperature, with the latter being the most influential.

2.4.1.1 Pyrolysis Temperature

Collard & Blin (2014) studied the thermal conversion of different biopolymers individually and the findings showed that the highest mass loss rates occur between 360 and 400°C for lignin, from 330 to 370°C for the cellulose, and from 200 to 350°C for the hemicellulose, which had the widest range for its highest decomposition rate. With a low heating rate and a temperature above the upper limits of those ranges, it would be expected for all the volatiles to be released. As stated by Collard & Blim (2014) hydrogen evolves from lignin at temperatures above 500°C, while in cellulose and hemicellulose it occurs at temperature ranges from 500 to 800°C and 480 to 800°C respectively. If it's desired to maximise the hydrogen production from the three pseudo components in the biomass, a temperature above 500°C should be chosen; once there has been a considerable mass loss in each of them.

On the other hand, García Barneto et al. (2009) studied the pyrolysis of alternative biomasses, Leucaena and Tagasaste, which can be used as energy crops, simulating the hydrogen signal and found the contributions of each biopolymer to hydrogen production: 27.5 wt.% for hemicellulose, 9.7 wt.% for the cellulose, 60.9 wt.% and for the lignin and 1.9% for the extractives in the Leucaena sample. This means that out of all the pseudo-components, the lignin has a higher contribution in the hydrogen yield.

Waheed & Williams (2013) studied hydrogen production a process involving high temperature pyrolysis, followed by steam reforming, with three different biomass samples: rice husk, sugar cane bagasse and wheat straw and their H_2 yields results after pyrolysis but before the steam reforming are summarised in Table 2-2. These studies exhibit similar properties to that of Garcia barneto et al. (2009), which proves the validity.

Table 2-2: Results obtained after pyrolysis from Waheed & Williams (2013)

Biomass Sample	**Hydrogen Yield (mmolg^{-1} biomass)**	**H (wt.%) (Ultimate Analysis)**
Sugar cane bagasse	2.07	5.63
Rice Husk	2.12	5.4
Wheat Straw	2.22	4.33

Research into the pyrolysis of biomass carried out by Lopez et al. (2002) looked at analysing the gases released during the process. The research, in particular, investigated the effect that temperature had on the composition of product gases. Despite a specific type of biomass being used in their investigation, their findings are highly relatable. In the paper, the gases identified were oxygen derived from the biomass feedstock, nitrogen which was fed into the experimental process to create an inert atmosphere, hydrogen, carbon monoxide, carbon dioxide and the light hydrocarbons: methane, ethene and ethane. In terms of the first two gases identified, they were consistently shown to be in

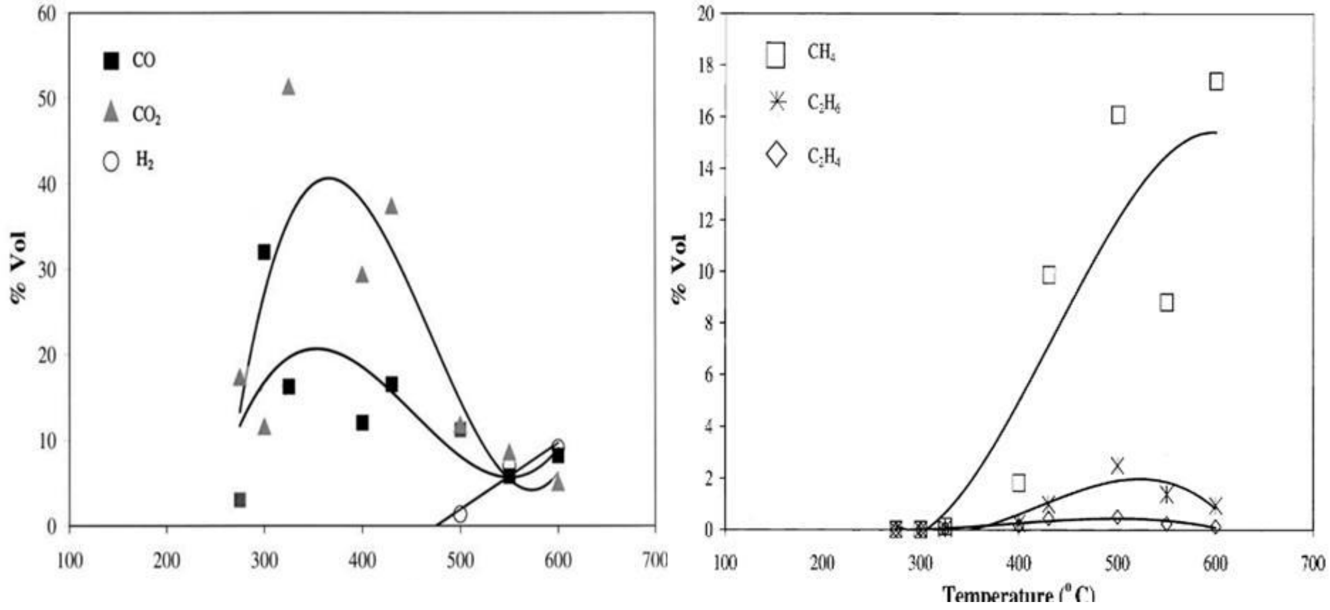

Figure 2-7:(a) Change in concentration of CO, CO_2 and H_2 with temperature during pyrolysis; **(b) Change in concentration of CH_4, C_2H_6 and C_2H_4.**

Source: Lopez et al. (2002)

the same ratio as they are found in air demonstrating that they are not products of pyrolysis.

From their results, which have been displayed above in figures *2-7a* and figure *2-7b*, it is shown that the majority of the gaseous mixture was made up of carbon monoxide and carbon dioxide with their concentrations reaching a maximum at 350°C before declining gradually with temperature. In terms of light hydrocarbons, it was found that their concentrations increased with temperature up to 500°C with CH_4 being the most abundant. The amount of hydrogen produced can also be seen to increase with temperature as can the total amount of gas produced. These results have also been reported by Couhert et al. (2009).

2.4.1.1.1 Effect of Highest Treatment Temperature (HTT) in Biomass Pyrolysis

In Biomass Pyrolysis, the highest treatment temperature (HTT) is the maximum temperature at which the biomass is subjected to in the respective reactors. Williams & Besler (1996) explored the effect of temperature in the slow pyrolysis of biomass, finding that, at higher temperatures, higher quantities of gas and oil were produced, and the char mass percentage decreased significantly. Also, at low temperatures, the production of H_2O, CO_2, and CO was promoted, while at higher temperatures the main products were oil, H_2O, H_2, hydrocarbon gases and CO, with lower concentrations of CO2. Figure 2-8 shows the influence of temperature in the composition of the gas in a slow pyrolysis process.

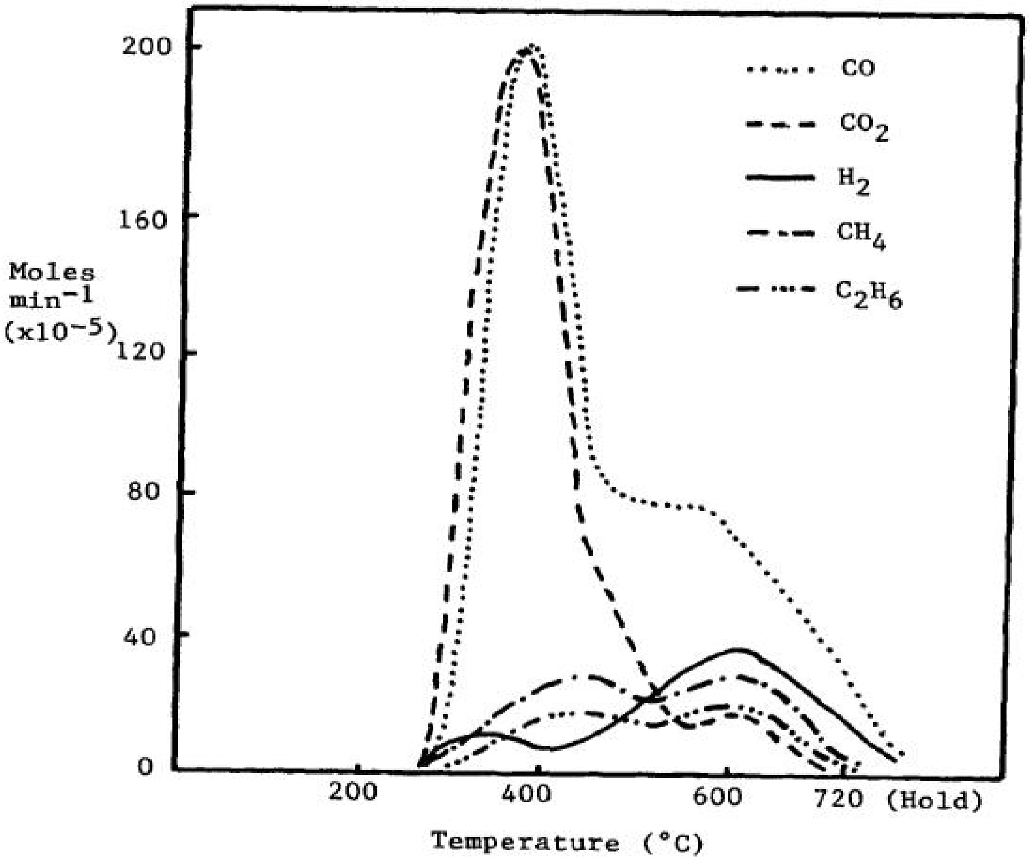

Figure 2-8: Effect of temperature in the composition of pyrolysis gas (Williams & Besler, 1996)

Additionally, other studies, summarised in Table 2-3, explored the effect of the final temperature in different samples of biomass:

Biomass feedstock	**Biomass temperature (O⁰C)**	**Char yield (wt%)**	**Gas yield (wt%)**	**Authors**
Hazelnut shell	775	29.6	32.3	Demirba et al 2004
	850	27.5	36.5	
	1025	22.9	44.6	
Spruce	800	30	20	Parthasarathy et al. 2017
Sawdust	800	30	20	
Pinecone	800	40	15	

Grapeseed	800	32	20	
Mallee	350	28	11	Garcia-Perez et al 2008
	390	21	12	
	500	14	23	
Spruce	700	16.5	0.52	Duffio et al 2009
	800	14.2	0.70	
	1000	13.3	0.78	

Table 2-3: Studies about temperature effect on biomass pyrolysis products

Studies, as shown in table 2-3, show that char yield decreased when the temperature was increased. This in effect also means that the gas yield increases gradually with temperature increase, first from the decomposition of the char and then at higher temperatures the tar starts degrading into gases (Dermirba et al. 2004). Figure 2.9a depicts the results of the char yields for hazelnut shell, beechwood, spruce wood and MSW and Figure 2.10 the char yield for wood, straw, green waste and algae. An approximation of the gas yield can be deducted by the difference in Figure 2.9b, while in Figure 2.10, it cannot be calculated by the difference because the liquid yield was not quantified.

Since higher temperatures would lead to higher gas yields, it would be expected to use a high temperature for the pyrolysis step, but since this process is followed by a Catalytic steam reforming

(CSR) stage, then medium temperatures, but higher than 500°C are required for tar to be produced and reformed with steam.

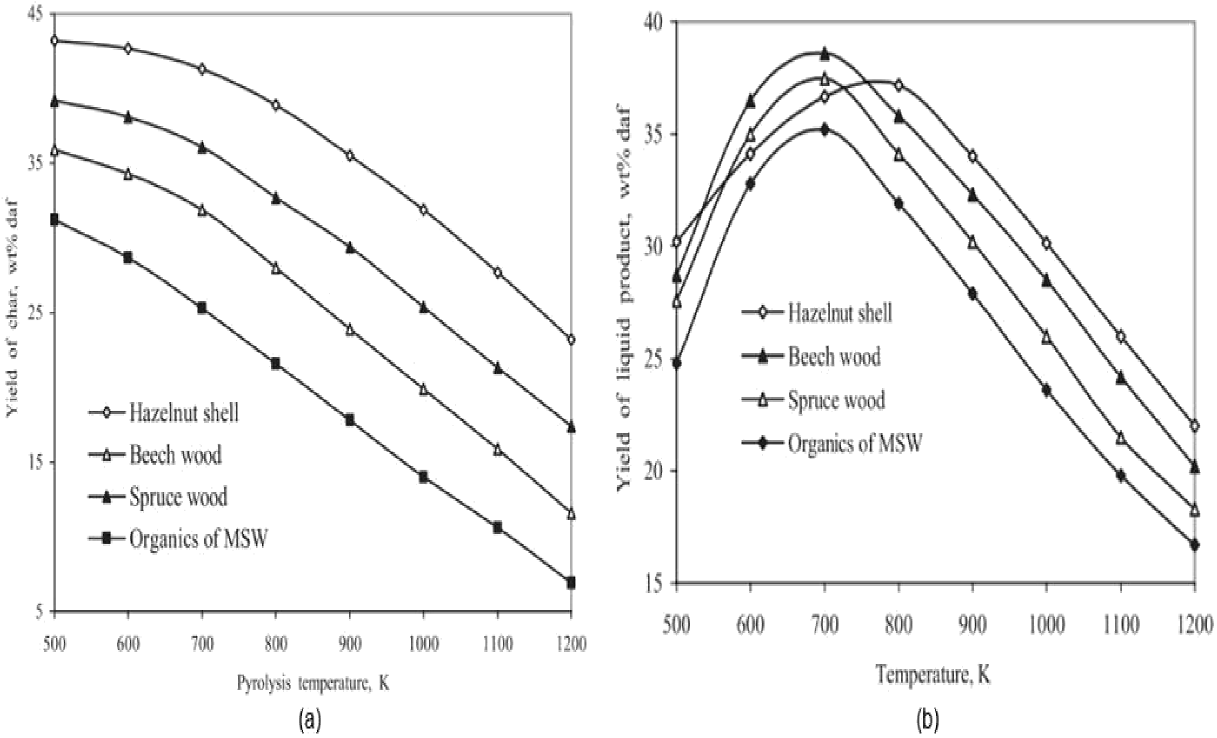

Figure 2-9: Effect of temperature in (a) char yield and (b) liquid yield (Demirbas, 2007).

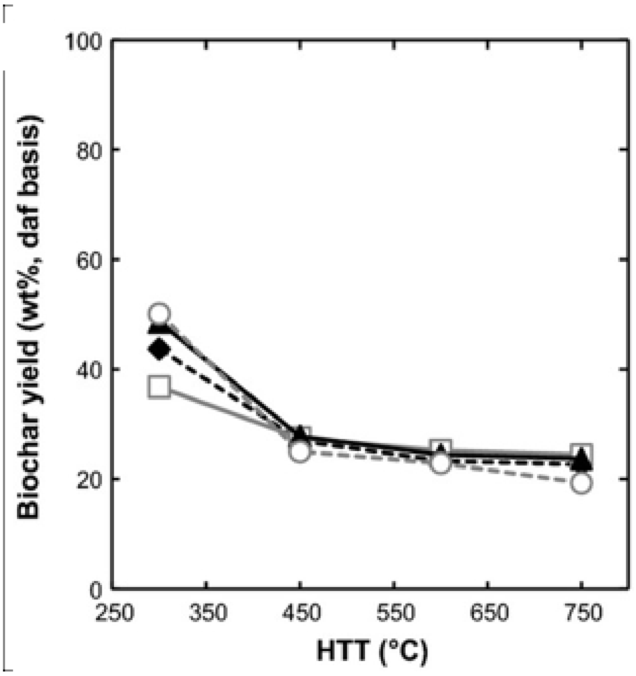

Figure 2-10: Effect of highest treatment temperature in wood with a residence time of 60 min (◆), straw (□), green waste (▲) and algae (○) (Ronsse, et al., 2014)

For this reason, high temperature should be used in the pyrolysis stage of this investigation. With respects to the figures produced, the trends provided do not effectively fit the data being displayed. This suggests that more research should be carried out to analyse the effect of temperature on the gaseous products of pyrolysis.

2.4.1.1.2 Effect of Heating Rate in Biomass Pyrolysis

The heating rate was found to have substantial influence on the product yields of biomass using a slow pyrolysis method. Chen et al. (2014) demonstrated with slow pyrolysis of Moso bamboo at 700°C that, with a low heating rate, the production of char and bio-oil is promoted with the lower yield for gas. In contrary, when the heating rate increases the biochar yield decreases, meaning that more volatiles are released. Also, the bio-oil yield decreases, while the non-condensable gas yield increases as the high heating rates allow the biochar and the bio-oil to release the volatiles and produce more gas. The effect of the heating rate in the product yields can be observed in Figure 2-11.

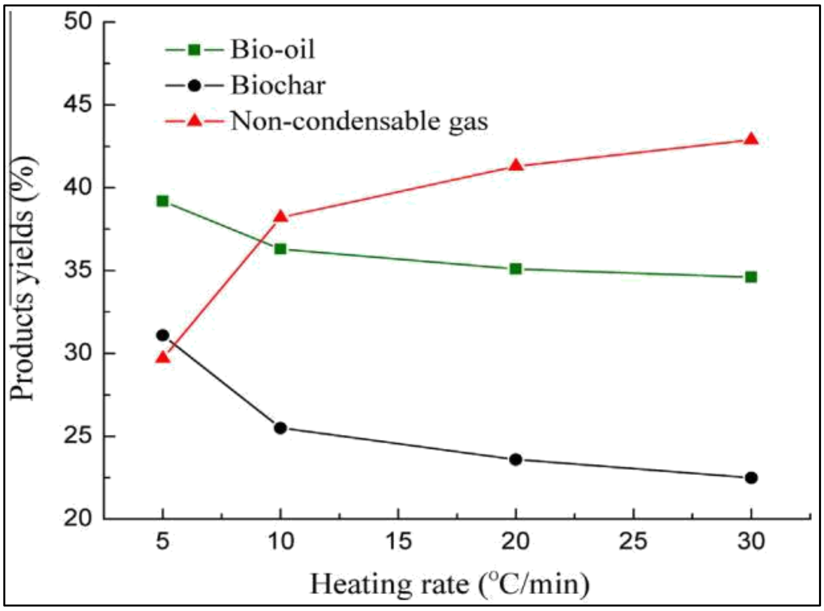

Figure 2-11: Influence of heating rate in product yields from Moso bamboo (Chen et al., 2014)

Then, after analysing the non-condensable gas, they found that there is no significant change in the concentration of hydrogen, but the concentration of CO_2 slightly decreases with increasing heating rate.

Previously, Williams & Besler (1996), had already studied the effect of the heating rate as well but with pine wood, getting similar tendencies: char yield decreased with increasing heating rate while aqueous, oil and gas yield increased, as observed in Figure 2-12.

y

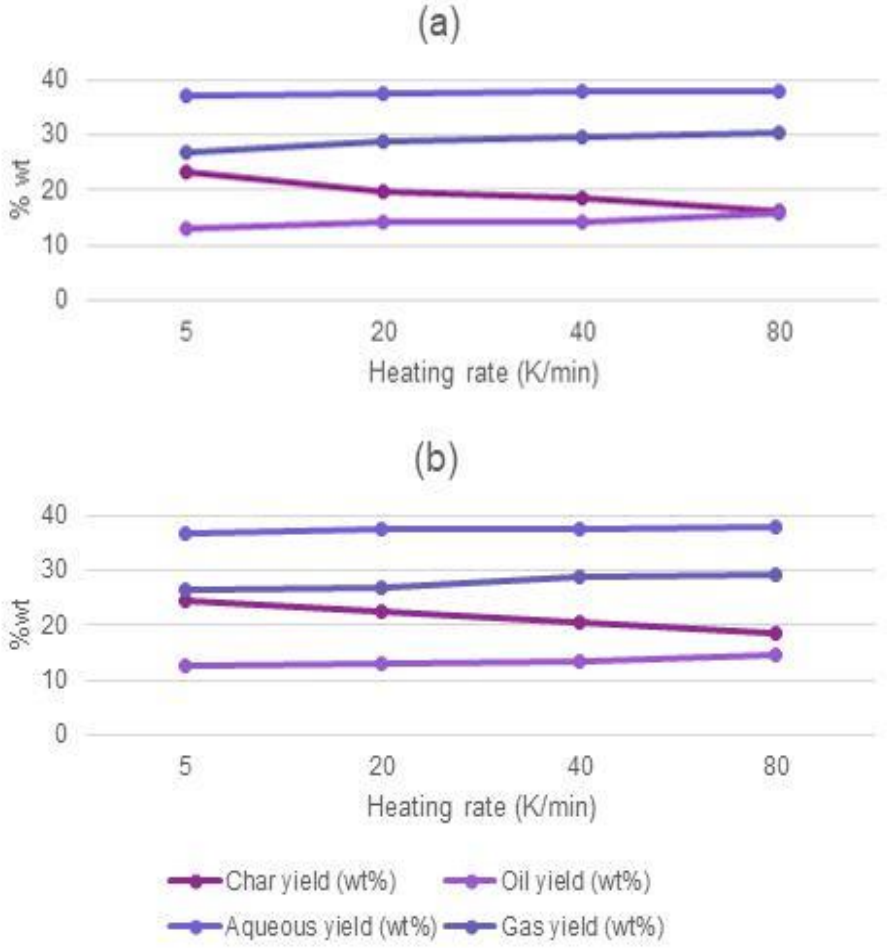

Figure 2-12: Effect of heating rate in char, aqueous, oil and gas yields at temperatures from 300°C to (a)600°C and (b) 720°C. Adapted from Williams & Besler (1996)

Consistent with Chen et al. (2014), William & Besler (1996) found that the H_2 concentration remained somewhat constant regardless of the difference in heating rates; however, the concentration of CO increased significantly while CO_2 decreased. This means that, when the process is driven only by slow pyrolysis, the reforming of hydrocarbons and the WGS reaction are not well defined since the only source of H_2O steam is the one released from the moisture in the biomass.

Considering the above, a high heating rate would be desired to maximise the gas yield and consequently, the hydrogen production from biomass pyrolysis. However, since there are subsequent steps which also must be taken account, an average heating rate could also be used.

In general, the studies by Collard and Blin (2014) and Lopez et al. (2018) both revealed that, the amount of gaseous products being produced as a result of pyrolysis reaches a maximum value around a specific temperature and heating rate. The two studies utilised different sources of biomass; this suggests that there are an optimum temperature and heating rate for biomass feedstocks depending on its source. In order to optimise the hydrogen product from biomass deconstruction, it is therefore necessary to first focus on identifying the most suitable temperature and heating rate of pyrolysis reaction.

2.4.1.2 Effect of Source of Biomass

Similarly, to temperature, the type of biomass used can greatly affect the composition of gases produced from pyrolysis. This is due to the varying amounts of cellulose, hemicellulose and lignin that make up each type of biomass. This has been widely researched and was investigated by Couhert et al. 2009. When conducting their experiments, several types of biomass were used to provide a range of biomass compositions. They included beech wood, spruce and fir mix, rice husk, grass and wood bark.

It should be noted that due to it being difficult to determine the composition of biomass, average compositions were adopted from literature. This could have been a potential source of error in their results. When testing the biomasses, they were all heated to a temperature of 950°C. This is far higher than temperatures commonly used for pyrolysis.

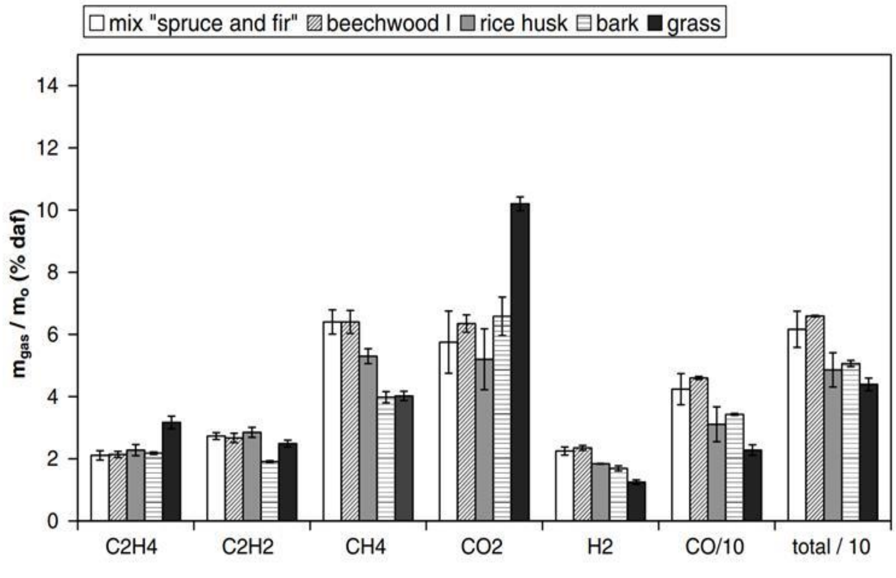

Figure 2-13: Gas composition and yield from various biomasses
Source: Couhert et al. (2008).

The results shown in figure *2-13*, prove that composition greatly affects the gas yields. The grass was shown to produce far more CO_2 than its counterparts, therefore making it an unattractive biomass source for hydrogen production. The mixed spruce and fir and beech wood were shown to give the greatest yield of gas. Additionally, they were shown to produce the highest amount of CH_4 and CO which would be highly beneficial to both steaming reforming and water-gas shift operating units. The ability to manipulate the gases produced during pyrolysis by using a particular biomass source is highly attractive. By reducing the amount of high molecular weight carbon-containing products, the amount of carbon formation on subsequent catalysts could be reduced. This would diminish the risk of deactivation and extend their lives. Furthermore, increasing the amount of carbon monoxide, methane and hydrogen would be beneficial to later stages of the system and the production of hydrogen itself.

2.4.1.3 Effect of Residence Times in Biomass Pyrolysis

A further important parameter is the residence time of the biomass in the reactor, especially at the peak temperature. It has been shown that, the longer the residence time of the volatile phase, the higher the gas yield will be, since the gaseous and liquid products have more time to undergo cracking reaction, and in addition, an increase in hydrogen concentration is obtained (Chen et al., 2003; Solar, et al., 2016), as seen in Figure 2-14.

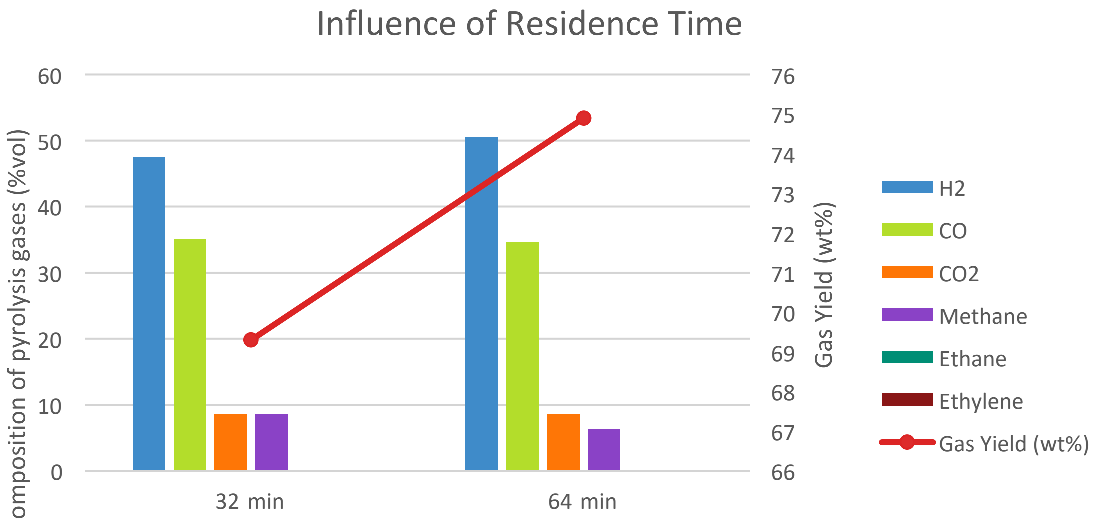

Figure 2-14: Effect of residence time in gas yield and composition for a constant temperature of 1173 K. Source: Solar, et al. (2016)

It can also be seen that there is also a high concentration of carbon monoxide and relatively low concentrations of methane and other hydrocarbon gases, because the tarry components allow for further cracking with longer residence times.

2.4.1.4 Pyrolysis Reactions

In order to understand the process of pyrolysis further, it is essential to review the reactions and stages that occur during the production and release of gaseous components. As explained previously, when the pyrolysis of biomass is carried out, volatile compounds are released as a result of chemical bonds within the material being broken due to the increase in temperature. Figure 2-15 below demonstrates this loss of mass due to the components being released during the pyrolysis of Xylan, which is an example of hemicellulose. In addition to the bonds being broken, rearrangement reactions occur as a direct impact of the process. These reactions are known as primary mechanisms. Collard and Blin (2014) described how these mechanisms could be separated into three main categories based on the nature of the chemical bond being broken. They consist of char formation, depolymerisation and fragmentation.

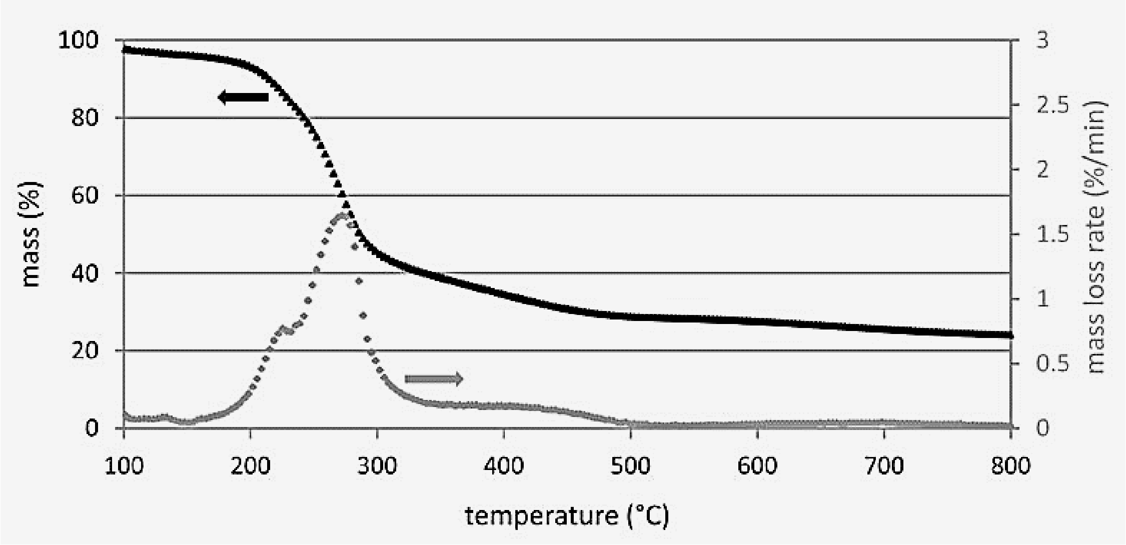

Figure 2-15: The change in mass and mass transfer rate with temperature during the pyrolysis of Xylan. Source: Collard and Blin (2014)

According to Collard and Blin (2014), char formation is described as the conversion of biomass into a solid residue which is favoured by Intra- and intermolecular rearrangement reactions. Depolymerisation is specified as the process whereby bonds joining individual monomer units are broken. This leads to a decrease in the degree of polymerisation until the molecules being produced become volatile. The final primary mechanism mentioned in the paper, fragmentation is defined as the breaking of covalent bonds of the polymer to form incondensable gases and a range of short-chain organic molecules.

Later in the paper, Collard et al. mentioned how secondary mechanisms often occur during pyrolysis due to the volatile components produced as a result of the primary mechanisms being unstable. These secondary mechanisms consist of cracking and recombination reactions. Cracking entails the breaking down of the bonds within the volatile components leading to the production of molecules with a lower molecular weight. This is quite an attractive mechanism as hydrocarbons with a higher molecular weight are much more reactive than those with a lower molecular weight which can lead to the problem of carbon formation on catalysts (Welaya et al., 2012). Since catalysts are critical to later stages in the production of hydrogen, the ability to enhance the amount of cracking occurring during the pyrolysis of biomass would be highly desirable.

There is a consensus between Chen et al. (2003) and Collard (2014) that due to the similarity of fragmentation and cracking, it is hard to determine which route is most prominent in the production of low molecular weight molecules such as H_2 and CH_4. As stated above, the other secondary mechanism is recombination. Contrary to fragmentation, this mechanism sees the volatile components join to form higher molecular weight molecules that may no longer be volatile depending on the reactor conditions. When this occurs, secondary char is produced and can lead to the formation of a deposit on the catalyst of the unit and subsequent units, resulting in their deactivation. This is a mechanism that should be minimised.

2.4.2 Catalytic Steam Reformation Reaction

As mentioned previously in section 2.4.1, pyrolysis is followed by steam reforming in the production of hydrogen from biomass. The steam reformation of gaseous fuel is currently the primary source of hydrogen globally and accounts for 95% of the total hydrogen production in the United States (Wei et al., 2012). During the process, hydrocarbons are reacted with steam to produce hydrogen and carbon monoxide. This reaction has been outlined below for methane. Steam reforming can be carried out using a variety of feedstocks which include methane, ethane, methanol, ethanol, acetone and higher hydrocarbons. Currently, most emphasis is on methane as the feedstock due to its favourable by-product formation (Wei et al., 2012). The reaction (equation 2.2 and 2.3) itself is strongly endothermic; this means that it is often carried out at high temperatures from 750 to 1450 °C (Nquyen et al., 2008).

$$CH_4 + H_2O \rightarrow CO + 3H_2 \qquad 2.2$$

$$C_nH_m + nH_2O \rightleftharpoons nCO + \left(n + \frac{m}{2}\right)H_2 \qquad 2.3$$

There has been considerable research conducted into steam reforming due to the fact that it has been used commercially for more than 40 years (Sehested, 2006). The conditions under which a reaction takes place can dramatically affect its outcome. The steam forming reaction is no different from this and has seen its operating conditions rigorously tested.

Findings have shown that efficient conversion performance of steam reforming reaction is influenced by several factors, out of which temperature and the choice of catalyst play an essential role (Duman & Yanik, 2017; Peng et al.,2017; Lang et al.,2017; Wu et al.,2011).

Notably, the biggest challenge in this process is tar formation which, according to Ni, et al. (2006), can be faced by an optimal gasifier design, the right parameters and the correct catalyst choice.

2.4.2.1 Influence of the choice of catalysts

The general characteristics that the catalysts in the steam reforming process should have to perform optimally and to be viable should have the following characteristics (Sutton et al., 2001):

- Tar removal effectiveness.
- Methane reforming capability
- Syngas ratio maximisation.
- Resistance to deactivation due to carbon fouling and sintering
- Easy regeneration
- Costly effective

Different researchers have studied the effect different catalysts and support in the steam reforming step and some of them have proven to even double gas and hydrogen yields (Dong et al., 2016; Shahbaz et al., 2017). Table 2-4 shows some of the studied catalysts in various research papers and their most relevant outcomes.

Table 2-4: Effect of catalysts in Gas and H2 yields

Authors	**Catalyst(s) tested**	**Gas yield**	**Units**	**H_2 yield (mmolg^{-1})**
Dong et al., 2016	9Ni1FeAl[a]	62.8	%wt.	11.4
	8Ni2FeAl[a]	57.1		10.7
	6Ni4FeAl[a]	58.4		9.2
	5Ni5FeAl[a]	51.3		8.7
	4Ni6FeAl[a]	49.6		8.4
	2Ni8FeAl[a]	50		7.7
	1Ni9FeAl[a]	53.2		8.3
Rapagna et al. 1998	Ni fresh catalyst	~1.88	M^3/kg daf biomass	
Wu et al. 2011	5 wt.% Ni/MCM-41	40.7	%wt	6.2
	10 wt.% Ni/MCM-41	46.7		8.3
	20 wt.% Ni/MCM-41	58.1		13.2
	40 wt.% Ni/MCM-41	62.8		18.2
Peng et al. 2017	20%Ni/Al_2O_2	1.31	M^3/kg	-
	40%Ni/Al_2O_2	1.45		
	20%Ni/CeO_2/Al_2O_2	1.51		
	40%Ni/CeO_2/Al_2O_2	1.66		

[a] The number stand for the Ni/Fe molar ratios

In industry, nickel on oxide supports (aluminium or magnesium) is the catalyst most commonly used (Xu, 2017). This is due primarily to its relatively high activity to cost ratio (Abdalla, 2017) compared to precious metal catalysts like Ru and Rh; they also have high effectiveness (Dong et al., 2016). Emphatically, an ideal catalyst for steam reforming would have high selectivity towards both hydrogen and carbon monoxide, high activity and would also show excellent resistance to poisoning, coking and sintering.

2.4.2.2 Nickel Catalysts

Of all the metals tested to catalyse the steam reforming reaction nickel has mostly attracted most of the research effort due to its low cost and relatively dynamic nature (Dal Santo, 2012). Despite these advantages, nickel-based catalysts are known to have four significant issues. Defined by Sehested (2006), these issues are due to the activity of nickel, Sulphur poisoning, carbon formation on the catalyst while in operation and sintering. With regards to the first issue raised in the paper, despite nickel catalysts having relatively high activity in comparison to other metals, when used in operation they still require high temperatures in order to achieve a significant production rate. This, in turn, can lead to high energy costs for a hydrogen plant. The second issue is Sulphur poisoning which affects many catalysts. Despite industries' greatest efforts to remove sulphur and sulphur-containing compounds from process streams, using processes such as flue-gas desulphurisation, small amounts are often still able to reach steam reforming catalysts. When an interaction occurs between sulphur and nickel catalysts, hydrogen sulphide is formed which blocks the active sites. This leads to the poisoning of the nickel catalyst. Eradicating sulphur impurities is not feasible, and therefore, more work needs to be done to add various promotors to nickel catalysts to reduce their effect.

Similarly, to sulphur poisoning, carbon formation can affect all catalysts and subsequently lead to their deactivation. Sehested (2006) discussed the three main types of carbon formation. The first is pyrolytic carbon which is a result of the catalyst being exposed to high molecular weight hydrocarbons at high temperatures. The second is encapsulation carbon which formed due to the reforming of feeds with a high content of aromatic compounds. The final type of carbon discussed is whisker carbon. This is described as being the most destructive of the carbon formations. The whiskers form due to the reaction of carbon monoxide or hydrocarbons on the catalyst surface to form graphitic carbon. Figure 2-16 below displays electron microscope images of each type of formation. The enlargement of the nickel particle causes the final issue of sintering during operation due to the high temperatures. This, in turn, increases the total surface area of the nickel catalysts which can lead to fracturing and lower activity. Due to the change in the surface area caused by sintering, the process directly affects all other issues discussed. Accordingly, it is critical that its effects are reduced.

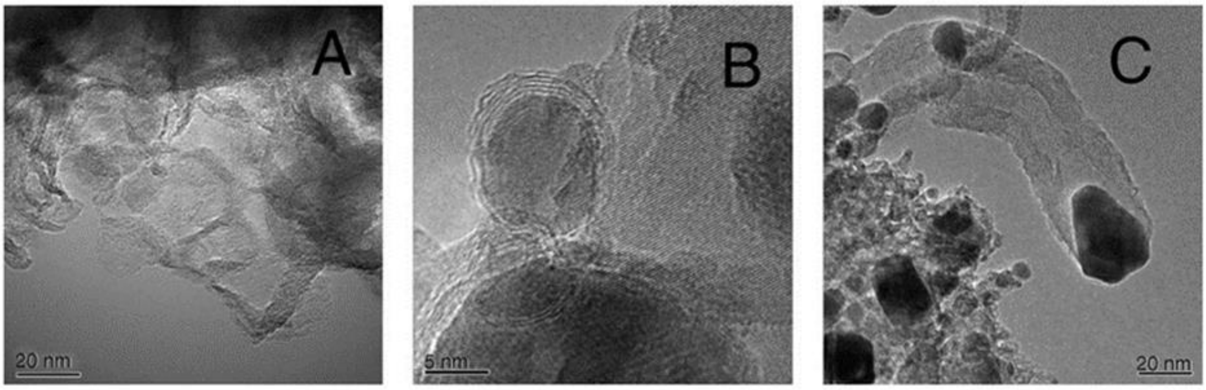

Figure 2-16: Electron microscopy images of a) pyrolytic carbon, b) encapsulating carbon and c) whisker carbon. Source: Sehested. (2006)

Research carried out by Nieva et al. 2014 looked at the possibility of conducting steam reforming at a low temperature using nickel-based catalysts. As explained previously, the issue with conducting the process at low temperatures is caused by its extremely exothermic nature. In the paper, they also identify the problems surrounding nickel use and deduce that by experimenting with a lower temperature, the effects of sintering and carbon formation could be significantly reduced. They also mentioned that the high performance of the system should also be maintained. During their investigation, four catalysts were tested including Ni/SiO_2 (NS), Ni/α-Al_2O_3 (NA), Ni-Mg-Al (NMA) and Ni-Zn-Al (NZA). To produce the catalyst two synthesis techniques were used which included incipient wetness impregnation (NS and NA) and co-precipitation (NMA and NZA). The catalysts were placed in a fixed bed continuous flow reactor operated at atmospheric pressure. Reduced temperatures of 500°C

and 600°C were tested in comparison to the conventional temperatures mentioned previously in the report. When in operation, a stream of steam and methane was injected continuously into the reactor in a ratio of 2 to 1. Hydrogen was used to dilute the stream. Criticism of this research is that the nickel loading was not consistent throughout all the catalysts. The loading ranged from 7 to 8.6 wt. %. An excess amount of nickel could result in a superior performance due to more catalytic material being present. This could lead to a false conclusion being reached on which catalyst performed best.

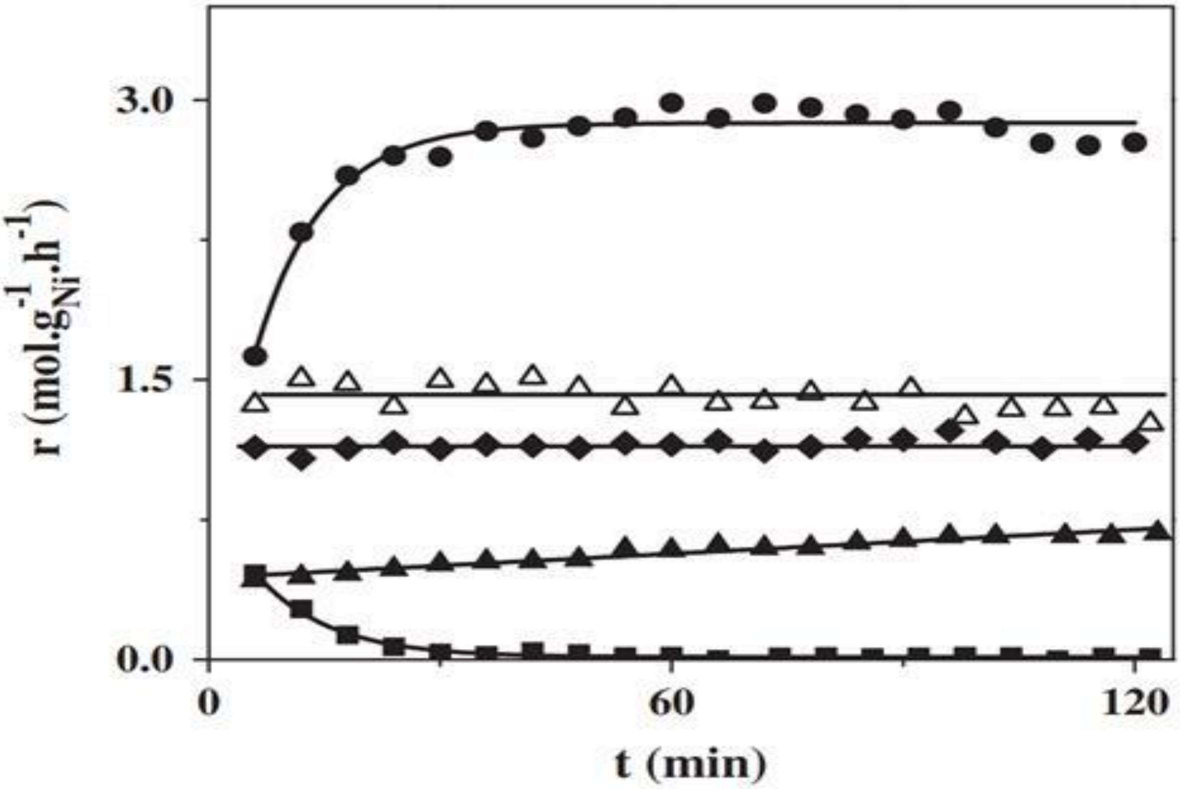

Figure 2-17: Conversion rate of methane in steam reforming at 500°C. NS (□), NA (◊), NMA (Δ) and NMZ (○). Source: Nieva et al. (2013)

From their investigation, Nieva et al. [2013] found that of the nickel catalysts tested, Ni-Zn-Al showed the highest activity with the lowest amount of coking. The variation of methane conversion rate with time for their experiments has been provided above in figure *2-17*. This shows that the activity of the NA and NMA catalysts showed little change during the investigation. Also shown was that the NS catalyst was deactivated within 30 minutes of the experiment beginning. Finally, it shows that the activity of the NZA catalyst increased during the first 20 minutes then maintained a relatively constant value for the remaining duration. Nieva et al. concluded that the trend shown by NZA was due to excess zinc, from its synthesis, covering the active sites of the catalyst. As the experiment continued, the zinc was sublimated, which led to an increase in the active surface area and turned an increase in the conversion rate.

Through catalyst analysis, it was shown that sintering was not occurring within the catalyst under the test conditions. Nieva et al., [2013] also conclude that carbon deposition on the catalysts can be significantly reduced when the active phase consists mainly of fine nickel particles instead of large clusters. The amount of carbon formation is described by the temperature-programmed oxidation curves shown below in figure 2-18 for the two temperatures tested.

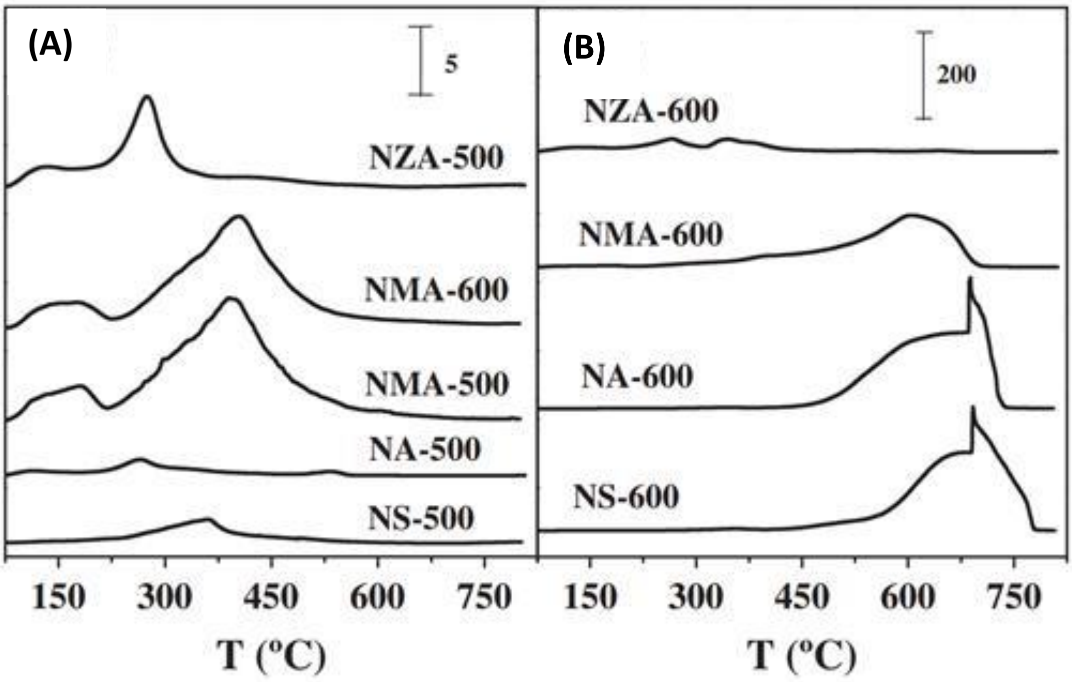

Figure 2-18: TPO profiles of reacted catalysts used in the steam reformation of methane at temperatures of a) 500°C and b) 600°C. Nieva et al. (2013).

The two curves show that a higher amount of carbon formation occurs when high steam reformation temperatures are used. They also show that the NA catalyst, when tested at 600°C, showed the highest amount of carbon formation. However, when tested at the lower temperature, it showed the lowest amount of formation in comparison to the other catalysts tested.

Wu and Williams (2011) carried out exhaustive research on Ni-based catalysts considering their preparation conditions, reaction conditions and the catalyst stability. Their principal findings are summarised in table 2-5 below:

Table 2-5: Key findings of Ni-based catalysts

Catalysts	Preparation Method	Findings
Ni/Al_2O_3	Impregnation	Higher conversion with higher Ni content. Higher H_2 yield with higher temperatures.
Ni-Al	Co-precipitation	Higher catalytic activity than Ni/Al_2O_3 by impregnation Higher H_2 yield with lower calcination temperature. Higher H_2 yield with higher temperatures. No deactivation at catalyst/biomass ratio higher than 0.65
Ni-Al-other metals	Co-precipitation	Addition of magnesium gives lower gas yield. Addition of lanthanum increases carbon conversion With $NiMGAl_4O_8$ higher temperatures increase H_2 yield.
Ni/CeO_2	Co-precipitation	The reaction between carbon and water is promoted. Moderately low tar reduction ability and medium stability
Ni/CeO_2/Al_2O_3	Co-precipitation	The reaction between carbon and water is promoted. Moderately high tar reduction ability and medium stability
Ni/dolomite	Impregnation	Low cost. Medium tar reduction ability and medium stability
Ni/zeolite	Impregnation	Zeolite addition reduces tar content but increases coke deposition in the catalyst. Medium tar reduction ability but low stability.
Ni commercial	Varies	Most Ni content from NiO less than 25%, Al_2O_3 the most abundant support, CaO, K_2O, SiO_2 and MgO added. Higher tar conversion with increasing steam/carbon ratio and temperature.

In the light of these, further research is required in this area of nickel catalysts as the ability to conducted steam reforming at a reduced temperature would not only prolong the life of the catalyst but also reduce the running cost of the system.

Furthermore, another investigation in the use of nickel as a catalyst for steam reformation has shown that the addition of boron as a promotor can significantly decrease the rate of deactivation and also enhance the conversion of methane when alumina is used as the support (Xu et al., 2009). Additionally, many other metals have been tested in combination with nickel alumina catalyst. Both lanthanum and molybdenum were shown to increase conversion and decrease coking in research by Hufschmidt et al. (2010) and Maluf and Assaf (2009), respectively.

Activated Carbon Catalyst

A more unconventional material used for steam reforming is activated carbon (AC). As well as its low cost, AC has a porous structure which provides a vast surface area for reactions to take place, making it an ideal for catalysing reactions (Rodríguez-reinoso, 1998). For this reason, AC is often also used as a support for other catalysts. The major disadvantage to the catalyst is the fact that it cannot be utilised in hydrogenation reactions above 427°C or the presence of oxygen above 227°C (LeValley et al., 2014). This is due to the carbon reacting with both H_2 and O_2 to form CH_4 and CO_2 respectively. Liu et al. (2016) looked at performing low-temperature catalytic steam reforming using AC supported nickel catalysts as a replacement for alumina.

Similarly, to some of the catalysts discussed previously, the wet impregnation method was used to produce the catalysts. Catalysts of 8, 10, 12 and 15 wt.Nickel were produced as well as 10 wt. % nickel on alumina and olivine supports. This was for comparative reasons. The first test aimed at determining the influence that nickel content had on the performance of the catalyst. Their results have been provided below in figure *2-19*.

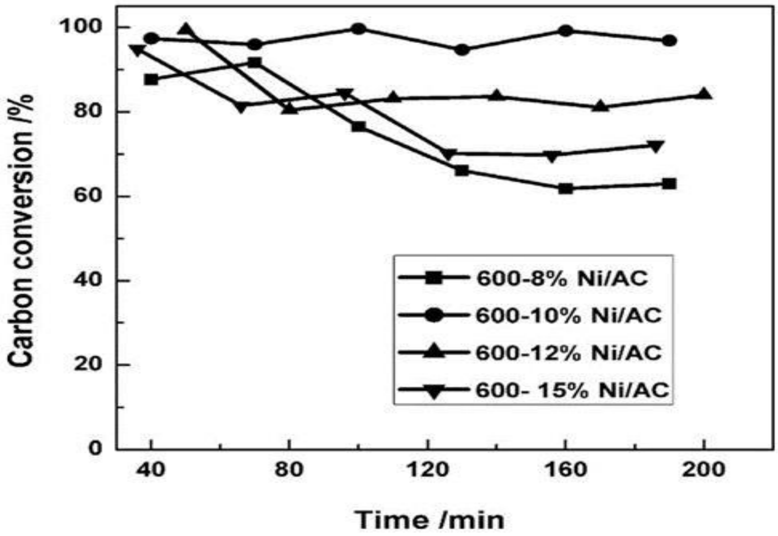

Figure 2-19: Carbon conversion on Ni/AC catalysts of varying composition. Source: Liu et al. (2016)

From figure 2-19, it is evident that carbon conversions of all catalysts were very high for the first hour of the experiment. The conversion then gradually decreased over time with the exception of the 10 wt. % nickel catalyst. Liu et al. concluded that the inferior performance of the 8 wt. % catalyst was due to a ‘lack of enough nickel-active components’ and carbon deposition, which led to the deactivation of the catalyst. In terms of both the 12 and 15 wt. % catalysts, Liu et al. attributed their lesser performance to the agglomeration of active particles within the catalyst which led to a decrease in the active surface area of the catalysts. This conclusion was supported by transmission electron microscopy (TEM) images taken of the reacted catalysts. Additional research could look at refining the nickel content further to find the optimum composition of the catalyst. Their next test looked at comparing the performance of the AC supported catalyst with other nickel catalysts. Their results are shown set out below in figure *2-20.*

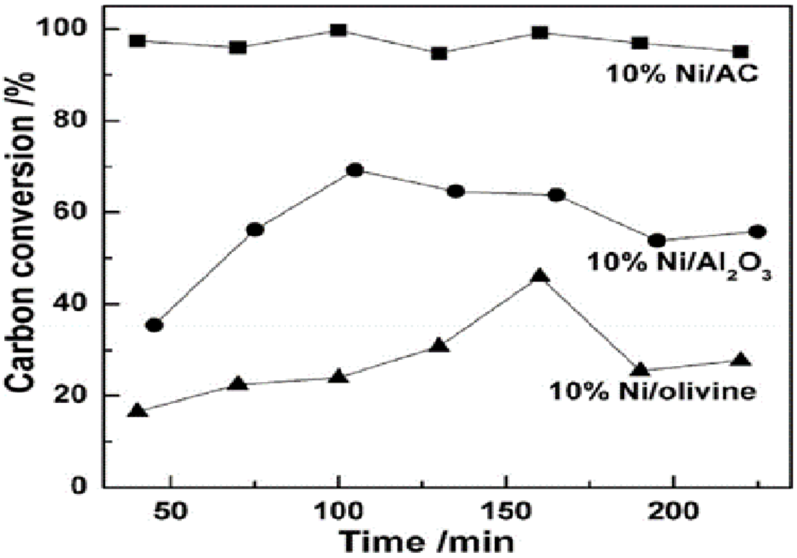

Figure 2-20: Carbon conversion during steam reforming using Ni-based catalysts on various supports. Source: Liu et al. (2016).

As can be seen in figure 2-20, showing their results for the nickel-based catalysts at 600°C, it is clear that the AC-supported catalyst had the best stability and activity during the experiment. Liu et al. discussed that the high performance of the AC catalyst is due to its larger specific surface area and more microporous structure. They also discussed whether the poor performance of the two other catalysts could be due to the fact that they were not completely reduced during their synthesis. This problem was also reported by Zhang et al. (2007). In further research, the performance of the AC catalyst should be compared to the other catalysts discussed when they are tested at the more conventional steam forming temperature. This is where the catalysts are shown to have their best performance. Using the catalysts at reduced temperatures gives the AC supported catalyst an advantage.

2.4.2.4. CaO as an absorber/catalyst in the Catalytic Steam Reforming (CSR)

Carbon dioxide removal in the whole process would lead to higher H_2 content, for this, various absorbents have been studied, Calcium oxide-based catalyst are an optimal choice due to their high-temperature resistance and their carbon dioxide capture capacity (Lee et al., 2015). The carbonation reaction is given in equation 2.4 as:

$$\mathrm{CaO}(s) + CO_2(g) \rightarrow CaCO_3(s) \tag{2.4}$$

Mahishi & Goswami (2007) added CaO to the biomass gasification process for hydrogen production and their results showed that there were higher hydrogen volume percentage and lower carbon dioxide. However, in time, this composition would reach an equilibrium, as shown in Figure 2-21.

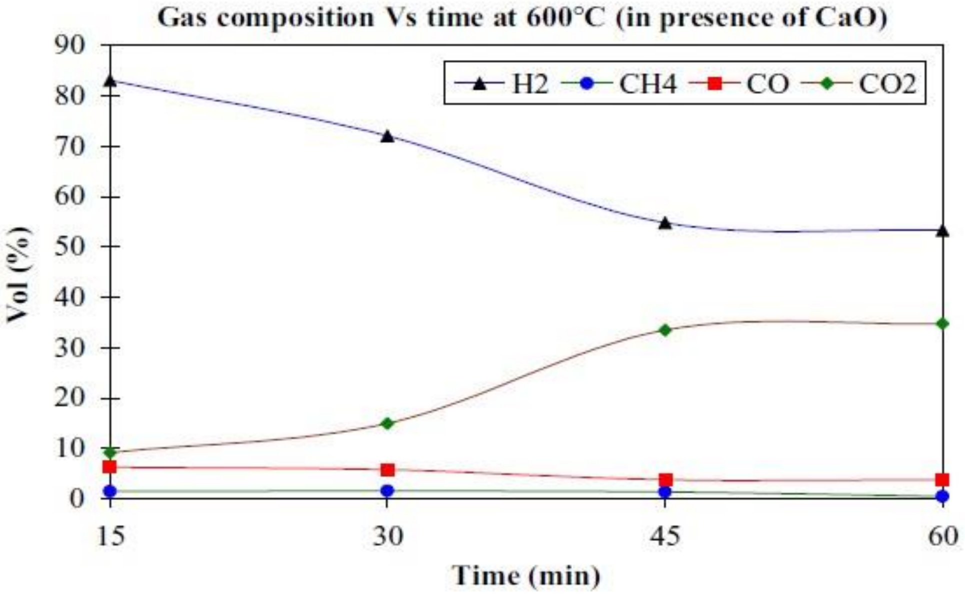

Figure 2-21: Effect of CaO addition to biomass gasification on gas composition (Mahishi & Goswami, 2007)

Zhou et al. (2014) studied the effect of calcium oxide in the steam gasification of municipal solid waste, which can be assumed to have similar behaviour as biomass CSR. Their studies proved that the H_2 increased while the CO_2 decreased when the CaO was added to the process, suggesting that CO_2 absorption happens in the catalyst to some extent. This behaviour can be seen in Figure 2-22.

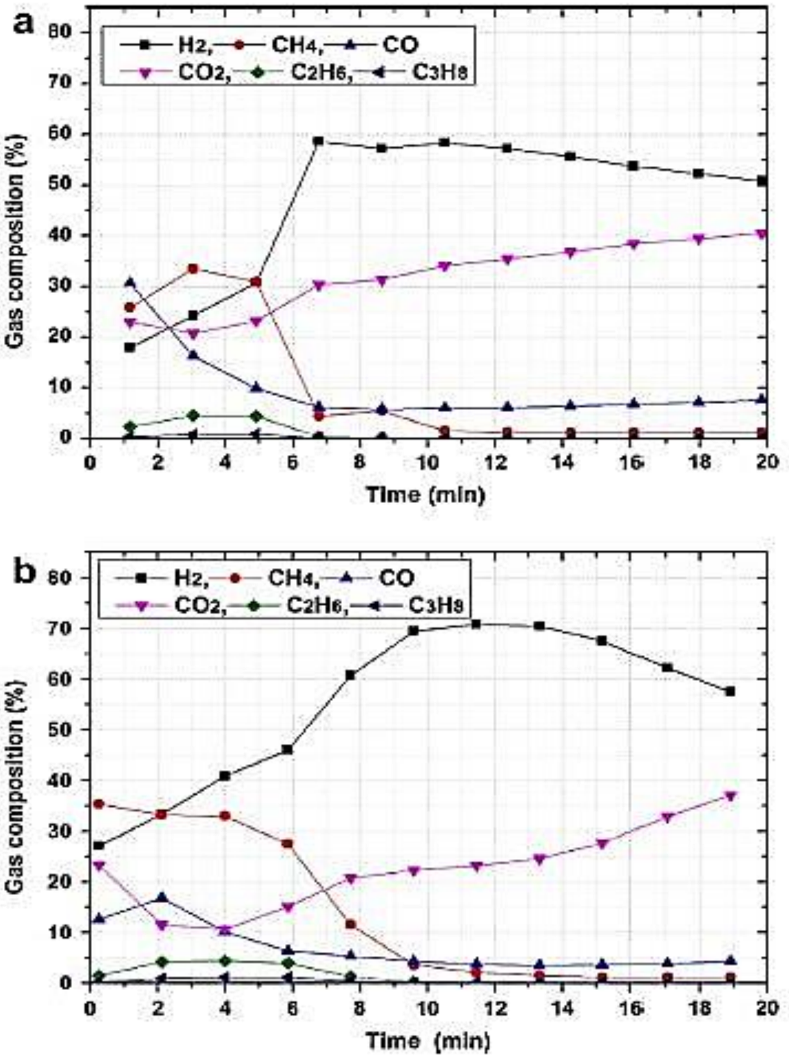

Figure 2-22: Composition of syngas without and with CaO addition (Zhou et al., 2014)

Likewise, Xu et al. (2005) studied the effect of CaO in dried coffee grounds as biomass in a fluidised bed gasifier, and they got higher hydrogen concentration when they added CaO as an absorber in comparison to no addition, as can be seen in Figure 2-23. This means that the CO_2 sorbent also behaves as a catalyst for the gasification process and consequently, in the WGS reaction (Hanaoka et al., 2005).

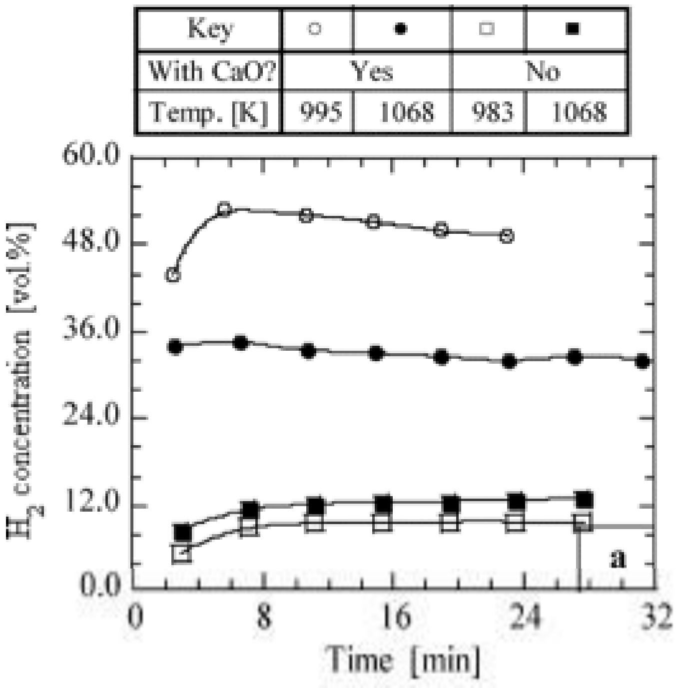

Figure 2-23: H_2 molar concentrations with time with and without CaO addition (995 and 1068K) (Xu et al., 2005)

In this case, the CaO sorbent would be introduced for a Water-gas shift (WGS) reaction process, but it is still important to know its influence in Catalytic steam reforming (CSR), as they are two processes that usually occur at the same time.

2.4.2.3 Effect of Temperature in Catalytic steam reforming (CSR)

Being one of the parameters that most affect the different stages of the process, the temperature profile is critical. According to Kumar, et al. (2009), hydrogen production increases and tar is destroyed and reformed with high temperatures too, and this is due to the endothermic characteristic of the reaction (equation 2.3).

The effect of temperature in biomass steam gasification was also investigated by Luo et al. (2009), finding similar behaviours: the hydrogen yield increased along with the temperature. However, this study was made in a single stage FBR, so all the different processes considered for this work takes place in one step. The findings are depicted in Figure 2-24.

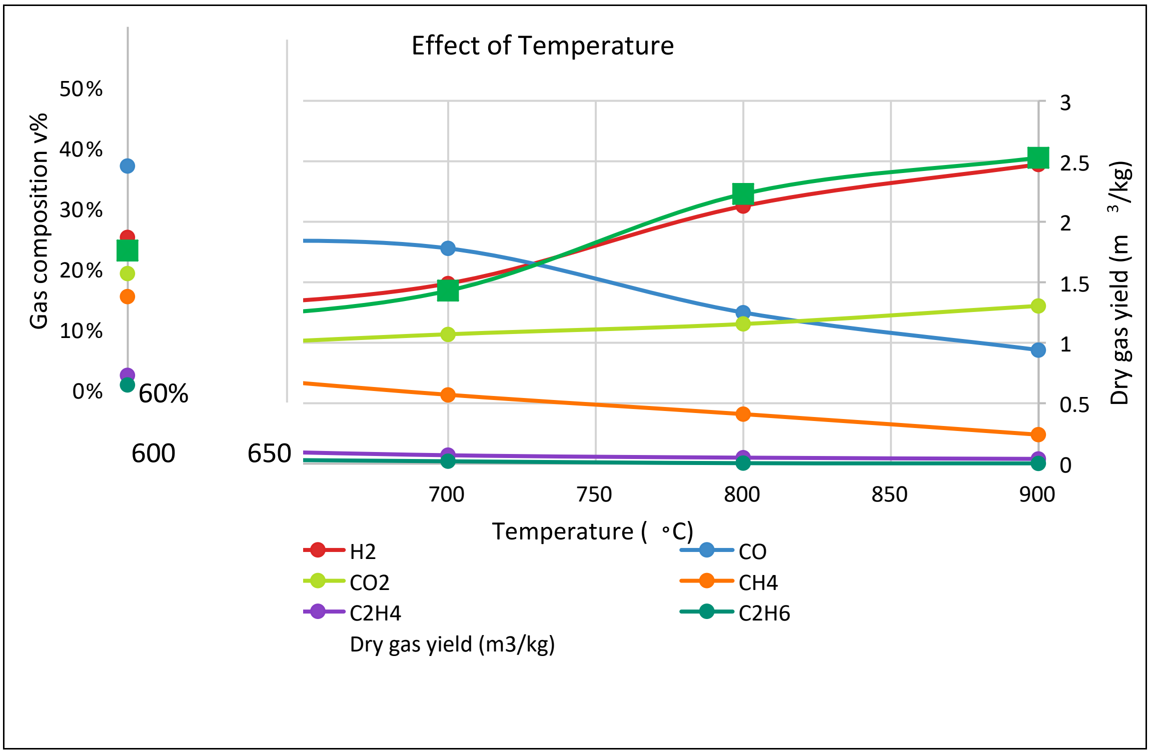

Figure 2-24: Effect of temperature in gas composition and gas yield in catalytic steam gasification. Adapted from the data in Luo et al. (2009)

Also, CO_2 is produced with higher temperatures while CO is decreased, meaning that, in this case, the WGS reaction is promoted at high temperatures. Gas yield is also maximised when high temperatures are used giving more syngas quantity for each kg of biomass, which is desired, yet it is desirable that this product gas contains a high H2 concentration.

Ning et al. (2018) obtained different results with the CSR of corncob char, using a 6 wt.% KOH solution and a steam flow rate of 0.4 g/min. The results showed a negative trend in hydrogen concentration when temperature was increased, obtaining 63.8% (vol.) at 800°C but 58.3% (vol.) at 950°C, however, the hydrogen yield increased drastically from 800°C to 850°C, and then there was a small increase when temperature increased to 900°C, being 124.6 g/kg char at first and 197.8g/kg char at 900°C, and at 950°C it remained constant. The decrease of hydrogen concentration is due to the decrease of reactivity of the WGS reaction, while the increase of hydrogen yield is because of the increase of gas yield due to the high temperatures. The reactivity decrease can also be seen in the increase of CO and decrease of CO2 concentrations, as seen in Figure 2-25.

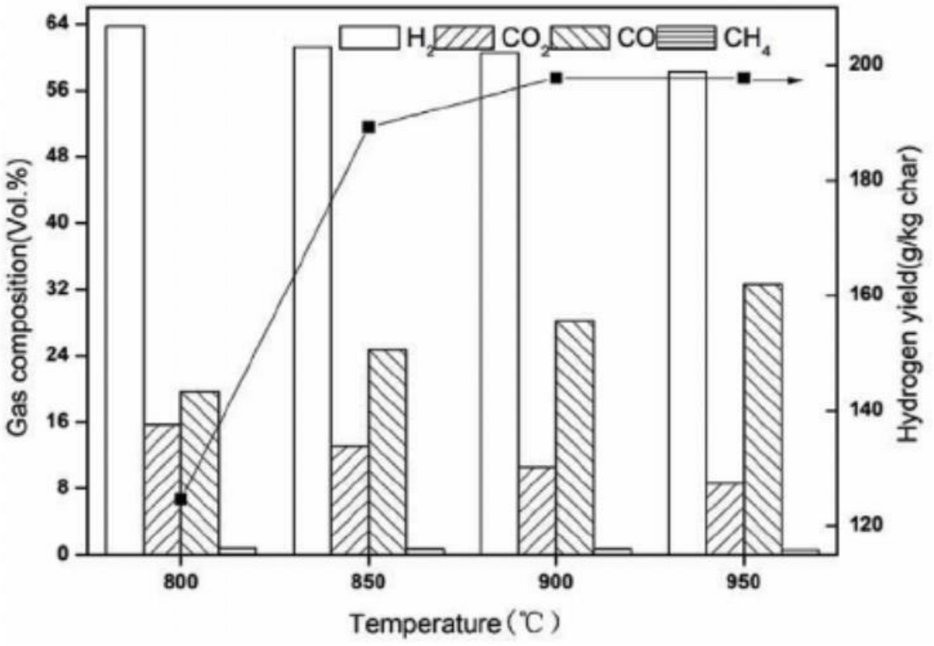

Figure 2-25: Influence of temperature in gas composition and hydrogen yield from corncob char CSR.

More so, Hu et al. (2003) investigated the effect that temperature and the ratio of carbon and steam has on SR performance using a nickel zirconium catalyst. During their investigation, the steam reforming was carried out using a number of temperatures ranging from 650°C to 850°C and a variety of steam to carbon ratios. From their results which are displayed in figures 2-26 and 2-27, it is demonstrated that both the conversion of methane and the selectivity of carbon monoxide both increase with temperature. In both cases, a maximum value was obtained at approximately 800°C. This represented a conversion of 100% methane and a carbon monoxide selectivity of 84%. Above this temperature, both values were shown to remain constant with the increase in temperature. This is a result that has been shown in previous papers reviewed. Hu et al. discuss that the increase in conversion is due to the exothermic nature of the reaction itself and the fact that the reaction rate increases with temperature.

Similarly, to temperature, it can be seen from figure 2-27 that increasing the ratio of steam to methane results in an increase in overall conversion of methane. The maximum value for the conversion of 100% was reached at a ratio of 3.5:1. The conversion remained constant above this ratio. Their results, therefore, suggest that it is unnecessary to use high steam to carbon ratio as it is not advantageous to the reaction and would result in increased operating cost due to an increase in raw materials. This increase in catalytic activity is to be expected due to the increase in the concentration of steam, increasing the number of reactant particles. This results in there being a greater probability of a collision occurring between reactants which in turns increases the rate of reaction. This, however, does not explain why the conversion of methane does not increase above a ratio of 3.5:1. Although not discussed by Hu et al. this could be due to the reactor system becoming oversaturated with steam.

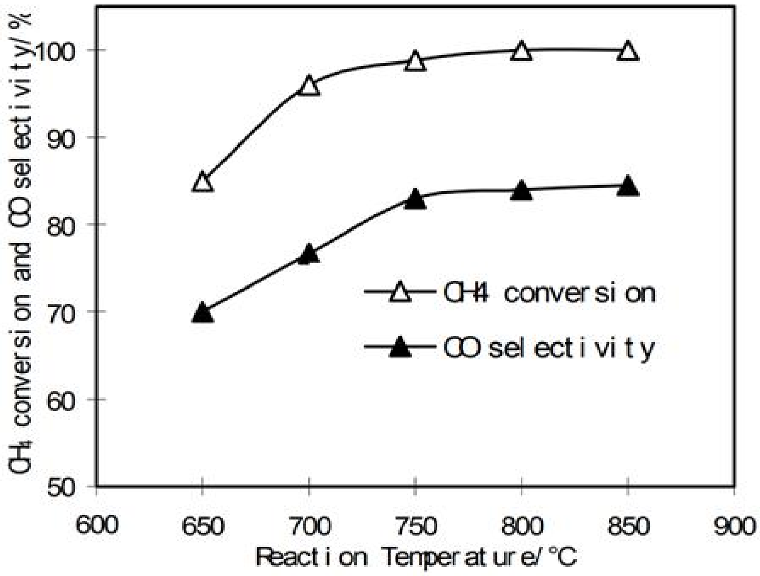

Figure 2-26: Effect of temperature on the performance of a Ni/ZrO2 catalyst in terms of CH4 conversion and CO selectivity. Source: Hu et al. (2003).

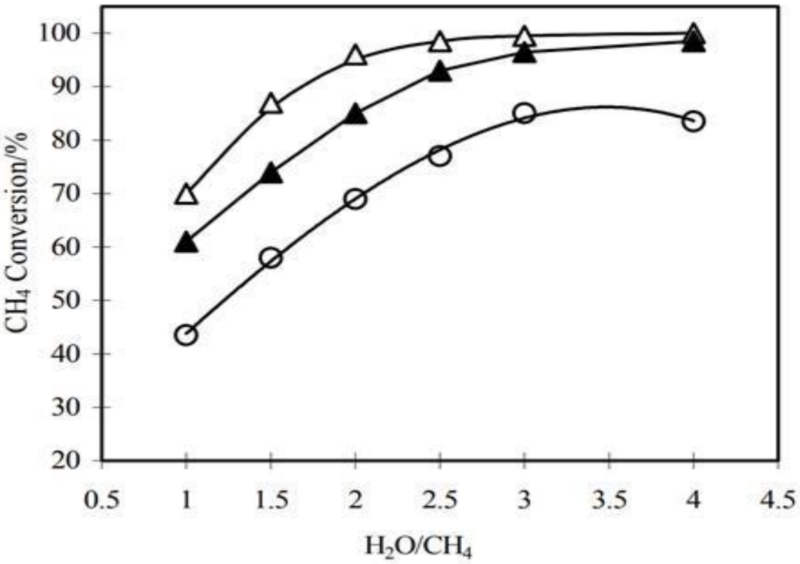

Figure 2-27: Effect that varying the steam to methane ratio has on the conversion of CH_4 at temperatures of 700°C (Δ), 650°C (Δ) and 600°C (○). Source: Hu et al. (2003).

A further paper which also examined the conditions at which SR takes place was published by Jalama (2012). As well as the temperature and the steam to methane ratio, Jalama also investigated the effect that the operating pressure has on performance. While conducting their simulation, pressures ranging from 1 to 20 bar, temperatures of 300°C to 1000°C and steam to water ratios of 3:1, 6:1 and 9:1 were all tested. Their research found that in terms of pressure, no significant effect on conversion was shown at high temperatures when the pressure was adjusted. For this reason, it was concluded in the paper that at the high temperatures used commercially, it is unnecessary to conduct SR at high pressure. In doing so, the overall cost of the plant would be significantly increased due to the increased reinforcement required for the reactor. Similar to the study conducted by Hu at al., the results show that the conversion of methane increases with both temperature and the steam to methane ratio until a maximum value is obtained. It is also demonstrated in the paper that conducting SR at low temperatures and pressure can significantly increase carbon formation on the catalyst. This is in disagreement with the results produced by Nieva et al. The two papers discussed above show that it is advantageous to carry out steam reforming at a high temperature and with high steam to methane ratio in order to obtain the highest possible production rate of hydrogen. Also indicated by both papers is that when increasing the two parameters, a maximum value is obtained for the conversion of methane. Consequently, it is unnecessary to conduct SR at temperatures or ratios above these values as it will only result in an excess running cost for the hydrogen plant.

2.4.2.4 Effect of Residence Times in Catalytic steam reforming of methane

The final product distribution from steam reforming of methane is greatly influenced by the residence time. Several studies have shown that there is a high possibility of achieving significant methane conversion and syngas (CO and H_2) selectivity at low residence times (Hickman et al., 1993; Foulds and Lapzewicz, 1994; Basile et al., 2001). Contrary to this, Bridgwater (2006) found that, whilst low residence time and temperature favour charcoal production, high product gas yield is favoured by longer residence times and higher temperatures. However, Bridgwater (2006) investigation focused on pyrolysis products unlike the Basile et al. (2001) that focused on steam reforming of methane.

In agreement with Bridgwater (2006), Antal (1981) studied the influence of gas-phase residence times in gas production in biomass gasification and found out that the H_2 yield increases with residence times. Also found that the production of H_2, CO_2, and CO reached a maximum with longer residence times. Figure 2-28 shows the experimental results of gas production with varying residence times.

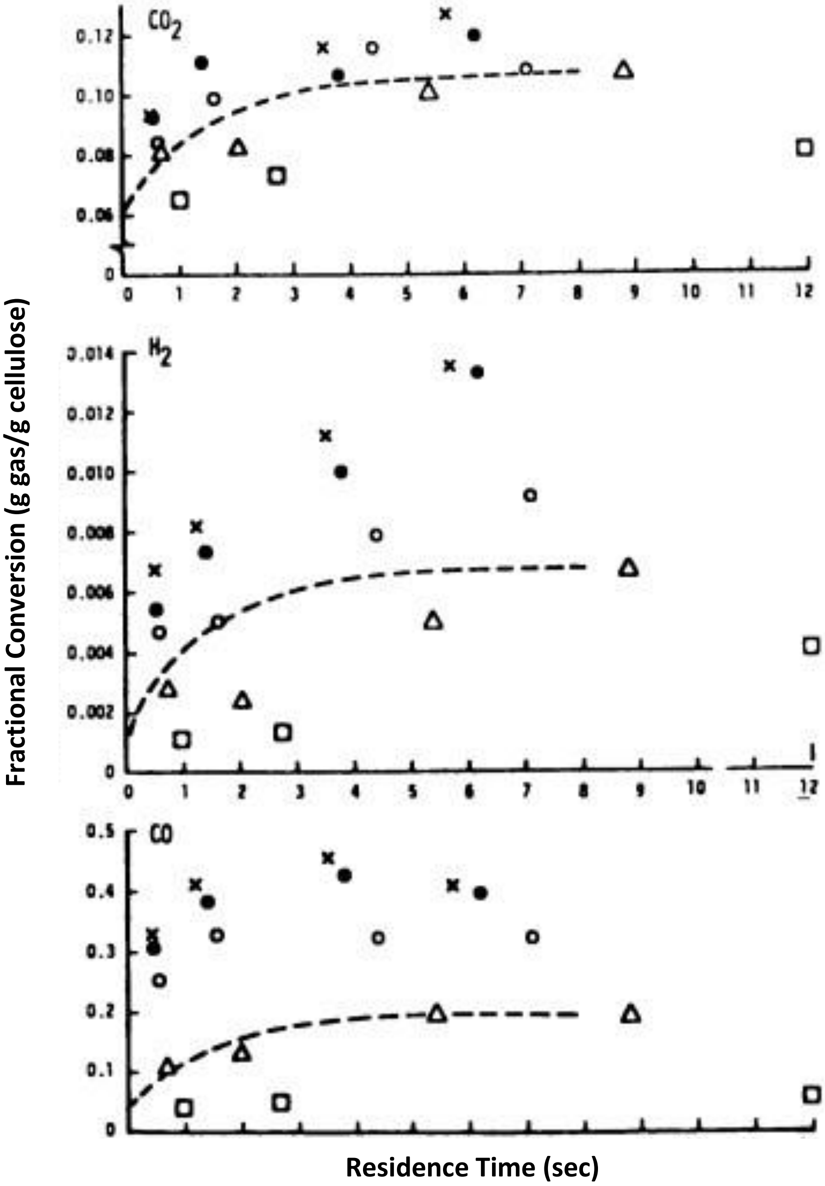

Figure 2-28: Gas production vs residence time at different temperatures (Michael J. Antal, 1981)

Peng et al. (2017) investigated the effect of residence time, using different catalysts, on tar yield and their study concluded that lower tar quantities were produced at higher residence times (Figure 2-29). When catalysts were added, even lower tar yields were achieved.

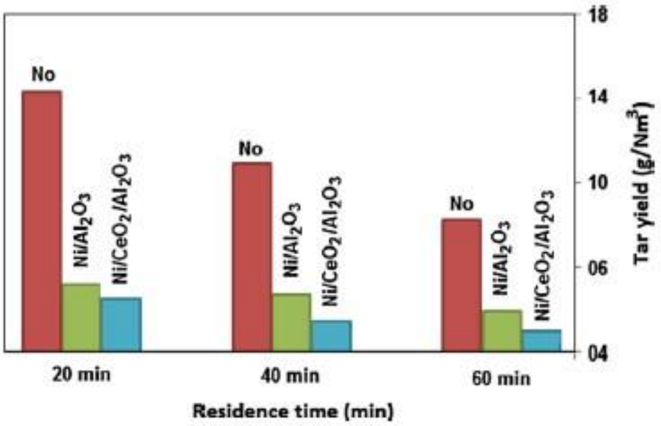

Figure 2-29: Residence time of various catalysts - influence on tar yield (Peng et al., 2017)

Basile et al. (2001) in their investigation found out that the influence of residence time was highly pronounced in methane reforming as very high methane conversions and selectivities towards syngas were observed with decreasing residence than when different catalysts were used under the same residence time. This is explained by the fact that lowering the residence time of methane conversion in a reforming reactor broadens the initial hot zone and at the same time raises the outlet temperature; this consequentially enhances methane conversion and syngas selectivity. On the opposite at elevated residence times, the outlet temperature plummets resulting in a negligible influence on the conversion of methane.

This might not apply to all steam reforming systems, especially when multiple reactors are linked together with simultaneous discrete reaction mechanisms. Since this work aims to maximise H_2 production using three-stage reactors, therefore the effect of residence times at each reactor will be challenging to monitor or control since their operations are not mutually exclusive, the effect of residence times will therefore not be considered.

2.4.2.5 Summary of Steam Reforming Catalysts

One key challenge facing steam reforming of methane is carbon formation. The three distinct forms of carbon deposits on catalysts are whiskers, encapsulating deposits ("polymers"), and pyrolytic carbon (Cortright et al., 2010). Since carbon deposition is linked to the kinetics, therefore the selectivity of the catalyst is an essential factor. Nickel-based catalysts are commonly used in catalytic steam reforming of methane to adsorb hydrocarbons on its metal sites which after that dehydrogenate and crack them. The outcome of this is low molecular weight hydrocarbons (CxHy) adsorbed fragments which can undergo further polymerisation reaction to form coke. One advantage of the Ni-based catalysts is that they supply sufficient adsorbed H_2O-derived species which are predominantly radicals (OH and H), to circumvent the coke formation reaction. This effectively plays a dominant role in the production of hydrogen (Cernik et al. 2002).

In the future, it hoped that through advancements in the catalyst composition, preparation techniques and reaction conditions, the amount of hydrogen produced via steam reforming could be significantly increased. Also, it is hoped that the catalysts can be synthesised to be highly selective towards carbon dioxide instead of carbon monoxide as this would decrease the need for two water-gas shift reactors which would dramatically reduce operating costs. Other future advances would include the use of microchannel and membrane reactors instead of the conventional fixed bed reactor which has been shown to contain areas of high and low temperature which can result in sintering and low conversion, respectively (Amphlett, 1998). Murphy et al. (2013) also showed that fixed bed reactors have greater start-up times. Finally, it also hoped that catalysts with activity in both the steam reforming and water-gas shift reactions could be combined and used at intermediate operating conditions which would significantly reduce processing costs.

2.4.3. Water-Gas Shift reaction (WGS)

Water-gas shift (WGS) reaction is employed for removing carbon monoxide, the by-product of steam reformation, and also for increasing hydrogen production from biomass deconstruction for industry purposes rather than fuel applications. The record shows that it was first studied in the year 1888 (Smith et al., 2010).

The WGS reaction's aims at reacting the CO produced in the previous pyrolysis and steam reforming stages with steam to increase the production of hydrogen and produce CO_2. WGS reaction is the equation 2.5 by Meshkani & Mehran, (2015):

$$CO + H_2O \leftrightarrows CO_2 + H_2 \qquad 2.5$$

Therefore, the global reaction for the whole process, by joining reaction in equation 2.3 and 2.5 would be equation 2.6:

$$CnHm + 2nH_2O \leftrightarrows nCO_2 + (n + m - 2)\ H_2 \qquad 2.6$$

Some applications such as fuel cells do not allow the mixtures of H_2 with CO because the latter poisons the catalysts, leading to the deactivation of electrodes. Hence the importance of the WGS reaction as a solution to remove all the undesired CO (Pal et al., 2018).

Dong et al. (2016), Wu, et al. (2011) and Duman & Yanik (2017) have previously studied hydrogen production in a two-stage fixed reactor system in which both the steam reforming and the WGS reactions take place in the same stage. This work, unlike the previous ones, tries to separate both processes by adding a third stage and explore them independently and selecting individual parameters for each one.

Lang et al. (2017) and Ma, et al. (2017) worked with two steps for WGS reaction called high-temperature shift (HTS) and low-temperature shift (LTS), which could also be explored in the three-stage fixed bed reactor.

The water-gas shift reaction is an integral part of the hydrogen production process. The reaction itself is a moderately reversible reaction which sees carbon monoxide reacted with steam to produce hydrogen and carbon dioxide. Due to the forward reaction being thermodynamically favoured at lower temperatures and kinetically favoured at higher temperatures, a compromise is often required to achieve both high conversion and production. Due to these constraints, in the industry, the reaction is often split up into two separate reactors. These are termed the high-temperature shift reactor (HTSR) and the low-temperature shift reactor (LTSR). HTSR is often carried out at a temperature between 310°C and 450°C. In comparison, LTSR is carried out at 210°C to 240°C (Zhu et al., 2015).

2.4.3.1 Effect of Catalysts selection on Water Gas Shift Reaction

Like the steam reforming step, the catalyst selection is crucial for promoting the WGS reaction and increasing the H_2 production too. Table 2-6 contains some of the catalysts studied in various research papers, specifically applied in the WGS reaction.

The WGS reaction catalysts are classified, according to Pal et al. (2018), in High-Temperature shift (HTS) catalysts, Low-Temperature shift (LTS) catalysts, Cerium based catalysts, Ceria and noble metal-based catalysts and Nanostructured catalysts. The high-temperature shift catalysts are the most studied of them all, but these typically include chromium, which is highly polluting (Pal et al., 2018).

Table 2-6 Catalysts covered in different research papers for WGS reaction

Authors	Catalyst(s)
Ma, et al. (2017)	ZnO supported Ruthenium catalysts
Kahn & Smirniotis (2008)	F_2O_3 doped with transition/non-transition/inner-transition metal ions (Ce, Ni, Cu, Zn, Mn, Cr and Co)
Lang et al. (2017)	Iron/ceria/foam catalysts
Meshkani & Rezaei (2015)	Promoted Fe_2O_3-Al_2O_3-CuO Chromium-Free Catalysts

Mostly, promoted Fe catalysts have been explored for the promotion of WGS reaction to enhance H_2 production. It was investigated that Ni addition to Fe catalysts promoted the WGS reaction (Lee et al., 2011) and that Ni-Fe-Al oxide catalysts reduced methanation and enhanced WGS reaction activity (Watanabe et al., 2009).

Regarding catalysts different from those which include Fe, Si et al. (2012) studied Cu promoted with CeO_2 catalysts for fossil fuels, which could also be studied in biomass samples. They found out that the highest CO conversion to hydrogen and carbon dioxide is achieved with higher Cu content and at high temperatures, as seen in Figure 2-30.

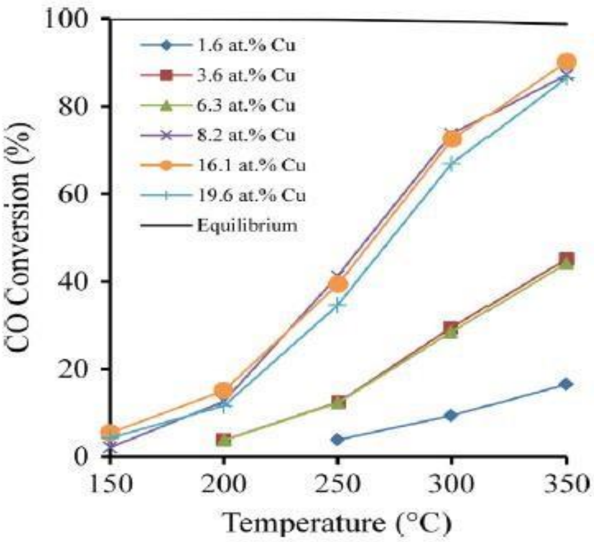

Figure 2-30: CO Conversion for different Cu/CeO_2 catalysts (Si et al., 2012)

Typically, the effect of the catalyst in the WGS reaction can be related to the conversion of CO to CO_2, according the following equation 2.7 (Gradisher et al., 2015):

$$X_{CO} = \frac{yCO, - yCO,}{yCO,in} \times 100\% \qquad 2.7$$

In the three-stage reactor a different approach is needed to know the effect of catalysts in the WGS reaction which could be by comparing H_2, CO_2 and CO concentrations in the produced gas, knowing the estimate carbon content in the feedstock.

2.4.3.1.1 Iron Catalysts

For many years iron-based catalysts have been known to be active in water gas shift reactions. During the intermediate reaction, iron contained within the catalysts is reduced from Fe2O3 to Fe3O4. Iron/chromium catalysts are predominantly used in industry as the catalyst for the reaction. The use of chromium is due mainly to reducing sintering. Despite this, deactivation still limits the catalyst to a lifespan of approximately 2-4 years. This section will look to review current research into the catalyst used as well as the effects that reaction conditions have on the reaction's performance. Due to the toxic nature of chromium and the high disposal costs that come with it, some of the earliest research carried out into iron-based catalysts has been dedicated to replacing the metal while maintaining a high conversion and stability.

Costa et al. (2002) suggest that chromium could be entirely replaced with the introduction of thorium to the iron catalyst as the support. The paper also investigated the effect that adding both thorium and copper to the iron catalyst has on the performance. In order to test the effects of thorium, separate samples of iron oxide (M), thorium oxide (T), copper oxide (C) and a commercial catalyst were also tested. All catalysts were produced by sol-gel synthesis. During their experiments, a process gas stream, of composition 10% carbon monoxide, 10% carbon dioxide, 60% hydrogen and 20% nitrogen, was passed over the catalysts to represent gases produced by a stream reforming unit. This, therefore, means that Costa et al. have assumed that all hydrocarbons would have been reformed before entering the water-gas shift reactor. This gives a poor representation of pure process gases and will minimise the opportunity for coking on the catalysts. Steam was also injected into the system at two separate ratios to the process gas. The first was used to represent an industrial plant and the second to minimise the steam consumption. All experiments were carried out at a temperature of 370°C which represents that of a high-temperature steam reforming (HTSR).

Additionally, Costa et al. (2002) concluded that the thorium doped iron catalyst was more selective than the conventional catalyst. This was shown by their experimental results for activity, activity per area and selectivity which are provided below in table 2-7. This result, however, was bettered by the iron catalyst doped with both copper and thorium. It should be noted that analysis of the reacted catalysts demonstrated that thorium could damage the active sites of the catalyst. From this paper, it can be concluded that the use of thorium has several advantages over chromium including being non-toxic, greater performance and having the ability to be prepared in the active phase. For these reasons and the negative impact of its addition, further research should be carried out to find the optimum amount of thorium.

Table 2-7: The catalytic activity, activity per area and the selectivity of the WGS reaction for pure iron oxide (M), copper doped iron oxide (C), thorium doped iron oxide (T), thorium and copper doped iron oxide (TC) and a commercial catalyst. Source: Costa et al. (2002).

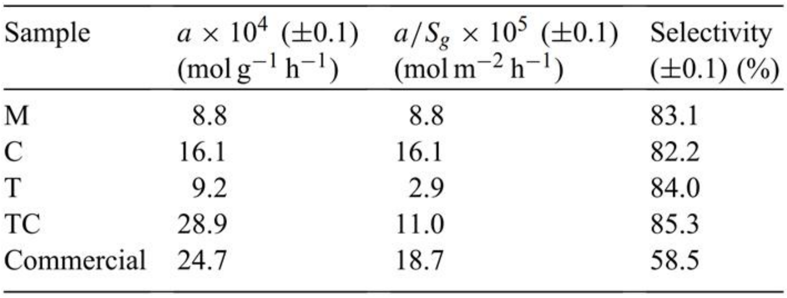

Sample	$a \times 10^4$ (±0.1) (mol g^{-1} h^{-1})	$a/S_g \times 10^5$ (±0.1) (mol m^{-2} h^{-1})	Selectivity (±0.1) (%)
M	8.8	8.8	83.1
C	16.1	16.1	82.2
T	9.2	2.9	84.0
TC	28.9	11.0	85.3
Commercial	24.7	18.7	58.5

With chromium still predominately used, Rhodes et al. (2002). Studied the effect that the addition of promoters, including Cu, B, Pb, Ba, Ag and Hg, in varying amounts had on the activity of an iron/chromium catalyst and in turn its performance. Unlike, Costa et al. it is stated that the catalysts were produced using the co-precipitation method and were made so that the promotor accountant for 2 wt%. They were tested in a fixed bed microreactor at a variety of temperatures. During the tests, a gas stream with a composition of 50vol% (hydrogen), 12.5vol% (carbon monoxide) and 2 37.5vol% (nitrogen) was injected into the system. As a gas stream, this again does not give an excellent representation of process gases produced by a preceding steam reformer. Process gases would typically also contain carbon dioxide and a number of low molecular weight hydrocarbons. Their result is shown below in Table 2-8 and Figure 2-31.

Table 2-8: Effect of promotors on WGS reaction performance and its activation energy. Source: Rhodes et al. (2002).

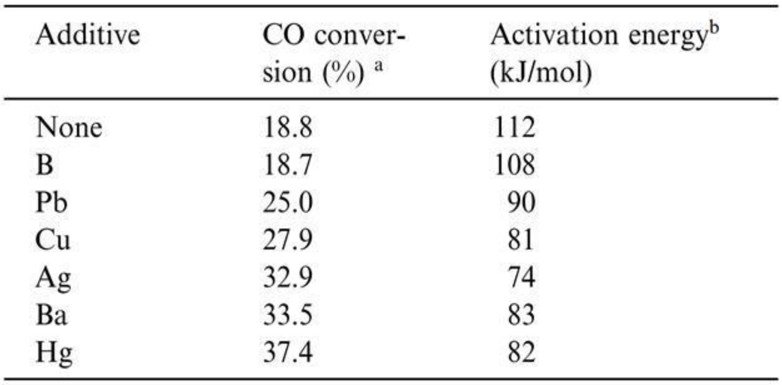

Additive	CO conversion (%) [a]	Activation energy[b] (kJ/mol)
None	18.8	112
B	18.7	108
Pb	25.0	90
Cu	27.9	81
Ag	32.9	74
Ba	33.5	83
Hg	37.4	82

From their investigation, it was found that at a temperature of 400°C the addition of mercury (Hg) as a promotor resulted in a conversion of carbon monoxide that was double that of the un-promoted catalyst. This was the highest conversion achieved by any promoted catalyst at that temperature. It was also shown that of all the promotors tested; only boron resulted in the conversion of carbon depletion. It was suggested that this could be due to the metal catalysing an unwanted side reaction. In addition to this, it was shown that the addition of mercury resulted in the catalyst with the lowest activation energy (Rhodes et al. 2002).

More so, Rhodes et al. 2002 found that the conversion of carbon monoxide increases with temperature, as shown below in figure 2-31 for all promoted and un-promoted catalysts. One area, in particular, that is not covered by Rhodes at al. is the analysis of the reacted catalysts.

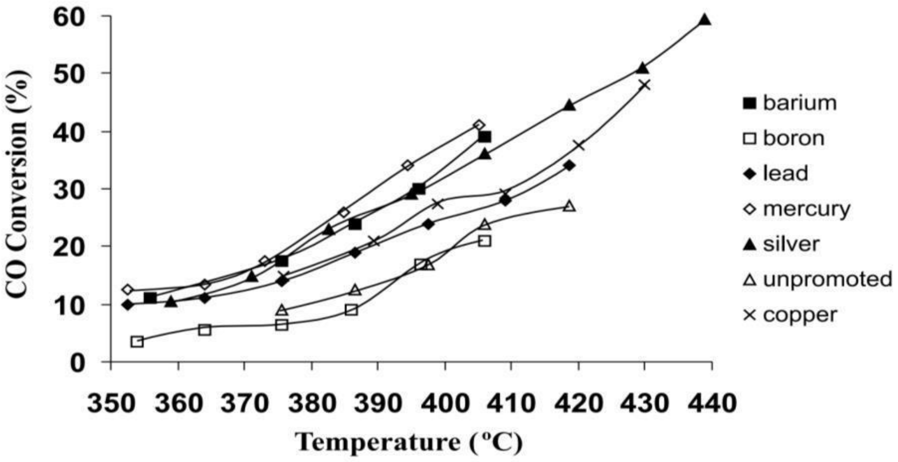

Figure 2-31: Effect of temperature on CO conversion on various promoted Fe3O4/Cr2O3 catalysts. Source: Rhodes et al. (2002).

More recent work into iron catalysts for the WGS reaction looks at using the innovative technique of single-atom doping. Single-atom catalysis uses isolated metal atoms that are stabilised on applicable carriers and is currently one of the most innovative and fast-growing research areas in catalyst science (Mitchell et al., 2017). Lin et al. (2013) investigated an iron catalyst with single-atom doping using iridium (Ir). During their investigation, four separate catalysts were tested which contained varying amounts of Ir. The metal loading of Ir tested was 0.01 wt% of the total catalyst. Similar to previous papers, the catalysts were prepared using the co-precipitation technique. By using STEM imaging, Lin et al. were able to perform statistical analysis on the distribution of Ir throughout the catalyst. They found that as the weight percentage of Ir was increasing in the catalyst, the number of single atoms decreased. This was due to an increase in the concentration of Ir within the catalyst. Provided below are the HAADF-STEM images used to identify the Ir single atoms contained within the different catalysts. The atoms have been made visible by the white circular rings provided on the images.

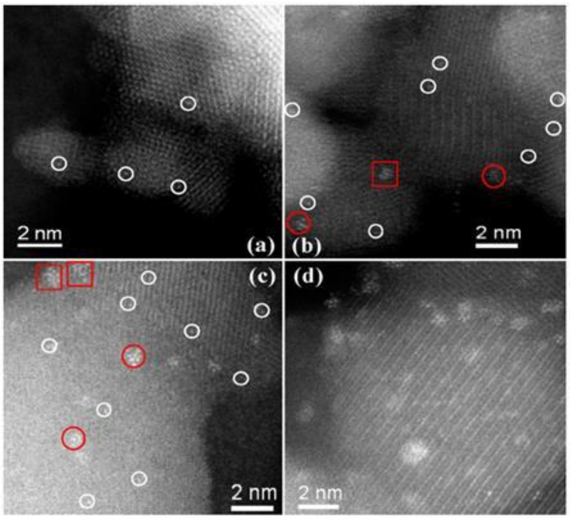

Figure 2-32: HAADF-STEM images for the four iridium doped iron catalysts indicating the single Ir atoms: (a)Ir/FeOx; (b) Ir/FeOx-0.22; (c) Ir/FeOx-0.32; (d) Ir/FeOx-2.40. Source: Lin et al. (2013).

After analysis, the catalysts were then tested in a microreactor at a temperature of 300°C. From their results, they showed that a single atom doped iron catalyst using Ir (Ir/FeOx) could significantly increase the conversion of CO via the WGS reaction. Furthermore, of the catalysts tested, the one with the lowest Ir loading was shown to have the greatest activity. By comparison with literature, it was suggested that this high performance is superior to the most active catalysts in industry. Further research is required in this field, but, if correct, it will have great implications on the future of WGS catalyst. This is due to it not only increasing activity and conversion but also reducing material cost, as less metal is required in the catalyst. Possible further research into this particular Ir doped iron catalyst could look at varying the temperature at which the WGS reaction takes place. Also, work should be carried out in which the Ir is substituted with various other metal but maintaining the single atom dispersion.

2.4.3.1.2 Carbon catalysts

Similar to steam reforming, carbon has also been looked at as potential support for a water-gas shift catalyst. Due to the lower temperature used within a water-gas shift unit in comparison to a steam reformer, carbon is a much more viable option for use in a water-gas shift reactor. Yu et al. (2006) produced a carbon catalyst using char from the gasification of coal and doping it with iron. During their investigation, several catalysts were tested at a range of temperatures. Also varied was the flow rate of gas through the system. Their results showed that when the char catalysts were tested, the WGS shift reaction was detectable at temperatures as low as 275°C and became more significant at temperatures above 300°C.

Yu et al. suggested that when the iron was loaded into the brown coal, it underwent a transformation process. Evidence of this is provided below in figure 2-33. This led to the iron becoming dispersed throughout the char in nano-sized particles of magnetite, which they concluded, resulted in a highly active catalyst shown for the WGS reaction over a broad range of temperatures. There are obvious benefits to using carbon including its abundance, cheap production cost and ease of disposal. Yu et al. discuss how the iron used in the production of this catalyst can be regenerated after use via regasification, therefore, reducing the cost further.

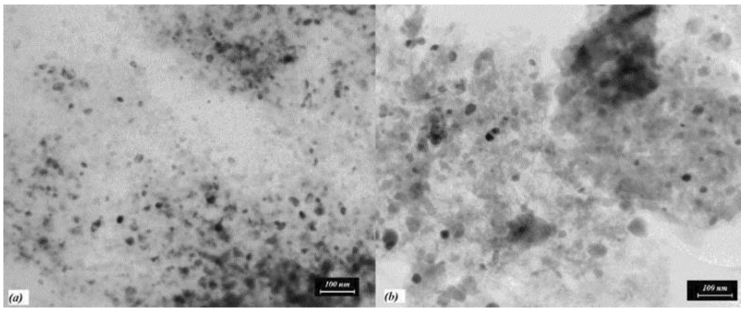

Figure 2-33: Transmission electron microscopy images of carbon supported iron catalyst. A) Unreacted catalyst and B) Reacted catalyst. Source: Yu et al. (2006).

2.4.3.1.3 Ceria Catalysts

One component that has shown potential for both steam reforming, as discussed in section 2.4.3.1 and the water-gas shift reaction stages of hydrogen production is ceria or cerium oxide. Ceria based catalysts have been showed to be highly reducible and also decrease activation energy when rare-earth or transition metal is added as support. This has led to ceria being researched extensively. Gunawardana et al. (2009) identified ceria loaded with copper as a potential candidate to catalyse the WGS reaction. Similarly, to some of the previous papers discussed in this section, the co-precipitation method was used to produce catalysts. Several catalysts were produced with a varied amount of copper loading and were tested in a novel U-tube reactor.

During their investigation, the catalysts were tested at temperatures ranging from 150 to 350°C. From their results which have been displayed below as figure 2-34, it is shown that increasing the temperature at which the water-gas shift reaction takes place increases the overall conversion of carbon monoxide until a maximum value is reached at around 300°C. They conclude that this could be due to the thermodynamic limitations of the reaction itself because of its reversible nature. This fits in with the use of a two-shift reactors system currently used in industrial applications as explained at the start of the water-gas shift review. Of the catalysts tested, the one consisting of 80at% copper performed best over the temperature range. Their results showed that increasing the copper content increases the overall performance of the catalyst. However, 90at% copper showed the least infinity to the water-gas shift reaction over the range of temperatures.

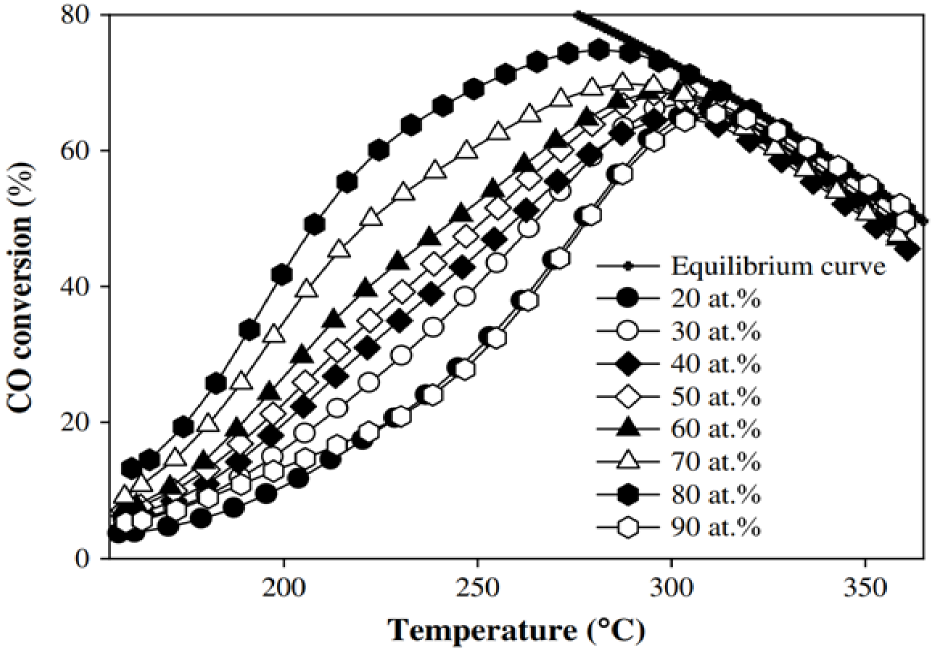

Figure 2-34:The performance of various catalysts with different copper loading. Source: Gunawardana et al. (2008).

Gunawardana et al. then tested the stability of the catalysts by extending the temperature range up to 420°C. During their testing, they completed five separate runs over the range and recorded the conversion at 300°C. Their results showed that the catalysts were not stable during the testing. The conversion decreased as the number of runs increased. This is shown below in figure 2-35 by the open symbol trend lines. The rate at which this occurred was found to become more severe during further testing. The catalysts with the lowest copper content were shown to be the least stable. This suggests that more testing is required in this ceria catalyst.

Further research could look at introducing a promoter to the composition of the catalyst to increase its stability. In addition to this, more work could be done to determine the cause of this decrease in instability. This could be achieved through the use of techniques such as electron microscopy.

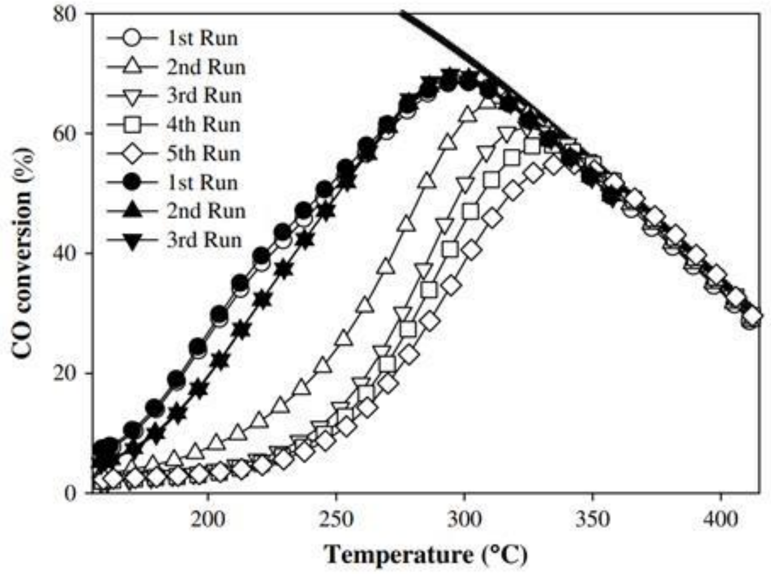

Figure 2-35: Comparison of stability and activity of a 60 at% copper-ceria catalyst over temperatures rates of 150°C to 360°C and 150°C to 420°C. The solid symbols represent the first temperature range and the open symbols represent the second range. Source: Gunawardana et al. (2009).

Further research into ceria catalysts was conducted by Hilaire et al. (2001). During their investigation, they looked at the use of ceria as a support for different metallic catalysts. Unlike previous catalysts discussed for the water-gas shift in this section of the report, wet impregnation was used as the catalyst synthesis method. During their preparation, the ceria supports were loaded with various transition metals which included lead, cobalt, nickel and iron. In each case, the loading was equal to 1% of the total catalyst weight. To replicate process gases, carbon dioxide, carbon monoxide and hydrogen were fed into the system. Before entering the reactor, the feed was passed through activated-carbon, and NaOH traps to ensure that no unwanted metals could enter the system. Hilaire et al. concluded that the WGS reaction mechanism involving a transition metal loaded ceria catalyst is a redox process. During the process, ceria is oxidised by steam. The oxygen is then transferred from the ceria support to the metal which then reacts with the carbon dioxide absorbed onto its surface from the process gas stream. Their results for the various promotors showed that the lead/ceria and nickel/ceria have very similar activities. Their activities were better than the iron/ceria, cobalt/ceria, and ceria catalysts.

2.4.3.1.4 Aluminium Catalysts

Another metal that has been tested to catalyse the WGS reaction is Aluminium. One example of an aluminium catalyst used in industry is Cu/Zn/Al. This is often used in the LTSR at temperatures between 240°C and 200°C (Rhodes et al., 1995). Rhodes et al. (1995) reported that the catalyst has been able to achieve a conversion of nearly 100%. Later in their paper, they discuss how the catalyst undergoes rapid poisoning and subsequent deactivation when sulphur is present in the process stream. This, therefore, means that a non-sulphur feed, or a sulphur removal step, is required when this catalyst is used. This would increase the running costs of hydrogen production plant dramatically. As well as poisoning, Rhodes et al. explain that the catalyst is also highly susceptible to sintering. Due to the extremely high conversion claimed by Rhodes et al. More research should be conducted which looks at reducing the effects of both sintering and poisoning on the catalyst by changing reaction conditions or by varying the composition of the catalyst.

2.4.3.1.5 Nickel Catalysts

Just as for the steam reforming stage of hydrogen production, nickel has also been shown to be active in the water-gas shift reaction. Hwang et al. (2011) presented a novel catalyst that uses potassium to modify the nickel. As a catalyst, nickel has many advantages over other materials due to its high thermal conductivity which enables it to control the heat of reaction in a highly exothermic reaction. Another advantage is the fact that nickel can be moulded and shaped by various methods. As a catalyst for the WGS reaction, however, nickel has one major disadvantage. This is due to it also catalysing the methanation reaction in the temperature range at which the WGS reaction is usually conducted. The reaction itself is the reverse of SR and sees methane and water produced from carbon monoxide, or carbon dioxide, and hydrogen. This was identified by

Hwang et al. and led them to investigate the addition of potassium as a possible way of suppressing this reverse reaction while maintaining a high conversion of carbon monoxide.

When conducting their investigation, Hwang et al. produced three separated catalysts for comparison. The first consisted of pure nickel and was prepared by grinding down to pre-dried nickel powdered to an average particle size of 3.4 µm. The second was the potassium-modified nickel-metal catalyst. This was produced via wet impregnation and saw 5 wt. % of potassium loaded onto nickel metal powder. The final catalyst was one currently used commercially which was tested for comparative reasons.

Hwang et al. use a process gas stream consisting of only carbon monoxide and hydrogen. This is a poor representation of a process stream found in industrial hydrogen production. However, it is suggested that by using this stream, it will be easier to identify whether the catalyst being tested has more of an affinity to the methanation reaction or the water-gas shift reaction. The tests were conducted at 350°C and the process gases examined by gas chromatography. In order to determine the selectivity towards each reaction discussed, Hwang et al. used the following equations 2.8 and 2.9:

$$CO\ Conversion\ (\%) = \frac{moles\ of\ CO\ consumed}{moles\ of\ CO\ \ FED}\ X\ 100 \qquad 2.8$$

$$CO\ Conversion\ (\%) = \frac{moles\ of\ CH4\ produced}{moles\ of\ CO\ \ consumed}\ X\ 100 \qquad 2.9$$

Their results, which are displayed graphically below in figure 2-36, show that the two nickel catalysts produced a similar conversion of CO at around 98%. This is an astounding conversion and is one of the highest found while conducting the research for this literature review. From the results, it is clear that for a pure nickel a larger proportion of the CO absorbed by catalyst was converted to methane via the unwanted methanation reaction. Hwang et al. discussed how the potassium modified nickel catalyst showed signs of suppressing this reaction. This is shown by the minuscule amount of methane produced during the test. In terms of comparing the potassium modified and commercial catalysts, both performed similarly in terms of the conversion and production of selected gases. In future research, more could be done to adjust the composition of the nickel catalyst as only one composition was tested by Hwang et al. 2011.

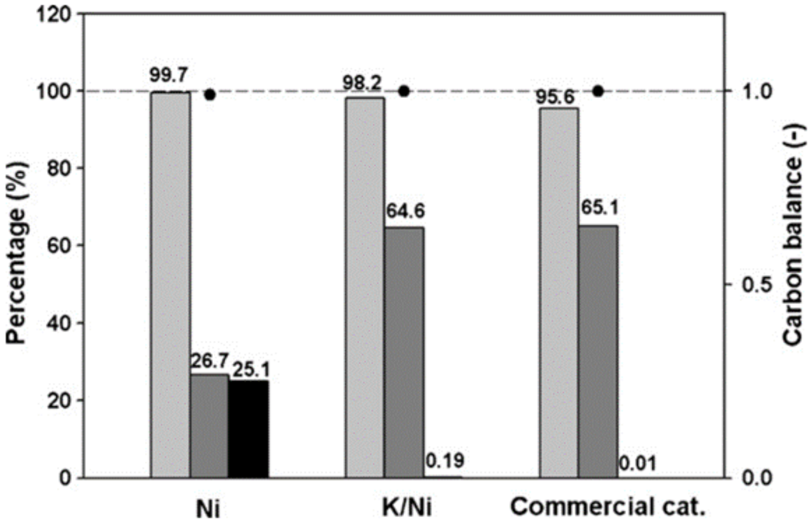

Figure 2-36: A Comparison of the performance of three catalysts for WGS reaction. Grey bar represents CO conversion; Dark Bar represents H_2 Production. Black Bar represents CH_4 production. The black dot is to represent the carbon balance. Source: Hwang et al. (2011)

2.4.3.1.5 CaO as an absorber/catalyst in the WGS reaction

An absorbent whose behaviour could be investigated as both absorber and catalyst for the WGS reaction stage is CaO. According to Müller et al. (2009), it could move the WGS reaction to the right, promoting H_2 production with a small content of CO_2. This process is driven by reaction (equation 2.5) in section 2.4.3.

Li et al. (2014) studied the WGS with enhanced absorption by CaO, and they proved that it could act as both catalyst and absorbent, giving high hydrogen content of 71 vol.% when used with pure H_2O and CO. This would be different when used with a biomass sample but should behave similarly. They found that at temperatures higher than 700°C the CO conversion rate to CO_2 decreased; thus, lower temperature for WGS reaction is required to use CaO as absorbent/catalyst. The same decreasing effect was shown by hydrogen, which was high at temperatures of about 450°C. Contrarily, the CO_2 absorption rate presented a more drastic decrease, to almost 0 at temperatures above 700°C, and the WGS reaction was no longer enhanced. This influence is depicted in Figure 2-37

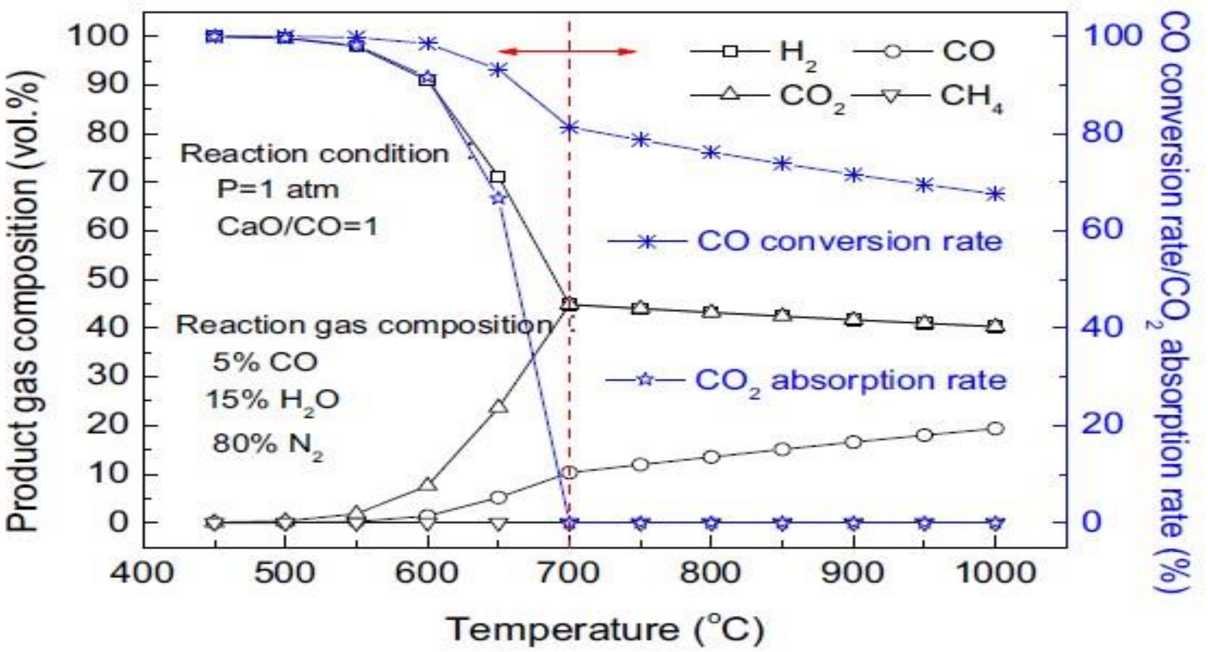

Figure 2-37: Influence of CaO in WGS reaction between pure water and carbon monoxide at different temperatures (Li et al., 2014)

2.4.3.2 WGS Catalyst Synthesis

Letichevsky et al. (2005) investigated the effect that the preparation technique has on performance. In particular, the paper looked at varying the preparation conditions with co-precipitation taken as the standard method of catalyst synthesis. Once prepared, the catalysts were characterised by several techniques. These included X-ray diffraction, Raman spectroscopy, temperature-programmed reduction, infrared spectroscopy, oxygen storage capacity and surface area tests. The conditions tested included pH, the salt precursor used to produce the catalyst and finally the introduction of drying and ageing steps. The compound of choice for the catalyst was CeO2-ZrO2. Letichevsky et al. identified that similar investigations carried out by Hori et al. (1998) and Rossignol et al. (1999) produced conflicting results. Therefore, their report aimed to systematically analyse the procedure of the co-precipitation technique in order to develop a methodology that would enhance the performance of the catalyst. Letichevsky et al. identify that a high specific surface area is key to a high performing catalyst. Their results, as well as the sample notation meaning, have been provided below in table 2-9 and 2-10.

Table 2-9: Specific area (S) and oxygen storage capacities (OSC) of the various catalyst produced using different precursors and synthesis techniques. Source: Letichevsky et al. (2005).

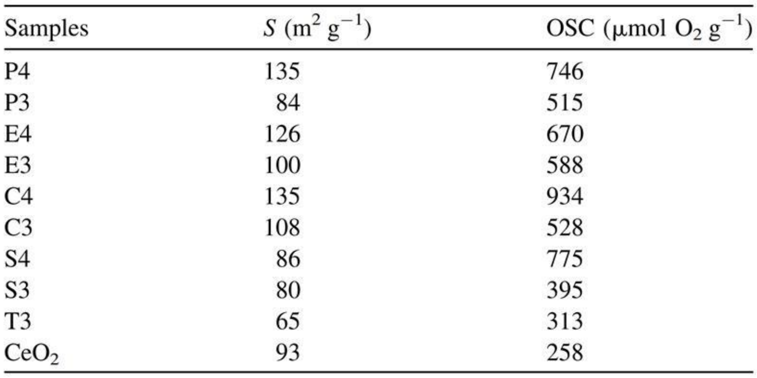

Samples	S ($m^2\ g^{-1}$)	OSC ($\mu mol\ O_2\ g^{-1}$)
P4	135	746
P3	84	515
E4	126	670
E3	100	588
C4	135	934
C3	108	528
S4	86	775
S3	80	395
T3	65	313
CeO_2	93	258

Table 2-10: Conditions used to create samples using in the work by Letichevsky et al. Source Letichevsky et al. (2005).

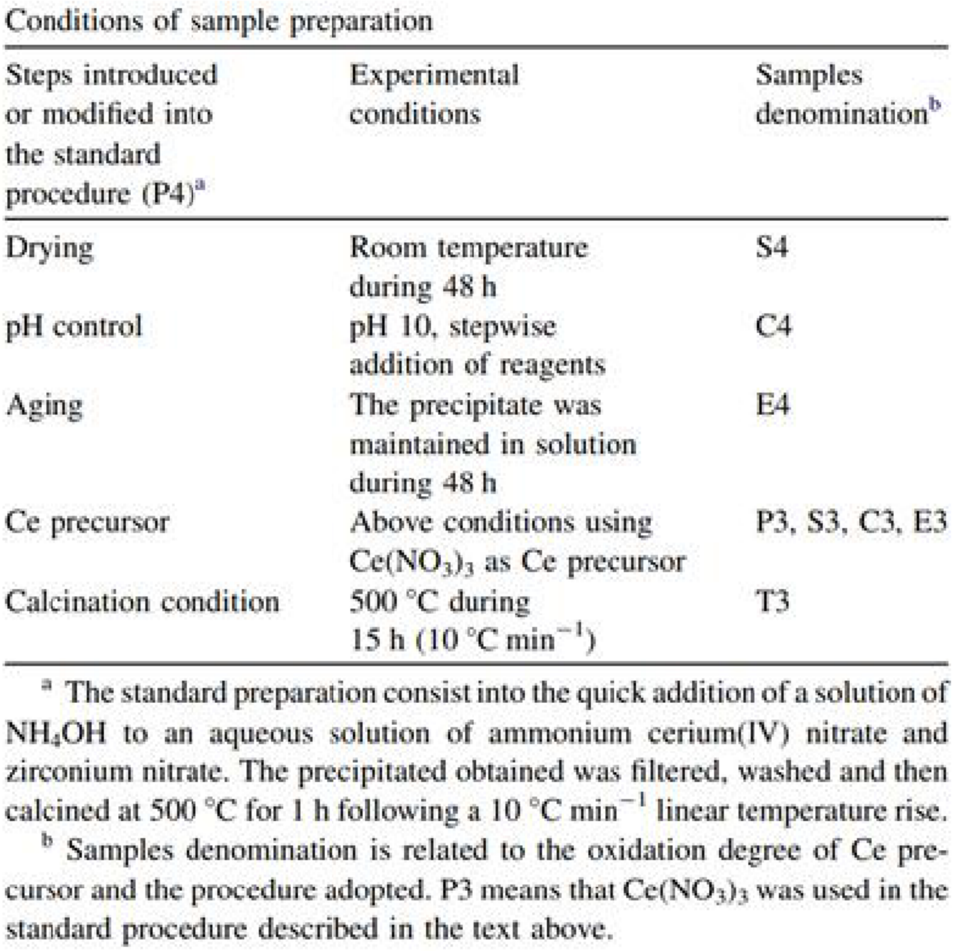

Conditions of sample preparation

Steps introduced or modified into the standard procedure (P4)[a]	Experimental conditions	Samples denomination[b]
Drying	Room temperature during 48 h	S4
pH control	pH 10, stepwise addition of reagents	C4
Aging	The precipitate was maintained in solution during 48 h	E4
Ce precursor	Above conditions using $Ce(NO_3)_3$ as Ce precursor	P3, S3, C3, E3
Calcination condition	500 °C during 15 h (10 °C min^{-1})	T3

[a] The standard preparation consist into the quick addition of a solution of NH_4OH to an aqueous solution of ammonium cerium(IV) nitrate and zirconium nitrate. The precipitated obtained was filtered, washed and then calcined at 500 °C for 1 h following a 10 °C min^{-1} linear temperature rise.

[b] Samples denomination is related to the oxidation degree of Ce precursor and the procedure adopted. P3 means that $Ce(NO_3)_3$ was used in the standard procedure described in the text above.

Letichevsky et al. (2005) concluded from their investigation that of all the parameters varied, the precursors used in synthesis had the greatest effect on the catalyst. For example, the use of $Ce(NO_3)_3$ led to the formation of tetrahedral ZrO_3 and cubic CeO_2 mixed oxides. On the other hand, when $(NH_4)_2Ce(NO_3)_6$ was used as the precursor a solid solution was formed. Letichevsky et al. considered that the reason it is the most significant parameter is because it defines the crystalline phases of the resulting catalyst which in turn results in it defining the reducibility of the CeO_2-ZrO_2 itself. All other parameters adjusted were shown not to cause any significant changes to the resulting catalyst. This research could be extended further to include different synthesis techniques such as wet impregnation and sol-gel which have been shown to be used in many of the other papers discussed. The catalysts could then be tested to investigate their affinity to the WGS reaction. This would provide evidence as to which technique is best for synthesis.

Table 2-11: Summary for catalytic metals and their supports discussed for the water-gas shift reaction.

Catalyst	Description	T (°C)	S:C	XA (%)	Source
Th/Fe	Th used reduce toxicity of Cr	370	0.6	-	Costa et al
Cr/Fe	Promotion by addition of Hg, B, Pb, Ag, Ba and Cu	400	6	37.4	Rhodes et al
Ir/Fe	Single atom doping	300	5	93	Lin et al
Fe/C	Char support for inexpensive catalyst	350	5	-	Yu et al
Cu/Ce	Copper loaded ceria catalyst with increased activity	300	-	68.5	Gunawardana et al.
Pd/CeO2	Ceria support promoted with Pb	400	-	-	Hilaire et al
Cu/Zn/Al	Easily poisoned by sulphur	250	-	100	Rhodes et al
Ni/Al	Methanation reduced with promotor Addition	350	3	99	Hwang et al

T means temperature, S:C means steam to carbon ratio, XA means metal loading

2.4.3.3 Effect of Temperature and Pressure in WGS reaction

The WGS reaction is a moderately reversible reaction. Therefore, due to Le Chatelier's principle the equilibrium of the reaction itself can be manipulated by adjusting the volume, pressure, temperature and or the concentration. For this reason, a vast amount of research has been carried out to determine the optimum condition for the WGS reaction to take place. Kim et al. (2012) examined the effects that both pressure and temperature have on the performance of the WGS reaction. Although the paper concentrates on the use of a novel membrane reactor (MR), results are also discussed for the traditional packed bed system (TR). The catalyst used in the work was a cerium doped iron catalyst which was prepared using co-precipitation. Once prepared, the iron contained within the catalyst was transformed into magnetite by controlled reduction. Reddy et al. have shown that this catalyst has a high tolerance to sulphur components contained within the process stream.

During their investigation, the temperature of the system was varied from 400°C to 550°C degrees and the pressure from 2 atm to 6 atm. The high temperatures used give a better representation of a HTSR reactor used commercially, however, they are considerably higher than temperatures previously discussed in this report for the water-gas shift reaction. The feed for the investigation consisted of carbon monoxide and nitrogen. Similar to other studies, this gives a poor representation of process gases usually found in the water-gas shift unit. Their results have been outlined below in figures 2.38a to 2.38d. Each figure represents the chang in conversion with temperature at each individual temperature tested.

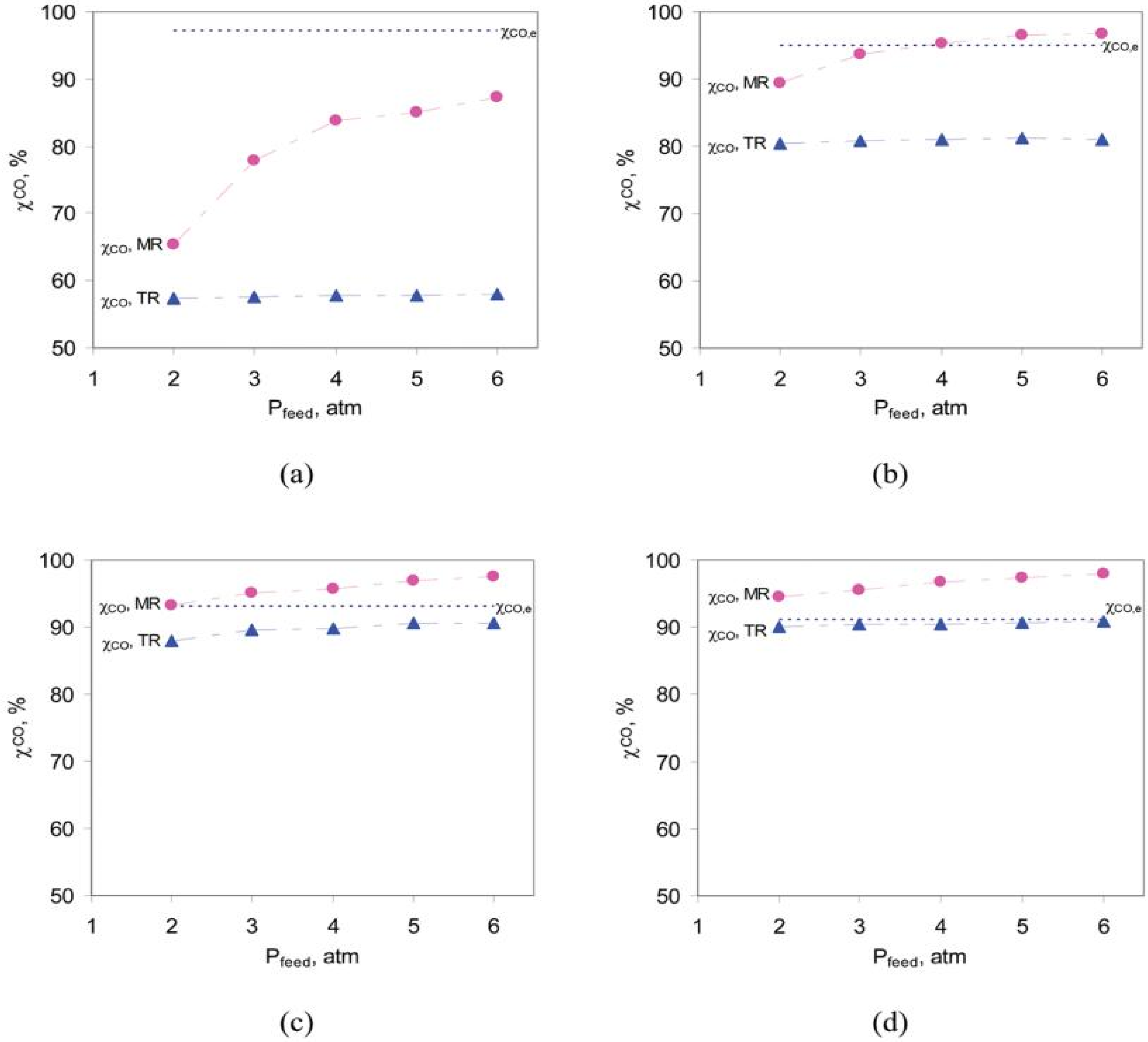

(a) (b) (c) (d)

Figure 2-38: Effect of pressure on the conversion of carbon monoxide at a variety of temperatures: a) 400°C b) 450°C c) 500°C and d) 550°C. Source: Kim et al. (2012).

These results show that increasing the pressure has very little effect on the conversion of carbon monoxide within the TR. Kim et al. conclude that the slight increase in conversion may be due to a more effective utilisation of catalyst bed under higher pressures. The reason for there being no change due to an increase in pressure can be explained by the water-gas shift reaction equation itself. By looking at the equation it is evident that the same moles of gas are present on both sides of the reaction. When there is an imbalance in the moles of gas, an increase in pressure will result in the equilibrium of the reaction shifting to the side with the least number of moles of gas in order to decrease pressure. The opposing result is shown when the system pressure is decreased. As there is no imbalance in the water-gas shift reaction equation these effects are not shown. This therefore means that the results produced by Kim et al. are in agreement with equilibrium reaction theory.

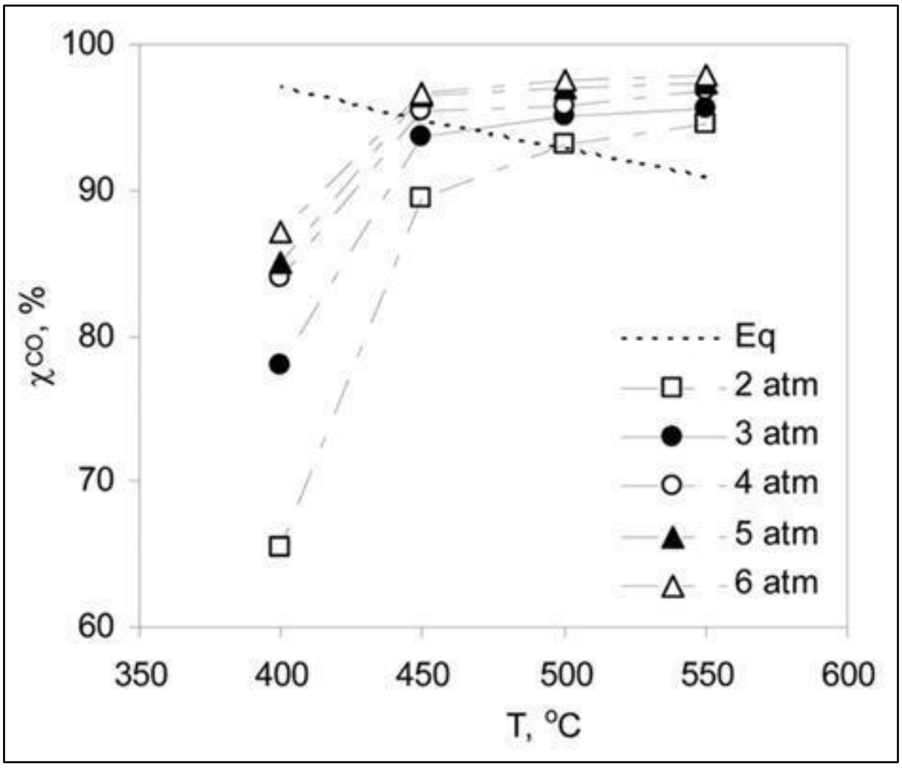

Figure 2-39: The effect of temperature on the conversion of carbon monoxide at various pressures. Source: Kim et al. (2012).

Figure 2-39 shows the results when the temperature of the TR unit was increased. From the figure it is clear that for all pressures tested, the conversion of carbon monoxide increases with temperature. This is not in accordance with the theory of Le Chatelier's principle as the forward reaction is exothermic. An increase in temperature should result in the equilibrium shifting in the endothermic direction of the reaction in order to reduce the temperature. The increase in conversion can be explained, however, by an increase in reaction rate due to the increased temperature. In addition, this result shows the increase in selectivity towards carbon monoxide cause by the catalyst.

Similarly, Meshkani & Mehran (2015) studied the effect of temperature particularly in WGS reaction (Figure 1.6.38) and higher temperatures led to higher CO to CO_2 conversion. In addition, Duman & Yanik (2017) found that higher H_2 yield was achieved with increasing temperatures (Figure 2-*40a*).

The temperature influence was investigated in Ceria-supported iron oxide catalyst, and it was found that the higher the temperature is, the higher the CO conversion is achieved (Bali, et al., 2010).

However, other studies showed a different trend in which the conversion increased to a maximum and then it decreased when Fe/Cu catalysts were added (Gawade, et al., 2010). This suggests that there’s a temperature at which the WGS reaction is mostly promoted but this depends greatly on the selected catalyst. Results from both studies are depicted in Figure 2-40a and Figure 2-40b respectively.

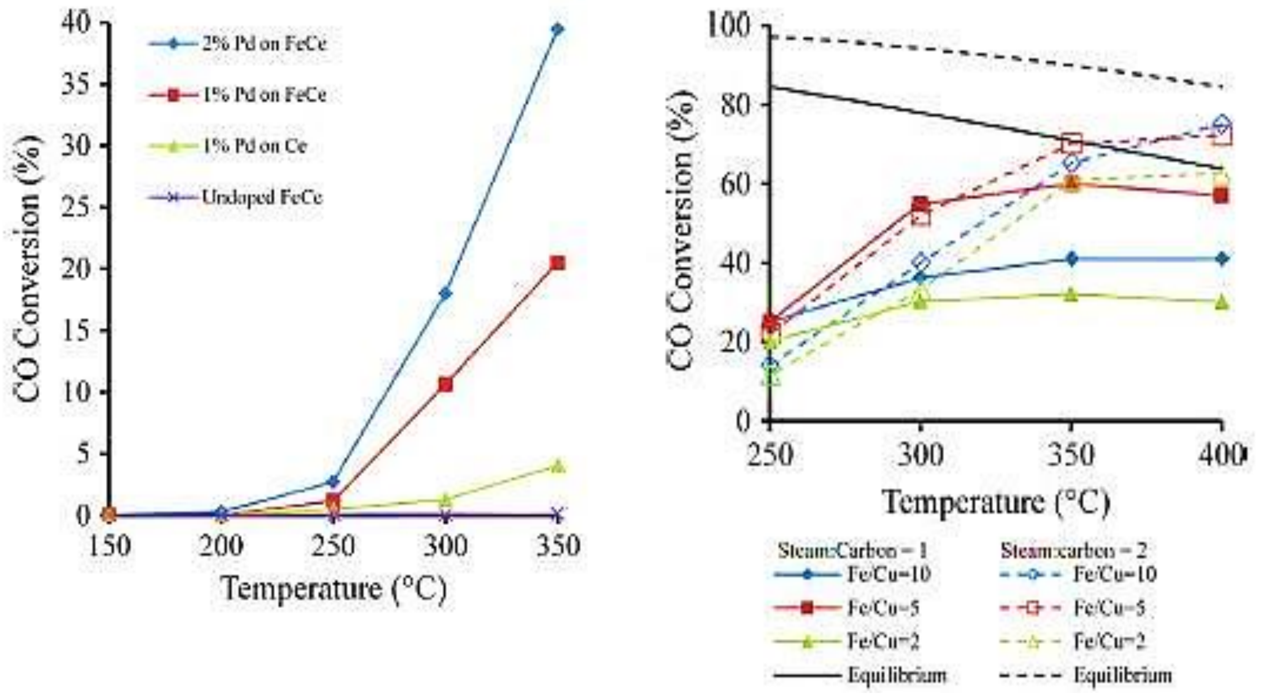

Figure 2-40: (a) Effect of temperature using different Pd/Fe/Ce catalyst in CO conversion Bali, et al., (2010)

(b) Effect of temperature using different Fe/Cu catalysts in CO conversion (Gawade et al., 2010)

2.4.3.4 Effect of steam to biomass ratio (S/B) on WGS reaction

Since the steam maximizes hydrogen production in both steam gasification and WGS reaction steps following reaction. (equation 2.4) and (equation 2.5), the S/B ratio is considered another parameter of high relevance. According to Kumar, et al. (2009), the higher the S/B the higher the conversion efficiency but the adequate temperature is required. Other research papers have proven the contrary, when steam flow rate increases, H_2 yield does as well until it reaches a maximum point and then it decreases. The challenge is finding the optimal steam flow rate at a determined temperature (Salami & Skála, 2015). These behaviours are shown in Figure 2-41a and Figure 2-41b respectively.

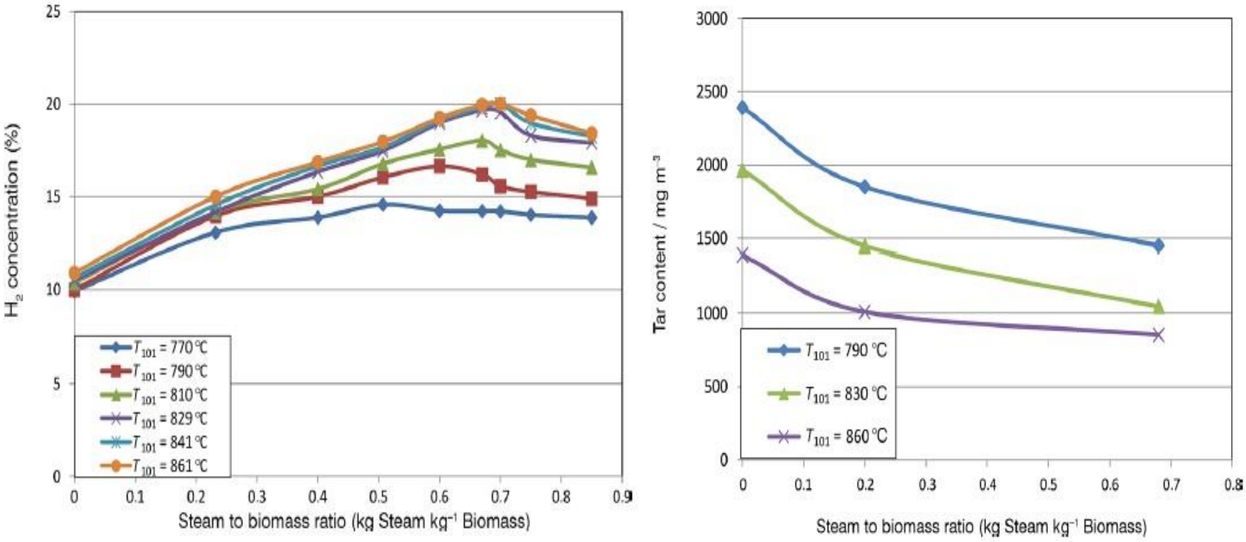

Figure 2-41:(a) S/B influence on H_2 production (Salami & Skála, 2015)

(b) S/B influence on tar content (Salami & Skála, 2015)

Luo, et al. (2009) also investigated the effect of S/B, with dolomite as a catalyst, and found that the hydrogen concentration is maximized with increasing S/B and with higher steam flow rate the hydrogen production decreases, like what Salami & Skála (2015) found. However, CO_2 also increases, while CO is reduced; other hydrocarbons like methane and ethane are also further converted with higher S/B. This would mean that the WGS reaction (reaction. (R.6)) is promoted when steam is increased until it reaches a maximum and H_2 starts decreasing, therefore the optimal S/B should be achieved for maximum H_2 yield. This effect is showed in Figure 2-43. Additionally, the gas yield in m^3/kg reaches its maximum of at a S/B of 1.43 which is different to the S/B at which H_2 reaches its maximum (2.10).

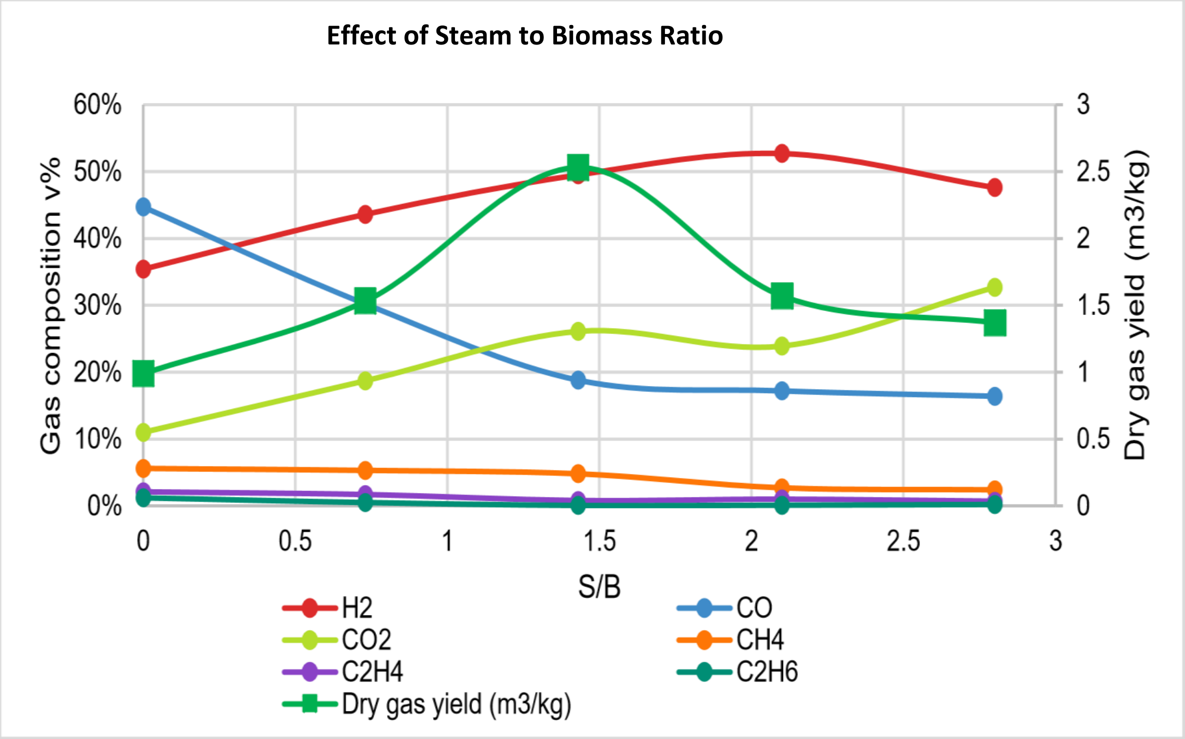

Figure 2-42: Effect of Steam to Biomass in gas composition and gas yield in catalytic steam gasification. Adapted from the data in Luo, et al. (2009)

2.4.3.5. Summary on Water-Gas Shift

Similarly, to the process of steam reforming, through the use of renewable feedstocks such as biomass, the water-gas shift will play a pivotal role in hydrogen production for the foreseeable future. As described in this report, ceria has shown strong potential for industrial applications in the future due to its high activity and ability to be reduced easily. In addition to this, ceria catalysts have been shown to have the ability to catalyse both the steam reforming and water-gas shift reaction, as described previously, when loaded with other transition metals. This gives the opportunity for hydrogen production to enhance further in future applications.

In the future, it is also hoped that new techniques such as electro catalysis will enable the surface chemistry of catalysts to be better controlled. As described by Calle-Vallejo et al. (2013) this will allow composition and the interactions that occur at the surface of a catalyst to be manipulated more accurately and effectively and will in turn enhance performance. Finally, it is hoped that new synthesis techniques such as single-atom doping will enable highly efficient hydrogen production through the water-gas shift reaction by having very low oxygen vacancies (LeValley et al., 2014).

2.5 General issues with steam reforming and water-gas shift

The greatest issue facing catalysts for both the steam reforming and water-gas shift reactions is that they are affected by a vast number of variables. The two reactions are affected by reaction conditions including temperature, steam to carbon ratio, the reactor used and residence time. Secondly, the catalysts are also affected by physical conditions such as composition, metal dispersion, coking, poisoning, and sintering. As asserted by Chen et al. (2008) all these factors, in turn, affect the performance of the water-gas shift reaction and can lead to a wide range of results being produced for the same catalyst.

More so, deactivation due to coking is a significant issue for both steam reforming and water-gas shift catalysts. Mostly dependent on the reaction conditions, coking can be found in many different forms. Despite engineers' best efforts to minimise the issue, techniques currently being used, such as increased steam to carbon ratio and the addition of rare earth metal oxides are proving to increase production costs for hydrogen significantly. A further method of deactivation described was sulphur poisoning. Like coking, sulphur poisoning has been shown to affect both water-gas shift and steam reforming catalysts. Despite Trimm et al. (1999) suggesting that a small amount of sulphur can marginally increase catalytic activity, sulphur is often shown to block active sites on catalyst surfaces. Successful techniques have been found to reduce this issue significantly; however, they often involve rare metals which again leads to increased production costs. Finally, sintering has been shown to be a significant problem for catalysts due to the occurrence of hot spots with reactor systems.

2.6 Summary of hydrogen production from biomass via the thermochemical method

Currently, hydrogen production is produced mostly from fossil fuels such as naphtha, natural gas or coal, and a small portion is produced from water photolysis, electrolysis or thermolysis. The first sources are not considered sustainable as they employ non-renewable sources and the latter are still in development and are not considered cost-effective (Alvarez et al., 2014). One of the most promising long-term alternatives to replace fossil fuels as a source for H_2 production is biomass, which is any material that originates from living organisms and is composed mainly of hydrogen and oxygen with negligible amounts of nitrogen and sulphur (Bizkarra et al., 2017).

Hydrogen production from biomass methods can be divided into two categories: thermochemical and biological. The different paths for hydrogen production can be seen in Figure 2-43. Notably, the approach of this work is to study the production of hydrogen from biomass following a thermochemical route in which first biomass is pyrolysed, and then the products are later reacted with water steam for the steam reforming, followed by the WGS reaction.

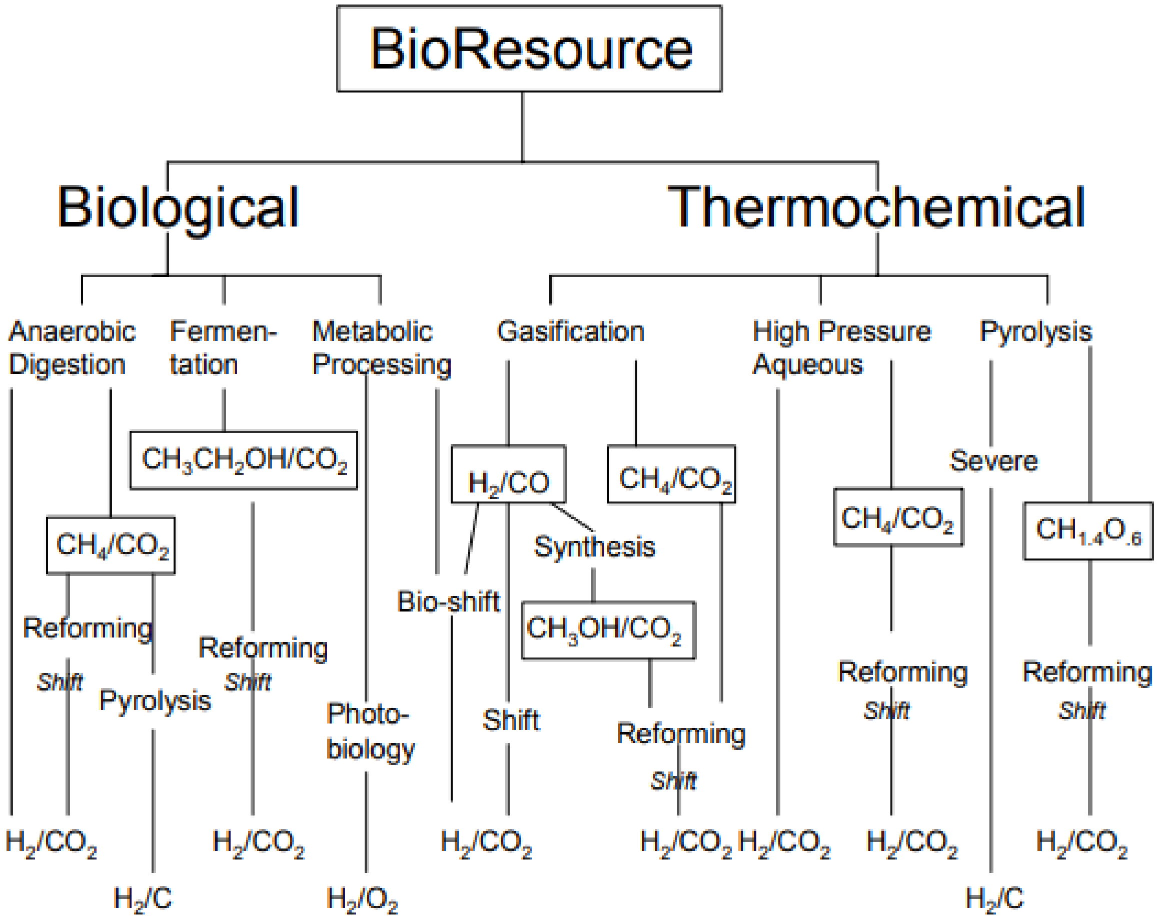

Figure 2-43: Hydrogen Production from Biomass Routes (Milne, et al., 2002)

The slow Pyrolysis of biomass consists of thermal degradation of organic matter at high temperatures and relatively low heating rates, and it is commonly used to produce biochar, bio-oil and non-condensable gases (hydrogen H_2, carbon monoxide CO, carbon dioxide CO_2, methane CH_4 and other hydrocarbon gases). The yields of each one of them depend on different parameters. Since this work aims to maximise hydrogen production, then the gas yield is prioritised over the liquid and char yields.

The constituents and the feedback type of the biomass are essential to have a rough prediction of the gas yield of the products from biomass pyrolysis, from the pseudo components. The lignin content of the biomass has a moderate correlation to hydrogen production (García Barneto et al., 2009). The most influential parameters in slow pyrolysis are the residence times, the heating rate and the HTT, which in turn are related to each other. The longer the time the biomass resides at the HTT, the higher the amount of gas that is produced (Solar et al., 2016). When the HTT is increased, the biomass produces more bio-oil until it reaches a maximum, then it decreases, as it would consequently release more non-condensable gases. In like manner, the char yield decreases but still the mass loss rate decreases, so treating the biomass with higher temperatures would eventually produce the same amount of char (Demirbas, 2007; Ronsee et al., 2014; Parthasarathy & Sheeba, 2017). In the same way, the gas yield increases with higher heating rate, but it does not a significant effect on the concentration of hydrogen. However, the concentrations of CO and CO_2 vary significantly (Chen et al.,2014; William & Besler, 1996).

The CSR is a process in which the volatiles are reacted with steam to produce carbon monoxide. The most critical parameters in the CSR process are the temperature, the steam to biomass ratio and the catalysts. The reforming reaction is promoted to a higher extent when higher temperatures are used in the process, resulting in a higher hydrogen yield and higher hydrogen content. This high hydrogen content is additionally driven by the WGS reaction (Luo et al., 2009; Kumar et al.,2018; Ning et al., 2018). Likewise, long residence times cause further reforming of the tar and higher hydrogen yields (Bridgwater, 2006; Peng et al., 2017; Michael J. Antal, 1981). The choice of the catalyst is fundamental for a high CSR performance, Ni catalyst have been widely studied, proving to reduce tar in the product (Wu & Williams, 2011) and increasing hydrogen yields (Dong, et al., 2016; Rapagna, et al., 1998; Wu, et al., 2011; Peng, et al., 2017).

The WGS reaction uses the carbon monoxide produced in by the reforming of volatiles to increase hydrogen production with steam addition, and the parameters to be explored for its H_2 enhancement are the same as the CSR: temperature, steam to biomass ratio and the catalyst. With increasing temperatures, but lower than the temperature required for CSR, hydrogen production is promoted (Meshkani & Mehran, 2015; Duman & Yanik, 2017; Bali et al., 20100). In some cases, the conversion reaches a maximum at a specific temperature, and then it decreases (Gawade et al., 2010). A similar effect is given by the S/B ratio, where the H_2 production increases to reach a maximum to then decrease; higher S/B ratios produce less tar content as well (Salami & Skála, 2015). The catalyst plays an essential role in improving WGS reaction performance; the use of Fe-based catalysts leads to enhanced WGS reaction activity (Lee et al., 2011; Watanabe et al., 2009).

CaO has been studied as it is capable of removing the CO_2 and converting it to $CaCO_3$, therefore serving as a potential sorbent for the WGS reaction. Studies prove that the CaO behaves not only as a sorbent but as a catalyst too, achieving high CO conversion and CO_2 at temperatures below 600°C (Li et al., 2014).

2.7 References

Abu El-Rub, Z., E. Bramer, and G. Brem, Review of catalysts for tar elimination in biomass gasification processes. Industrial & engineering chemistry research, 2004. 43(22): p. 6911-6919.

Aigner, I., U. Wolfesberger, and H. Hofbauer, Tar content and composition in producer gas of fluidized bed gasification and low-temperature pyrolysis of straw and wood-influence of temperature. 2009: na.

Al-Salem, S., P. Lettieri, and J. Baeyens, Recycling and recovery routes of plastic solid waste (PSW): A review. Waste management, 2009. 29(10): p. 2625-2643.

Arregi, A, Amutio, M, Lopez, G, Bilbao, J, Olazar, M. 2018. Evaluation of thermochemical routes for hydrogen production from biomass: A review. Energy Conversion and Management. 165. Pp 696-719

Asadullah, M., et al., Catalyst development for the gasification of biomass in the dual-bed gasifier. Applied Catalysis A: General, 2003. 255(2): p. 169-180.

Basile, F., Fornasari, G., Trifirò, F., Vaccari. A. 2001.Partial oxidation of methane: Effect of reaction parameters and catalyst composition on the thermal profile and heat distribution. Catalysis Today. 64(1-2), pp 21-30

Basu, P., Combustion and gasification in fluidized beds. 2006: CRC press.

Blanco, P.H., et al., Characterization and evaluation of Ni/SiO 2 catalysts for hydrogen production and tar reduction from catalytic steam pyrolysis- reforming of refuse derived fuel. Applied Catalysis B: Environmental, 2013. 134: p. 238-250.

Blanco, P.H., et al., Characterization of tar from the pyrolysis/gasification of refuse derived fuel: influence of process parameters and catalysis. Energy & Fuels, 2012. 26(4): p. 2107-2115.

Brage, C., Q. Yu, and K. Sjöström, Characteristics of evolution of tar from wood pyrolysis in a fixed-bed reactor. Fuel, 1996. 75(2): p. 213-219.

Bridgwater, A., et al., The nature and control of solid, liquid and gaseous emissions from the thermochemical processing of biomass. Biomass and bioenergy, 1995. 9(1): p. 325-341.

Bridgwater, A.. The technical and economic feasibility of biomass gasification for power generation. Fuel, 1995. 74(5): p. 631-653.

Bridgwater, A.V., Renewable fuels and chemicals by thermal processing of biomass. Chemical Engineering Journal, 2003. 91(2): p. 87-102.

Britt, P., et al., Mechanistic investigation into the formation of polycyclic aromatic hydrocarbons from the pyrolysis of plant steroids. Fuel, 2001. 80(12): p. 1727-1746.

Britt, P.F., A. Buchanan, and C.V. Owens Jr, Mechanistic investigation into the formation of polycyclic aromatic hydrocarbons from the pyrolysis of terpenes. Prepr. Pap.-Am. Chem. Soc., Div. Fuel Chem, 2004. 49(2): p. 868.

Brown, M. and V. Kearley, Role of wood waste as source of biomass fuel in the UK. Energy Materials, 2009. 4(4): p. 162-165.

Burnley, S., The impact of the European landfill directive on waste management in the United Kingdom. Resources, Conservation and Recycling, 2001. 32(3): p. 349-358.

Castaldi, M.J. and N.J. Themelis, The case for increasing the global capacity for waste to energy (WTE). Waste and Biomass Valorization, 2010. 1(1): p. 91-105.

Chen, G., Andries, J., Luo, Z., Spliethoff. H. 2003. Biomass pyrolysis/gasification for product gas production: the overall investigation of parametric effects. Energy Conversion and Management. 44(11), pp.1875-1884

Collard, FX and Blin, J. 2014. A review on pyrolysis of biomass constituents: Mechanisms and composition of the products obtained from the conversion of cellulose, hemicelluloses and lignin. Renewable and Sustainable Energy Reviews. Vo 38, Pp 594-608

Comission, E. Directive 2008/98/EC on waste (Waste Framework Directive). 2009; Available from: http://www.ec.europa.eu/environment/waste/framework/

Comission, E. Directive 2008/98/EC on waste (Waste Framework Directive). 2009; Available from: http://www.ec.europa.eu/environment/waste/framework/.

Cornelissen, T., et al., Flash co-pyrolysis of biomass with polylactic acid. Part 1: Influence on bio-oil yield and heating value. Fuel, 2008. 87(7): p. 1031-1041.

Cortright, R. D. Davda, R. R. and Dumesic, J. A. 2010. Hydrogen from catalytic reforming of biomass-derived hydrocarbons in liquid water. Materials for Sustainable Energy, pp. 289-292 (2010)

Costa, I., G. Massard, and A. Agarwal, Waste management policies for industrial symbiosis development: case studies in European countries. Journal of Cleaner Production, 2010. 18(8): p. 815-822.

Czernik, S. French, R. Feik, C. Chornet, E. 2002. Hydrogen by Catalytic Steam Reforming of Liquid Byproducts from Biomass Thermoconversion Processes. Ind. Eng. Chem. Res.200241174209-4215

DECC, A., UK Bioenergy Strategy. UK Department of Energy and Climate Change, 2012.

DEFRA, Wood Waste: A Short Review of Recent Research 2012: London

DEFRA. UK Statistics on Waste. 2015; Available from: https://www.gov.uk/government/uploads/system/uploads/attachment_data/file/487916/UK_Statistics_on_Waste_statistical_notice_15_12_2015_update_f2.pdf

DEFRA. UK Statistics on Waste. 2015; Available from: https://www.gov.uk/government/uploads/system/uploads/attachment_data/file/487916/UK_Statistics_on_Waste_statistical_notice_15_12_2015_update_f2.pdf.

DEFRA. UK Statistics on Waste. 2015; Available from: https://www.gov.uk/government/uploads/system/uploads/attachment_data/file/487916/UK_Statistics_on_Waste_statistical_notice_15_12_2015_update_f2.pdf.

DEMIRBAS, A., Hazelnut shell to hydrogen-rich gaseous products via catalytic gasification process. Energy sources, 2004. 26(1): p. 25-33.

Demirbas, A., Hydrogen production from carbonaceous solid wastes by steam reforming. Energy Sources, Part A, 2008. 30(10): p. 924-931.

Department for Environment Food and Rural Affairs (DEFRA). 2019. UK Statistics on Waste. https://assets.publishing.service.gov.uk/government/uploads/system/uploads/attachment_data/file/784263/UK_Statistics_on_Waste_statistical_notice_March_2019_rev_FINAL.pdf

Devi, L., K.J. Ptasinski, and F.J. Janssen, A review of the primary measures for tar elimination in biomass gasification processes. Biomass and bioenergy, 2003. 24(2): p. 125-140.

DfT, D., Defra. 2012 UK bioenergy strategy. London, UK: Department of Energy and Climate Change, 2014.

Directive, C., 31/EC of 26 April 1999 on the landfill of waste. Official journal L, 1999. 182(16): p. 07.

Domine, M.E., et al., Hydrogen production from biomass-derived oil over monolithic Pt-and Rh-based catalysts using steam reforming and sequential cracking processes. Catalysis Today, 2008. 133: p. 565-573.

Dou, B., et al., Catalytic cracking of tar component from high-temperature fuel gas. Applied thermal engineering, 2003. 23(17): p. 2229-2239.

Dou, B., et al., Steam reforming of crude glycerol with in situ CO 2 sorption. Bioresource technology, 2010. 101(7): p. 2436-2442.

Dti, U., Meeting the energy challenge: A white paper on energy. Department for Trade and Industry, Cm7124, 2007.

Dufour, A., Girods. P., Masson. E., Rogaume. Y., Zoulalianb. A., 2009. Synthesis gas production by biomass pyrolysis: Effect of reactor temperature on product distribution. International Journal of Hydrogen Energy. 34(4), pp. 1726-1734

Dupont, V., et al., Production of hydrogen by unmixed steam reforming of methane. Chemical Engineering Science, 2008. 63(11): p. 2966-2979.

Elliott, D.C., Analysis and comparison of biomass pyrolysis/gasification condensates: Final report, 1986, Pacific Northwest Lab., Richland, WA (USA).

European Comission Eurostat. Waste generation in EU-28 by type 2016 [cited 2016 28th June]; Available from: https://www.epthinktank.eu/2016/01/07/closing-the-loop-new-circular-economy-package/waste-generation-in-eu-28-by-type-2012/.

Eurostat Statistic, Waste generation by economic activities and households, EU-28, 2016. Available at: https://ec.europa.eu/eurostat/statistics-explained/index.php?title=File:Waste_generation_by_economic_activities_and_households,_EU-28,_2016_(%25).png

Eurostat, E.C. Generation of waste by economic activity and hazardousness (2012). 2012; Available from: http://www.ec.europa.eu/eurostat/tgm/refreshTableAction.do;jsessionid=p4yYpYQPoPG05kjt-OBSIxvpIyAyKuddwaxRQMB_EjyOfjWS3_4k!-518880487?tab=table&plugin=1&pcode=ten00107&language=en.

Fagbemi, L., L. Khezami, and R. Capart, Pyrolysis products from different biomasses: application to the thermal cracking of tar. Applied energy, 2001. 69(4): p. 293-306.

Fahmi, R., et al., The effect of lignin and inorganic species in biomass on pyrolysis oil yields, quality and stability. Fuel, 2008. 87(7): p. 1230-1240.

Fermoso, J., et al., High-pressure co-gasification of coal with biomass and petroleum coke. Fuel Processing Technology, 2009. 90(7): p. 926-932.

Florin, N.H. and A.T. Harris, Enhanced hydrogen production from biomass with in situ carbon dioxide capture using calcium oxide sorbents. Chemical Engineering Science, 2008. 63(2): p. 287-316.

Florin, N.H. and A.T. Harris, Hydrogen production from biomass coupled with carbon dioxide capture: the implications of thermodynamic equilibrium. International Journal of Hydrogen Energy, 2007. 32(17): p. 4119-4134.

Foulds, G.A. Lapszewicz, J.A. Catalysis, The Royal Society of Chemistry, Cambridge, UK, Vol. 11, 1994 (Chapter 10).

Galvagno, S., et al., Steam gasification of tyre waste, poplar, and refuse-derived fuel: A comparative analysis. Waste management, 2009. 29(2): p. 678-689.

Gao, N., A. Li, and C. Quan, A novel reforming method for hydrogen production from biomass steam gasification. Bioresource technology, 2009. 100(18): p. 4271-4277.

Gao, N., et al., Hydrogen-rich gas production from biomass steam gasification in an updraft fixed-bed gasifier combined with a porous ceramic reformer. International journal of hydrogen energy, 2008. 33(20): p. 5430-5438.

Garcia-Perez, M., Shan Wang, X., Shen, J., Rhodes, M.J., Tian, F., Lee, W., Wu, H., and Li, C. 2008. Fast Pyrolysis of Oil Mallee Woody Biomass: Effect of Temperature on the Yield and Quality of Pyrolysis Products. Industrial Engineering and Chemical Research. 47, pp. 1846-1854

Gil, J., et al., Biomass gasification in atmospheric and bubbling fluidized bed: effect of the type of gasifying agent on the product distribution. Biomass and Bioenergy, 1999. 17(5): p. 389-403.

Gil, J., et al., Biomass gasification in fluidized bed at pilot scale with steam-oxygen mixtures. Product distribution for very different operating conditions. Energy & Fuels, 1997. 11(6): p. 1109-1118.

Gómez-Barea, A., R. Arjona, and P. Ollero, Pilot-plant gasification of olive stone: a technical assessment. Energy & fuels, 2005. 19(2): p. 598-605.

González, J., et al., Investigation on the reactions influencing biomass air and air/steam gasification for hydrogen production. Fuel Processing Technology, 2008. 89(8): p. 764-772.

Gordillo, G. and K. Annamalai, Adiabatic fixed bed gasification of dairy biomass with air and steam. Fuel, 2010. 89(2): p. 384-391.

Greenhalf, C., et al., A comparative study of straw, perennial grasses and hardwoods in terms of fast pyrolysis products. Fuel, 2013. 108: p. 216-230.

Greenhalf, C., et al., Sequential pyrolysis of willow SRC at low and high heating rates–Implications for selective pyrolysis. Fuel, 2012. 93: p. 692-702.

Grosso, M., A. Motta, and L. Rigamonti, Efficiency of energy recovery from waste incineration, in the light of the new Waste Framework Directive. Waste Management, 2010. 30(7): p. 1238-1243.

Grosso, M., A. Motta, and L. Rigamonti, Efficiency of energy recovery from waste incineration, in the light of the new Waste Framework Directive. Waste Management, 2010. 30(7): p. 1238-1243.

Guan, Y., et al., Steam catalytic gasification of municipal solid waste for producing tar-free fuel gas. International journal of hydrogen energy, 2009. 34(23): p. 9341-9346.

Guoxin, H. and H. Hao, Hydrogen rich fuel gas production by gasification of wet biomass using a CO 2 sorbent. Biomass and Bioenergy, 2009. 33(5): p. 899-906.

Han, J. and H. Kim, The reduction and control technology of tar during biomass gasification/pyrolysis: an overview. Renewable and Sustainable Energy Reviews, 2008. 12(2): p. 397-416.

Hanaoka, T., Sasaki, H., Sakanishi, K. and Edashige, Y., 2009. Syngas production by woody biomass gasification with a CO_2/O_2 mixture. Journal of the Japan Institute of Energy, 88(10), pp.862-868.

He, M., et al., Hydrogen-rich gas from catalytic steam gasification of municipal solid waste (MSW): Influence of catalyst and temperature on yield and product composition. International Journal of Hydrogen Energy, 2009. 34(1): p. 195-203.

He, M., et al., Syngas production from catalytic gasification of waste polyethylene: influence of temperature on gas yield and composition. International journal of hydrogen energy, 2009. 34(3): p. 1342-1348.

Hernández, J.J., G. Aranda-Almansa, and A. Bula, Gasification of biomass wastes in an entrained flow gasifier: effect of the particle size and the residence time. Fuel Processing Technology, 2010. 91(6): p. 681-692.

Hickman, D.A., Haupfear, E.A. and Schmidt, L.D., 1993. Synthesis gas formation by direct oxidation of methane over Rh monoliths. Catalysis letters, 17(3-4), pp.223-237.

Higman, C. State of the gasification industry: Worldwide Gasification Database 2014 update. in Gasification Technologies Conference. Washington, DC. 2014.

Hu, M., et al., Hydrogen-rich gas production by the gasification of wet MSW (municipal solid waste) coupled with carbon dioxide capture. Energy, 2015. 90: p. 857-863.

Iliuta, I., A. Leclerc, and F. Larachi, Allothermal steam gasification of biomass in cyclic multi-compartment bubbling fluidized-bed gasifier/combustor–New reactor concept. Bioresource technology, 2010. 101(9): p. 3194-3208.

Jamasb, T. and R. Nepal, Issues and options in waste management: A social cost–benefit analysis of waste-to-energy in the UK. Resources, Conservation and Recycling, 2010. 54(12): p. 1341-1352.

Jess, A., Mechanisms and kinetics of thermal reactions of aromatic hydrocarbons from pyrolysis of solid fuels. Fuel, 1996. 75(12): p. 1441-1448.

Kalinci, Y., A. Hepbasli, and I. Dincer, Biomass-based hydrogen production: a review and analysis. International journal of hydrogen energy, 2009. 34(21): p. 8799-8817.

Kamińska-Pietrzak, N., N. Howaniec, and A. Smoliński, The influence of feedstock type and operating parameters on tar formation in the process of gasification and co-gasification. Ecological Chemistry and Engineering S, 2013. 20(4): p. 747-761.

Kan, T., et al., High efficient production of hydrogen from crude bio-oil via an integrative process between gasification and current-enhanced catalytic steam reforming. international journal of hydrogen energy, 2010. 35(2): p. 518-532.

Karagoz, S., Energy production from the pyrolysis of waste biomasses. International Journal of Energy Research, 2009. 33(6): p. 576-581.

Kimura, T., et al., Development of Ni catalysts for tar removal by steam gasification of biomass. Applied Catalysis B: Environmental, 2006. 68(3): p. 160-170.

Kirubakaran, V., et al., A review on gasification of biomass. Renewable and Sustainable Energy Reviews, 2009. 13(1): p. 179-186.

Kirubakaran, V., et al., Studies on auto-gasification of bio-residues. Energy Sources, Part A, 2009. 31(11): p. 967-973.

Knight, R.A., Experience with raw gas analysis from pressurized gasification of biomass. Biomass and Bioenergy, 2000. 18(1): p. 67-77.

Kobayashi, N., et al., High temperature air-blown woody biomass gasification model for the estimation of an entrained down-flow gasifier. Waste management, 2009. 29(1): p. 245-251.

Le Duc Dung, K.M. and T. Takarada, Catalytic Decomposition of Biomass Tars at Low-Temperature. 2013.

Letichevsky, S, Tellez, CA, de Avillez, RR, da Silva, MIP, Fraga, MA and Appel, LG. 2005. Obtaining CeO2–ZrO2 mixed oxides by coprecipitation: role of preparation conditions. Applied Catalysis B: Environmental. 58(3-4), pp 203-210.

Li, J., et al., Hydrogen-rich gas production by steam gasification of palm oil wastes over supported tri-metallic catalyst. International Journal of Hydrogen Energy, 2009. 34(22): p. 9108-9115.

Lu, H., et al., Effects of particle shape and size on devolatilization of biomass particle. Fuel, 2010. 89(5): p. 1156-1168.

Luo, S., et al., Effect of particle size on pyrolysis of single-component municipal solid waste in fixed bed reactor. International Journal of Hydrogen Energy, 2010. 35(1): p. 93-97.

Luo, S., et al., Hydrogen-rich gas from catalytic steam gasification of biomass in a fixed bed reactor: influence of particle size on gasification performance. International Journal of Hydrogen Energy, 2009. 34(3): p. 1260-1264.

Mahishi, M.R. and Goswami, D.Y., 2007. An experimental study of hydrogen production by gasification of biomass in the presence of a CO_2 sorbent. International Journal of Hydrogen Energy, 32(14), pp.2803-2808.

Maniatis, K. and A. Beenackers, Tar protocols. IEA bioenergy gasification task. Biomass and Bioenergy, 2000. 18(1): p. 1-4.

Maroño, M., J. Sánchez, and E. Ruiz, Hydrogen-rich gas production from oxygen pressurized gasification of biomass using a Fe–Cr water gas shift catalyst. international journal of hydrogen energy, 2010. 35(1): p. 37-45.

McKendry, P., Energy production from biomass (part 3): gasification technologies. Bioresource technology, 2002. 83(1): p. 55-63.

Milne, T.A., Elam, C.C. and Evans, R.J., 2002. Hydrogen from biomass: state of the art and research challenges (No. IEA/H2-TR-02/001). National Renewable Energy Lab., Golden, CO (US).

Miyazawa, T., et al., Catalytic performance of supported Ni catalysts in partial oxidation and steam reforming of tar derived from the pyrolysis of wood biomass. Catalysis Today, 2006. 115(1): p. 254-262.

Mohan, D., C.U. Pittman, and P.H. Steele, Pyrolysis of wood/biomass for bio-oil: a critical review. Energy & fuels, 2006. 20(3): p. 848-889.

Neeft, J., H. Knoef, and P. Onaji, Behavior of tars in biomass gasification systems, Novem EWAB programme report 9919. Novem, Maarn (The Netherlands), 1999.

Ono, A., et al., Evaluation of waste pyrolysis characteristics in a pressurized fluidized bed reactor. Waste Management, 2001. 21(5): p. 451-456.

Panepinto, D., et al., Environmental performances and energy efficiency for MSW gasification treatment. Waste and Biomass Valorization, 2015. 6(1): p. 123-135.

Părpăriţă, E., et al., Pyrolysis behaviors of various biomasses. Polymer Degradation and Stability, 2014. 100: p. 1-9.

Pasel, C. and W. Wanzl, Experimental investigations on reactor scale-up and optimisation of product quality in pyrolysis of shredder waste. Fuel Processing Technology, 2003. 80(1): p. 47-67.

Phuphuakrat, T., et al., Characterization of tar content in the syngas produced in a downdraft type fixed bed gasification system from dried sewage sludge. Fuel, 2010. 89(9): p. 2278-2284.

Pober, K.W. and H.F. Bauer, The nature of pyrolytic oil from municipal solid waste. Fuels from waste, 1977. 1: p. 73-85.

Ponzio, A., S. Kalisz, and W. Blasiak, Effect of operating conditions on tar and gas composition in high temperature air/steam gasification (HTAG) of plastic containing waste. Fuel Processing Technology, 2006. 87(3): p. 223-233.

Price, J.L., The landfill directive and the challenge ahead: demands and pressures on the UK householder. Resources, Conservation and recycling, 2001. 32(3): p. 333-348.

Qin, Y., et al., Characterization of tar from sawdust gasified in the pressurized fluidized bed. Biomass and Bioenergy, 2007. 31(4): p. 243-249.

Renewable Energy Association (REA). 2018. Waste to Energy: Information on Waste to Energy. Available at: https://www.r-e-a.net/renewable-technologies/energy-from-waste

Sheth, P.N. and B. Babu, Production of hydrogen energy through biomass (waste wood) gasification. International Journal of Hydrogen Energy, 2010. 35(19): p. 10803-10810.

Skoulou, V., et al., Process characteristics and products of olive kernel high temperature steam gasification (HTSG). Bioresource technology, 2009. 100(8): p. 2444-2451.

Strategy, W., for England and Wales. CM4693-1. DETR: London, 2000.

Sun, S., et al., Experimental and numerical study of biomass flash pyrolysis in an entrained flow reactor. Bioresource technology, 2010. 101(10): p. 3678-3684.

Sun, S., et al., Experimental study on cyclone air gasification of wood powder. Bioresource technology, 2009. 100(17): p. 4047-4049.

Tomishige, K., M. Asadullah, and K. Kunimori, Syngas production by biomass gasification using Rh/CeO 2/SiO 2 catalysts and fluidized bed reactor. Catalysis Today, 2004. 89(4): p. 389-403.

Umeki, K., et al., High temperature steam-only gasification of woody biomass. Applied energy, 2010. 87(3): p. 791-798.

Valin, S., et al., Comprehensive study of the influence of total pressure on products yields in fluidized bed gasification of wood sawdust. Fuel Processing Technology, 2010. 91(10): p. 1222-1228.

Van Paasen, S., J. Kiel, and H. Veringa, Tar formation in a fluidised bed gasifier. Impact of fuel properties and operating conditions, 2004.

Wang, J., et al., Hydrogen-rich gas production by steam gasification of municipal solid waste (MSW) using NiO supported on modified dolomite. international journal of hydrogen energy, 2012. 37(8): p. 6503-6510.

Wang, T., et al., Reforming of raw fuel gas from biomass gasification to syngas over highly stable nickel–magnesium solid solution catalysts. Fuel Processing Technology, 2006. 87(5): p. 421-428.

Warnecke, R., Gasification of biomass: comparison of fixed bed and fluidized bed gasifier. Biomass and Bioenergy, 2000. 18(6): p. 489-497.

WASTE TO ENERGY; A Technical Review of Municipal Solid Waste Thermal Treatment Practices, 2010.

Williams, P.T. and S. Besler, Polycyclic aromatic hydrocarbons in waste derived pyrolytic oils. Journal of Analytical and Applied pyrolysis, 1994. 30(1): p. 17-33.

Williams, P.T., Waste treatment and disposal.2005: John Wiley & Sons.

WRAP, Wood Waste Market in the UK, 2009: Pöyry Forest Industry Consulting Ltd and Oxford Economics Ltd.

Wu, C. and P.T. Williams, Hydrogen Production from the Pyrolysis− Gasification of Polypropylene: Influence of Steam Flow Rate, Carrier Gas Flow Rate and Gasification Temperature. Energy & Fuels, 2009. 23(10): p. 5055-5061.

Wu, C., et al., Hydrogen production via catalytic steam reforming of fast pyrolysis bio-oil in a two-stage fixed bed reactor system. Fuel Processing Technology, 2008. 89(12): p. 1306-1316.

Xiao, R., et al., Air gasification of polypropylene plastic waste in fluidized bed gasifier. Energy Conversion and Management, 2007. 48(3): p. 778-786.

Yan, F., et al., Hydrogen-rich gas production by steam gasification of char from biomass fast pyrolysis in a fixed-bed reactor: Influence of temperature and steam on hydrogen yield and syngas composition. Bioresource Technology, 2010. 101(14): p. 5633-5637.

Yanik, J., et al., Pyrolysis of algal biomass. Journal of Analytical and Applied Pyrolysis, 2013. 103: p. 134-141.

Zhang, L., C.C. Xu, and P. Champagne, Overview of recent advances in thermo-chemical conversion of biomass. Energy Conversion and Management, 2010. 51(5): p. 969-982.

Zhang, Q., et al., Review of biomass pyrolysis oil properties and upgrading research. Energy conversion and management, 2007. 48(1): p. 87-92.

Zhao, Y., et al., Experimental study on sawdust air gasification in an entrained-flow reactor. Fuel Processing Technology, 2010. 91(8): p. 910-914.

Zhou, J., et al., Biomass–oxygen gasification in a high-temperature entrained-flow gasifier. Biotechnology advances, 2009. 27(5): p. 606-611.

Chapter 3: Experimental

3.1 Introduction

There are three main sections which compose the experimental part of this research:

- The first section, presented in chapter 4, involved the preparation of a two-stage pyrolysis reactor. The reactor and methodology were initially tested to ensure that results obtained were suitable and repeatable. All pyrolysis products were collected, ensuring mass balances were as close to 100% as practically possible. This section allowed for the production of hydrogen from raw biomass based on the two-stage process described later in this chapter then a three-stage process. The test experiments also allowed for the development of analytical methodologies although these were further developed throughout the research. Once the reactor was fully prepared, the initial experimental section examined the pyrolysis of wood pellets to produce pyrolysis gases, followed by catalytic steam reforming (CSR) and water-gas-shift (WGS) reactions in a fixed bed reactor. Emphasis is placed on the catalytic steam reforming (CSR) stage to investigate the optimum nickel catalyst for optimising hydrogen yield.
- The second section presented in chapter 5 investigated the influence of metal catalysts types and process parameters in the third stage of the water-gas shift (WGS) reaction. The catalytic performance of different metals (Co, Cu, Zn, Mn, Fe) on Alumina (Al_2O_3) catalysts with respect to activity and selectivity at a constant metal loading of 40% were studied. Empirical evidence of high activity shifted emphasis to Iron (Fe) coated on alumina support catalyst. Therefore, the effect of metal loading of this catalyst was considered by varying the metal loading from 5 % to 100 %. Another critical process parameter that was studied is the effect of steam flowrate on the gas yield, hydrogen yield and coke formation, testing the steam to carbon ratio at 1:1, 1:2, 1:4 and 1:8. The reacted catalysts for each experiment were characterised by temperature-programmed oxidation (TPO) to investigate the coke amount deposited over the catalyst which reflects the potential for catalysts deactivation. The experimental procedure detailed in chapter 3 was used for all experiments.

- The third section presented in chapter 6 investigated the effect of adding reduced 10% nickel supported on alumina in the catalytic steam reforming (CSR) stage with no catalyst at the water gas shift stage. This was investigated in order to determine the influence on hydrogen production. The third section also investigated the influence of adding CaO at states (reduced or unreduced) and different metal loadings to enhance water gas shift reaction performance. The impact of this on the CO/CO_2 ratio, and CO_2 absorption was elucidated. Finally, the third section looked at the reacted catalysts being subjected to different characterisation techniques; Temperature Programmed Oxidation and X-ray diffraction (XRD) so as to investigate the type and extent of carbon depositions on the reacted catalysts.

Figure 3-1: Photograph of the biomass sample.

3.2 Biomass

The biomass sample used was a mixed source wood pellet supplied by Liverpool Wood Pellets (Liverpool wood pellets 2019), a company which manufactures wood pellets from the UK sourced virgin wood off cuts from North America, and these pellets are equivalent to those that would be used in a domestic heating system. Figure 3-1 shows photographs of the biomass before they were prepared for analysis or pyrolysis experiments. The biomass material was in a homogenous, pelletized form.

3.3 Sample preparation

The biomass samples were received in pellet form and were then prepared for pyrolysis or material analysis. The Biomass was prepared using coning and quartering from 1kilo of biomass sample to make sure they are uniform and the same. The biomass pellets were approximately 10mm by 5mm by 5mm and were prepared for the pyrolysis experiments using a cutting mill to produce a homogenous woodchip which was passed through a multiple sieve system to collect a sample between 2.8mm and 1.0mm in size. Thermogravimetric Analysis (TGA) analysis was undertaken to gain insight into the thermal degradation of the biomass samples prior to starting experiments using the pyrolysis reactor.

3.4 Proximate and ultimate analysis

Proximate and ultimate analysis was used to determine the composition of the pyrolysis samples. The proximate analysis used a furnace to devolatilize and combust samples according to set standards to determine the relative proportion of char, ash, volatile gases and moisture which are formed by thermal decomposition of the samples under standard test conditions. The procedure used followed standards which were developed for use with biomass. The procedure requires samples to be milled to smaller than 1000 µm, after which three methods were used for the analysis.

Moisture content was determined according to standard BS EN 14774-3:2009. This involves heating the sample for 2 hours in a furnace at a fixed temperature of 105°C. A pre-dried and pre-weighed glass vessel with a lid was used for this method in accordance with the standard. The lid was heated in the oven with the vessel throughout the procedure as was then placed onto the vessel immediately on removal from the furnace to prevent moisture returning to the sample during cooling. The weight of the vessel and the remaining sample was determined using a balance and the moisture content determined as the change in sample mass between the original sample and the sample after the drying process.

Volatile content was determined using the standard BS EN 15148:2009. A pre-dried sample was heated in a furnace fixed at 900°C for 7 mins in a pre-dried and pre-weighed silica crucible with a lid which remained on the vessel throughout the procedure. Once the sample was removed from the furnace, it was allowed to cool before being weighed on a balance. The mass change between the initial sample and the sample post-heating is due to loss of volatiles from the sample.

Ash content was measured in accordance with the standard BS EN 14775:2009. Each sample was heated in a furnace in an inert shallow flat-based silica dish with the temperature of the furnace ramping from room temperature through to 250°C at a heating rate of approximately 5°Cmin^{-1}. After this temperature was reached, the furnace remained at 250°C for 60 mins before a further heating stage from 250°C through to 550°C at a rate of 10°Cmin^{-1}. This temperature was held for 120 mins. This was undertaken in a furnace with adequate oxygen supply for all carbon material to be completely combusted.

The fixed carbon content of the samples was determined using the formula below

$$\%wtFC = 100 - \&wtM - \%wtVM - \%wtAsh \tag{3.1}$$

(Bridgeman et al. 2010)

The determination of the percentage of constituent elements of a chemical substance by weight components of Carbon, Hydrogen, Nitrogen and Sulphur in the biomass sample was measured via Ultimate or Elemental Analysis, (CHNS) according to the standard BS EN 15104:2011 (1993) using a Thermo EA-2000. This involved combusting a known quantity of sample, in a tin capsule, in the presence of a predetermined quantity of an oxidising agent, in this case, vanadium pentoxide (V_2O_5). The combustion at 1000°C causes oxidation of all present carbon, nitrogen and sulphur atoms into CO_2, NO_2 and SO_2. The NO_2 is reduced to N_2 in a secondary reaction step, and the three gases are separated through a gas chromatograph (GC) column and passed across a thermal conductivity detector (TCD) using an inert carrier gas (Helium) at which point they are quantified. Standards are analysed alongside the unknown samples to confirm that the analysis is providing accurate values. In this case, repeated measurement of oatmeal and BBOT (2,5-Bis(5-tert-butylbenzoxazol-2-yl) thiophene) were used as standards alongside an empty tin capsule, and blank samples with barley flour were analysed after every eighth unknown sample to confirm that the values remained consistent.

The high heating value of all the samples was calculated on a dry basis using the formula below.

$$HHV\ (MJKg^{-1}) = \frac{3.55C^2\ - 232C - 2230H + 51.2(C\ \times H) + 131N\ + 20{,}600}{1000} \qquad 3.2$$

(Bridgeman et al. 2010)

The oxygen content was calculated by difference.

3.4.1 Biomass composition

Table 3-1: Proximate Analysis Biomass

PROXIMATE ANALYSIS BIOMASS			
Component	**As Received (%)**	**Dry (%)**	**Dry Ash Free (%)**
Moisture	6.73	-	-
Volatiles	79.24	84.96	85.72
Ash	0.760	0.89	-
Carbon	13.27	14.15	14.28

The biomass material contained a relatively low ash and moisture content, as seen in table 3-1 and table 3-2. These values were compared to the Phyllis database to get a baseline

Table 3-2: Ultimate Analysis for Biomass

ULTIMATE ANALYSIS BIOMASS		
Component	**As Received (%)**	**Dry (%)**
Moisture	6.73	-
Carbon	45.96	49.28
Hydrogen	5.30	5.68
Nitrogen	0	0

Sulphur	0	0
Ash	0.76	0.82
Oxygen	41.25	44.22
Total	100	100
Heating Value MJ/kg [Friedl et al.2005]	18.15	19.45

TGA was also used to provide further elucidation of the manner in which the material undergoes devolatilisation in an oxygen-free atmosphere comparable with pyrolysis.

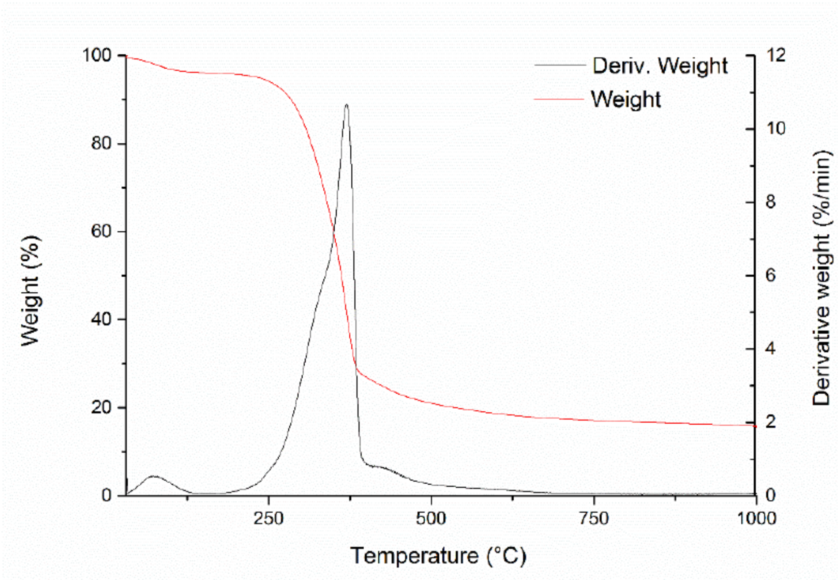

Figure 3-2: TGA and DTG showing devolatilisation of biomass sample heated from room temperature to 1000°C at 10°C/ min in a nitrogen atmosphere.

The TGA was undertaken using a TA TGA Q5000 IR with the sample heated from room temperature through to 1000°C at a ramping rate of 10°Cmin^{-1} in a nitrogen atmosphere flowing at a rate of 10mlmin^{-1}. The prepared sample (~25mg) was placed in a pre-weighed and tared platinum pan which remains inert high temperatures. A data point was collected every 0.1s during heating. The weight change and differential weight change gave vital information about the devolatilization process and the rate at which the biomass decomposes. The TGA provided vital information with regards to the composition of the biomass sample. This informed the maximum temperature used in the pyrolysis stage (550°C). This temperature ensured that all the volatiles were evolved, and complete decomposition of the biomass was ensured.

Table 3-1 and 3-2 shows that the sample contains approximately 7 wt.% moisture. Guedes et al (2018). found that in general, a higher heating rate and higher maximum temperature will both lead to more volatile and therefore less fixed carbon.

The ash content is low at just 0.76 wt.% while elemental analysis of the biomass sample puts carbon at 46 wt.%, hydrogen at 5 wt.% and oxygen at 41 wt.% with nitrogen at 0 wt.%. This provides all the elements necessary for hydrocarbon bio-gas production.

The TGA results initially showed a weight loss below 100°C which is associated with moisture being evaporated from the sample. At approximately 250°C, there is a reduction in the sample weight, this reduction in sample weight continues until approximately 400°C, as seen in figure 3-2. Most of the weight change is concluded by around 500°C.

These are some thermochemical processes that are solely responsible for biomass weight loss. The significant weight loss between 250°C and 400°C is due to the thermal decomposition of cellulose and thermal degradation of hemicellulose. Hemi-cellulose is similar in composition to cellulose, but hemicellulose degrades at a slightly lower temperature. Between 400°C and 500°C, the major weight loss is due to lignin decomposition which occurs over a broader temperature range than either hemicellulose or cellulose. (Di Blasi 2008, Burhenne et al., 2013)

Once a temperature of 500°C is reached there remains approximately 20 wt.% of the original material which indicates that pyrolysis experiments using a similar heating profile are likely also to produce around 20 wt.% char yield. This is consistent with the char yield of the experimental results ranging between 20 – 25 wt.%

3.4.2 Catalyst Development

Since the selection of catalyst is one of the most critical parameters in the thermochemical production of hydrogen, special attention must be paid to its preparation. The different types of catalysts utilised in this study were supported on alumina and were synthesised in the University of Leeds laboratories. Alumina was purchased from Sigma Aldrich having the surface area of 7.62 m^2g^{-1}. Impregnation method was used in the catalyst synthesis throughout the study; this preparation method is based on the one used by Li, et al. (2006) and the general method is depicted in Figure 3-3.

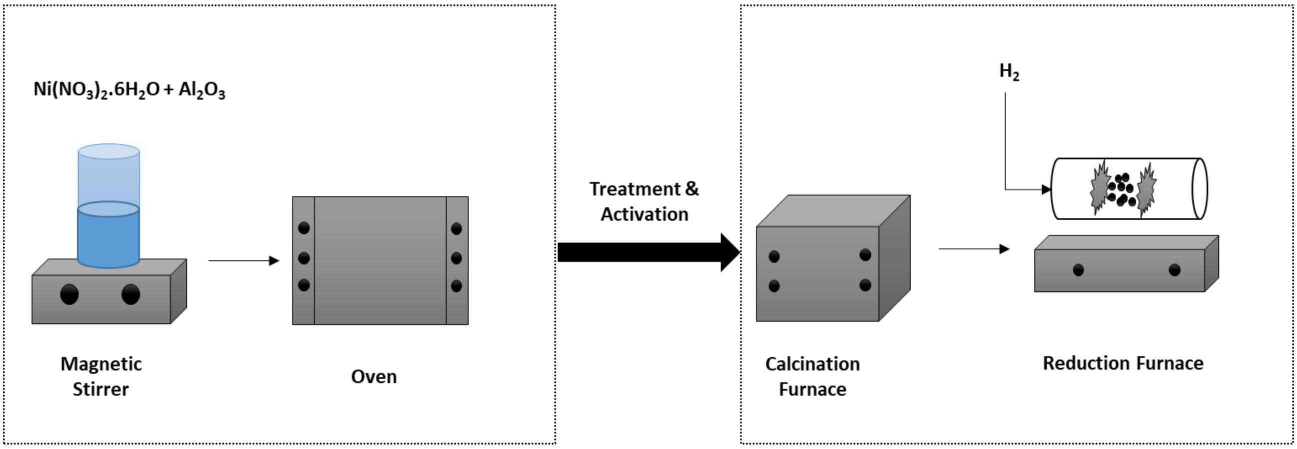

Figure 3-3: General procedure for the catalyst preparation method by impregnation.

3.4.3 X_A/Al_2O_3 catalysts preparation

All the catalysts used for steam reforming and water gas shift reaction were prepared by wet impregnation method. 10 wt% nickel on alumina support was used consistently throughout each investigation. For the first investigation in section 4.1, cobalt, copper, iron, zinc and manganese were all prepared as catalysts for the third stage. Again, alumina was used as the support for the catalyst. In each case, the metal being tested were made up 40 wt% of the total mass of the catalyst. In the first stage of the catalyst synthesis, solutions were produced by dissolving a known amount of metal salt in deionised water. The salts used to produce each catalyst and related data can be found in the tables 3-2 and 3-3 below. In order to calculate the amount required, the following equation was used. A sample calculation has been provided below for 10 grams of iron.

$$Mass\ of\ salt = \frac{Molecular\ mass\ of\ salt}{molecular\ mass\ of\ metal}\ X\ desired\ mass\ of\ metal \quad \text{(E.3.3)}$$

$$Mass\ of\ salt\ required = \frac{404.0}{55.8} X\ 100 = 72.4\ grams. \qquad \text{(E.3.4)}$$

Table 3-3: Metal salts used in catalyst synthesis as well as their chemical formulas.

Metal (X_A)	Name of Salt	Salt Chemical Formula
Cobalt	Cobalt(II) nitrate hexa-hydrate	$Co(NO_3)_2·6H_2O$
Copper	Copper(II) nitrate penta-hydrate	$Cu(NO_3)_2·5H_2O$
Iron	Iron(II) nitrate nona-hydrate	$Fe(NO_3)_2·9H_2O$
Zinc	Zinc(II) nitrate hexa-hydrate	$Zn(NO_3)_2·6H_2O$
Manganese	Manganese(II) nitrate tetra-hydrate	$Mn(NO_3)_2·4H_2O$

Table 3-4: Molecular mass of metals and their salts used in mass calculations.

Metal	Molecular Mass of Metal (kg/mol)	Molecular Mass of Salt (kg/mol)
Cobalt	58.9	291.0
Copper	63.5	232.6
Iron	55.8	404.0
Zinc	65.4	297.5
Manganese	54.9	251.0

Once fully dissolved, a suspension was formed through the addition of the alumina support in an appropriate amount depending on the desired weight per cent of metal. For example, to make 4g Fe^{2+} or 4g $Fe(NO_3)_2·9H_2O$, 6 grams of support would be added to a solution containing 4 grams of dissolved iron. Prior to adding the support, it was ground down to achieve an average particle size of between 50 and 212 microns. The suspensions were then placed in a fume cupboard where they were gently heated to remove some of the excess water. During this process, the suspensions are continuously mixed on a magnetic hotplate stirrer. This is will not only enhance the evaporation of water but also promote excellent diffusion of the metals on the alumina support. Care was taken to avoid rapid evaporation or excessive turbidity in the mixing system as this could result in the loss of iron and, or, support which could alter the weight percentages of the catalysts produced.

Once the suspensions had formed a sol, the impregnated samples were then calcined at 850°C for approximately one hour in an oxygen atmosphere with a flow rate of 60 ml min^{-1}. Defined as the 'thermal treatment of a catalyst in an oxidising atmosphere,' calcination is most commonly undertaken at a temperature slightly above that of the system operating temperature (Jentoft, 2003). Numerous research papers, including those by Ramu et al. (2004), Lopez et al. (2007) and Wongmaneenil et al. (2009), have shown that the temperature at which calcination is conducted is a critical factor in catalyst synthesis. In addition to this, research by Nayebzabeh et al. (2013) showed that catalyst activity is greatly affected by calcination temperature.

The metal ions contained within the solid catalysts were then reduced to the active phase for 4 hours in a hydrogen flow of 150 ml min^{-1} at a temperature of 800°C. Once sufficiently reduced, the catalyst particles were decreased in size by grinding and sieved to obtain particle diameters of between 50-212 microns. In terms of the iron catalysts examined in the second investigation, the same synthesis methodology was used, however, the amount of iron-containing salt added during the first step of the technique was varied and the amount of alumina support added was increased to produce catalysts of 5, 20, 40 and 100 wt.% iron.

3.4.4. CaO/Al$_2$O$_3$ Catalyst Preparation

This Catalyst will help produce more hydrogen using the water gas shift (WGS) stage in addition to the steam reforming (SR) stage.

This catalyst will be used in the water gas shift (WGS) stage. This catalyst aims to adsorb CO$_2$ using the presence of:

$$CO + H_2O \rightarrow CO_2 + H_2 \qquad (E.3.5)$$

CaO will adsorb CO$_2$ from the water gas shift equation as seen in the equation above and released heat:

$$CaO + CO_2 \rightarrow CaCO_3 \qquad (E.3.6)$$

All the catalysts were prepared by the impregnation of the metals and the calcium oxide on alumina support Al$_2$O$_3$.

For the catalysts, the Al$_2$O$_3$ support and the nickel, iron or calcium oxide nitrates (depending on the planned catalyst) were mixed in 50ml of deionised water and stirred at 80°C to get a semi-solid. Then the semi-solids were dried at 100°C in an oven during the night, to be then calcinated at 750°C for 3 hours. The salts used for the impregnation of nickel, iron and calcium oxide were $Ni(NO_3)_2 \bullet 6H_2O$ (4.9547g for one gram of Ni), $Fe(NO_3)_3 \bullet 9H_2O$ (7.234g for one gram of Fe) and $Ca(NO_3)_2 \bullet 4H_2O$ (4.217g for one gram of CaO) respectively. The powder was sieved to obtain a particle size between 50 to 212 µm. Some of the catalysts were reduced. The catalysts are identified by the weight percentage of the metal or calcium oxide, followed by the compound formula and the support at the end, which was Al for all of them, e.g. $10Fe_{20}CaOAl$, 10 wt.% iron content, 20 wt.% calcium oxide content and the resting 70 wt.% alumina content.

The same catalyst, 10 wt% NiAl was constantly used in the steam reforming (SR) stage across the different experiements. The catalysts for the water-gas shift (WGS) stage were CaO in different weight percentages with alumina support and CaO with added Fe in different proportions with alumina support.

In addition to the steam gasification of biomass, in the presence of a calcium oxide (CaO) sorbent for carbon dioxide capture, is an innovative pathway to improve H_2 (Lin et al. 2005, Dou et al. 2010)

Previous research has shown Fe to be a suitable catalyst for water gas shift reactions, but by adding CaO to Fe, the adsorption of CO_2 can simultaneously occur while the water gas shift reaction is taking place. Fe to enhance water gas shift while CaO for CO_2 adsorption.

3.5 Reactor Systems

3.5.1 Design of a two-stage fixed-bed reactor System

The pyrolysis and the catalytic steam reforming were carried out in the 2-stage fixed bed reactor. Schematic diagram of the 2-stage fixed bed reactor is shown in Figure 3-4. Both the stages of the reactor were made of stainless steel. Biomass sample was placed in the 1st stage of the reactor in the boat crucible. While the catalyst was placed in the centre of the 2nd stage on the quartz wool. Quartz wool was kept in place by putting a stainless-steel mesh under it. 2 separate furnaces controlled the temperature in both the stages of the reactor. To monitor the temperature; thermocouples were provided in both the stages. Steam was injected directly in the second stage of the reactor through a stainless-steel pipe using a water syringe pump.

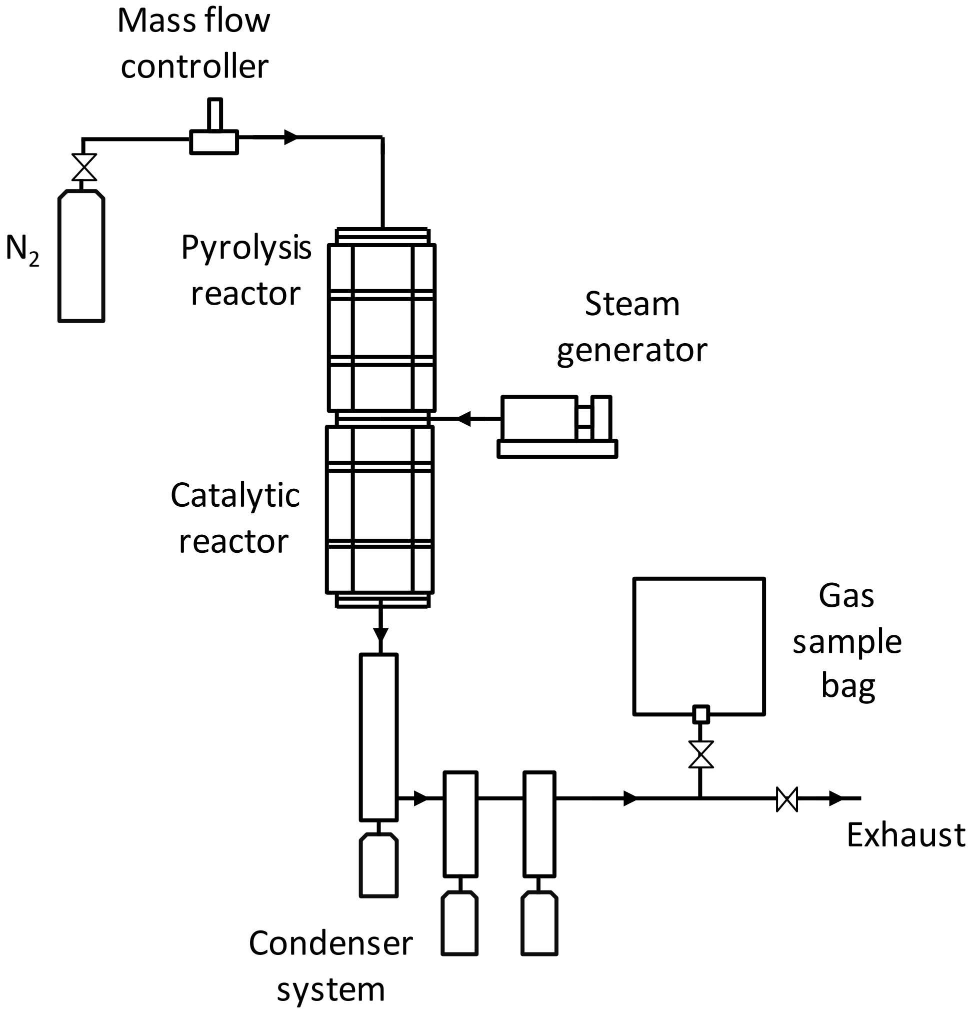

Figure 3-4: Schematic Diagram of the 2-stage fixed bed reactor

Figure 3-4 and Figure 3-5 depicts a schematic diagram and a photograph respectively of the 2-stage Fixed Bed Reactor to be used for the experiments. This reactor went through a recommisioning phase.

Figure 3-5: 2-stage fixed bed reactor for pyrolysis catalysis/catalytic steam reforming experiments: (A) pyrolysis reactor, (B) catalysis/reforming reactor, (C) condensers, (D) water pump for steam injection, (E) reactor temperature control equipment, (F) gas flow meter and (G) thermocouple temperature displays (H) temperature controllers.

3.5.2 Parameters for the experiments based on literature and commissioning trials

These are the constant parameters for the operating conditions throughout all the experiments involving 2-stage fixed bed reactor system, with some exceptions, and these are specified in Table 3-5

Table 3-5: Constant parameters in the experiments

Parameter	Value	Units
Temperature in the 1st stage (Biomass Pyrolysis) (HTT)	550	°C
Heating rate in the 1st stage (Biomass Pyrolysis)	20	°C/min
Temperature in the 2nd stage (CSR)	850	°C
N_2 flow rate	100	ml/min
Steam Flow Rate in the 2nd stage (CSR)[a]	6.64	ml/hr
Gas collection time after rig shut down.	20	min
Biomass mass	2	g
Catalyst weight in the 2nd stage (CSR)	1	g

3.5.3 Procedure of the Experiment involving two-stage reactors

Before running any experiment, the rig and the parameters were set up, and the process consists of the following:

In procedure initially, the reactor was appropriately cleaned and all the traces from the last experiment were removed. After cleaning, the feed (wood pellets) was weighed accurately and placed in the boat, and the catalyst after weighing was dispersed on the quartz wool. After hanging the boat in the first stage of the reactor and dispersing the catalyst in the 2nd stage of the reactor was appropriately closed with nuts and bolts to prevent the entering of air inside the reactor. The reactor was then placed between the furnace and attached the bottom of the reactor to the already weighed dry ice-condensers. After setting up the reactor, N_2 at a fixed flow rate was allowed to pass through the reactor for 5 min to remove the air present inside the reactor. After N_2 purging, the 2nd stage containing catalyst bed was preheated up to the required temperature. Once the required temperature was achieved and stabilised, the first-stage furnace was heated up to the particular temperature, and steam was injected via water pump directly in the 2nd stage of the reactor to promote the reforming reaction. All the gases were collected directly in the Tedlar**TM** gas sample bag and analysed with offline GCs.

3.5.4 The design and reproducibility of products with three stages fixed-bed reactor

A novel reactor was developed to enhance the hydrogen yield. This reactor involved the 3 stages of the reactor. Each stage was provided with a separated furnace to control the temperature. In order to monitor the temperature, each stage was also provided with a separate thermocouple. Biomass pyrolysis took place in the first stage of the reactor; therefore boat was hung into the first stage of the reactor. While in the 2nd and 3rd stage of particular reactor reactions were promoted to increase the H_2 yield. Mesh was placed in the 2nd and 3rd stage of the reactor to place the catalyst. Also, the 2nd and 3rd stage of the reactor was equipped with 2 separate water pumps. The output of the 3rd stage of the reactor was connected to the condenser to condense the higher hydrocarbons produced during the process.

Figure 3-6 and Figure 3-7 depicts a schematic diagram and a photograph, respectively of the 3-stage Fixed Bed Reactor used for the experiments.

A novel extension to the 2nd stage is the furnace that enhances hydrogen production from carbon monoxide using a water gas shift

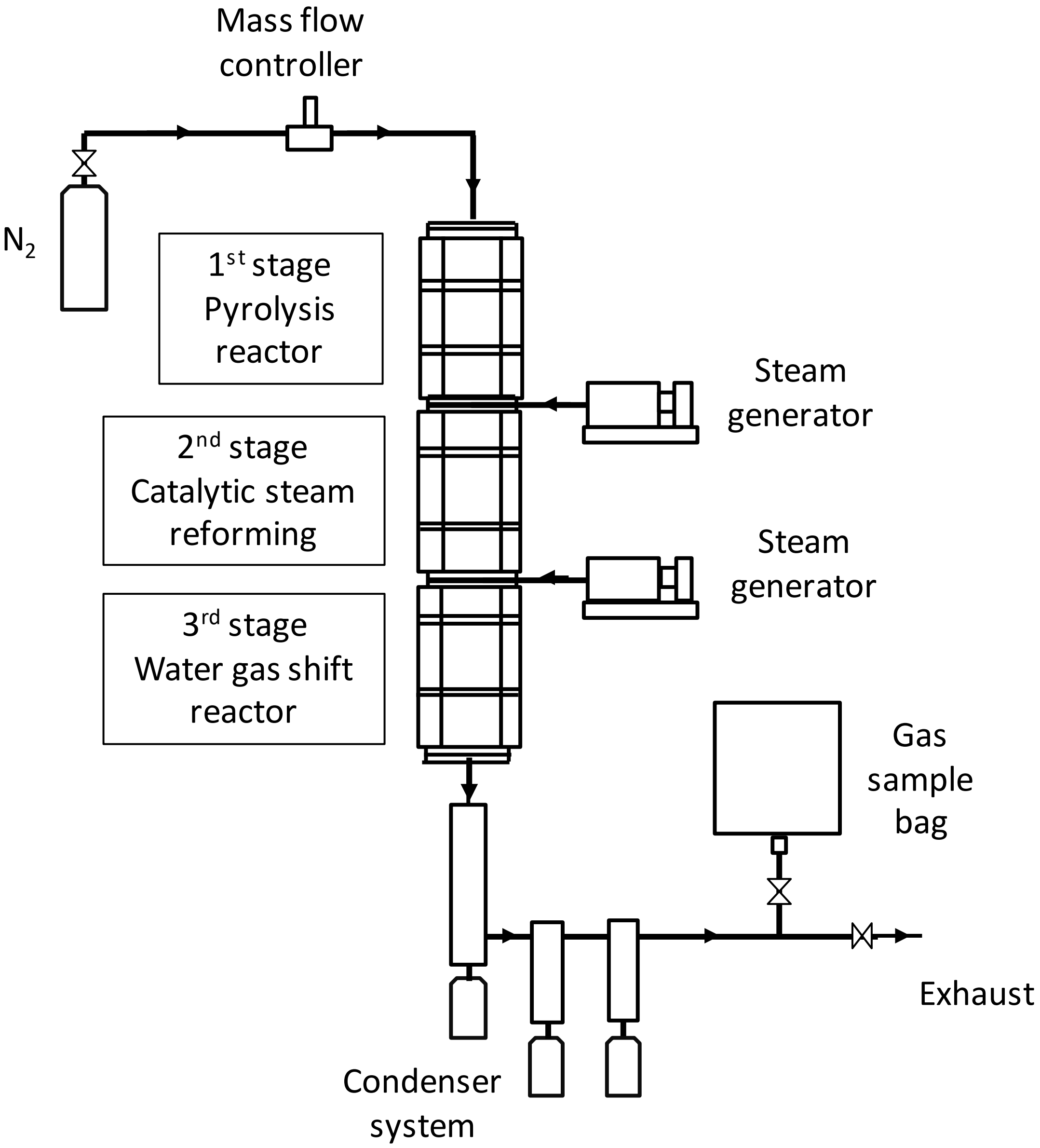

Figure 3-6:Schematic Diagram of the 3-stage fixed bed reactor

Figure 3-7: 3-stage fixed bed reactor for pyrolysis catalysis/catalytic water gas shift experiments: (A) pyrolysis reactor, (B) catalysis/reforming reactor, (C) water gas shift reforming reactor (D) condensers, (E) water pump for steam injection, (F) reactor temperature control equipment, (G) gas flow meter and (H) thermocouple temperature displays (J) timer (K) gas sampling bag

3.5.5 Parameters for the experiments

There are some conditions which remained constant throughout all the experiments, with some exceptions, and these are specified in Table 3-6

Table 3-6: Constant parameters in the experiments.

Parameter	Value	Units
Temperature in the 1st stage (Biomass Pyrolysis) (HTT)	550	°C
Heating rate in the 1st stage (Biomass Pyrolysis)	20	°C/min
Temperature in the 2nd stage (CSR)	850	°C
Temperature in the 3rd stage (WGS reaction)	350	°C
N_2 flow rate	100	ml/min
Steam Flow Rate in the 2nd stage (CSR)[a]	6.64	ml/hr
Steam Flow Rate in the 3rd stage (WGS reaction)[a]	1.80	ml/hr
Time to reach HTT	30	min
Residence time of biomass at HTT	20	min
Gas collection time after rig shut down.	20	min
Biomass mass	2	g
Catalyst weight in the 2nd stage (CSR)	1	g
Catalyst weight in the 3rd stage (WGS reaction)	0.5	g

The parameters that were mostly explored in the experiments were; the catalyst compositions, metal loading, and steam flow rate. This is due to the fact that these parameters from research and trials have shown the greatest affinity to enhancing hydrogen production from the experimental process.

3.5.6 Running the experiment

In the procedure to operate a 3-stage fixed bed reactor, the reactor was cleaned first to remove all the impurities from the last experiment. Biomass was then weighed accurately and placed in the boat. Quartz wool in the 2nd and 3rd stage was placed over the mesh in order to prevent the catalyst from falling. Catalysts for the 2nd and 3rd stage was then weighed accurately and dispersed over the quartz wool. The reactor was then tightened up properly in order to prevent the leakage and then placed between the furnaces. Bottom of the 3rd stage of the reactor was then connected to dry ice-cooled condensers. All these 3 stages were provided with the thermocouple in order to monitor the temperature. Both the 2nd and 3rd stage of the reactor was fitted with the steam pumps to promote the steam reforming reaction in the 2nd stage and water gas shift reaction in the 3rd stage of the reactor.

To perform the experiments in the novel 3-stage fixed bed reactor, N_2 at a fixed flow rate was allowed to pass through the reactor to purge the reactor. Then the temperature in the 2nd and 3rd stage was raised initially. Once the operating temperature in the 2nd and 3rd stage were reached, the 1st stage furnace and steam injections were turned on simultaneously. Schematic diagram of the process is shown in Figure 3-7

3.5.7 Validation of the fixed bed reactor

As a way of validating the experimental fixed reactor-bed system, preliminary tests were carried out three times for fast pyrolysis, catalytic steam reforming and water gas shift reaction at the temperature of 550^0C, 850^0C and 350^0C respectively. 2 g of wood pellets biomass was pyrolysed in the top stage as feedstock, no catalyst was added, and no steam was introduced in the repeat experiments.

The data displayed in Table 3-7 reveals the validation of the experimental fixed bed reactor system. The repeatability is excellent with low standard deviation, especially with respect to char yield. The char yield was between 7.30 wt.% to 7.34 wt.% with a mean of 7.31 wt.% and a standard deviation of 0.02. The gas yield also has a very low standard deviation. From all the above, the standard deviation for all products was less than 2% of the mean value which indicate the acceptable repeatability for the process conditions. In addition to this, in order to maintain this level of high accuracy of data, numerous experimental repetitions were carried out at regular intervals within the course of this research.

Table 3-7: Reproducibility analysis of the products mass balance

Parameters	**1st Experiment**	**2nd Experiment**	**3rd Experiment**	**Mean**	**Standard deviation**
Gas yield (wt.%)	54.05	52.47	55.46	53.99	1.50
CO (vol.%)	38.80	38.80	38.80	38.80	0.00
H_2(vol.%)	28.20	25.90	29.20	27.77	1.69
O_2 (vol.%)	0.00	0.00	0.00	0.00	0.00
CO_2 (vol.%)	16.20	19.20	16.20	17.20	1.73
CH_4 (vol.%)	12.10	11.30	12.10	11.83	0.46
C_nH_m (vol.%)	3.70	4.00	3.70	3.80	0.17
Char (wt.%)	7.30	7.34	7.30	7.31	0.02
Mass balance (%)	98.88	99.60	100.04	99.79	1.16

3.6 Gas analysis

Gas was collected during the pyrolysis experiments during sample heating using a 25 L Tedlar® gas bag. This gas was analysed offline using three GC instruments which were configured and calibrated for quantitative analysis of key compounds. The first instrument, a Varian CP-3380 analysed the permanent gases (H2, O2, N2 and CO) using argon as the carrier gas and a 2 m x 2 mm column packed with a 60-80 mesh molecular sieve and a thermal conductivity detector (TCD). The second instrument was also a Varian CP-3380 but with a HayeSep column and was configured to measure carbon dioxide also using a TCD. The third instrument was used to determine hydrocarbon gases (C1-C4), used nitrogen as a carrier gas and a 2 m x 2 mm stainless steel column packed with Hysesp, 80-100 mesh using a flame ionisation detector (FID). Calibration was achieved using known standards these were used to calculate response factors (RF) for each gas. The results indicate a relative proportion of each gas. From these values, two assumptions can be used to calculate the weight of each gas produced during the experiment. Firstly, that the nitrogen flow rate in the reactor was constant and recorded accurately, secondly that 1 mole of gas at standard temperature and pressure has a volume of 22.4l in accordance with the ideal gas law. Each gas sample was injected three times with the average used to calculate the gas yield.

Table 3-8: Gas Chromatographs and Detectors used for gas analysis

Gas Chromatograph	**Detector**	**Gases analysed**	**Carrier gas**
Varian CP-3800 (Figure 3-8)	Thermal Conductivity Detector	CO_2	Argon
Varian CP-3380	Thermal Conductivity Detector	H_2, N_2, O_2, CO	Argon
Varian CP-3380	Flame Ionization Detector	Hydrocarbon Gases (methane, ethane, ethene, propene, propane, butene, butadiene)	Nitrogen

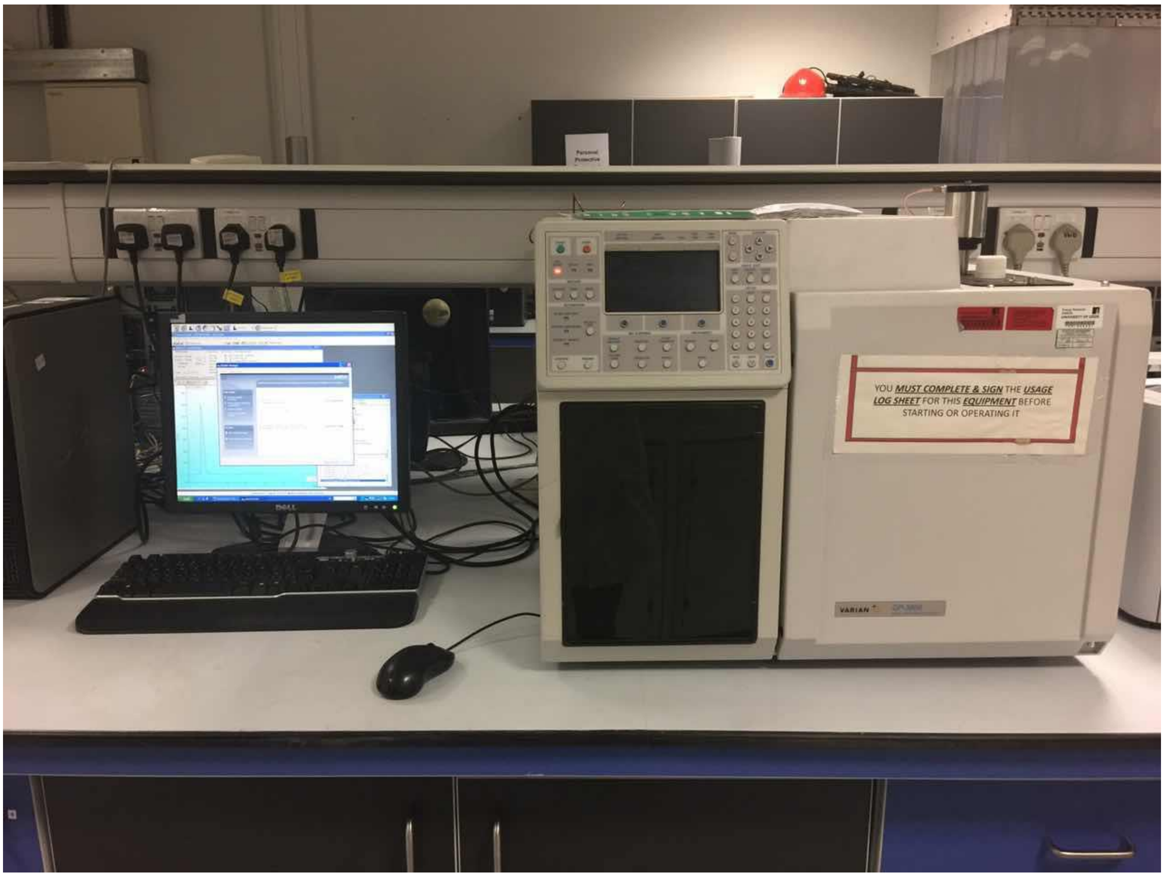

Figure 3-8: Varian CP-3800 with thermal conductivity detector (TCD)

3.6.1 Calculations

After GC analysed the gases, a further calculation was needed to obtain the char residue yield (wt.%), the mass balance (wt.%) and the H_2 production in mmol per grams of biomass using the following equations (Dong et al., 2016; Nahil et al., 2013):

$$char\ residue\ yield\ (wt\%) = \frac{weight\ of\ char\ residue}{weight\ of\ biomass\ sample} \times 100 \qquad \text{(E.3.5)}$$

$$mass\ balance\ (wt\%) = \frac{weight\ of\ char\ residue, gas\ and\ liquid}{weight\ of\ biomass\ sample + weight\ of\ injected\ water} \times 100 \qquad \text{(E.3.6)}$$

$$Hydrogen\ Production\ (mmolg^{-1}) = \frac{mmol\ H_2}{g\ Biomass} \qquad \text{(E.3.7)}$$

The yield of CO and CO_2 are calculated in the same way as hydrogen production:

$$CO\ yield\ (mmolg^{-1}) = \frac{mmol\ CO}{g\ Biomass} \tag{E.3.8}$$

$$CO_2\ yield\ (mmolg^{-1}) = \frac{mmol\ CO_2}{g\ Biomass} \tag{E.3.9}$$

In this case, the gas yield was calculated in a different way to the one proposed by Dong et al., (2016), also using the difference in weight between the water added to the system with the syringes and the water in the condenser system, which is the water that reacted in the rig:

$$gas\ yield\ (wt\%) = \frac{weight\ of\ gas}{weight\ of\ Biomass + weight\ of\ H_2O\ injected - weight\ of\ H_2O\ in\ condenser} \tag{E.3.10}$$

To evaluate the performance of the CSR and WGS reactions and the overall process two indicators are introduced, which are the hydrogen to carbon monoxide, hydrogen to carbon dioxide and hydrogen to total carbon compounds produced ratios:

$$H/CO = \frac{mmolg^{-1}\ H_2}{mmolg^{-1}\ CO} \tag{E. 3.11}$$

$$H/CO_2 = \frac{mmolg^{-1}\ H_2}{mmolg^{-1}\ CO_2} \tag{E. 3.12}$$

$$H/C = \frac{mmolg^{-1}\ H_2}{mmolg^{-1}\ CO + mmolg^{-1}\ CO_2 + mmolg^{-1}\ CH_4 + mmolg^{-1} C_nH_m} \tag{E.3.13}$$

3.7 Materials Characterization

Different methods were adopted in characterising the spent catalysts. These help to identify and understand the best quality catalysts for hydrogen production and optimisation in terms of selectivity, carbon deposition and deactivation. The methods used in this study are discussed briefly below.

3.7.1 Temperature programmed reduction (TPR)

Temperature programmed reduction (TPR) of the prepared catalysts was undertaken using a Stanton–Redcroft thermos gravimetric analyser (TGA) as shown in figure 3-9. The TPR was conducted to investigate the adsorption of hydrogen on all active sites of the fresh catalysts and test the reducibility characteristic of the catalyst. TPR was used to determine what temperature the fresh catalyst should be reduced to change the catalyst state from passive (oxide form) to an active state (metal form).

During the TPR analysis, each fresh catalyst sample 20 mg fresh catalyst sample was placed in the TGA, and preheated to 150 °C at a heating rate of 20°C min^{-1} and held for 30 min in the atmosphere of N_2 at a flow rate is 50 ml min^{-1} to remove the moisture, then heated at 10 °C min^{-1} to a final temperature of 900 °C. TPR was carried out with H_2 at a concentration of 5 vol.% (95% N_2). The sample is cooled down to room temperature.

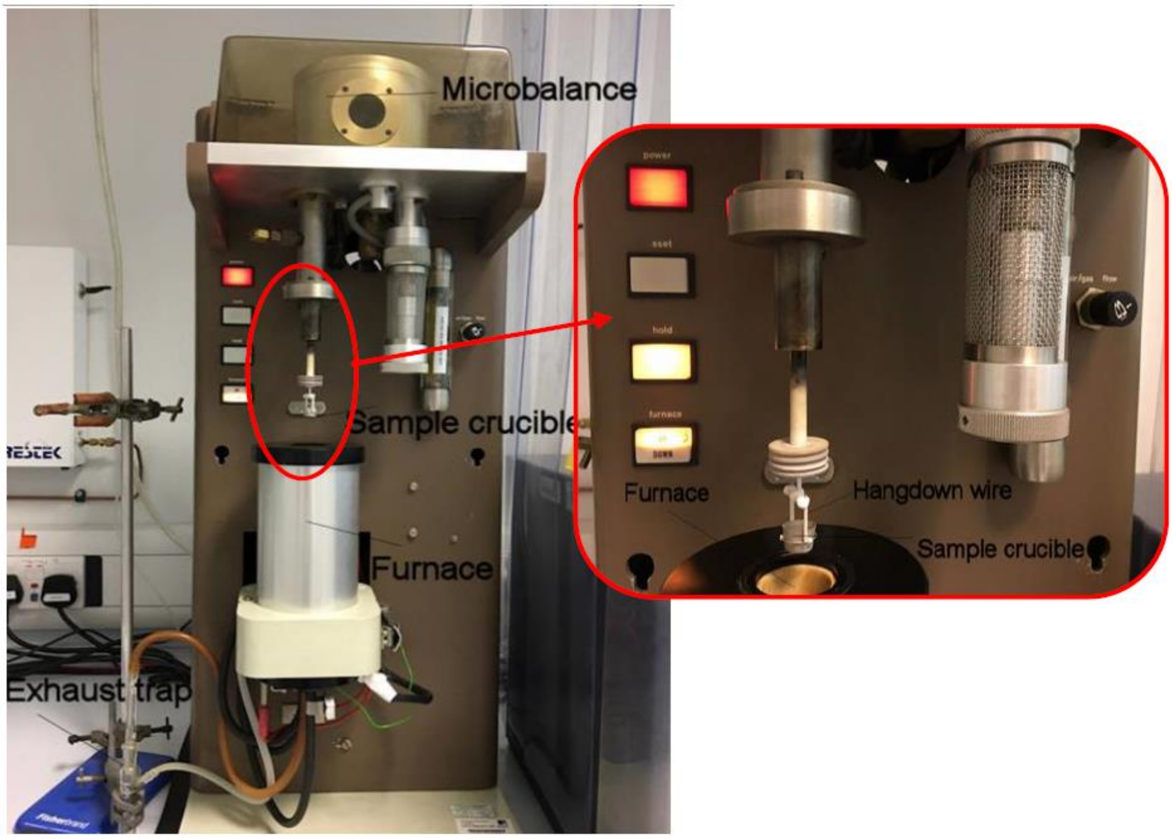

Figure 3-9: Stanton-Redcroft thermos gravimetric analyser

3.7.2 Temperature programmed oxidation (TPO)

In order to analyse each reacted sample of catalyst for carbon deposition properties, temperature-programmed oxidation was undertaken using a Stanton-Redcroft thermogravimetric analyser. Before beginning the analysis, care was taken to ensure that the sample was representative of the entire catalyst sample with the colouration and size at approximately the mid-point of the sample where variation in size and colour existed. 10 mg of the sample was loaded into the pre-tared alumina pan analyser. This is done to reduce the effect that diffusion has on the analysis and to maintain a narrow range of the catalyst particle distribution (Chen et al., 2013). The reacted catalysts samples were then heated gradually at a ramp rate of 15°C min-1 to a temperature of 800°C in the presence of oxygen. The dwell time for the system was 10 minutes. As the samples are heated, any carbon deposits will react with the surrounding oxygen. The temperature at which this occurs is dependent on the type of carbon deposit. Examples include amorphous, heavy hydrocarbon and filamentous carbons. As the reaction takes place, the mass of the catalyst reduces as carbon dioxide is produced. This change in mass was recorded and plotted on a TPO thermal profile by plotting its variation with time. An advantage of this, particular, method over microscopy techniques is that it can detect deficient levels of carbon that may not be visible with the most advanced microscopes (Wang et al. 2010).

TPO results of different reacted catalysts reveal the specific phases of carbon deposition as a result of the different thermal stability of the various kinds of carbon deposits. For example, amorphous carbon is usually oxidised at lower temperatures while filamentous carbon due to higher thermal stability is oxidised at elevated temperature (Zhang et al. 2016, Zhang et al. 2017). Therefore, the weight loss in TPO thermograms reflects the oxidation level of the carbon deposit on the reacted catalyst surface.

3.7.3 X-ray diffraction (XRD)

In order to identify the composition of the reacted catalysts in terms of crystallographic structure, X-ray diffraction (XRD) analysis was carried out on a Bruker D8, using Cu α1radiation X-ray tube. The X-ray scans were conducted from 20 to 80 ° 2θ using a step size of 0.032.

The XRD samples were prepared by grinding the reacted catalyst into powders and loading it on sample holders and loading into the machine holder. The resulting data for analysis was collected from XRD data acquisition software which was connected to the Bruker D8. The Phase identification was carried out using 4 and the International centre for diffraction data powder diffraction files (ICDD PDF4+) database (Degen et al 2014)

XRD analysis is premised on Bragg's law (equation 3.14). Therefore, the diffraction peak position is gotten from the atomic bond distance in the crystal [8-9].

$$Bragg'sLaw: \lambda = 2d_{hkl}sin\theta \qquad (E. 3.14)$$

Where λ is the X-ray wavelength, dhkl is calculated by the lattice parameters of the unit cell and 2θ is the specific diffraction peak angle.

3.7.4 Brunauer, Emmett and Teller (BET) surface area analysis

The surface area analysis using nitrogen adsorption with a Quantachrome Corporation (FL, US) Autosorb 1-C instrument shown in figure 3-10 was used to characterise the porous properties of the reacted catalysts. (Naderi M 2015) This was investigated using static volumetric principles to measure the quantity of nitrogen adsorption and desorptions on the surface of the catalyst. The BET technique is a computational technique used to relate nitrogen adsorption to surface area and porosity of catalysts at equilibrium vapour pressure (Hammes et al., (2008).

Nitrogen adsorption was carried out by measuring the quantity of the nitrogen (adsorbate) that was adsorbed onto or desorbed from the reacted catalysts at various equilibrium vapour pressures using the static volumetric method. A specific quantity of N_2 was added or removed from the solid reacted catalyst structure which was maintained the critical temperature of N_2 corresponding to a constant temperature of -196 °C. Equilibrium marks the end of the reaction and evaluation after a series of adsorption or desorption pressure changes occur within the sample walls. These changes in vapour pressure were recorded. During the equilibrium pressure point, the amount of N_2 which was adsorbed or desorbed is calculated by the difference between the quantity of N_2 needed to fill the space around the sample and the quantity of N_2 admitted or removed. The data extracted was utilised to plot adsorption and desorption isotherms, from which the surface area of the sample can be determined.

Figure 3-10: NOVA 2200e instrument used to characterise the porous properties of catalysts

The principle of this method is based on the BET equation proposed by Brunauer et al. 1938, as shown in equation 3.8.

$$1 / v((P_0/P)-1) = (1/V_m.C) + (C-1 / V_m.C) \times (P/P_0) \quad (E.3.15)$$

Where v is the volume of adsorbed gas at relative pressure (P/P0) (cm^3), P is pressure, P_0 is the saturated vapour pressure, Vm is the volume of adsorbate adsorbed when the entire adsorbent surface is covered with a complete unimolecular layer (cm^3), and C is the BET constant.

Vm can be obtained from a combination of the slope and the intercept with the Y-axis of the BET plot as shown in equations 3.15, 3.16 and 3.17 below.

$$\text{Slope} = (C - 1) / (V_m.C) \text{ Intercept} = 1 / (V_m C) \quad (\text{E.3.16})$$

$$V_m = 1 / (\text{Slope} + \text{Intercept}) \ (\text{E.3.17})$$

The total surface area of the sample can be determined from equation 3.18 below.

$$S = (V_m.N_a.A) / V \ (\text{E } 3.18)$$

Where A is the molecular cross-sectional area of the adsorbate (m^2), Na is Avogadro's number (6.023 x 1023 mole-1), and V is the molar volume of the adsorbate (cm^3 $mole^{-1}$).

The BET surface area of the sample can then be determined by equation 3.19.

$$S_{BET} = S / W \ (\text{equation } 3.19)$$

Where W is the weight of the sample (g).

3.7.5 Thermogravimetric analysis of catalysts

The thermogravimetric analyses of the reacted catalysts were carried out in order to determine their thermal behaviour in terms of weight loss in relation to temperature and from which a proximate analysis was determined. The proximate analysis provided data on the moisture, volatile, fixed carbon and ash content of the samples. The thermogravimetric analysis was carried out using a Shimadzu thermal gravimetric analyser TGA-50. The TGA was made up of an aluminium pan held in a microbalance which was coupled to a precisely controlled furnace. The procedure involved placing a known quantity of the sample into the aluminium pan which was suspended in the microbalance within the furnace. Figure 3-11 shows a photograph of the Shimadzu thermal gravimetric analyser TGA-50.

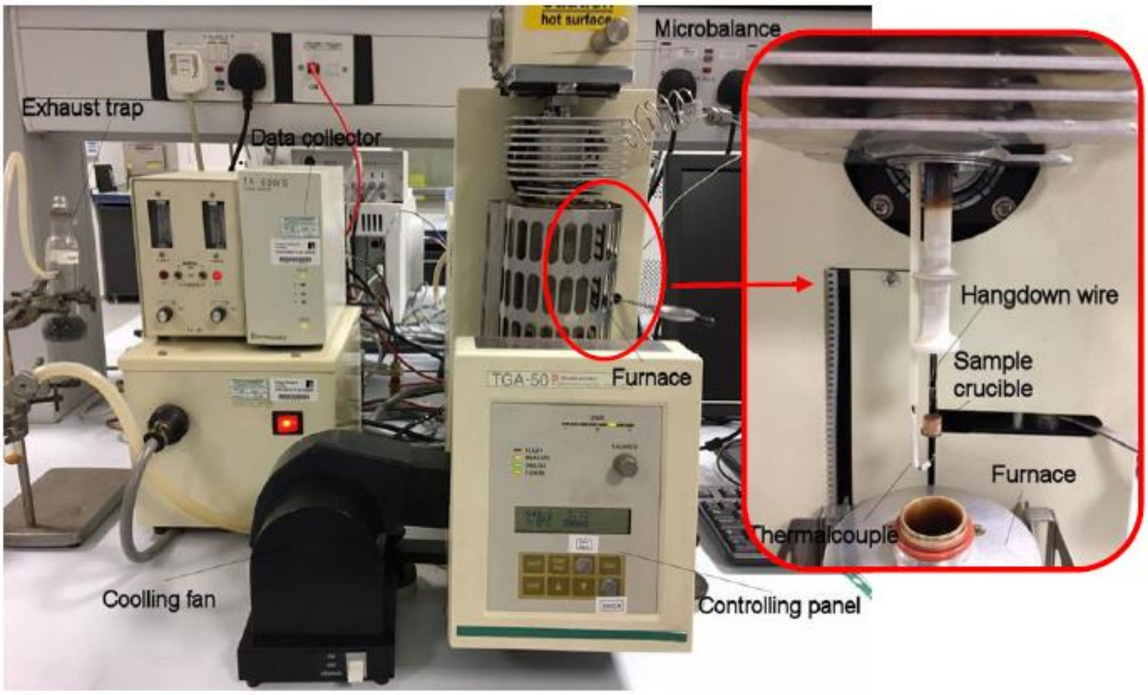

Figure 3-11: Shimadzu thermal gravimetric analyser (TGA-50).

3.8 Reference

B. Dou, Y. Song, Y. Liu and C. Feng, Journal of Hazardous Materials, 2010, 183, 759-765.

Burhenne, L., Messemer, J., Aicher, T. and Laborie M.P. The effect of the biomass components lignin, cellulose and hemicellulose on TGA and fixed bed pyrolysis. Journal of Analytical and Applied Pyrolysis. [Online]. 2013. 101, pp.177-184. [Accessed 28th March 2019]. Available from: https://www.sciencedirect.com/science/article/pii/S0165237013000168.

Brunauer, S., Emmett, P.H. and Teller, E., Adsorption of Gases in Multimolecular Layers. Journal of the American Chemical Society, 1938. 60(2): p. 309-319.

Chen, D., Zhou, J. & Zhang, Q., 2014. Effects of heating rate on slow pyrolysis behaviour, kinetic parameters and products properties of Moso bamboo. Bioresource Technology, Volume 169, pp. 313-319.

Degen, T., Sadki, M., Bron, E., König, U. and Nénert, G., 2014. The high score suite. Powder Diffraction, 29(S2), pp.S13-S18.

Di Blasi, C. Modeling chemical and physical processes of wood and biomass pyrolysis. Progress in Energy and Combustion Science. [Online]. 2008. 34(1), pp.47-90. [Accessed 28th March 2019]. Available from: http://www.sciencedirect.com/science/article/pii/S0360128507000214.

Dong, L. et al., 2016. Development of Fe-Promoted Ni−Al Catalysts for Hydrogen Production from Gasification of Wood Sawdust. Energy Fuels, Volume 31, pp. 2118-2127.

Friedl, A., et al., Prediction of heating values of biomass fuel from the elemental composition. Analytica Chimica Acta, 2005. 544(1): p. 191-198.

Guedes, R.E, Luna, A.S. and Torres, A.R. Operating parameters for bio-oil production in biomass pyrolysis: A review. Journal of Analytical and Applied Pyrolysis. [Online]. 2018. 129, pp.134-149. [Accessed 8 January 2018]. Available from: https://www.sciencedirect.com/science/article/pii/S0165237017305697

Hammes, K., Smernik, R. J., Skjemstad, J. O., & Schmidt, M. W. (2008). Characterisation and evaluation of reference materials for black carbon analysis using elemental composition, colour, BET surface area and 13C NMR spectroscopy. Applied Geochemistry, 23(8), 2113-2122.

Jentoft, FC. 2003. Thermal Treatment of Catalysts. Modern Methods in Heterogeneous Catalysis Research. University of Massachusetts.

Li, G., Hu, L. & Hill, J. M., 2006. Comparison of reducibility and stability of alumina-supported Ni catalysts prepared by impregnation and co-precipitation. Applied Catalysis A: General, Volume 301, pp. 16-24.

Lopez, DE, Suwannakarn, K, Bruce, DA, and Goodwin, JG. 2007. Esterification and transesterification on tungstated zirconia: Effect of calcination temperature. Journal of Catalysis. 247, pp. 43-50.

Luo, S., Xiao, B., Hu, Z. and Liu, S., Effect of particle size on pyrolysis of single-component municipal solid waste in fixed bed reactor. International Journal of Hydrogen Energy, 2010. 35(1): p. 93-97.

Naderi, M., 2015. Surface Area: Brunauer–Emmett–Teller (BET). In *Progress in filtration and separation* (pp. 585-608). Academic Press.

Nahil, M. A. et al., 2013. Novel bi-functional Ni-Mg-Al-CaO catalyst for catalytic gasification of biomass for hydrogen production with in situ CO2 adsorption. RSC Advances, Volume 3, pp. 5583-5590.

Nayebzadeh, H, Saghatoleslami, N, Maskooki, A, and Vahid, BR. Effect of Calcination Temperature on Catalytic Activity of Synthesis SrO/S-ZrO2 by Solvent-free Method in Esterification of Oleic Acid. The Journal of Chemical and Biochemical Engineering Quarterly. 27(3), pp. 267-273.

Ramu, S, Lingaiah, N, Prabhavathi Devi, BLA, Prasad, RBN, Suryanarayana, I, and Sai Prasad, PS. Esterification of palmitic acid with methanol over tungsten oxide supported on zirconia solid acid catalysts: effect of method of preparation of the catalyst on its structural stability and reactivity. Applied Catalysis A: General. 276(1), pp. 163-168.

S. Lin, M. Harada, Y. Suzuki and H. Hatano, Energy Conversion and Management, 2005, 46, 869-880

Wang, D., Xiao, R., Zhang, H. and He, G., 2010. Comparison of catalytic pyrolysis of biomass with MCM-41 and CaO catalysts by using TGA–FTIR analysis. Journal of Analytical and Applied Pyrolysis, 89(2), pp.171-177.

Wongmaneenil, P, Jongsomjit, B, and Praserthdam, P. 2009. Journal of Catalyst Communications. 10, pp. 1079.

Wu, C. and Williams, P.T., Hydrogen Production from the Pyrolysis Gasification of Polypropylene: Influence of Steam Flow Rate, Carrier Gas Flow Rate and Gasification Temperature. Energy & Fuels, 2009. 23(10): p. 5055-5061.

Zhang, Y, et al., 2017. Pyrolysis-catalysis of waste plastic using a nickel-stainless steel mesh catalyst for high value carbon products. Environmental Technology, pp1-27

Zhang, Y., et al., 2016. High-value resource recovery products from waste tyres. Proceedings of the Institution of Civil Engineers-Waste and Resource Management, 169(3), pp 137-145

Chapter 4: Investigation of Catalysts Influence on Hydrogen Production from Two and Three -Stage Catalytic Steam Reforming of Biomass

In this chapter, Nickel-based catalysts on different supports have been investigated. These were done in order to compare the influence of the different nickel catalysts as well as their metal loadings on the hydrogen production by the thermochemical deconstruction of biomass in different fixed-bed reactors as described in Chapter 3. The core aim of this investigation is to produce high hydrogen yield from lignocellulosic biomass by pyrolysis-catalytic-reforming-water gas shift process. The catalysts utilised were all synthesised through a wet impregnation method. As reported by Contreras et al. (2015), impregnation synthesis technique gave rise to the best noble metal catalysts with respect to selectivity and catalytic conversion. The set-up of the fixed bed reactor systems and catalyst preparation method were described in Chapter 3, section 3.5.

This chapter is divided into two sections vis-à-vis catalysts investigation in a two-stage thermochemical process; Pyrolysis-catalytic steam reforming of biomass and catalyst Investigation in the three-stage thermochemical process; Pyrolysis-catalytic steam reforming of biomass and water gas shift reaction for hydrogen production.

Section 4.1 principally analyses the results obtained from the deconstruction of waste wood biomass via two stage pyrolysis and catalytic steam reforming reactor. The influence of catalysts on hydrogen production at the catalytic steam reforming reaction was chiefly investigated. At the pyrolysis stage, the temperature was kept constant at 550^0C while the catalysts used in the catalytic steam reforming stage were varied between 650^0C and 950^0C. Different nickel loadings (0%, 5%, 10% and 20%) supported on alumina was studied. 10%Nickel on different oxide supports (alumina, dolomite, silica, and zeolite) were also investigated. Section 4.2 discusses results obtained from the introduction of third stage water gas shift reactor to enhance hydrogen yield. The most suitable catalyst for optimising hydrogen yield was also the prime investigation focus. Unlike in the first experiments in section 4.1, the pyrolytic temperature was kept constant at 850^0C. The catalytic steam reforming catalysts were varied using constant 10% nickel on the different support (NiAl, NiDo, NiSi, NiZe) while the third stage, water gas shift reaction was kept constant using 5FeAl. The influence of bimetallic catalysts on total gas and hydrogen yield in the water gas shift reaction which involved the use of different metal catalysts but supported on the same alumina support ($NiAl_2O_3$/2.5Fe2.5Cu, $NiAl_2O_3$/2.5Fe2.5Co, $NiAl_2O_3$/2.5Fe2.5Mn, $NiAl_2O_3$/2.5Fe2.5Zn) was also investigated.

4.1 Catalysts investigation in two-stage pyrolysis-catalytic steam reforming of Biomass

Nickel-based catalysts have been reported to have a strong influence on the total gas production and hydrogen yield from a pyrolysis-steam reforming reaction (Charisiou et al. 2019, Gai, et al. 2019; Karaismailoglu et al. 2019; Zamzuri et al. 2017). Based on cost implication, Nickel-based catalysts are also considerably cheaper than other transition metals like Ru and Rh (Miranda et al., 2015). Ni-based catalysts have different catalytic performances attributed to several factors such as, the quantity of the active metal component (that is, nickel loading), the type and amount of support component (such as alumina, dolomite, zeolite, silica and char) and the promoter component which boosts the catalyst' stability and the reactivity (Damatzis and Zabaniotou, 2011; Hu et al 2015; Marono et al 2010, Galvagno et al, 2009; Solid biofuel, 2010a,b,c).

4.1.1 Effects of different nickel loadings on total gas and hydrogen production

The influence of changing the nickel loading on the catalyst was investigated using Ni-Al_2O_3 catalysts prepared with various loadings of the nickel-metal (0, 10 and 20%) on the alumina (Al_2O_3) support. The results obtained are presented in Table 4-1 and 4-2. The results of total gas yields (expressed in wt%), the char residue yield and the mass balance are shown in Table 4-1. The results showed that the difference in nickel loadings has an influence on the production of gas yield and hydrogen. Sand was utilised as a reference catalyst representing zero catalysts. As the amount of nickel on the catalyst was increased from 0 to 20%, the gas yield steadily Although all the catalysts had a mass balance close to each other with a standard deviation of 1.6%, however, the highest mass yields of the different gases were generated from the highest nickel loading. 20% nickel loading also had the highest gas yield at 1.53g while 5% nickel loading is the lowest at 1.45g. Notably, 5% and 10% nickel loading had the lowest char content of 0.41g while 20% of nickel loading had the highest char content at 0.47g. It is evident that beyond 10% loading, the gas yield was relatively constant, and the char yield increased. The increase in char yield is entirely disassociated from the elevation of nickel loading because residual char is mainly pyrolytic.

Similar findings on the influence of nickel loading have been found in other literature (Costa et al., 2010; Grosso et al. 2010). According to Akande et al. (2005), for the steam reforming of ethanol, the gas yield and catalytic activity rose with increased nickel loading from 10 to 15 %, but upon further increase of Ni loading to 20 wt %, no significant gas yield increase was found. Therefore, this suggests that the rise in gas yield from increasing the nickel loading was as a result of the active catalytic sites on the catalyst surface being increased. In effect, this makes the catalyst more selective towards steam reforming since Ni is the catalyst-active component.

Table 4-1: Experimental summary for effect of nickel loading based on 3 samples for each conditions

Catalysts	**Char yield**	**Liquid**	**Gas**	**Mass Balance**
Sand	23	5.93	61	100.09
5% Nickel Alumina	20.5	5.20	72.5	96.99
10% Nickel Alumina	20.5	5.74	76	100.24
20% Nickel Alumina	23.5	5.81	76.5	101.25

Figure 4-1 reveals the influence of nickel loading on product gases production and total gas yield (expressed in gas yield/feed wt%) while figure 4-2 shows the nickel loading influence on hydrogen yield and syngas production (expressed in gas yield mmol per gram). A similar trend to total gas yields and CO_2 yields in table 4-1 was obtained as the nickel loading increased. The 20% nickel loading had the highest carbon dioxide and second-highest hydrogen yields at 20.86mmol/g, followed by 10% metal loading. The H_2 yield was quite relatively the same as that of 10% loading. The catalyst produced the least CO yield at 8.41mmol/g. A similar result was obtained for the hydrocarbon yield, where they both produced the least. 20% of nickel loading has produced the least methane. These imply that it is not susceptible to coking and sintering under the utilised process conditions.

Evaluating the effect of 10% nickel loading on product gases production, the catalyst is best selective towards H_2, having produced the highest H_2 yield at 20.90mmol/g and third-highest CO yield representing 12.71mmol/g relative to other catalysts studied. This suggests that it has the best catalytic activity in promoting a steam reforming reaction. Producing the least hydrocarbons and significantly low CH_4 yield also implies that the catalyst has a strong resistance to coking effect and deactivation.

5% Nickel loading produced the highest amount of carbon monoxide at 33.93mmol/g, the second-lowest amount of hydrogen at 3.38mmol/g, second-lowest CO_2 yield and second highest hydrocarbon yield. The considerably high amount of hydrocarbon and methane suggests that the catalyst has poor activity in steam reforming of methane. Under this condition, methanation was promoted at the expense of steam reforming.

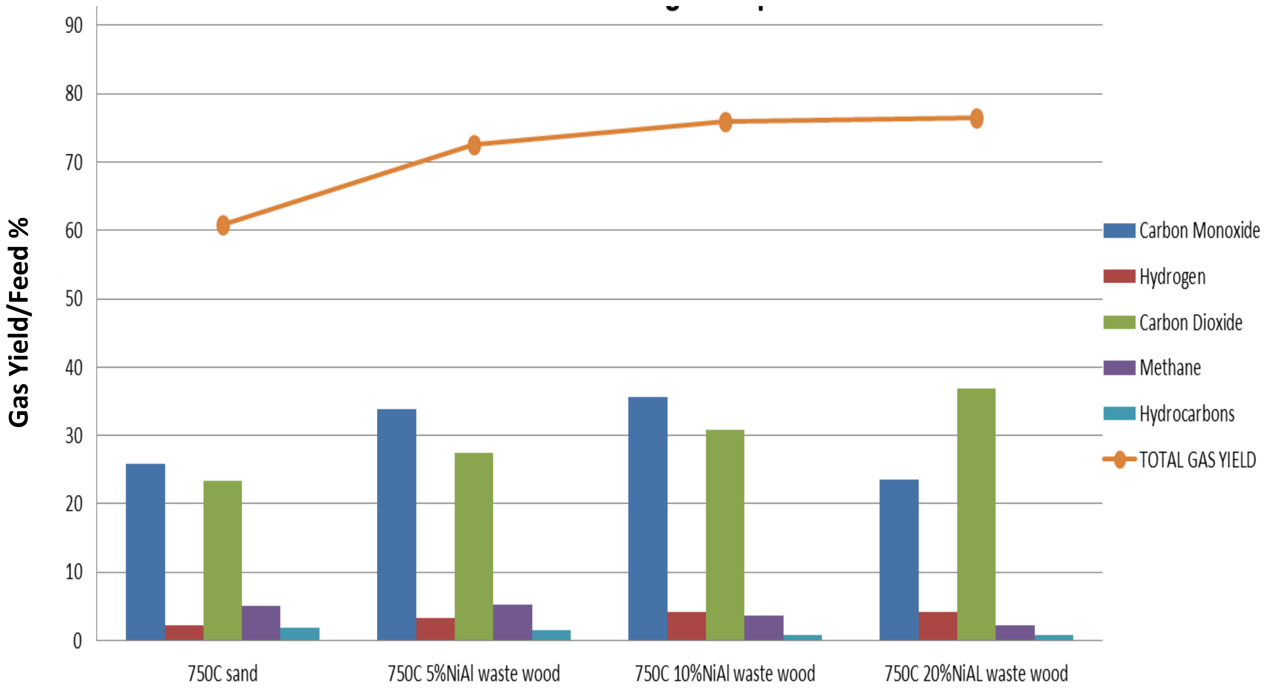

Figure 4-2: Gas Volume percentage comparison of catalysts with different Nickel Loading

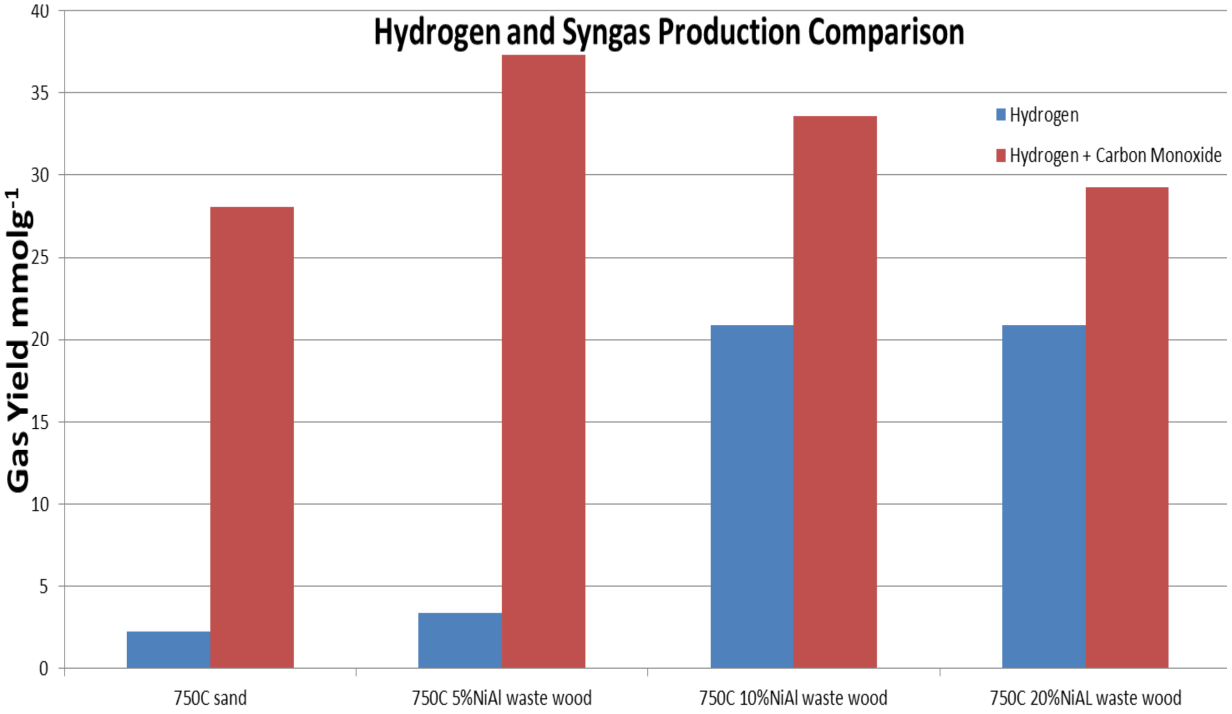

Figure 4-1: Hydrogen and Syngas Yield for catalysts with different Nickel Loadings

Sand representing 0% nickel loading behaved poorly in catalysing the steam reforming of methane, this reflects in the highest yield of CH_4 and hydrocarbon obtained. Sand produced the least hydrogen yield at 2.24 mmol/g, unlike 10% nickel loading that produced 20.90mmol/g. These results confirm the importance of catalyst in a steam reforming reaction. 5% Nickel loading produces the highest amount of carbon monoxide at 33.93mmol/g followed by sand at 25.80mmol/g followed by 10% at 12.71mmol/g followed by the 20% at 8.41mmol/g. 5% produces the second-lowest amount of hydrogen with sand being the lowest in the data set, as seen from figure 4-2. 10% Nickel loading produced the highest amount of hydrogen at 20.90mmol/g followed by 20% nickel loading at 20.86mmol/g followed by 5% nickel loading at 3.38mmol/g then lastly sand at 2.24 mmol/g.

The syngas and hydrogen yield revealed in figure 4-2 showed that sand (0% nickel) had poor selectivity towards H_2 while 10% and 20% Nickel loading had high selectivity. Notably, 10% metal loading catalyst of all the investigated catalysts had the best performance with respect to hydrogen yield representing 20.90mmol/g. The syngas production of 5% nickel loading proved to be the best followed by 10% while sand represents a blank to establish baseline. The poor selectivity of sand (SiO_2) is expected because it is absolutely inert and often used as a mere heat carrier (Kechagiopoulos et al., 2007). As obtained by Biswa and Kunzru, (2007), the selectivity towards H_2 by Ni catalysts on the same support, increased with an increase in metal loading from 10 to 30 wt% metal loading and decreased at higher loading (40 wt%). However, the catalyst support utilised (ZrO_2) is different from the one used in this study which is alumina. This accounts for the variation in products selectivity across the metal loadings. The effectiveness of Nickel-metal loading is therefore premised on the type of support.

4.1.2 Effect of oxide support on syngas and hydrogen production

Table 4-2: Experimental summary for effect of oxides support

Experiment	**Char (wt%)**	**Liquid**	**Gas (wt%)**	**Mass Balance**
Sand	23	5.93	61	100.09
10% Nickel Alumina	20.5	5.74	76	100.24
10% Nickel Dolomite	19.5	5.55	84.5	102.54
10% Nickel Silica	20	5.30	80	100.11
10% Nickel Zeolite	20.5	5.46	80.5	98.36
20% Nickel Alumina	23.5	5.81	76.5	101.25
20% Nickel Dolomite	19	5.60	92.5	101.80
20% Nickel Silica	21	5.42	86	100.08
20% Nickel Zeolite	24	5.16	80.5	98.21

The results of the influence of different catalyst support on the activity and product distribution on catalysts with nickel loadings of 10 and 20 wt% are shown in Table 4-2. Table 4-2 shows the mass balance of all the experiments in this particular data set; the standard deviation for the mass balances is 1.35%. There is no significant difference between 10 wt% and 20 wt% nickel loading of the same alumina support unlike dolomite and silica (SiO_2) which has significantly higher gas yield and mass balance produced by its respective 20 wt% loading. Among the three supports tested, Dolomite support on 10 wt% Nickel loading yielded the highest amount of gas and the best mass balance. However, studies have shown that Al_2O_3 and SiO_2 promote higher sintering resistance and a higher metallic surface area in comparison to other oxide supports [Gil et al. 1994].

Figure 4-3 and figure 4-4 illustrate the effect that different oxide support compositions have on the production of syngas and hydrogen. Nickel dolomite produced the highest amount of syngas than any of the other oxides investigated. Nickel alumina produced the lowest amount of hydrogen as seen in figure 4-4 this is probably due to low catalytic activity; dolomite also produced the highest amount of hydrogen which indicates highest conversion and selectivity towards the target H_2 gas. Again, it means that contingent on the support composition, the conversion and product selectivities were quite distinctive.

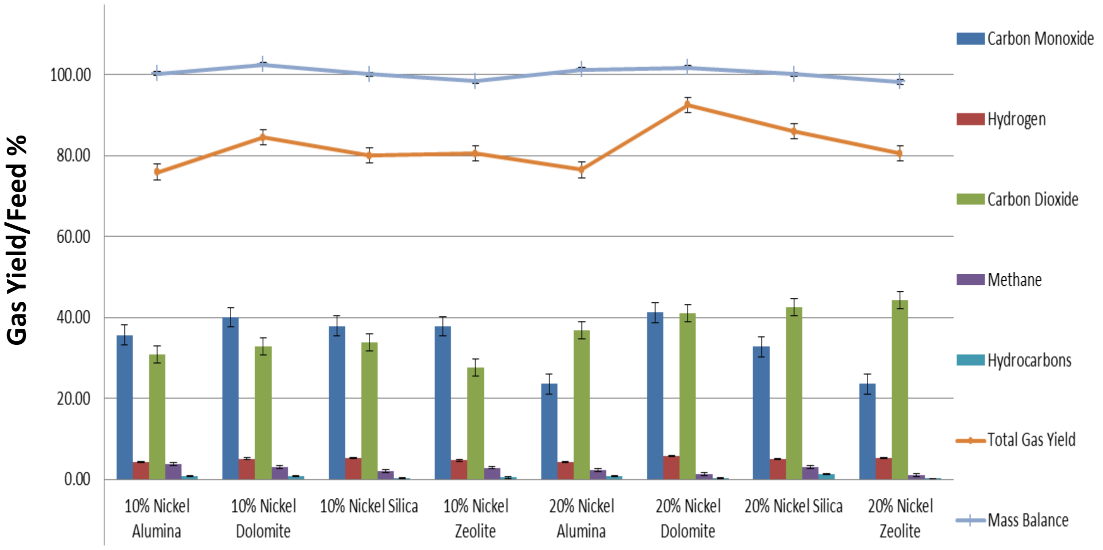

Figure 4-3: Gas Volume percentage comparison of Nickel catalysts with different Supports

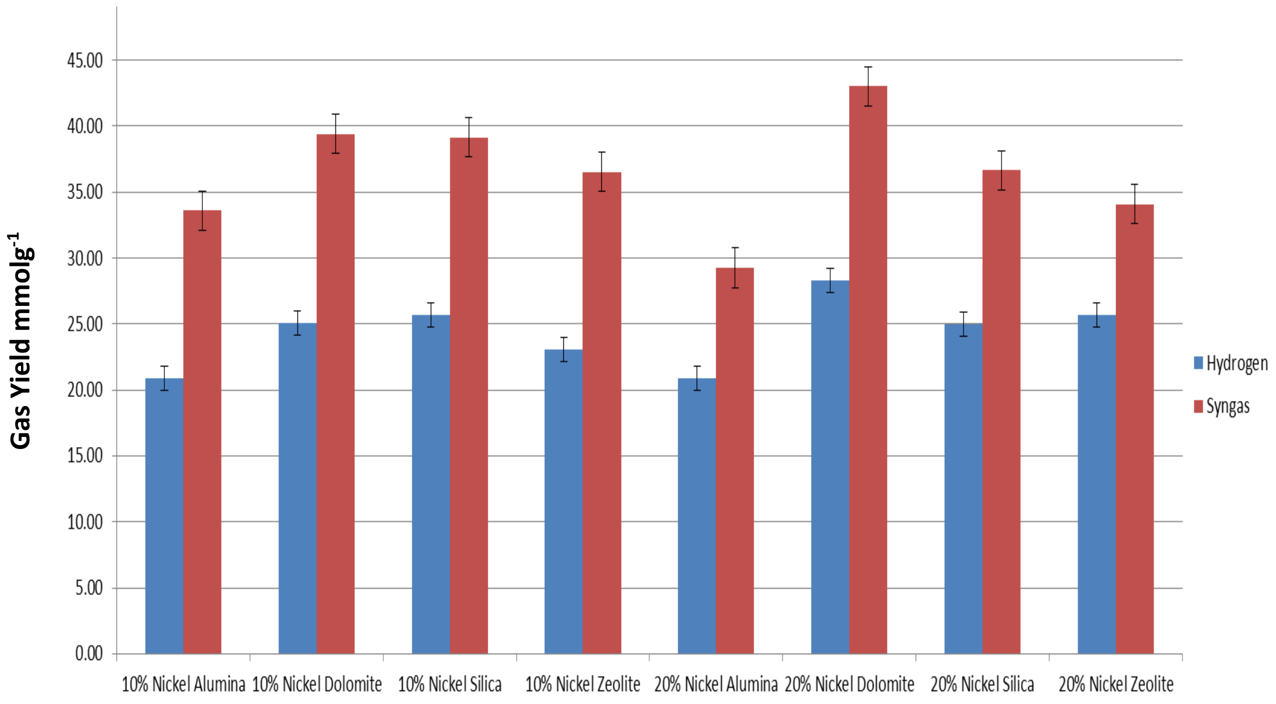

Figure 4-4: Hydrogen and Syngas Yield for Nickel Catalysts with Different Supports (*error bars represent standard deviation*)

4.2 Investigating catalyst for optimum hydrogen production from the three-stage process

In this section, the three-stage fluidised bed reactor for hydrogen production was introduced. This approach to producing hydrogen from raw biomass in the three-stage process is described in Chapter 3 which comprised; Pyrolysis of wood pellets to produce pyrolysis gases, followed by catalytic steam reforming (CSR) and water-gas-shift (WGS) reactions in a fixed bed reactor. Emphasis is still predominantly placed on investigating the best catalyst for enhancing hydrogen yield in the CSR and WGS stages.

Imperatively, the catalyst type, composition, temperature and steam to carbon ratios are essential factors for hydrogen production. In the choice of catalysts, several conditions are considered, these include; catalytic activity, selectivity, stability, mechanical strength and cost (Freni et al. 2001, Moulijn, et al. 2001, Mitchell et al. 2013, Ellis, et al. 2013).

Many studies have focused on identifying suitable catalyst for hydrogen production, there is a consensus among them that Ni is one of the most effective metals, especially for steam reforming (Shahbaz et al 2017, Shen and Yoshikawa, 2013; Guan et al, 2016; Frusteri et al (2004); Andre et al

(2007); Fatsikostas et al (2002); Lasa et al, 2011 Bartholomew and Farrauto, 2006). Nickel-based catalysts from both laboratory and commercial applications are shown to have a high catalytic activity for tar reduction by cracking and reforming (Chan and Tanksale, 2014). Additionally, they find the ease of application as primary catalysts, especially in downstream catalytic processes. In a recent study by Soria et al. (2019), high-quality H_2 production by water gas shift process was investigated using different four reactors namely; membrane reactor (MR), sorption-enhanced reactor (SER; specifically utilized for CO_2 absorption) and sorption-enhanced membrane reactor (SEMR; for concurrent CO_2 and H_2 removal), and with fixed-bed conventional reactor (TR).

The key findings in this investigation involved that there is a great potential for obtaining high hydrogen yield from water gas shift process, and the production of high purity H_2 gas through the SER and SEMR was the best, but the apparent drawbacks are the cost implication of these two specialized reactors as well as the chains of processes involved such as sorption, rinse, regeneration, among others before a constant hydrogen production is achieved. Bruni et al. (2019) showed evidence of hydrogen yield and high energy efficiency with low-cost implication by using a two-stage reactor involving methane steam reforming and water gas shift processes. Although this does not mirror the reality of industrial plant where the biomass is required to be first deconstructed, and the product gases contain other compounds other than methane, nevertheless, this finding provides useful information on why a three-stage thermochemical should be given a thorough consideration because it reflects a real-life plant operation.

Based on the above, the overall aim of this section is to obtain higher hydrogen yield by investigating parameters in the second stage of the three-stage thermochemical conversion of wood pellet biomass and the influence of using bimetallic catalysts on hydrogen yield. Different nickel-based catalysts are tested to ascertain their performance in removing hydrocarbons and optimising hydrogen production, the five chosen nickel-based catalysts are, Ni-Al, Ni-Do, Ni-Si, Ni-Ze and Ni-MCM41.

4.2.1 Influence of 10% Nickel loading of different support on hydrogen production in steam reforming stage

In this section, the catalysts used in the second stage were varied; 10NiAl, 10NiDo, 10NiMCM41, 10NiSi, and 10NiZe and a blank experiment for the catalytic steam reforming (CSR) process while 5FeAl catalyst in the third-stage water gas shift (WGS) reactor was kept constant. The other parameters kept unchanged were the temperature at 750°C, steam/carbon ratio (1:4) and steam flowrate (6.64ml/hr)

Tan et al. (2019) showed the evidence of the excellent catalytic performance of co-impregnated prepared nickel catalyst with dolomite as a promoter, a high hydrogen yield representing 66.2% and carbon conversion to gas representing 77.7% with the least amount of filamentous coke deposit under the steam reforming of gasified tar at 700^0C. This explains why Ni/Do was chosen. Other selected catalysts were also based on empirical evidence from the literature. Nejat et al. (2019) showed 90% and 80% for conversion of ethanol and yield of hydrogen respectively from catalytic steam reforming of ethanol using bimetallic catalysts (NiCo/MCM-41) where MCM-41 significantly enhance the catalyst performance. The oxide of silica (SiO_2) was found to have low interaction with nickel-metal in low-temperature steam reforming of methane, a non-oxide form of silica might proof otherwise because of the low price of silica (Kho et al. 2015). Studies have also shown that several metal loadings (3–7 wt.%) of Nickel when impregnated different zeolite types at 700 °C, has depicted different levels of carbon deposit. For example, the 7 wt.% Ni-Ze showed the highest coke deposition. The highest and least methane conversions of 91.6% and 12.3% were achieved with 7 wt.% Ni/zeolite-Y and 7 wt.% Ni/zeolite-A, respectively. More so, mild CH_4 catalytic conversion of 57.8% was observed with 7 wt.% Ni/ZSM-5 (Muraza et al. 2015; Luengnaruemitchai and Kaengsilalai, 2008).

Table 4-3: Product yields (wt%) from pyrolysing, catalytic steam reforming and water gas shift of wood pellet with and without catalyst in the second stage

Catalyst	Blank-Blank	10Ni-Al: Blank	10Ni-Al: 5Fe-Al	10Ni-Do: 5Fe-Al	10Ni-MCM41: 5Fe-Al	10Ni-Si: 5Fe-Al	10Ni-Ze: 5Fe-Al
Gas/Biomass (wt%)	45.47	62.68	74.52	80.72	62.44	60.71	57.02
Residue char/Biomass (wt%)	23	22.5	23.5	23.5	24	23	25
Gas Yield (vol%)	10.83	19.43	22.05	23.60	19.33	18.56	19.66
mmolg^{-1} Feed of H_2	0.67	20.72	24.19	27.20	20.64	19.20	23.396
H_2/CO molar ratio	0.45	2.36	2.50	3.12	2.82	3.12	3.29

As depicted in Table 4-3, a relatively constant residual char was obtained, representing an average of 23.5 wt%. Since the process conditions in the water gas shift stage were kept constant, the variations in the gas/biomass weight per cent, gas yield and hydrogen yield were principally influenced by the different catalysts in the steam reforming reactor except for the 10Ni-Al: Blank system. The highest and lowest gas yields were observed in 10Ni-Do: 5Fe-Al and Blank-Blank catalysts. A similar result of very high catalytic performance was obtained for 10wt% Ni/dolomite catalysts by Srinakruang et al. (2005) which was attributed to the influence of the low calcination temperature (500^{0}C). In another study, NiO/Dolomite also showed high hydrogen production from municipal solid waste (MSW) gasification (Wang et al., 2012). Yoon et al. (2010) showed that reaction temperature has a significant influence on the product gas yields of reforming with dolomite catalyst, that is, the composition of hydrogen rose with temperature. At above 700°C, the yield of H_2 rose while a decline in CO was observed, the CO_2 yield was not affected. They concluded that then a rather steam reforming reaction is alone occurring, water gas shift reaction (WGSR) was also activated. This means that the steam reforming and the WGSR were taking place simultaneously. This provides for the carbon monoxide gas (CO) to interact with steam, therefore increasing hydrogen yield and decreasing the CO yield. However, at a higher temperature (above 750°C), H_2 yield declined which was as a result of friability and low attrition properties of dolomite (Simell et al. 1997; Sutton et al. 2001). Therefore, in the choice of dolomite catalyst, the temperature factor should hence be considered.

Newly developed Ni on dolomite catalyst (Ni/dolomite) exerted high activity and stability under a short contact time of W/F: 0.55 g h/mol, for the gasification of tar by steam, which was investigated by using toluene as the model compound. Moreover, the performance of the Ni/dolomite catalysts gave negligible carbon deposition, while the conventional supported Ni catalysts gave fairly large carbon deposition. It was found that the calcination temperature significantly influences the property and the activity of the Ni/dolomite catalyst

As expected, Blank-Blank (that is, no catalysts utilised) showed the lowest gas and hydrogen yields. This shows the important role catalyst play in enhancing gas yield and H_2 production. The order of catalytic performance of the catalysts based on the total gas yield under the investigated process conditions in this study are:

10Ni-Do > 10Ni-Al > 10Ni-MCM41 > 10Ni-Si > 10Ni-Ze > Blank-Blank

Another striking observation in these results is the difference between the gas yield of 10Ni-Al: Blank and 10Ni-Al: 5Fe-Al catalyst. Without a catalyst in the water gas shift stage, the total gas yield was 62.68%, this yield rose by 18.9% when 5wt% FeAl was utilised. This showed the evidence of a good catalytic performance of 5FeAl.

Table 4-4: Gas composition (wt%) from pyrolysing, catalytic steam reforming and water gas shift of wood pellet with and without catalyst in the second stage

Product gases	**Blank/ Blank**	**10NiAl/ Blank**	**10NiAl/ 5FeAl**	**10NiDo/ 5FeAl**	**10NiMCM41/ 5FeAl**	**10NiSi/ 5FeAl**	**10NiZe/ 5FeAl**
CO(vol%)	38.8	21.8	21.9	18.1	21.4	20	18.6
H_2(vol%)	17.6	55.0	54.7	56.4	55.2	53.9	61.2
CO_2 (vol%)	19.2	20.1	20.8	23	20.6	21.9	18.6
CH_4(vol%)	16.4	2.3	2.0	2.5	2.2	3.8	1.4
C_nH_m(vol%)	8.0	0.7	0.5	0.10	0.6	0.4	0.3
Total (wt%)	45.47	71.52	74.51	80.72	62.44	60.71	57.02

As shown in Table 4-4, the dominant product gases obtained H_2, CO, CO_2, CH_4 and other products are the light molecular weight hydrocarbons; methane, ethene, ethane, propene, propane, butene & butadiene, and butane. However, it is worth mentioning that these observed gases are the direct product of pyrolysis of the wood pellet pyrolysis and the secondary reactions (steam reforming and water gas shift reaction). In other words, they are primarily condensable and non-condensable gases, char and steam. Steam produced is being used up during the steam reforming and water shift stages through the influence of selected catalysts.

The highest yield of H_2 and the lowest CO_2 yield was found with 10Ni-Ze representing 61.2 and 18.6 (vol%) respectively. This is an evidence of higher reforming reactivity (that is, excellent steam-methane reforming reaction) having a high $CO:H_2$ of about 1:3. As can be seen in table 4-3, the CH_4 level for NiZe was the lowest which means that the methane produced in the pyrolysis has been significantly converted to H_2. A meagre amount of hydrocarbons produced by this catalyst representing 0.3 vol% is also an indication of good resistance to coking and high retardation of catalyst deactivation. Several authors have reported high selectivity (above 90%) of NiZe to H_2 production and good chemical stability due to the strong interaction between zeolite support and the active nickel metal (Kwak et al. 2010; Inokawa et al. 2011; Contreras et al., 2014).

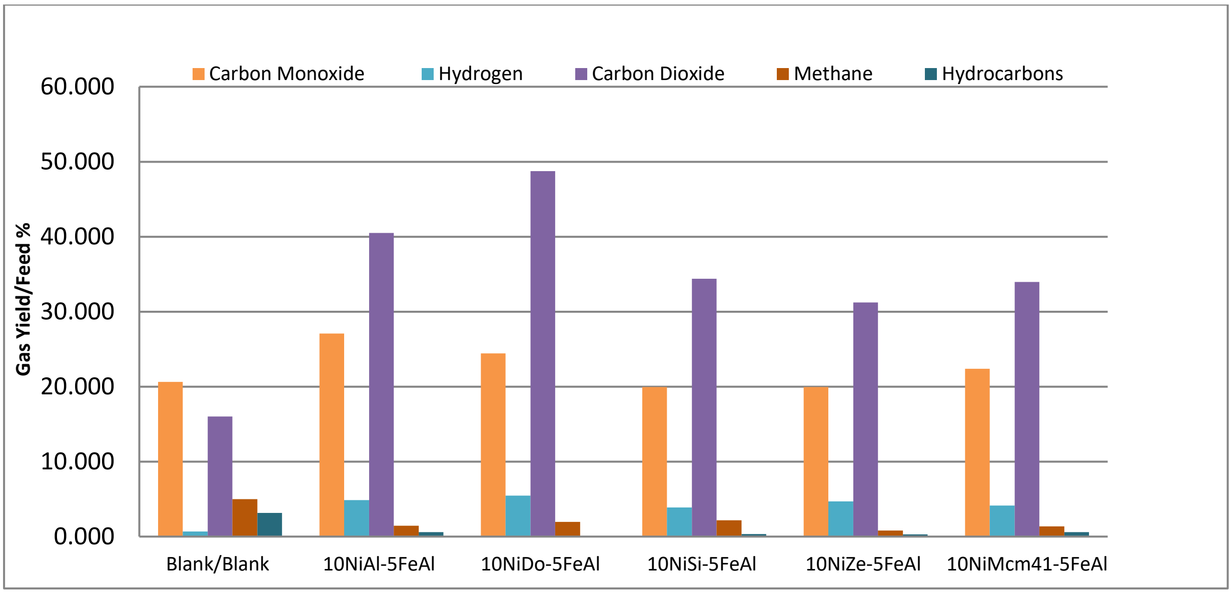

Figure 4-5: Gas Volume Percentage Comparison

As shown in figure 4-5, there was a significant difference in the total gas yield and gas compositions across the different catalysed and non-catalysed processes; The residual char was relatively constant across the experiments (21-25wt%) because the process conditions at the pyrolysis stage were kept constant. Jong et al. (2003) similarly obtained a constant char yield of 13.8wt% from 13-16mg wood pellet sample, a slight decrease in their char yield was due to their pyrolysis high temperature of 900°C compared to 750°C used in this study, this supports the claim that a high temperature and smaller particle sizes increase the heating rate and leading to a decreased in char yield (Arregi et al. 2018).

As can also be seen in Figure 4-5, the H_2 volume per cent ranges from 3.174 to 24.426 while the gas composition is predominantly CO_2 (in the range of 4.403 to 48.74wt%), and CO (in the range of 1.0537 to 27.097wt%) which suggests that the catalysts significantly promoted the water gas shift reaction and the steam reforming reaction. Hydrogen yield expressed in mmol per gram of biomass ranges from 0.674 to 27.195. It is also observed from the results obtained that there was a significant difference in the catalytic conversion performance of the different catalysts tested in terms of selectivity towards H_2 in the steam reforming stage under the same process conditions. For all the catalysts tested, the selectivity towards H_2, CO and CO_2 varied due to different factors as explicitly discussed below.

4.2.2 Steam reforming and water gas shift without catalyst

The gas composition obtained with Blank-Blank catalyst in the second and third stage reactions were shown in figure 4-5. The Blank-Blank catalyst means the absence of catalyst in the steam reforming stage as well as in the water gas shift stage. It is evident that without catalyst usage, the cost implication of the production is the least, but what amount of product gases can be gotten from this and what is the quantity of hydrogen can be generated? As obtained, the total gas yield and the hydrogen yield of 10.83% and 0.674mmol/g biomass respectively were the lowest while the CH_4 and the C1-C4 light hydrocarbons produced were the highest representing 16.4 and 8.0 vol% respectively. Takanabe et al. (2004) on sustainable hydrogen from bio-oil found out that in the absence of catalysts (blank experiment) in steam reforming no conversion was observed. In contrast, an empty reactor tube representing a blank experiment gave rise to the production of CO, H_2, CH_4, CH_3CHO as well as a trace amount of C_2H_4 in the gas phase upon steam reforming of ethanol at 400°C (Fatsikostas et al. 2004).

Homogenous dehydrogenation of the alcohol was responsible for the decomposition of the C-C bond of the aldehyde (CH_3CHO), hence leading to the production of CO and CH_4. Homogenous activity is favoured when the catalyst is absent in steam reforming reactions at higher temperatures, lower temperature (usually <600°C) leads to dehydrogenation while elevated temperatures above 700°C favour dehydration and cracking or dissociation (Fatsikostas et al. 2004). Similarly, above 617°C selectivity towards acetaldehyde due to dehydrogenation of ethanol was observed with optimum at about 630°C but temperatures ranging from 700°C and above selectivity towards CO, CH_4 and C_2H_4 increased as shown in equation 4.1 and 4.2 below (Liberatori et al. 2007).

$$C_2H_5OH \leftrightarrow CH_2 = CH_2 + H_2O \qquad 4.1$$

$$C_2H_5OH \leftrightarrow CH_3CHO + H_2 ® \, CH_4 + CO \; + H_2 \qquad 4.2$$

The results obtained in this present study agrees with the above previous empirical results, at a higher temperature the reforming was selectivity towards hydrocarbons and carbon monoxide (CO) accounting for the highest among all the tested catalysts (8.0 vol% and 38.8vol% respectively) and lowest H_2 yield (17.6 vol%). The low proportion of CO_2 obtained is indicative of the fact that no water gas shift reaction took place (Chiodo et al. 2010; Matter et al. 2004). In addition to this, based on the observed 1:2, H_2:CO respectively, there is also no possibility that steam reforming reaction took place, the idea H2/CO for steam reforming ranges from 1.82-2.10(Xing et al. 2010). One important finding is that in the absence of catalysts in the reactor, the total gas yield diminished, and the undesired hydrocarbon products generation are favoured.

4.2.3 Steam reforming with 10Ni-Al catalyst and water gas shift without catalyst

In the advent of using 10NiAl catalyst in the second stage while the WGR stage is uncatalyzed, the gas volume per cent composition is in the order of $CH_4 < C_nH_m < CO_2 < CO < H_2$ representing 2.3, 8.0, 20.1, 21.8 and 55.0vol% respectively. As shown in table 4.6, in the absence of catalysts in the steam reforming and water gas shift reactors, there was high selectivity towards CO, CH_4 and C_nH_m indicating the absence of water gas shift and steam reforming reaction. Upon the addition of 10NiAl to the second stage, steam reforming reaction but without catalyst in the third stage, a sharp rise in hydrogen yield by 46.3% from17.6vol% was observed. In the same vein, the H_2:CO also increased from 1:2 to 2.5:1 which significantly indicated high catalytic activity of 10NiAl in the steam reforming stage. The total gas and CO_2 yield also rose by 57.29% and 4.6% respectively. In an investigation by Arcotumapathy et al. (2014), the presence of 10Ni/a-Al catalyst significantly reduced the activation energy of the Steam reaction (that is, the CH_4 consumption); hence, the yield of H_2, CO and total gas increased. As can also be seen in table 4.6, the level of C_nH_m hydrocarbons declined steeply, but in comparison to other results obtained where the water gas shift reaction was catalysed with 5FeAl, it was relatively high, and this suggests that the WGR stage was not promoted. More so, a dip in total gas yield was also observed relative to other investigations with catalysts at the third stage. The obtained selectivity to hydrogen (20.723mmol of H_2 per gram of feed) shows that 10NiAl catalyst is effective in Steam reforming. The CH_4 content (2.3 vol%) cannot be linked with methanation due to the large CO per cent that was not converted representing 21.1vol%. There is no available literature on three-stage fixed bed reactor that involved pyrolysis, steam reforming and water gas shift; hence there is sufficient information that could lead to the conclusion that water gas shift reaction did not take place in the third stage. However, studies had been reported on the two-stage fluidised reactor. Yi et al. (2010) attempted to find a suitable catalyst for optimum hydrogen yield via both steam reforming and water gas shift reactions. Au–ceria catalyst was found possessing both high SRM and WGSR activity with high selectivity to CO_2 at temperatures below 250°C. Nevertheless, the SRM and WGSR were discrete experiments that did not account for product gases compositions in the absence of catalysts in the WGSR stage. Xing et al. (2010), reported that an elevated H_2/CO value (>3) of the syngas from SRM depicts the presence of water gas reaction as shown in figure 4-6, this may not always be true because there different process conditions that could trigger higher H_2/CO which include catalyst type, temperature, nature of feedstock, among others (Nakamura et al. 1994).

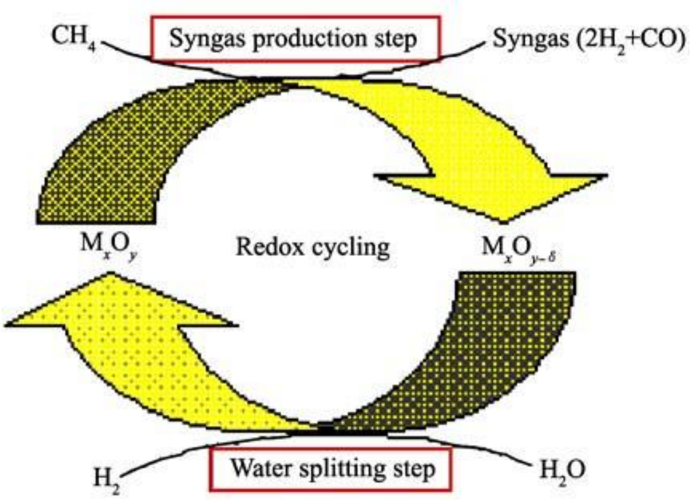

Figure 4-6: Schematic of two-step reforming of methane (Xing et al 2010)

In another study, Kemppainen et al. (2015) found out that in a blank experiment (empty layer furnace), water gas shift reaction occurred at a low rate at a temperature above 500^{0}C but even at lower temperatures ranging between 300^{0}C to 400^{0}C forward water-gas shift reaction was promoted. Wheeler et al. (2004) intermittently ran Blank experiments (that is, without catalytic material on the support) to confirm homogeneous reactions or reactions on impurities in the water gas shift reactor. Common to all the blank experiments conducted was that CO conversions were negligible even at a higher temperature at 1000 °C, as shown in figure 4-7.

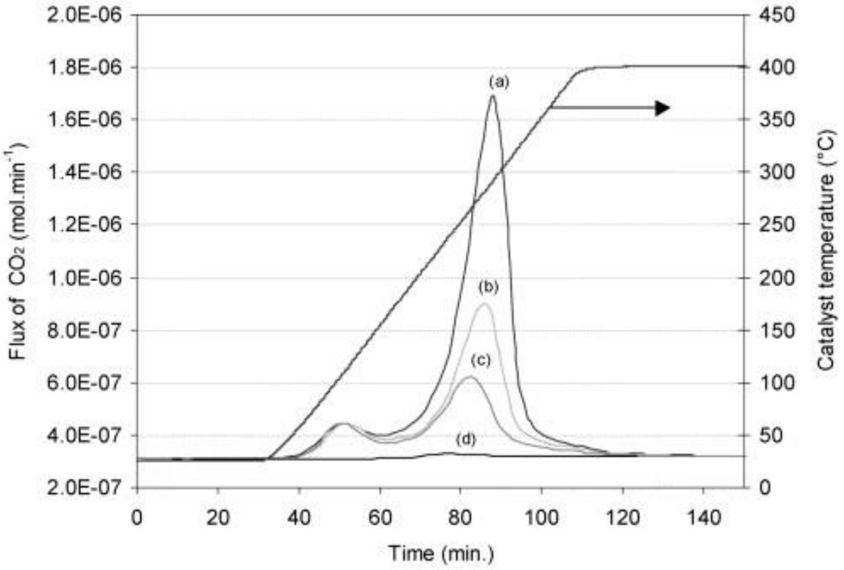

Figure 4-7: TPO profiles for the 2% Pt/CeO$_2$ exposed to 10% CO for (a) 126 min, (b) 45 min, (c) 15 min, and (d) blank experiment (no catalyst and flowing of 10% CO for 60 min between zones A and B). (Wheeler et al. 2004)

One substantial deduction from this result is that 10NiAl catalyst showed strong catalytic performance which gave rise to higher total gas yield and excellent selectivity towards Hydrogen in the steam reforming reactor, and there is no enough evidence to show that water gas shift reaction was absolutely inactive in the third stage.

4.2.4 Steam reforming with 10Ni-Al catalyst and water gas shift with 5Fe-Al catalyst

Figure 4.5 presents the gas composition obtained by using two different catalysts 10Ni-Al and 5Fe-Al at the secondary reaction stages; steam reforming and water gas shift reactors respectively. As observed, the yield of syngas; CO_2, CO and H_2 (20.8, 21.9 and 54.7vol% respectively) were higher while there was a gross reduction in the yield of CH_4 and C_nH_m hydrocarbons (2.0 and 0.5vol% respectively) compared to when no catalyst was used (2.3 and 0.70vol%). This suggested that both SR and WGR were favoured, the 5Fe-Al catalyst therefore reliable plays a more significant role. As also can be seen, the hydrogen yield increased from 20.723 to 24.194mmol g^{-1} biomass, representing 16.75% rise in the hydrogen yield from when no catalyst was used. Again the CO_2 and CO selectivity were low; this suggested that reverse water gas shift and reverse steam reforming were not significantly promoted.

In a recent study on Steam reforming of different biomass tar model compounds over Ni/Al_2O_3 catalysts, Williams et al. (2017), found out that increasing the Ni metal loading in the catalyst (5 - 20%) significantly improves the catalytic property of carbon conversion and selectivity towards H_2 formation in the SR system. Coking effect is also found to increase with increasing metal loading until the optimum level is found for 40% Ni (6.5 wt.%). This is, however, inconsistent with that of Alberton et al. (2007), this might be as a result of the different feedstock gases used for steam reforming, while Alberton et al. utilizes ethanol, Williams, on the other hand, uses biomass pyrolysis product gases which would reflect the actual potentials of reacting gases.

According to Vicente et al. (2014), at below 500^0C 10NiAl is prone to deactivation due to coke deposition, and above 700°C, the catalyst is susceptible to sintering. As seen in Table 1, the concentration of C_1 - C_4 hydrocarbons is relatively high (0.50vol%) representing the third highest after the WGS blank test. Furthermore, in their findings, 10NiAl have higher catalytic stability compared to 10CoAl catalysts; this strength is a direct effect of their metal dispersion, hence impedes the blockage of the metallic site. Choong et al. (2011) modified this catalyst into a bimetallic catalyst by adding Calcium (Ca) at different metal loadings; they found that coking effect is removed grossly, and its catalytic conversion and stability improve at 10Ni/3Ca-Al_2O_3. However, the cost implication of the added Ca poses another hurdle. Therefore, incorporating another metal into the catalyst can significantly reduce the formation of the undesired C_nH_m.

4.2.5 Steam reforming with 10Ni-Do catalyst and water gas shift with 5Fe-Al catalyst

As revealed in figure 4.5 nickel supported on dolomite catalyst among all tested catalysts generated the highest gas to feed weight per cent (80.72wt%). Similarly, the selectivity of H_2 and yield of both CO_2 and H_2 were the highest (48.74 and 5.48wt%). The lowest level of C_mH_n was also recorded (0.102wt%), and also a reduced concentration of CH_4 (1.97wt%), this is an evidence that methane has undergone reforming The gas yield, hydrogen concentration and the H_2/CO molar ratio rose to the optimum (23.595, 27.195mmolg^{-1} and 3.119 respectively). The high H_2/CO ratio representing >1 agreed with the understanding of Xing et al. (2010) that water gas shift reaction was active. Among the tested catalyst, this empirical result presented 10NiDo as the best catalyst for enhancing the production of hydrogen and CO_2 under the investigated process conditions. It showed that the CO produced during the steam reforming and were used up in the WGR process. The low level of the light hydrocarbons and CH_4 is proof that 10NiDo is effective in eliminating coke deposition and the possibility of catalyst poisoning through chemical kinetics.

A rise in CO_2 selectivity is also observed, while CO declines, this is because water gas shift reaction is taking place, this also explains the rise in hydrogen selectivity. However, despite the minimum CO concentration, at 550 °C, with a steep rise in hydrogen selectivity, there is a slight escalation for methane selectivity. According to Vizcaino et al. (2007) investigation, where the concentration of CH_4 and CO, while CO2 level rises, is probably because the CH_4 SR starts to extend further while the WGSR equilibrium is displaced towards H_2 and CO_2 formation. As the temperature rises, the catalytic properties of CH_4 SR also rises, may while the WGSR reaches equilibrium, in order for CO to remain unconsumed. This consequently results in an increase in its production and a relatively constant CO_2 level.

In general, Dolomite being an ore of calcium and magnesium [$CaMg(CO_3)_2$] in recent times is gaining attention as one of the best efficient catalyst for tar and coke elimination in a reactor from product gases, promoting SR and WGS reaction most especially the calcined dolomite (Siedlecki et al. 2009, Hu et al. 2006, Roche et al. 2014, Williams, et al. 2015). Similar to the result obtained in this study, Hu et al. in their investigation found out that the calcined dolomite catalyst proved to be the best active downstream catalyst for marginally optimising hydrogen yield (130.9gH_2/kg daf biomass). However, Hu et al. further found out that the calcined dolomite catalyst became friable and brittle, which suggests poor mechanical intensity as they cannot withstand high-temperature nature of steam reforming.

Consistent, with the result of this study, is the findings of Wei et al. (2007). They find that dolomite produces the least tar yield, which accounts 11.2 g/Nm^3 and 9.4 g/Nm^3 tar content in the gas for legume straw and pinewood respectively at 800 °C. They also find that dolomite has the weakest mechanical resistance as it undergoes severe attrition, especially in fluidised beds.

Hence, their application in a fluidised bed reactor and commercial-scale systems is seemingly unrealistic.

4.2.6 Steam reforming with 10Ni-MCM41 catalyst and water gas shift with 5Fe-Al catalyst

Nickel incorporated MCM-41 mesoporous molecular sieves (Ni-MCM-41) as observed in table 1 has an excellent catalytic activity of CH_4 conversion profile of the steam reforming reaction. Under the conditions used for other catalysts, a selectivity towards hydrogen (53.2vol %) which is quite similar to that of 10NiAl catalyst (54.7vol %) is obtained. A considerable good yield of H_2, CO and CO_2 are recorded (20.64mmol per biomass gram, 21.4vol% and 20.6vol% respectively). Of all the catalyst tested 10NiMCM41 catalyst is the fourth-best with respect to the total gas yield of 19.325vol%. The relatively equal volume per cent of H_2 (55.2%) suggests that the catalyst is more selective towards CH_4 SR.

However, catalytic stability and carbon formation problems are the drawbacks to the use of this catalyst, Lau et al. (2009) report that Ni-MCM-41 catalyst synthesised by direct incorporation method have better catalytic stability than the impregnated catalysts. More so, Ni-MCM-41 with high metal loading has high stability with a contrasting high carbon formation, which by implication means both reforming and carbon deposition are simultaneously taking place on the active metal surface. This is conspicuous in this experiment as hydrocarbons concentration is the third highest (0.58wt%) compared to other tested catalysts. Similar findings are also reported by Williams et al. 2011 and Arbag et al. 2010. Therefore, one would deduce that CO_2 reforming of CH_4 is highly susceptible to carbon formation. An increase in the steam to carbon ratio can significantly reduce this.

4.2.7 Steam reforming with 10Ni-Si catalyst and water gas shift with 5Fe-Al catalyst

Similar to 10NiDo-5FeAl performance, 10NiSi-5FeAl catalyst actively reformed the volatile product gases, leading to high CO_2 yield (21.9vol %) and relatively low CO yield (20vol %). The selectivity of hydrogen is, however, the lowest compared to other catalysts tested. One pitfall of this catalyst is the high yield of CH_4 which suggests that methanation is favoured; this is possibly a function of weak interaction between nickel and silica supports. Therefore, the catalytic activity of SR is reduced, which also account for the dip in the total gas yield. The implication of this is that nickel supported on silica is not active for steam reforming of pyrolysis product gases. Nevertheless,10NiSi has relatively high thermal and mechanical stability, but its selectivity to CH_4 is its application major drawback. According to Zhang et al. 1998 in Shen and Yoshikawa (2012), NiSi catalysts are easily prone to quick deactivation due to coking resulting from the deposition on their surfaces enormous carbon.

4.2.8 Steam reforming with 10Ni-Ze catalyst and water gas shift with 5Fe-Al catalyst

Fig 4-5 presents the gas composition obtained from nickel supported on zeolite catalyst over steam reforming. The lowest methane yield is observed (1.4vol%) and second-lowest hydrocarbon yield (0.3vol%) while a good yield of CO_2, CO and H_2 are obtained representing (18.6, 18.6 and 61.2vol % respectively). The hydrogen yield of 23.396mmol per gram of biomass is only second to dolomite supported catalyst (27.195mmol/g biomass). This result suggests that NiZe actively catalysed the steam reforming reaction. However, it is very likely that the zeolite conversion performance (92.3%) and total gas yield of 57.017vol. is affected by reverse steam reforming but not high temperature nor susceptible to coking.

In a similar investigation by Gayubo et al. (2014), the catalytic activity (H_2 yield) of Ni catalyst supported on SiO_2 (10Ni/Si) increases steadily along the 20hrs slope. The conversion performance of 10NiSi exceeds that of 10Co/Si, 20NiSi and 5NiSi which can be attributed to its ease of decomposing

C-C bond. High metal loading of 20wt% performs poorly as a result of the strong agglomeration of metal crystals. They also studied the effects of temperature on the catalyst and reforming of ethanol, at a temperature below 500^0C, H_2 yield declines and carbon deposition escalates leading to deactivation as well as above 700^0C. At 500 and 600°C, the highest H_2 yields are recorded. In general, several studies agree that there is a reliable prospect for the industrial application of nickel supported on Zeolite.

Based on these results, 10NiZe is a better catalyst for obtaining high hydrogen yield over a long period with less coking effect due to high temperature unlike 10NiDo of high propensity to friableness under the conditions of this study.

4.3 Influence of Bimetallic catalysts in the Water Gas Shift stage

In recent times, bimetallic catalysts have been found to exert huge catalytic activity, excellent thermal and chemical stability, selectivity to desired products and strong resistance to both coke deposition and sintering as result of the functional interactions between the two incorporated metals. These qualities account for their increasing utilisation for thermochemical reactions (Dai et al. 2012, Wei et al. 2012, Lin et al. 2010, Ni et al. 2007). As reported in Dai et al. (2010), the incorporation of cobalt to Ni-based systems offers a significant influence on the metal-support interaction thereby reducing reaction temperature and product yields. 6CoNi/Al catalysts were found to enhance H_2 yield in the water shift reaction better than a monometallic 6Co/Al system. The addition of 1%wt of Ni to 10%wt Co Alumina catalyst raised the H_2 yield from 3.4mol H_2 per EtOH to 3.9 at 273^0C (Andonova et al. 2011).

Choong et al. (2011) incorporated Rh in a Ni-MCM-41-V catalyst; their finding shows that the Rh-Ni-MCM-41-V incorporated bimetallic catalysts resulted in higher methane conversion more than the conversion profile obtained with Ni-MCM-41-V. This implies that Rh improves the catalytic activity of the reforming reaction.

In catalytic dehydrogenation, the incorporating of Sn into Pt catalyst (Pt-Sn/Al_2O_3) is proven to increase the activity, selectivity, stability and poisoning of the bimetallic catalyst. The Sn influences the electronic characterises and morphology of Pt surface or reduces the concentration of Pt ensembles which is required for coke production (Resasco, 2003, Cortright and Dumesic, 1995).

A recent investigation by Zhaoa and Lu (2016) reveals higher ethanol conversion, anti-coking and stabilities properties of addition of nickel to Cobalt alumina catalysts (Ni-Co/Al_2O_3) for steam reforming of ethanol (SRE) than the addition of Cobalt to nickel alumina catalyst (Co-Ni/Al_2O_3). In their findings, the catalytic activity depends mostly on the surface species dispersion over the support which could be modulated by the synthesis process. Secondly, higher metal loading corresponds to higher steam reforming of ethanol, that is Ni-Co/Al_2O_3, Co/Ni/Al_2O_3 and Ni/Co/Al_2O_3 catalysts at the metal loading of 31.5%, 29.1% and 28.0%, respectively results in conversion performance of 68.7%, 50.9%, 36.6% at 350 °C. They also find high H_2 and CO_2 selectivities of 97.2%, 88.9% and 87.4%, respectively during a 100 h SRE over Ni-Co/Al_2O_3 catalyst at 550°C.

Similarly, Carrero et al. (2017) incorporated Cu, Co, and Cr to the Ni/SBA-15 catalyst to build smaller crystallites of the Ni phase. Out of these catalysts, Ni-Cr/SBA-15 catalyst indicates the best reduction profile towards higher temperatures which depicts a stronger metal-support interaction and hence produces the best glycerol conversion, hydrogen production and coke reduction compared especially to the Ni/SBA-15 material.

In this current investigation, all the process conditions were kept constant (second stage catalyst - 10NiAl, temperature for pyrolysis 500°C, steam reforming 850°C and water gas shift 350° C. The WGS catalysts which were substituted with bimetallic catalysts made of 2.5wt%Fe and the following 2.5wt% metals (Mn, Co, Cu and Zn). The results obtained are presented in figure 4-7 and table 4-5.

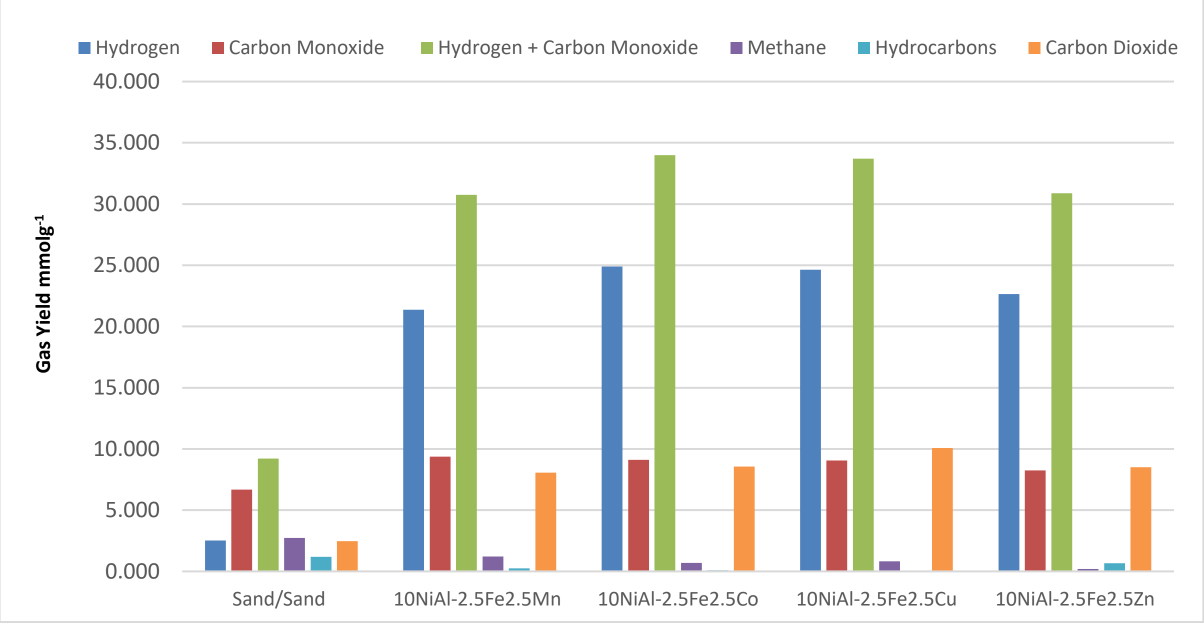

Figure 4-8: Comparison of Hydrogen and Syngas production from bimetallic catalysts

Table 4-5: Gas Volume Percentage Comparison

GAS	10NiAl-5FeAl	10NiAl-2.5Fe2.5Mn	10NiAl-2.5Fe2.5Co	10NiAl-2.5Fe2.5Cu	10NiAl-2.5Fe2.5Zn
Carbon Monoxide	21.9	23.3	21.0	20.3	20.4
Hydrogen	54.7	53.0	57.4	55.2	56.2
Carbon Dioxide	20.8	20.0	19.7	22.6	21.1
Methane	2.0	3.0	1.6	1.8	1.8
Hydrocarbons	0.5	0.7	0.2	0.1	0.5
H_2 mmolg/g biomass	24.19	21.37	24.90	24.64	22.66
TOTAL GAS YIELD (wt%)	74.51	68.67	69.53	76.15	66.80

As seen in table 4-5, the H_2 and CO_2 selectivity of the bimetallic catalysts of Cu and Zn are higher than that of single metal 5FeAl catalyst, indicating the evidence of optimisation of WGS. The total gas yield of Cu based was the highest which is entirely consistent with that of Zheng et al. (2016) that studied the influence of the quantity of Cu and Fe in optimising selectivity to hydrogen in steam reforming and water-gas reaction. It was found that a 2.5Fe2.5Cu-Nickel catalyst obtained optimum catalytic performance, the reduction in the hydrocarbon was associated with the excellent structure and morphology of the Cu and Fe phases. In the present study, the bimetallic Fe-Cu catalyst indicated a strong resistance to coking or sintering due to producing the lowest hydrocarbon content (0.1Vol%)

The 2.5Fe2.5Mn catalyst has the highest CO, CH_4 and hydrocarbons selectivity, and the lowest H_2 selectivity among all the bimetallic catalysts and the single metal catalyst. As reported in Wang et al. (2010), Mn-promoted catalysts have higher hydrocarbon and olefin selectivity as a result of enrichment of Mn atoms on catalyst surface which can be susceptible to sintering effect and hence low total gas and hydrogen yields. On the other hand, 2.5Fe2.5Co catalyst has the best hydrogen yield (57.4vol% and 24.90mmol per gram of biomass, about 2.9% increase above the single 10FeAl catalyst. However, the concentration of hydrocarbon was best reduced by bimetallic Cu and Co catalysts.

In general, there is no significant difference in hydrogen yield except for 10NiAl-2.5Fe2.5Co and 10NiAl-2.5Fe2.5Cu which shows a remarkable reduction in their undesirable hydrocarbon and methane selectivity by 60% and 20% respectively relative to 10FeAl single catalyst. The catalysts are also selective towards CO_2 corresponding with the single metal catalyst which indicates the occurrence of reverse water gas shift reaction.

In a reforming of methane study conducted by Arbag et al. (2010) using a single Ni metal (Ni-MCM-41-V) and bimetallic Rh-Ni catalyst (Rh–Ni-MCM-41-V), CO selectivity (with respect to CH_4 conversion) produced with Rh–Ni-MCM-41-V is lower than with Ni-MCM-41-V under the same process conditions. During the first 4-h period, CO was about 2.5 with the Ni-MCM-41-V catalyst while a reduction is obtained with the Rh–Ni-MCM-41-V catalyst. Their findings also reveal that Rh incorporation increased the relative catalytic activity for the dry reforming reaction, with respect to the reverse water gas shift reaction. Hence, a decline in the relative significance of the reverse WGS reaction with respect to dry reforming of CH_4.

In another investigation by Charisiou et al. (2016), as temperature rises, CH4 reforming and C_2H_4O reforming and decomposition (to CO and CH_4) are improved with both Ni and Co catalysts, especially with Ni ones, for which the hydrocarbon (C_2H_4O) selectivity above 500 °C is zero and that of CH_4 declines significantly. Therefore, CH_4 selectivity above 600 °C is lower with Ni catalysts than with Co ones; this leads to a higher H_2 yield with the Ni catalysts. However, upon equal amounts of metal loading, the two catalysts (5Ni5Co/Al under the same process conditions, a midway conversion performance is observed. Choon et al. (2011) incorporated Ca into Ni/Al_2O_3 catalyst in ethanol reforming, an excellent stability was found but as the Ca loading increases (1, 3 and 10%), coking rate increases resulting in deactivation because the Ca addition lessens the alumina surface area and also immobilize the chemical interaction between Ni and Al_2O_3. Nonetheless, the selectivity of CH_4, H_2 and CO_2 also increase. According to Bartholomew and Farrauto (2006), one factor that affects the selectivity and catalytic properties of bimetallic catalysts is the differences in the extent of interaction between metals and or alloying. Therefore, further research is required with varying process conditions; perhaps a better result is obtained.

4.4 Conclusion

The key findings of the study include:

1. The nickel loading was instrumental in the production of hydrogen and carbon monoxide. 10% of nickel loading produced the highest amount of hydrogen at 20.90mmol/g while under the same conditions, the sand produced the lowest amount of hydrogen at 2.24mmol/g. 5% nickel loading produced the highest amount of carbon monoxide at 33.93mmol/g with the lowest amount produced by the 20% nickel loading at 8.41mmol/g
2. The 20 wt.% nickel dolomite catalyst produced the highest amount of syngas from the thermal processing of the biomass at 43 mmol syngas $^{g-1}$ which was 33% higher than the 20 wt.% nickel alumina catalyst at 29 mmol syngas $^{g-1}$
3. Due to the increased nickel content in the nickel dolomite, the catalytic activity increased in relation to hydrogen production. Due to the increased nickel content in the nickel silica, the catalytic activity decreased in relation to hydrogen production.
4. Catalyst is undoubtedly required for catalysing the steam reforming stage of the hydrogen generation from biomass. The blank test indicated negligible non-catalytic steam reforming before the catalytic experiments. The results obtained show that without catalyst in the second stage of the thermochemical conversion, the production of hydrocarbons (C_nH_m) and Methane were favoured representing 19.2vol% and16.4vol%. Hence, the potential of hydrogen production from biomass is underutilised and a long cleaning process will be required to generate pure hydrogen fuel, this drives the production cost up.
5. It is also evident that the third stage is also not inconsequential in optimising the production of syngas, a 10NiAl catalyst with zero catalysts in the WGS stage yielded the higher level of the unwanted C1-C4 hydrocarbons and Methane gas (0.7vol% and 2.3vol% respectively) compared to a 10NIAl-5FeAl (0.5vol%CH_4 and 2.0vol% CmHn respectively).
6. Although, nickel supported on dolomite catalyst appears to be the most effective catalyst for optimising the production hydrogen (56.4vol% and 27.195mmol per gram of biomass and reduction in other permanent gases (18.1vol%CO and 23vol%CO_2), it is surpassed potentially by nickel supported on Alumina because of its weak mechanical intensity and friableness. The nickel alumina on the other hand, as supported by several experimental studies can withstand high temperature, actively destroy tars and are relatively cheap. This makes it the most suitable for fixed-bed pyrolytic, catalytic steam reforming and water gas shift process of producing hydrogen fuel.

7. There is no significant improvement in H_2 yield under the bimetallic catalysts relative to the single metal catalysts.
8. The best catalytic activity occurs over the 10Ni-Do among the 5 catalysts tested (Ni-Al, Ni-Si, Ni-Do, Ni-Ze and Ni-MCM41), having a total gas yield of 80.722, H_2 yield of 27.195mmol per gram of feed and H_2/CO molar ratio of 3.12. However, 10NiZe under the process conditions are undertaken in this study proved to be an excellent alternative catalyst to replace Ni-Al which is the conventional industrial catalyst due to its low selectivity to CH_4 and C_1-C_4 hydrocarbons (0.829 and 0.287wt% respectively).

4.5 Reference

Alberton, AL, Souzab, MMVM, Schmala, M. 2007. Carbon formation and its influence on ethanol steam reforming over Ni/Al2O3 catalysts. Catalysis Today. 123(1-4) pp 257-264

Andonova, S. C.N. de Ávila, K. Arishtirova, J.M.C. Bueno, S. Damyanova. Applied Catalysis B, 105 (2011), pp. 346-360

Andre, L. Albertona, Mariana MVM. Souzab, Schmala, M. 2007. Carbon formation and its influence on ethanol steam reforming over Ni/Al2O3 catalysts. Catalysis Today, 123 (1-4), pp257-264

Arbag,H, Yasyerli,S, Yasyerli,N, and Dogu, G . 2010. Activity and stability enhancement of Ni-MCM-41 catalysts by Rh incorporation for hydrogen from dry reforming of methane International journal of hydrogen energy. 35, pp 2296 – 2304

Arcotumapathy, V., Vo, D. V. N., Chesterfield, D., Tin, C. T., Siahvashi, A., Lucien, F. P., & Adesina, A. A. (2014). Catalyst design for methane steam reforming. Applied Catalysis A: General, 479, 87-102.

Arregi, A, Amutio, M, Lopez, G, Bilbao, J, Olazar, M. 2018. Evaluation of thermochemical routes for hydrogen production from biomass: A review .Energy Conversion and Management. 165. Pp 696-719

Bartholomew and Farrauto, RJ. 2006. Fundamentals of Industrial Catalytic Processes. second edition, A John Wiley and Sons incorporate publication, USA

Bruni, G., Rizzello, C., Santucci, A., Alique, D., Incelli, M., & Tosti, S. (2019). On the energy efficiency of hydrogen production processes via steam reforming using membrane reactors. International Journal of Hydrogen Energy, 44(2), 988-999.

Carrero, A, Calles, JA, García-Moreno, L and Vizcaíno, AJ. 2017. Production of Renewable Hydrogen from Glycerol Steam Reforming over Bimetallic Ni-(Cu, Co, Cr) Catalysts Supported on SBA-15 Silica Catalysts, 7(2), 55

Chan, FL Tanksale, A. 2014. Review of recent developments in Ni-based catalysts for biomass gasification. Renewable Sustainable Energy Review, 38, pp. 428-438

Charisiou, N. D., Papageridis, K. N., Siakavelas, G., Tzounis, L., & Goula, M. A. (2016). Effect of active metal supported on SiO2 for selective hydrogen production from the glycerol steam reforming reaction. Bio Resources, 11(4), 10173-10189.

Chiodo, V., Freni, S., Galvagno, A., Mondello, N., & Frusteri, F. (2010). Catalytic features of Rh and Ni supported catalysts in the steam reforming of glycerol to produce hydrogen. Applied Catalysis A: General, 381(1-2), 1-7.

Choong, CKS, Zhong, Z, Huang, L, Wang, Z, Ang, TP, Borgna, A, Lin, J, Hong, L, Chena, L. 2011. Effect of calcium addition on catalytic ethanol steam reforming of Ni/Al2O3: I. Catalytic stability, electronic properties and coking mechanism. Applied Catalysis. 407(1-2), pp.145-154

Contreras, J. L., Salmones, J., Colín-Luna, J. A., Nuño, L., Quintana, B., Córdova, I., ... & Fuentes, G. A. (2014). Catalysts for H2 production using the ethanol steam reforming (a review). International Journal of Hydrogen Energy, 39(33), 18835-18853.

Cortright, RD, and Dumesic, JA, 1996. Reactions of Isobutane and Isobuytlene over Silica-and L-Zeolite-Supported Pt/Sn and Pt/Sn/K Catalysts, in Studies in Surface Science and Catalysis, Vol. 101, eds. J.W. Hightower, W.N. Delgass, E. Iglesia and A.T. Bell, p.1185

Dal Santo, V., Gallo, A., Naldoni, A., Guidotti, M., & Psaro, R. (2012). Bimetallic heterogeneous catalysts for hydrogen production. Catalysis Today, 197(1), 190-205.

DIRECTIVE 2010/31/EU of the European Parliament and of the Council of 19 May 2010 on the energy performance of buildings. The European parliament and the council of the European union; 19 May 2010.

Ellis, P. R., Enache, D. I., James, D. W., Jones, D. S., & Kelly, G. J. (2019). A robust and precious metal-free high performance cobalt Fischer–Tropsch catalyst. Nature Catalysis, 1.

Fatsikostas, A. N., & Verykios, X. E. (2004). Reaction network of steam reforming of ethanol over Ni-based catalysts. Journal of Catalysis, 225(2), 439-452.

Fatsikostas, AN, Kondarides, DI, Verykios, XE. 2002. Production of hydrogen for fuel cells by reformation of biomass-derived ethanol. Catalysis Today, 75, p145

Freni, S., Calogero, G., & Cavallaro, S. (2000). Hydrogen production from methane through catalytic partial oxidation reactions. Journal of Power Sources, 87(1-2), 28-38.

Frusteri, F, Freni, S, Chiodo, V, Spadaro, L, Bonura,G, Cavallaro, S. 2004. Steam reforming of bio-ethanol on alkali-doped Ni/MgO catalysts: hydrogen production for MC fuel cell. Applied Catalysis. A, 270, p. 1

Gayubo, AG, Vicente, J, Ereña, J, Carolina Montero, Olazar, M, Bilbao, J. 2014. Comparison of Ni and Co Catalysts for Ethanol Steam Reforming in a Fluidized Bed Reactor. Catalysis Letters. 144(7), pp.1134-1143

Gil, A., et al., Influence of the preparation method and the nature of the support on the stability of nickel catalysts. Applied Catalysis A: General, 1994. 109(2): p. 167-179.

Guan, G, Kaewpanha, G, Hao, X, Abudula, A. 2016. Catalytic steam reforming of biomass tar: prospects and challenges. Renew Sustain Energy Review, 58, pp. 450-461

Inokawa, H. S. Nishimoto, Y. Kameshima, M. Miyake. 2011. Promotion of H2 production from ethanol steam by zeolite basicity. Int J Hydrogen Energy, 36 (23), pp. 15195-15202

Jong, WD, Pironea, A, and Wójtowiczb, MA. 2003. Pyrolysis of Miscanthus Giganteus and wood pellets: TG-FTIR analysis and reaction kinetics. Fuel, 82(9).pp 1139-1147

Kauranen P, Solin J, Törrönen K, Koivula J, Laurikko J. 2013. Hydrogen Roadmap – The possibilities of hydrogen energy for Finland (In Finnish: Vetytiekartta – Vetyenergian mahdollisuudet Suomelle). Research report. VTT, Espoo.

Kemppainen, A., Alatarvas, T., Iljana, M., Haapakangas, J., Mattila, O., Paananen, T., & Fabritius, T. (2014). Water-gas Shift Reaction in an Olivine Pellet Layer in the Upper Part of Blast Furnace Shaft. ISIJ international, 54(4), 801-809.

Kho, E. T., Scott, J., & Amal, R. (2016). Ni/TiO2 for low temperature steam reforming of methane. Chemical Engineering Science, 140, 161-170.

Kriston A, Szabó T, Inzelt G. 2010. The marriage of car sharing and hydrogen economy: a possible solution to the main problems of urban living. Int J Hydrogen Energy .708–35, pp 12697;

Kwak, B.S. J. Kim, M. Kang. 2010. Hydrogen production from ethanol steam reforming over core-shell structured NixOy-, FexOy-, and CoxOy-Pd catalysts. Int J Hydrogen Energy, 35 (21), pp. 11829-11843

Lasa, HD, Salaices, E, Mazumder, J, Lucky, R. 2011. Catalytic steam gasification of biomass: catalysts, thermodynamics and kinetics Chemistry Review, 111, pp. 5404-5433

Liberatori, J. W. C., Ribeiro, R. U., Zanchet, D., Noronha, F. B., & Bueno, J. M. C. (2007). Steam reforming of ethanol on supported nickel catalysts. Applied Catalysis A: General, 327(2), 197-204.

Lin, J. H., Biswas, P., Guliants, V. V., & Misture, S. (2010). Hydrogen production by water–gas shift reaction over bimetallic Cu–Ni catalysts supported on La-doped mesoporous ceria. Applied Catalysis A: General, 387(1-2), 87-94.

Liu, D, Lau, R, Borgnab, A, and Yanga, H. 2009. Carbon dioxide reforming of methane to synthesis gas over Ni-MCM-41 catalysts. Applied Catalysis A, 358(2), pp 110-118

Luengnaruemitchai A, Kaengsilalai A. Activity of different zeolite-supported Ni catalysts for methane reforming with carbon dioxide. Chemical Engineering Journal 2008; 144(1): 96– 102.

Matter, P. H., Braden, D. J., & Ozkan, U. S. (2004). Steam reforming of methanol to H_2 over non-reduced Zr-containing CuO/ZnO catalysts. Journal of Catalysis, 223(2), 340-351.

Mitchell, S., Michels, N. L., & Pérez-Ramírez, J. (2013). From powder to technical body: the undervalued science of catalyst scale up. Chemical Society Reviews, 42(14), 6094-6112.

Moulijn, J. A., Van Diepen, A. E., & Kapteijn, F. (2001). Catalyst deactivation: is it predictable: What to do. Applied Catalysis A: General, 212(1-2), 3-16.

Muraza, O., & Galadima, A. (2015). A review on coke management during dry reforming of methane. International Journal of Energy Research, 39(9), 1196-1216.

Nakamura, J., Aikawa, K., Sato, K., & Uchijima, T. (1994). Role of support in reforming of CH4 with CO2 over Rh catalysts. Catalysis letters, 25(3-4), 265-270.

Nejat, T., Jalalinezhad, P., Hormozi, F., & Bahrami, Z. (2019). Hydrogen production from steam reforming of ethanol over Ni-Co bimetallic catalysts and MCM-41 as support. Journal of the Taiwan Institute of Chemical Engineers, 97, 216-226.

Ni, M., Leung, D. Y., & Leung, M. K. (2007). A review on reforming bio-ethanol for hydrogen production. International Journal of Hydrogen Energy, 32(15), 3238-3247.

Resasco, D., 2003. Dehydrogenation-Heterogenous, in Encyclopaedia of Catalysis, ed. I.T. Horvath. John Wiley & sons, New jersey, pp 49-79

Shahbaz, M, Yusup, S, Inayat, A, Patrick, DO, Ammar, M. 2017. The influence of catalysts in biomass steam gasification and catalytic potential of coal bottom ash in biomass steam gasification: a review. Renew Sustain Energy Rev, 73, pp. 468-476

Shen, Y, Yoshikawa, K, 2013. Recent progresses in catalytic tar elimination during biomass gasification or pyrolysis – a review. Renew Sustain Energy Review, 21, pp. 371-392

Simell, P.A. J.O. Hepola, A. Krause. 1997. Effects of gasification gas components on tar and ammonia decomposition over hot gas cleanup catalysts. Fuel, 76 (1997), pp. 1117-1127

Soria, M. A., Rocha, C., Tosti, S., Mendes, A., & Madeira, L. M. (2019). COx free hydrogen production through water-gas shift reaction in different hybrid multifunctional reactors. Chemical Engineering Journal, 356, 727-736.

Srinakruang, J., Sato, K., Vitidsant, T., & Fujimoto, K. (2005). A highly efficient catalyst for tar gasification with steam. Catalysis Communications, 6(6), 437-440.

Stewart EM, Lutz AE, Schoenung S, Chiesa M, Keller JO, Fletcher J, Ault G, McDonald J, Cruden A. 2009. Modeling, analysis and control system development for the Italian hydrogen house. Int J Hydrog Energy, 34, pp 1638–46.

Sutton, D. B. Kelleher, J.R.H. Ross. 2001. Review of literature on catalysts for biomass gasification. Fuel Process Technol, 73 (2001), pp. 155-173

Takanabe, K., Aika, K. I., Seshan, K., & Lefferts, L. (2004). Sustainable hydrogen from bio-oil—Steam reforming of acetic acid as a model oxygenate. Journal of catalysis, 227(1), 101-108.

Tan, R. S., Abdullah, T. A. T., Mahmud, S. A., Zin, R. M., & Isa, K. M. (2019). Catalytic steam reforming of complex gasified biomass tar model toward hydrogen over dolomite promoted nickel catalysts. International Journal of Hydrogen Energy, 44(39), 21303-21314.

Vicente, J, Montero, C, Ereña, J, Azkoitib, MJ, Bilbaoa, J, Gayuboa, AG. 2014. Coke deactivation of Ni and Co catalysts in ethanol steam reforming at mild temperatures in a fluidized bed reactor. International Journal of Hydrogen Energy. 39(24), pp.12586-12596

Vizcaíno, AJA, Carrero J, Calles, A. 2007. Hydrogen production by ethanol steam reforming over Cu–Ni supported, 32(10–11), pp. 1450-1461

Wang, H, Yang, H, Xu, J, Wang, H, Ding, M, Li, Y. 2010. Study of bimetallic interactions and promoter effects of FeZn, FeMn and FeCr Fischer-Tropsch synthesis catalysts. Journal of Molecular Catalysis A: Chemical. 326, pp.29-40

Wang, J., Cheng, G., You, Y., Xiao, B., Liu, S., He, P., & Zhang, G. (2012). Hydrogen-rich gas production by steam gasification of municipal solid waste (MSW) using NiO supported on modified dolomite. international journal of hydrogen energy, 37(8), 6503-6510.

Wei, L, Xu, S, Zhang, L, Liu, C, Zhu, H, Liu, S, 2007. Steam gasification of biomass for hydrogen-rich gas in a free-fall reactor. International Journal of Hydrogen Energy, 32, pp. 24-31

Wei, Z., Sun, J., Li, Y., Datye, A. K., & Wang, Y. (2012). Bimetallic catalysts for hydrogen generation. Chemical Society Reviews, 41(24), 7994-8008.

Wheeler, C., Jhalani, A., Klein, E. J., Tummala, S., & Schmidt, L. D. (2004). The water–gas-shift reaction at short contact times. Journal of catalysis, 223(1), 191-199.

Williams, PT, Artetxe, M, Alvarez, J, Nahil, MA, Olazar, MB. 2017. Steam reforming of different biomass tar model compounds over Ni/Al2O3 catalysts. Energy Conversion and Management 136, pp. 119-126

Williams, PT, Wu, C, Wang, L, Shib, J, and Huang, J. 2011. Hydrogen production from biomass gasification with Ni/MCM-41 catalysts: Influence of Ni content. Applied Catalysis. 108-109, pp 6-13

Xing, Z. H. U., Hua, W. A. N. G., Yonggang, W. E. I., Kongzhai, L. I., & Cheng, X. (2010). Hydrogen and syngas production from two-step steam reforming of methane over CeO2-Fe2O3 oxygen carrier. Journal of rare earths, 28(6), 907-913.

Yi, N., Si, R., Saltsburg, H., & Flytzani-Stephanopoulos, M. (2010). Active gold species on cerium oxide nanoshapes for methanol steam reforming and the water gas shift reactions. Energy & Environmental Science, 3(6), 831-837.

Zhang, X, Chan, SH, Ho, HK, Tan, S, Li, M, Li, G, Li, J, Feng, Z. 2015. Towards a smart energy network: The roles of fuel/electrolysis cells and technological perspectives. International Journal of Hydrogen Energy Review, 40(21), pp 6866-6919

Zhaoa, X and Lu, G., 2016. Modulating and controlling active species dispersion over Ni–Co bimetallic catalysts for enhancement of hydrogen production of ethanol steam reforming. International Journal of Hydrogen Energy. 41(5), pp 3349-3362

Zheng, Z., Yang, D., Li, T., Yin, X., Wang, S., Wu, X., ... & Xie, X. (2016). A novel BEA-type zeolite core-shell multiple catalysts for hydrogen-rich gas production from ethanol steam reforming. Catalysis Science & Technology, 6(14), 5427-5439.

Chapter 5: Optimisation of water gas shift reaction following pyrolysis-catalytic reforming for hydrogen production

5.0 Summary

In this chapter, the influence of metal catalysts types and process parameters in the third stage reactor, water-gas shift (WGS) reaction was investigated. The catalytic performance of different metals (Sand, Co, Cu, Zn, Mn, Fe) on Alumina (Al_2O_3) catalysts with respect to activity and selectivity at a constant metal loading of 40% were studied. Empirical evidence of high activity shifted emphasis to Iron (Fe) coated on alumina support catalyst. Therefore the effect of metal loading of this catalyst was considered by varying the metal loading from 5 % to 100 %. Another key process parameter that was studied is the effect of steam flowrate on the gas yield, hydrogen yield and coke formation, testing the carbon to steam ratio at 1:1, 1:2, 1:4 and 1:8. The reacted catalysts for each experiment were characterised by temperature-programmed oxidation (TPO) to investigate the coke amount deposited over the catalyst which reflects the potential for catalysts deactivation. The experimental procedure detailed in chapter 3 was used for all experiments.

5.1 Introduction

As discussed in Chapter 2, the major issue confronting catalysts for both steam reforming and water-gas shift reactions is that they are negatively influenced by certain operating conditions such as temperature, steam to carbon ratio, the reactor used and residence time. More so, the catalysts are also influenced by physical conditions, including composition, metal dispersion, coking, poisoning, and sintering. According to Chen et al. (2008), all these indices, in turn, affect the conversion performance of the water-gas shift reaction and can lead to an increased CO_2 and decreased H_2 production for the same catalyst.

Notably, catalyst deactivation due to coking is a significant issue for both steam reforming and water-gas shift catalysts which is mainly dependent on the certain reaction conditions. Coking can be found in many different forms (Helveg et al. 2011; Sehested, (2006). Despite engineers' best efforts to minimise the issue, techniques currently being used such as increased steam to carbon ratio and the addition of rare earth metal oxides are proving to increase production costs for hydrogen significantly.

Another cause of catalysts deactivation described is sulphur poisoning. Like coking, sulphur poisoning has been shown to affect both water-gas shift and steam reforming catalysts. Regardless of Trimm et al. (1999) assertion that a small amount of sulphur can, in fact, marginally increase catalytic activity, several studies have shown that sulphur often blocks active sites on catalyst surfaces. Successful techniques have been found to reduce this significantly, however, they often involve rare metals which again leads to increased production costs. Finally, sintering has been shown to be a significant problem for catalysts due to the occurrence of hot spots with reactor systems (Wang et al. 2002).

This chapter aims to investigate different catalysts with the best performance in optimising hydrogen production from raw biomass. In addition, understanding of how process parameters influence the WGSR and determining to what extent coking affects the catalysts are elucidated.

5.2 Biomass sample and catalyst preparation

In this investigation, a wood pellet was utilised as the biomass material. The catalysts used in the second (SR) and third (WGS) stages of the reactor were prepared by wet impregnation method (Yurdakul et al., 2016). For the SR stage of the reactor, 10wt% nickel on Alumina support was utilised consistently throughout this chapter investigation. However, for the water gas shift stage, the catalysts used were Co, Cu, Fe, Zn and Mn were all prepared as co-impregnated nickel catalysts. Again, alumina was used as the support for the metal WGS catalysts. In each case, the metal being tested made up 40wt% of the total mass of the catalyst. In the first stage of the process, solutions were prepared by dissolving a calculated amount of metal salt in deionised water. The salts used to synthesise each catalyst are shown in tables 5-1 and 5-2, respectively. In order to calculate the amount of salts required, the following equation was used. A sample calculation has been provided below for 10 grams of iron.

Table 5-1: Metal salts used in catalyst synthesis and their chemical formulas

Metal	**Name of Salt**	**Salt Chemical Formula**
Cobalt	Cobalt (II) nitrate hexa-hydrate	$Co(NO_3)_2 \cdot 6H_2O$
Copper	Copper (II) nitrate penta-hydrate	$Cu(NO_3)_2 \cdot 5H_2O$
Iron	Iron (II) nitrate nona-hydrate	$Fe(NO_3)_2 \cdot 9H_2O$
Zinc	Zinc (II) nitrate hexahydrate	$Zn(NO_3)_2 \cdot 6H_2O$

Manganese	Manganese (II) nitrate tetra-hydrate	$Mn(NO_3)_2{\cdot}4H_2O$

Table 5-2: Molecular mass of metals and their salts used in mass calculations

Metal	Molecular Mass of Metal (g)	Molecular Mass of Salt (g)
Cobalt	58.9	291.0
Copper	63.5	232.6
Iron	55.8	404.0
Zinc	65.4	297.5
Manganese	54.9	251.0

$$Mass\ of\ salt = \frac{Molecular\ mass\ of\ salt}{Molecular\ mass\ of\ metal} \times desired\ mass\ of\ metal$$

$$Mass\ of\ salt\ required = \frac{404.0}{55.8} \times 10 = 72.4\ grams$$

Once fully dissolved, a suspension was formed through the addition of the alumina support in an appropriate amount depending on the desired weight per cent of metal. For example, to make 10 g of 40 wt.% iron alumina 6 g of support would be added to a solution containing 4 g of iron. Prior to adding the support, it was ground down to achieve an average particle size of between 50-212 microns. In terms of the iron catalysts examined in the second investigation, the same synthesis methodology was used. However, the amount of iron-containing salt added during the first step of the technique was varied, and the amount of alumina support added was increased to produce catalysts of 5, 20, 40 and 100 wt.% iron respectively. For the final investigation, the same methodology was followed to produce a catalyst of 40 wt.% iron.

5.3 Experimental process

The production of hydrogen from wood pellet biomass was carried out in the laboratory-scale fixed bed reactor, as discussed in Chapter 3. To provide steam for the second and third stages of the unit, water was injected in between the first and second stages and also into the third stage using syringes. For the first two investigations, the injection rate for both inlets were 6.64 and 1.66 ml hr^{-1} respectively to achieve a total steam-to-carbon ratio (S/C), of 5 with respect to the mole steam/mole carbon contained within the biomass which is similar to Garcia et al., 2000). For the final investigation, this ratio was adjusted by increasing the steam injection rate into the later stage of the system. It should be noted that the ratios investigated in this report only consider the steam injected into the latter stage of the reactor system. Ratios of 1:1, 1:2, 1:4 and 1:8 were all tested. If the steam injected into the second stage of the reactor system was also considered, the ratios would equate to 1:5, 1:6, 1:8 and 1:16, respectively. The injection was set to begin when the pyrolysis temperature reached 150°C.

5.4 Results and discussion

5.4.1 Influence of different catalysts (X_A/Al_2O_3) in the third stage, water-gas shift reaction on hydrogen production

The results of the performance of several catalysts in the third-stage water gas shift reactor with varying metal compositions on the yields of hydrogen, and other products gases (CO, CO_2, CH_4 and C_2H_4) through pyrolysis catalytic SR and WGSR from wood pellets are presented in table 5-3. The mass balance indicated that the quantity of char residue produced by the pyrolysis stage of the reactor unit was constant throughout the investigation. The char residue in terms of the mass of the biomass sample used was around 23% for each experiment. This depicts that 77% of the unpretreated starting biomass was converted into gaseous products during the process of pyrolysis. This level of consistency is expected as the stage should be unaffected by the change in catalysts used downstream.

Table 5-3: Mass balance for the pyrolysis/Steam Reforming/Water-Gas shift reaction over XA/Al2O_3 catalysts

Catalyst	Sand	Co	Cu	Zn	Mn	Fe
Gas/Biomass (wt. %)	75.79	72.31	78.39	77.24	85.37	92.38
Residue Char/Biomass (wt. %)	23.00	23.00	23.00	23.00	23.00	23.00
H_2 Yield (mmol H_2 g^{-1} biomass)	26.47	23.66	29.83	29.97	32.44	32.60
H_2/CO molar ratio	2.44	2.22	2.48	2.41	2.61	2.60

Comparing the conversion performance of the thermochemical system using sand in the water-gas-shift stage of the reactor with each catalyst, it was found that the addition of all, but one catalyst escalated both the total gas and hydrogen yields. From table 5-3, it can also be seen that the total gas yield rose from 76% to about 95% and the volume of hydrogen generated ranged from 26.5 to more than 30 mmol g^{-1} biomass. Although the incremental difference is relative, it was shown that the metals actively do catalyse the water-gas shift reaction. This rise in yield has also been reported in other previous studies for different metals tested (Yanik, et al., 2008; Bukur et al., 2016; Rodriguez et al., 2017). More so, of the metals tested, as shown in table 5-3, iron (Fe) showed the greatest affinity to catalysing the WGS reaction, consequent to the highest gas and hydrogen yields by this catalyst.

The product gases concentrations, as shown in Table 5-4 below, provided further support on the most effective and suitable metal in catalysing the WGS reaction. The results revealed that in the absence of a catalyst in the third stage of the reactor, the concentration of carbon monoxide was slightly higher. Additionally, the concentration of hydrogen in the product gases was much lower. This was not the case with the cobalt catalyst. However, it indicated that all but one of the five catalysts tested significantly catalysed the reaction, which agrees with the result discussed previously (Hilaire et al. (2001). Generally speaking, the build-up of CO and the partial pressure of steam along the reactor's length in the presence of a catalyst, promotes WGSR which in effect increases the stream conversion to CO_2 and H_2. According to Ang et al., (2015), the presence of potassium on a ceria-coated nickel catalyst (Ni/xK/CeO_2) leads to the adsorption of CO_2. Potassium (K) impedes the formation of Ni carbonyl compounds as a result of strong chemical bonding between Ni and K in addition to the adsorption of CO on Ni through the production of bridging carbonyls. More so, potassium also promotes CeO_2 reduction is reduced by K thereby producing hydroxyl (OH) groups. The OH radicals further decompose into adsorbed oxygen which in turns interacts with adsorbed CO on Ni and eventually lead to the formation of adsorbed carbon dioxide (CO_2).

$$CO_{(ads)} + 2OH \longrightarrow CO_{2(g)} + H_{2(g)} + O_L$$

Similarly, Bunluesin et al. (1998) opined that WGSR involves the active participation of both the metal and the catalyst support. They argued further that upon comparing ceria-supported Pt, Pd and Rh, activity rates are independent of the metal utilised because conversion occurs at the metal-ceria interface where the metal adsorbs CO and catalyses the CO oxidation to CO_2. A low activity observed in WGSR by Fe/ceria and Co/Ceria under reaction conditions is associated with the oxidation of the metals and the inability of the metals to stabilise CO adsorption (Hilaire et al., 2001). The catalytic activity of Cu is greatly influenced by high surface area, but upon high temperature above 300^0C, Cu not only loses its surface area and activity but also suffers sintering. However, the alumina support (Al_2O_3) helps inhibits the formation of Cu crystallites and also acts as a textural promoter in WGS reaction (Twigg and Spencer, 2001). According to Raynasamy and Wagner, 2009, the level of CO can be significantly reduced to about 0.3wt% when a resilient Cu-ZnO-Al_2O_3 catalyst in low-temperature shift reactors with an exit temperature of about 200°C is used.

In this study, in the presence of all the various metal/Al_2O_3 catalysts, the concentration of hydrogen ranged from 55 to about 60 vol. % and the concentration of carbon monoxide reduced to less than 24vol.%. The Ni/Al_2O_3 catalyst used in the second stage also catalysing the water-gas shift explains why a higher difference in carbon monoxide concentration was not recorded. More so, Williams et al. (2011 and 2013b) have suggested that reaction can be significantly optimised through the introduction of catalysts for the steam reforming of primary products produced from the pyrolysis of biomass.

Table 5-4: Gas compositions and fractions table for the pyrolysis/Steam Reforming/Water-Gas shift reaction over XA/Al_2O_3 catalysts

	Gas Concentration (Vol. %)				
Catalyst	**Hydrogen**	**Carbon dioxide**	**Carbon Monoxide**	**Methane**	**C_nH_m**
Sand	55.10	15.63	27.61	1.41	0.25
Co	54.05	18.15	24.37	2.90	0.53
Cu	57.19	15.14	23.03	4.51	0.14
Zn	57.59	13.14	23.53	5.51	0.24
Mn	59.42	12.96	22.74	4.73	0.15
Fe	57.16	19.79	22.01	1.01	0.04

Table 5-4 reveals that catalyst compositions influence the performance of the thermochemical system. It is apparent that hydrogen concentration varied marginally with different catalysts used in the conversion of wood pellet biomass. Manganese was shown to generate the highest concentration of hydrogen, followed by copper, iron, zinc and then cobalt. In terms of carbon monoxide, it was found to be in the greatest and smallest concentrations when the cobalt and iron catalysts were used, respectively. This suggests that, of the catalysts tested, iron is the best metal for catalysing the water-gas shift reaction. As noted earlier that carbon monoxide is used up in the reaction; hence, a low concentration fraction indicates that more of the gas has reacted. This assumption is also supported by the fact that, of the catalysts tested, Fe generated the greatest gas concentration of carbon dioxide. As this is a product of the water-gas shift, a high concentration also suggests that Fe is best for catalysing the reaction. This is in agreement with several previous scientific investigations which indicated that iron-based catalysts are highly active with respects to the water-gas shift reaction for many years (Schulz, 2007; Yu et al. 2007; Costa et al. 2002). In an investigation on novel WGSR catalyst from Fe-loaded Victorian brown coal by Yu et al. (2007), a significantly high catalytic activity was obtained because Fe excellently dispersed in the char matrix with a significantly low particle size (<50nm). The carbon content in the char inhibited the crystallisation of nano-iron particles and also maintained a high catalytic conversion of the catalyst during WGSR. Nevertheless, Fe-based catalysts are relatively less active at lower temperatures (190-250^{0}C), coupled with low equilibrium concentrations of CO at low temperatures. Hence, to achieve higher conversions of CO at lower temperatures (190–250°C), a second, more active catalyst, based on Cu-ZnO, was developed in the early 1960s and is used in the industry extensively (Zhu and Wachs, 2016).

With respect to manganese, the low carbon dioxide concentration is shown in table 5-4, and its superior hydrogen fraction suggests that the catalyst promotes dry reforming rather than the water-gas shift reaction. This assumption for greater selectivity towards dry reforming could also be applicable to the zinc catalyst which has a lower final concentration of carbon dioxide in comparison to the system in the abscess of a third stage catalyst. This assumption, however, is not supported by the fact that both systems show the most significant concentrations of methane in the process gases which is used up in the reaction.

This result agrees with the finding of Najfach, (2017) on the empirical study of the effect of Mn and Al_2O_3 composition on Ni catalysts for dry reforming of methane. One key finding of this is that the addition of Mn on nickel supported catalysts over time promotes a much more stable CO_2 conversion. The Mn-promoter strongly inhibited CH_4 decomposition and carbon formation as equally seen in this present where its C_mH_n vol% is 0.14.

A different result was obtained by Liu et al., (2018), where Mn inhibited the catalytic dry reforming reaction. Although they used the same wet impregnation method for catalysts synthesis as adopted in this study, the possible reasons for the discrepancy are partly due to differences in process conditions. First, purified natural clay was also used as a support in conjunction with Nickel. The natural clay might have still contained other minerals which interacted with Ni or Mn. Secondly, the process gases introduced into the reactor were not pyrolytic products and thirdly the residence time was short (30mins). As observed by Najfach, (2017) at initial time Mn dry reforming ability was negligible, but on a time-lapse of 24 hours, the CO_2 conversion not only became high but also stabilised.

A further reaction that could also be impeding hydrogen yields in each experiment is methanation. During the relatively basic reaction, as outlined below, carbon dioxide reacts with hydrogen to produce water and methane. It is therefore highly relevant that catalysts that are selective towards both hydrogen and carbon dioxide products are chosen in order to avoid this undesirable reaction. Sun et al. (2013) showed that cobalt has the potential to catalyse methanation, although, the results obtained in this investigation do not show this directly. It should be noted that, in larger-scale operations, although the reaction is still undesirable, methane produced can be used as a feed for steam reformation or burned to provide a source of energy for the process (LeValley et al., 2014).

Dry Reforming $CO_2 + CH_4 \rightarrow 2H_2 + 2CO$ 4.1.1.1

Methanation $CO_2 + 4H_2 \rightarrow CH_4 + 2H_2O$ 4.1.1.2

Reverse Water-Gas Shift $CO_2 + H_2 \rightarrow CO + H_2O$ 4.1.1.3

Other causes of this undesirable exothermic methanation are the changes in the WGS reaction conditions, precisely, temperature and catalysts composition. Cherkezova-Zheleva and Mitov (2010) tested WGSR at three process temperatures; 573, 623 and 673K and observed that that the Fe^{2+}/Fe^{3+} ratio reached an optimal at 623K and beyond this, the catalytic activity declined significantly. In their work, they further observed that over-reduction of the bulk iron oxide (Fe_3O_4) to lower iron oxides, iron carbides or metallic iron compounds in the course of catalysts preparation (reduction), activation and application (reaction), favoured methanation. This is because the metallic Fe and Fe-carbide actively catalyse the methanation reaction and at the same destroy the catalyst pellets. It is essential to mention that the mixture of a low concentration of steam and higher than the maximum reaction temperature is the potential source of over reduction (Zhu and Wachs, 2016). While Lywood and Twigg (1993) recommended the use of their empirical formula for accurate and suitable iron-based catalysts reduction during catalysts use, Lloyd et al. on the other hand recommended that a suitable combination of process gas stream containing H_2O, CO, CO_2, N_2 and H_2 will remedy methanation occurrence. Both in the two studies by Reddy et al. (2011 and 2012), it was also found out that methanation was inhibited when chromium or cobalt was added to iron-based catalysts (Fe-Ce oxide) at low steam to CO ratio which led to an increase in the catalyst stability.

Several works by Lee et al. (2009, 2011a, 2011b) attempted to incorporate Ni as a potential substitute for Cr. Although higher CO catalytic conversions were obtained, a significantly low selectivity as a result of undesirable methanation side reaction was found when the Ni content exceeded 40 wt % through a rise in the surface area of the catalysts. Other authors added Ce and Zn as promoters to impede the methanation reaction and concurrently escalated the selectivity of high-temperature WGSR. The copper-nickel (Cu-Ni) alloy catalysts have also proven potent to suppress the methanation reaction without altering its high activity potential (Jha et al. 2015 and Jeong et al. 2015). However, one drawback to these developments is the considerable cost implication associated with the reactants.

The promotion of Na among other alkali metal oxides to $Fe_2O_3{-}Al_2O_3{-}NiO$ catalyst has also been reported to inhibit methanation. In a study by Meshkani and Rezaei (2015), the addition of Na (3 wt%) under two process streams for more than two days (about 50hrs) recorded the optimal activity and stability of WGSR. The rise in the HTWGS activity by Na metal was a product of raising the number of weakly basic sites.

Another reaction that could be influencing the performance of the catalytic system is the reverse water-gas shift reaction (r-WGSR). Due to the reversible nature of the reaction, when under suitable conditions the equilibrium can be shifted towards the reactants of the forward reaction. The r-WGSR involves direct CO_2 hydrogenation and the intermediate H_2O removal.

This side reaction is mostly thermodynamically favoured by higher temperatures because it is endothermic, therefore increasing the H_2/CO_2 ratio optimises the CO_2 conversion to CO (Loiland et al. 2016).

In a review of kinetic reaction studies with respect to the power-law model for Fe-Cr catalysts by Zhu et al. (2016), the steady-state reaction order is shown in table 5-5. There is a dominant dependence on the partial pressure of CO by 1.0 and less on that of H_2O which is about 0.25. This indicates that the surface of the working catalysts possesses a better concentration of adsorbed H_2O that of CO. In effect, WGSR is promoted but in the case when the 0 and mean value of 0.3 are the reaction orders on the H_2 and CO_2 partial pressure dependence respectively, the transportation of H_2 and CO_2 to the surface are therefore unhindered, making CO_2 promote reverse water gas shift reaction (r-WGSR) at the expense of the forward reaction (WGS). As also seen in the table, the CO, H_2O, H_2 and CO_2 partial pressure dependence are ~1, ~0.1, ~0 and -0.26 respectively, adding Cu reduced the activation energy and also suppressed the r-WGS reaction.

Table 5-5: Kinetic Parameters of Power Law Kinetic Expressions for Iron-Based HT-WGSR, Zhu and Wachs et al. 2015

	Reaction orders				
Catalyst	**(CO)**	**H2O**	**CO2**	**H2**	**Activation energy**
Fe-Cr	0.9	0.25	-0.6	0	114
Fe-Cr	1.1	0.53	0	0	95
Fe-Cr	1	0	-	-	118
Fe-Cr-Cu	1	0	-	-	75-80
Fe-Cr-Cu	1	0	-0.36	-0.09	111
Fe-Cr-Cu	0.9	0.31	-0.61	-0.05	88

Therefore, selectivity towards CO is a potential result of r-WGSR. However, in this study as steam is not considered when determining the gas yield of the system, this could be one explanation as to why the gas yield dipped when cobalt was utilised to catalyse the reaction in comparison to sand. This is also supported by the fact that the yield and concentration of hydrogen decreased when cobalt was used. In contrast, the carbon monoxide and carbon dioxide concentrations were shown to decrease and increase, respectively, which is not in agreement with the reverse water-gas shift equation.

Despite research by Fu et al. (2005) and Chinchen et al. (1988) suggesting that both copper and zinc catalysts have high selectivity towards the water-gas shift reaction, they have been shown to perform relatively poorly in comparison to the iron catalyst in this investigation. This can be explained by the fact that both zinc and copper are typically used for low-temperature applications where temperature used is usually less than 250°C which is far less than the 350°C of this study (LeValley et al., 2014). On the other hand, iron is most commonly used in high-temperature reactions as previously reported meaning that the experimental conditions favoured its use. Another explanation for the difference in performance could also be the synthesis techniques used to make the catalysts. Taylor et al. (2003) reported that both copper and zinc catalysts are most commonly manufactured using the co-precipitation method rather than the wet impregnation method used in this investigation. This is also in agreement with the work produced by Letichevsky et al. (2005) which suggested that the synthesis technique significantly affects catalyst performance.

5.4.2 Analysis of coke formation on X_A/Al_2O_3 catalysts using Temperature Programmed Oxidation (TPO)

According to Horiuchi et al. (1996) and Helveg et al. (2011), the issue of coke formation on catalysts downstream from the initial pyrolysis stage is one the most critical pitfalls of catalysts efficiency which leads to their deactivation. Sehested (2006) also opined that the three main carbon formations on catalysts are pyrolytic, whisker and encapsulating. As there are little or no, aromatic compounds found in the product gas, it would be unlikely for encapsulating carbon formations to be incident on the surface of the catalysts. On the other hand, due to the high temperatures used in the reactor system and the high concentrations of both carbon monoxide and hydrocarbons, there is a high possibility that pyrolytic and whisker carbon formations may be present. In order to investigate this and analyse the characteristics of the formations found on the reacted catalysts temperature-programmed oxidation (TPO) was used.

As depicted in figure 5.1 and table 5.6 for the residual catalyst analysis, the metals tested, manganese showed the most significant amount of weight loss, with over 10% of the original mass being lost. This was followed by copper and iron with total losses of approximately 4%, cobalt with a loss of 1% and zinc with an overall increase of 1%. These results suggest that the manganese catalyst was the most affected by coking as the loss of mass means that a greater amount of carbon has been oxidised off the catalyst surface. This result is not in agreement with the assumption made in the previous section of the report, where it was suggested the low calculated mass balances shown by some of the catalyst tested was caused by increased coking. If this were the case, both copper and cobalt would have seen the greatest percentage loss.

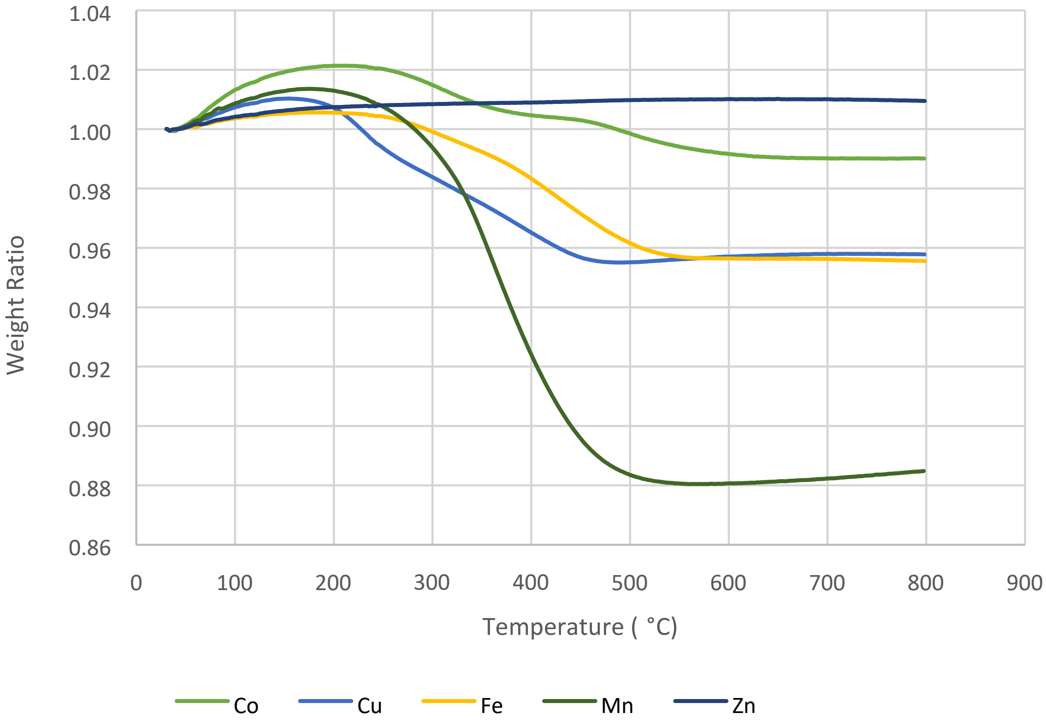

Figure 5-1: TPO analysis of reacted XA/Al2O3 catalysts

Table 5-6: Catalysts coke formation

Catalyst	Percentage change weight loss for carbon deposit on the surface of the catalyst
Cobalt	-1%
Copper	-4%
Iron	-4%
Manganese	-11%
Zinc	+1%

From figure 5-1 and table 5-6, it is also evident that there are several points of weight loss for the catalysts during the analysis, and each point of weight loss represents a type of carbon formed on the surface of the catalyst. Regarding the cobalt catalyst, it is clear that there were two types of carbon formed due to the two-stage weight loss. This was also the case for iron. However, for the remaining catalysts, it can be seen that there was only a single point of weight loss during TPO. With respect to the first stage of weight loss for the cobalt catalyst, it has been shown in figure 5.1 to have occurred at around 275°C. Both Wu et al. (2013) and Liu and Au (2003) suggested that this loss is due to heavy hydrocarbon deposition. Similar losses are also seen to occur with the manganese, iron and copper catalysts. This result is, somewhat, in agreement with the gas compositions as the process gases from the manganese and copper experiments were shown to have the lowest concentrations of heavy hydrocarbons. Conversely, this is not in agreement with the process of gas concentrations produced when the iron was used. One possible reason that the iron gas composition results do not fit with the TPO analysis could be due to a greater amount of heavy hydrocarbons being produced during the pyrolysis of biomass in that particular experiment.

Concerning the second stage of weight loss for cobalt, shown to occur at around 470°C, it is possible to attribute this to the oxidation of amorphous carbons. It should be noted, however, that this weight loss cannot be said to be significant as it only accounts for about 2% of the starting mass. A similar weight loss was shown to occur for the iron catalyst. The amount of amorphous carbon on the surface of catalysts must be reduced as they are known to cause deactivation relatively easily by encapsulating the active sites (Chen et al., 2016). Despite the loss being higher than that shown by the cobalt catalyst, it can again not be considered to be significant. Regarding all the catalysts tested, it is clear that there was minimal weight loss above this temperature. For this reason, it can be assumed that they were not affected by carbon formation known to occur at high temperatures such as filamentous.

For each metal tested, it can be seen that there was an increase in mass at the start of the analysis. One possible explanation for this could be that the metal ions contained with the catalyst are being oxidised. This agrees with the method of catalyst synthesis, where the reduction was used to move the catalytic metal ions to the active phase. Chen et al. (2016) showed similar results for nickel-based catalysts. However, one difference between the results is the temperature at which oxidation took place. In the results presented in this chapter, oxidation can be seen to have occurred at temperatures ranging from 50 to 350°C which is significantly less than the temperatures shown by Chen et al., (2016).

It has been suggested in another work conducted by Urasaki et al. (2008) that the use of alumina as catalyst support can enhance the effects of coking. This was due to the presence of acidic active sites on the surface of the catalysts. It is clear from the results presented, however, that the metal loaded onto the alumina support has had the greatest effect on the level of coking present. One proposed method of reducing the acidity of an alumina supported catalyst is through the introduction of an alkaline metal such as sodium or calcium to the catalyst. It has been reported by Ashok et al., (2015) that the addition of an alkaline metal promotes steam-carbon reactions which result in a reduction in coke deposition. Future research could focus on adding small quantities of an alkaline metal to the catalysts.

5.4.3 Pyrolysis/ Steam Reforming/ Water-Gas shift reaction over Fe/Al_2O_3 catalysts with varying metal loading

As indicated, iron (Fe) is shown to be the most effective metal for catalysing the water-gas shift reaction; the second investigation was aimed at determining the best composition of the alumina supported iron catalyst for optimum hydrogen generation. The initial investigation was conducted with a catalyst metal loading of 40 wt%, but in this investigation, the loading was varied between 5 and 100 wt% iron. The results from the investigation as presented in tables 5-7 and 5-8 indicated that the residual char was again unaffected by the change in the catalyst used. This further supports the finding that the pyrolysis of biomass is unaffected by catalysts used in the downstream.

Table 5-7: Mass balance for the pyrolysis/Steam Reforming/Water-Gas shift reaction over Fe/Al_2O_3 catalysts

Catalyst	**Sand**	**Metal Loading**			
		5%	**20%**	**40%**	**100%**
Gas/Biomass (wt.%)	80.79	95.34	93.48	92.38	76.09
Residue Char/Biomass (wt.%)	24.00	24.00	24.00	24.00	24.00
Mass Balance (wt.%)	96.90	96.66	95.96	96.35	75.58
H_2 Yield (mmol H_2 g^{-1} biomass)	26.47	32.98	32.11	31.60	26.45
H_2/CO molar ratio	2.44	2.51	2.59	2.65	3.94

Additionally, it is also revealed in the results provided in table 5.7 that the yield of hydrogen remained relatively constant with the increase in metal loading until above 40 wt% iron. This, therefore, suggests that increasing the iron content of the catalyst has little effect on the water-gas shift reaction until high metal loadings of 100wt% where a negative impact on catalyst performance is observed. Similar to this result was Li et al. (2000), findings on copper loaded cerium oxide catalysts where at low metal loadings, the loaded species is present in the form of highly dispersed oxide clusters, while at high metal loadings, the species is not only present in oxide clusters of increasing size but also the form of solid inactive metal particles. The outcome of this is the reduction in the specific surface area of the catalyst with an increase in metal loading. In other recent studies, Bobrova et al. (2017) and Liu et al. (2016) for a nickel-based catalyst also showed this inverse relationship in specific surface area and agglomeration of active particles with metal loading. This decrease in surface area would in turn also result in a decrease in the activity of the catalyst as there is a less active surface area for the reaction to take place. It is worth noting, however, that this does not justify the consistency of performance shown at loading less than and including 40 wt% iron.

A contrast to the obtained consistency in performance shown by the catalysts loaded with less than 40 wt.% iron, was reported by Li et al. and Bobrova et al. where performance increases with metal loading until about 20 wt% of the catalyst is composed of the selected metal. Their results suggest that there is, in fact, an optimum composition, whereas the results shown in this current report suggest that above a particular metal loading, it is unnecessary to increase the active metal content further. This discrepancy might be as a result of the differences in metal loading used in these investigations which are far greater from each other. For example, Li et al. (2000) compares metal loading with a difference of 2.5 wt. % whereas in this investigation the difference was as big as 60 wt% between the 40 wt. % and 100 wt. % catalysts. This leaves a vast range of loadings where changes in performance could be shown. For this reason, further study using smaller changes in metal loading might lead to similar results being shown.

Regarding the experimental run using pure iron (100 wt.% Fe) to catalyse the water-gas shift reaction, this experiment not only provides information on the effect of iron loading but also reveals the necessity for the use of catalyst support. From Table 0-7, two things are clear, firstly, the lower metal loading catalysts (5, 10, 20 and 40wt %) have a consistent result which suggests that at low metal loading of iron catalysts, there is no significant difference in hydrogen yield. Secondly, pure iron catalyst shares similar results with that obtained in the absence of catalyst in the third stage of the reactor with respect to both the yield of hydrogen and gas. This suggests that the pure iron catalyst is ineffective at catalysing the water-gas shift reaction. As explained by Yu et al. (2006) iron catalysts for the water-gas shift reaction often start as ferric oxide (Fe_2O_3) and are reduced to magnetite (Fe_3O_4), which is known to be the active phase for iron catalysis. This lack of magnetite in the composition of the 100 wt.% catalyst, and therefore a lack of active material, could explain the poor performance of the catalyst. Another probable explanation could be the lack of support. In catalytic chemistry, supports are used to maximise the active surface area of the catalyst. Therefore, in this investigation, it can be assumed that, by completely removing all the alumina support, the active surface area has been reduced significantly due to the poor performance. This highlights the need for catalyst supports. Although not outlined in this investigation, supports also reduce the cost of catalysts by reducing the content of the active material by efficiently dispersing it.

Commercially a pure iron catalyst is feasible, as it is a relatively cheap commodity, but in most cases, it is unrealistic to be able to run a system with such a high metal loading. Regarding the 100 wt.% metal loading, the results in table 5.7 show that the calculated mass balance is far less in comparison to the others tested including when the sand was used. Similarly, to the first investigation, one assumption that could be made is that the pure catalyst experience much greater coking. A further explanation could be that the system was not secured successfully. This would have resulted in the release and loss of mass from the reactor unit in the form of process gases.

In order to provide a more in-depth insight into how the metal loading of iron in alumina supported catalyst affected performance, the gas concentrations and fractions for each catalyst are presented in table 5-8 below. When comparing the results with those shown in table 5-7, it is noticeable that they also show high similarity in the performance of the 5, 20 and 40 wt.% catalyst due to the concentrations of carbon monoxide, carbon dioxide and hydrogen is almost identical.

Interestingly, despite all three of these catalysts being shown to produce a far greater amount of hydrogen than the system with no catalyst, their concentrations were also very similar. This is unexpected as explained previously; the increased hydrogen production should reduce the carbon monoxide and increase both the hydrogen and carbon dioxide concentration. One explanation for this result could be the inconsistency of the pyrolysis stage of the system. Regardless of the relative yield of gas from the biomass feed being shown for each experiment, the gases being produced may have varied significantly. For example, one experiment may have produced a far greater amount of carbon dioxide but far less carbon monoxide.

Table 5-8: Gas compositions and fractions table for the pyrolysis/Steam Reforming/Water-Gas shift reaction over Fe/Al_2O_3 catalysts

	Gas Concentration (Vol.%)				
Metal Loading (wt.%)	**Hydrogen**	**Carbon dioxide**	**Carbon Monoxide**	**Methane**	**C_nH_m**
Sand	55.10	20.63	22.61	1.41	0.25
5%	56.78	20.12	22.60	0.48	0.02
20%	56.88	20.01	21.89	0.77	0.45
40%	57.16	19.79	22.01	1.01	0.04
100%	57.04	23.68	14.47	4.72	0.09

Also, table 5-8 shows the pure iron catalyst to have produced the product gases with the most significant of the water-gas shift reaction taking place. This is due to the concentration of carbon monoxide decreasing while carbon dioxide increased in line with the reaction equation. In addition, the figure shows that the amount of methane found in the product gases of the 100 wt% experiment was higher than all other experiments done. These results strongly suggest that the catalyst could be in fact catalysing the reverse reaction of steam reforming which sees hydrogen react with carbon monoxide to produce both methane and carbon dioxide. This would explain their increases in concentration. No literature has been found to support this assumption; however, it is unlikely that this was the source of the variation. This is due to the exothermic nature of the reaction and the extremely high temperatures being used strongly favouring the forward reaction. This is also not supported by there being no significant reduction in the concentration of hydrogen in comparison to the non-catalysed system.

5.4.4 Analysis of coke formation on Fe/Al_2O_3 catalysts using Temperature Programmed Oxidation (TPO)

TPO analysis was carried out to analyse any carbon formation on the reacted catalysts. Similar to the previous investigation, it is deducible that the pure iron catalyst may have been more susceptible to coking due to the lowest calculated mass balance occurring after its use. The results from the analysis are presented figure 5-2, which indicates that the iron-containing catalysts are not significantly affected by coking due to the TPO analysis showing losses of less than 5% for each catalyst tested. The results presented show no correlation between carbon deposition and metal loading on the Fe catalyst as seen from the results. 5% and 40% have roughly the same amount of weight loss of 5.5%, while 100% have a smaller weight loss of approximately 2%. The 20% had no weight loss which means no carbon deposition at all.

Furthermore, similar to the results shown in section 5.4.3, table 5-8 reveals several points of weight loss for the iron alumina catalysts. Despite this, the only catalyst that could be said to have undergone a two-stage weight loss was the 40 wt. % catalyst. Like the catalysts tested in section 5.4.3, it is evident that the weight loss was due to both heavy hydrocarbon deposition and the formation of amorphous carbon due to the majority of weight loss being shown to occurring within the ranges of 100 to 300°C and 400 to 550°C, respectively. In addition to this, the increase in mass shown by the catalysts can be again attributed to the oxidisation of metal irons within the catalyst. The small increase in the weight of pure iron catalyst suggests that there were some active irons present within the iron catalyst which somewhat invalidated the assumption made in the previous section of the report.

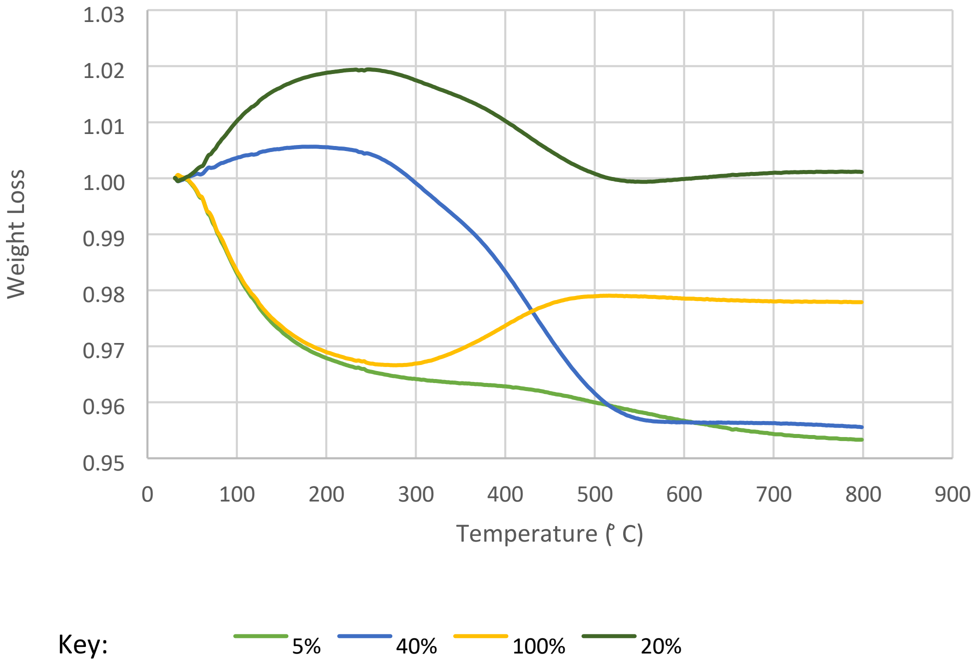

Figure 5-2: TPO analysis of Fe/Al_2O_3 catalysts with varying metal loading

5.4.5 Pyrolysis/Steam Reforming/Water-Gas shift reaction over Fe/Al_2O_3 catalysts with varying steam to carbon ratios

The final investigation conducted focused on examining the effects that varying the steam flowrate had on the yield of hydrogen from the water-gas shift reaction of catalytic steam reforming product gases. Notably, in a very recent investigation, Loughrey, (2018), suggested that the experimental rig used should be modified to enable steam to be injected into the third WGS stage of the reactor. This was due to the initial rig originally being used to only optimise the steam reformation (SR) stage of the reactor. It was considered that the performance of the unit could be affected by the third stage operating only with the remnants of the steam used in the second stage. As explained earlier in this chapter, the investigation was conducted at 850°C with steam to carbon ratios of 1:1, 1:2, 1:4 and 1:8 with respect to steam injected into the third stage of the reactor unit. It should be noted that the ratios do not include the steam used in the second stage which was constant throughout the investigation at 6.64 ml hr^{-1}. The results of this investigation are presented below in tables 5-9 and 5-10.

Table 5-9: Mass balance for the pyrolysis/Steam Reforming/Water-Gas shift reaction at various steam to carbon ratios.

Carbon : Steam	**1:1**	**1:2**	**1:4**	**1:8**
Gas/Biomass (wt. %)	92.38	84.90	71.73	72.24
Residue Char/Biomass (wt. %)	23.00	23.00	23.00	23.00
Mass Balance (wt. %)	96.35	93.49	90.97	89.77
H_2 Yield (mmol H_2 g^{-1} biomass)	32.60	28.02	21.78	18.64
H_2/CO molar ratio	2.60	1.58	2.25	1.75

Firstly, from table 5-9, it is apparent that the percentage of biomass converted to residue char remained consistent for each experiment run. This confirms that the pyrolysis stage of the reactor is not affected by downstream reactor conditions. Secondly, it is shown that increasing the steam to carbon ratio resulted in the yield of hydrogen decreasing consistently. In addition to this, table 5-9 shows that the increase also inhibited the amount of gaseous products being produced by the reactor unit and also reduced the hydrogen to carbon monoxide ratio in the final products. These results, however, are not in agreement with research conducted by Figueiredo et al. (2005), who concluded that the conversion of carbon monoxide to hydrogen increased continuously until a constant value is reached. It should be taken into account, however, that the ratios used in their investigation are far lower than those used in these experiments. For this reason, it could be assumed that their conclusion is incorrect and that above a certain steam to carbon ratio, the performance of the water-gas shift reaction does not remain constant but decrease. However, no literature has been found to support this assumption.

Table 5-10: Gas compositions and fractions table for the pyrolysis/Steam Reforming/Water-Gas shift reaction at various steam to carbon ratios

	Gas Concentration (Vol. %)				
Steam to Carbon Ratio	**Hydrogen**	**Carbon dioxide**	**Carbon Monoxide**	**Methane**	**C_nH_m**
1:1	57.16	19.79	22.01	1.01	0.04
1:2	53.31	20.97	23.07	2.24	0.41
1:4	52.45	20.49	23.33	3.16	0.56
1:8	47.11	19.40	26.92	5.19	1.39

As shown in Table 5-10, increasing the steam to carbon ratio of the system also significantly influenced the composition of the product gases. Firstly, it is shown that the fraction of both methane and other hydrocarbons increased as the steam to carbon ratio also increased. This suggests that the second stage of the reactor, where these gases are being converted to product gases for the water-gas shift reaction, is being impeded by the additional steam being added to the system. This could, therefore, provide an additional explanation as to why the overall performance of the reactor system is decreasing with the increase in steam to carbon ratio. This is due to a reduction in the conversion of methane not only reducing the amount of hydrogen from steam reformation but also reducing the amount of hydrogen from the water-gas shift reaction as there are fewer reactants available.

Hu et al. (2003) reported that the selectivity of carbon monoxide reduces with an increase in steam to carbon ratio, which supports these results. It can also be concluded from Table 5-10 that the fraction of carbon monoxide in the product gases also increases as the steam to carbon ratio is increased. This, therefore, shows that the performance of water-gas shift reaction is also reducing. This is also supported by the fact that the fraction of carbon dioxide decreases. One explanation for these results could be that the fixed bed reactor system unit becomes over-saturated with steam. As explained by Lopez et al. steam is also produced during the pyrolysis of biomass which would also add to the saturation of the system. This, in turn, could result in shorter contact times for the reactants and the surface of the catalyst. This would be highly unfavourable for both the activation and adsorption of reactants and would result in the reduction in methane and carbon monoxide conversion to produce hydrogen. Again, no literature was found to support this conclusion.

With respects to the water-gas shift equation itself, these results are not supported by equilibrium theory. As explained previously, the reaction is reversible; this means it involves a state of equilibrium whereby the rate at which forward reaction takes places becomes equal to the rate of the reverse reaction. This equilibrium can be manipulated by adjusting the reaction conditions. One way this can be achieved is by adjusting the concentration of reactants. This result in the equilibrium being shifted to the side that would reduce the change in concentration; hence, the forward reaction would begin to ensue at an increased rate. This is le Chatelier's principle and, from the results displayed above, it is clear that it is not in agreement with this investigation. This is because the increase in concentration, through the increase in steam flowrate, has not resulted in an increased yield of hydrogen. In addition to this, the results are not supported by basic reaction theory. In this theory, an increase in concentration increases the probability that reacting particles will come into contact which in turn increases the rate of reaction. Again, as the results show a decrease in the yield of hydrogen with increased concentration, they are not in agreement with theory.

5.5 Conclusion

The three-stage thermochemical process consisting of pyrolysis, catalytic steam reforming and water gas shift reaction has presented reliable route for the generation of hydrogen from raw biomass, most especially wood pellet which was utilised in this investigation. Previous studies have well established the enormous potential of hydrogen to become a possible clean alternative fuel due to its high energy density and its reaction producing only water as a by-product. This eventually will help to mitigate both the diminishing reserves globally of fossil fuels and the increasing environmental pollution associated with their use.

However, the possibility of birthing the future sustainable hydrogen economy is contingent on certain factors which must be resolved; this includes the requirement of a new renewable feedstock (biomass) for production and not the current natural gas and coal. Integrating a renewable biomass feedstock into hydrogen production is again problematic unless an ancillary operating unit is provided in addition to the steam reforming and water-gas shift unit currently being used. This is known as pyrolysis and is required to turn the biomass into a gaseous feed.

It is also established from the literature that the temperature at which pyrolysis takes place, and the type of biomass also used greatly influence both the composition and yield of product gases. With respect to steam reforming and water gas shift reaction, some metals such as Fe, Ni, Al, Mn, Zn among others can effectively catalyse the reaction. To optimise this conversion process, some process parameters, chiefly temperature, steam to carbon(S/C) ratio and steam flow rate were identified for probable manipulations. As the temperature is increased, the conversion of carbon monoxide also increased. Unlike temperature, the pressure of the system was reported to have little effect on performance. This was explained by the stoichiometry of the water-gas shift reaction equation.

More precisely, the findings from bench-scale three staged reactor system distinguished iron (Fe) as the best metal with the greatest affinity to catalysing the water-gas shift reaction. Fe-based catalyst produces the greatest yields of both gas and hydrogen, and a significantly low concentration of carbon on the reacted catalyst. All metals tested, apart from cobalt, catalysed the water-gas shift reaction. The poor performance of cobalt has been attributed to it catalysing the reverse water gas shift reaction. This assumption was supported by the fact that both the gas and hydrogen yields were less than the system with no catalyst present, although the high concentration of carbon dioxide did not support it. Despite literature suggesting that cobalt has the ability to catalyse the unwanted methanation reaction, the results presented in this report do not distinctly demonstrate this.

Another finding in this investigation is that manganese has greater selectivity towards dry reforming rather than the water-gas shift reaction. This assertion is made base on the high hydrogen yield shown when the catalyst was used despite the concentration of carbon monoxide remaining relatively low. When the reacted catalysts were analysed using TPO, it was shown that manganese suffered the most considerable weight loss suggesting that it is the most susceptible to coking.

It is evident also that metal loading does not significantly affect catalyst performance (about 32 mmol H_2 g^{-1} biomass) until high weight fractions (100 wt% iron) where performance decreases (26.45mmol H_2 g^{-1} biomass). It has been suggested that the reduction in performance of the pure catalyst (at high loadings of 100 wt%) is due to the agglomeration of active particles within the catalyst resulting in a reduction in active surface area (that is, the lack of magnetite present in the catalyst which is the active phase of iron catalysts). This was supported by a number of literature sources. On the other hand, the consistency shown in the performance of catalyst with metal loadings ranging from 5 wt. % to 40 wt. % was not supported by previous studies which suggest it should have increased. One conclusion drawn from this is the necessity of catalysts supports to increase the active surface area, especially by dispersion. The TPO analysis also has shown that carbon deposition varies with metal loading as the pure iron catalyst was most susceptible to coking.

One last finding from the investigation of the effects of steam to carbon ratio (S/C) on the water-gas shift reaction is that, increasing the level of steam results in a decrease in the yield of hydrogen. This, however, contrasts with equilibrium and reaction theory; the reason is not yet apparent. Hence, further findings are required.

Summarily, the findings in this study show that catalyst composition, metal loading, and steam to carbon ration are relevant matrices in upscaling hydrogen production in a 3-stage thermochemical technique.

Maximisation of hydrogen production from biomass has been investigated following three-stage reactions viz a viz pyrolysis, catalytic steam reforming and water-gas shift reactions in a fixed bed reactor at 850°C. Of these metals Co, Cu, Fe, Mn, and Zn, Fe-catalyst yielded the highest volume of hydrogen (32.6 mmol H_2 g^{-1} biomass) and gas (92.38wt %) with the lowest concentration of CO in the product gases. Fe also showed the least coke deposit on the reacted catalysts which were analysed through Temperature programmed oxidation (TPO). Notably, while Mn and Zn indicated the best selectivity to dry reforming consequent to the low concentration of CO_2 in the process gases Co, on the other hand, indicated the best affinity to methanation. A relative increase in H_2 production was promoted by increasing the metal loading of the Iron alumina catalysts from 5wt% to 40wt% above which a dip in production performance was observed; this suggests that the amalgamation of active particles. It was also found that the flow rate of steam into the third stage of the reactor has a significant influence on both the yield of hydrogen and other product gases. However, the observed inverse relationship between the flow rate of steam and H_2 yield was a result of over-saturation of the reactor system with steam bridging the contact times for the reactants and the surface of the catalyst.

5.6 Reference

Ang, M.L. Oemar, U. Kathiraser, Y. Saw, E.T. Lew, C.H.K. Du, Y. Borgna, A. Kawi, S., 2015. High-temperature water–gas shift reaction over Ni/xK/CeO2 catalysts: Suppression of methanation via formation of bridging carbonyls. Journal of Catalysis, 329.pp 130–143

Abdalla, S, Al-Marzouki, F and Obaid, A. 2017. High-efficient and low-cost catalyst for hydrogen evolution reaction: Nickel phosphide nano-spheres. Journal of Renewable and Sustainable Energy. 9, pp 23104-23105.

Amphlett, JC. 1998. Simulation of a 250 kW diesel fuel processor/PEM fuel cell system. Journal of Power Sources. 71, pp. 179-184.

Ashok, J, Kathiraser, Y, Ang, ML, and Kawi, S. Bi-functional hydrotalcite-derived NiO–CaO– Al2O3 catalysts for steam reforming of biomass and/or tar model compound at low steam-tocarbon conditions. Applied Catalysis B: Environmental. 172, pp. 116-128.

Blanco López, MC, Blanco, CG, Martıneź -Alonso, A and Tascón, JMD. 2002. Composition of gases released during olive stones pyrolysis. Journal of Analytical and Applied Pyrolysis. 65(2), pp 313-322.

Bobrova, L, Andreev, D, Ivanov, E, Mezentseva, N, Simonov, M, Makarshin, L, Gribovskii, A, and Saykov, V. 2017. Water–Gas Shift Reaction over Ni/CeO2 Catalysts. Journal of Catalysts. 7, pp 310-333.

Bukurab, D.B., Todica, B., Elbashira, N. 2016. Role of water-gas-shift reaction in Fischer–Tropsch synthesis on iron catalysts: A review. Catalysis Today. 275, pp.66-75

Bunluesin T., R.J. Gorte, G.W. Graham, Appl. Catal. B 15(1998) 107.

Calle-Vallejo, F, Koper, MTM, and Bandarenka, AS. Tailoring the catalytic activity of electrodes with monolayer amounts of foreign metals. The Journal of Chemical Society Reviews. 12, pp. 5210-5230.

Ceria-based model catalysts: fundamental studies on the importance of the metal–ceria interface in CO oxidation, the water–gas shift, CO2 hydrogenation, and methane and alcohol reforming. Chemical Society Reviews, 46(7), 1824-1841

Chen, F., Wu, C., Dong, L., Vassallo, A., Williams, P.T. and Huang, J., 2016. Characteristics and catalytic properties of Ni/CaAlOx catalyst for hydrogen-enriched syngas production from pyrolysis-steam reforming of biomass sawdust. Applied Catalysis B: Environmental, 183, pp.168-175.

Chen, K, Xue, Z, Liu, H, Guo, A and Wang, Z. 2013. A temperature-programmed oxidation method for quantitative characterization of the thermal cokes morphology. Fuel. 113, pp 274279.

Chen, WH, Hsieh, TC, and Jiang, TL. 2008. An experimental study on carbon monoxide conversion and hydrogen generation from water gas shift reaction. Journal of Energy Conversion Management. 49, pp. 2801-2808.

Cherkezova-Zheleva, Z.; Mitov, I. J. Phys.: Conf. Ser. 2010, 217,012044.

Chichen, GC, Denny, PJ, Jennings, JR, Spencer, MS, and Waugh, KC. 1988. Synthesis of Methanol: Part 1. Catalysts and Kinetics. Journal of Apllied Catalysis. 36, pp 1-65.

Collard, FX and Blin, J. 2014. A review on pyrolysis of biomass constituents: Mechanisms and composition of the products obtained from the conversion of cellulose, hemicelluloses and lignin. Renewable and Sustainable Energy Reviews. 38(1), pp 594-608.

Costa, JLR, Marchetti, GS and Rangel, MDC. 2002. A thorium-doped catalyst for the high temperature shift reaction. Catalysis Today. 77(3), pp 205-213.

Couhert, C, Commandre, JM and Salvador, S. 2009. Is it possible to predict gas yields of any biomass after rapid pyrolysis at high temperature from its composition in cellulose, hemicellulose and lignin? Fuel. 88(3), pp 408-417.

Figueiredo, RT, Ramos, ALD, Carvalho de Andrade, HM, and Fierro, JLG. 2005. Effect of low steam/carbon ratio on water gas shift reaction. Journal of Catalysis Today. 107, pp. 671-675.

Fu, Q, Deng, W, Saltsburg, H, and Flytzani-Stephanopoulos, M. Activity and stability of lowcontent gold–cerium oxide catalysts for the water–gas shift reaction. Applied Catalysis B: Environmental. 56, pp. 57–68.

Fu, Q, Deng, W, Saltsburg, H, and Flytzani-Stephanopulos, M. 2005. Activity and stability of low-content gold–cerium oxide catalysts for the water–gas shift reaction. Journal of Applied Catalysis B: Environmental. 56, pp. 57-68.

Gonzalez, RD, Lopez, T and Gomez, R. 1997. Sol-Gel preparation of supported metal catalysts. Catalysis Today. 35, pp 289-317.

Gunawardana, D, Lee, HC, Kim, DH. 2009. Performance of copper–ceria catalysts for water gas shift reaction in medium temperature range. International Journal of Hydrogen Energy. 34(3), pp 1336-1341.

Helveg, S, Sehested, J, and, Rostrup-Nielsen, JR. 2011. Whisker carbon in perspective. Catalysis Today. 178(1), pp. 42-46.

Hilaire, S, Wang, X, Luo, T, Gorte, RJ and Wagner, J. 2001. A comparative study of watergas-shift reaction over ceria supported metallic catalysts. Applied Catalysis A: General. 215(12), pp 271-278.

Hongrui Liu, H, Hadjltaief, H.B, Benzina, M.E.G, Costa, P.D. 2018. Natural clay-based nickel catalysts for dry reforming of methane: On the effect of support promotion (La, Al, Mn). International Journal of Hydrogen Energy. Pp.1-10 [accessed Mar 07 2019].

Hori, CE, Permanaa, H, Nga, KYS, Brennerb, A, Morec, K, Rahmoellerd, KM and Beltond, D. 1998. Thermal stability of oxygen storage properties in a mixed CeO2-ZrO2 system. Applied Catalysis B: Environmental. 16(2), pp 105-117.

Horiuchi, T, Sakuma, K, Fukui, T, Kubo, Y, Osaki, and Mori, T. 1996. Suppression of carbon deposition in the CO2-reforming of CH4 by adding basic metal oxides to a Ni/Al2O3 catalyst. Applied Catalysis A: General. 144(1), pp. 111-120.

Hu, J, Dehua, HE, Li, Y, Wang, H and Zhang, X. 2003. Influences of reaction conditions on steam reformation of methane over Ni/ZrO2 catalyst. Journal of Chemical Information and Modelling. 48(2), pp 738-739.

Hufschmidt, D, Bobadilla, LF, Romero-Sarria, F, Centeno, MA, Odriozola, JA, Montes, M, and Falabella, E. Supported nickel catalysts with a controlled molecular architecture for the catalytic reformation of methane. Journal of Catalysis Today. 149(3), pp. 394-400.

Hwang, KR, Lee, CB and Park, JS. 2011. Advanced nickel metal catalyst for water–gas shift reaction. Journal of Power Sources. 196(1), pp 1349-1352.

IPCC. 2014. Climate Change 2014: Mitigation of Climate Change. Cambridge: Cambridge University Press

Jalama, K. 2012. Effect of Pressure, Temperature and Steam to Carbon Ratio on Steam Reforming of Vegetable Oils: Simulation Study. International Conference on Nanotechnology and Chemical Engineering.

Jeong, D. W.; Jang, W. J.; Jha, A.; Han, W. B.; Jeon, K. W.; Kim, S. H.; Roh, H. S. J. Nanoelectron. Optoelectron. 2015, 10, 530–534.

Jentoft, FC. 2003. Thermal Treatment of Catalysts. Modern Methods in Heterogeneous Catalysis Research. University of Massachusetts.

Jha, A.; Jeong, D. W.; Shim, J. O.; Jang, W. J.; Lee, Y. L.; Rode, C. V.; Roh, H. S. Catal. Sci. Technol. 2015, 5, 2752−2760.

Kim, SJ, Xu, Z, Reddy, GK, Smirniotis, P and Dong, J. 2012. Effect of Pressure on High Temperature Water Gas Shift Reaction in Microporous Zeolite Membrane Reactor. Journal of Industrial and Engineering Chemistry Research. 51, pp 1364-1375.

Lazar, MD; Dan, M; Mihet, M; Almasan, V; Rednic, V, Borodi, G. 2011. Hydrogen production by low temperature methane steam reforming using Ag and Au modified alumina supported nickel catalysts, Rev. Rounm. Chim. 56, 637-642.

Lazar, MD, Mihet, M, Dn, M, Almasan, Y, Marginean, P. 2009. Preparation and characterization of nickel based multicomponent catalysts. Journal of Physical Conference Ser. 182

Lee, J. Y.; Lee, D. W.; Hong, Y. K.; Lee, K. Y. Int. J. Hydrogen Energy 2011, 36, 8173−8180.

Lee, J. Y.; Lee, D. W.; Lee, K. Y.; Wang, Y. Catal. Today 2009, 146, 260−264.

Lee, J. Y.; Lee, D. W.; Lee, M. S.; Lee, K. Y. Catal. Commun. 2011, 15, 37−40.

Letichevsky, S, Tellez, CA, de Avillez, RR, da Silva, MIP, Fraga, MA and Appel, LG. 2005. Obtaining CeO2–ZrO2 mixed oxides by coprecipitation: role of preparation conditions. Applied Catalysis B: Environmental. 58(3-4), pp 203-210.

LeValley, TL, Richard, AR and Maohong, F. 2014. The progress in water gas shift and steam reforming hydrogen production technologies – A review. International Journal of Hydrogen Energy. 39(30), pp. 16983-17000.

Li, Y, Fu, Q, and Flytzani-Stephanopulos, M. 2000. Low-temperature water-gas shift reaction over Cu- and Ni-loaded cerium oxide catalysts. Journal of Applied Catalysis B: Environmental. 27, pp. 179-191.

Lin, J, Wang, A, Qiao, B, Liu, X, Yang, X, Wang X, Liang, J, Li, J, Liu, J and Zhang, T. 2013. Remarkable Performance of Ir1/FeOx Single-Atom Catalyst in Water Gas Shift Reaction. Journal of the American Chemical Society. 134(41), pp 15314-15317.

Liotta, LF, Wu, H, La-Parola, V, Pantaleo, G, Puleo, F, and Venezia, AM. 2013. Ni-Based Catalysts for Low Temperature Methane Steam Reforming: Recent Results on Ni-Au and Comparison with other Bi-metallic systems. Catalysts, 3,563-583

Liu, BS, and Au, CT. 2003. Carbon deposition and catalyst stability over La2NiO4/γ-Al2O3 during CO2 reforming of methane to syngas. Applied Catalysis A: General. 244(1), pp 181195.

Liu, X, Yang, X, Liu, C, Chen, P, Yue, X and Zhang, S. 2016. Low-temperature catalytic steam reforming of toluene over activated carbon supported nickel catalysts. Journal of the Taiwan Institute of Chemical Engineers. 65, pp 233-241.

Lloyd, L.; Ridler, D. E.; Twigg. M. V. In Catalyst Handbook; Twigg, M. V., Ed.; Wolfe Publishing Ltd.: London, 1989; pp 283−306.

Loiland, J.A. Wulfers, M.J. Marinkovic, N.S. Lobo, R.F. 2016. Fe/γ-Al2O3 and Fe–K/γ-Al2O3 as reverse water gas shift catalysts. Catalyst Science Technology, 6, pp. 5267-5279

Lopez, DE, Suwannakarn, K, Bruce, DA, and Goodwin, JG. 2007. Esterification and transesterification on tungstated zirconia: Effect of calcination temperature. Journal of Catalysis. 247, pp. 43-50.

Loughrey, F. 2018. Interim report - Hydrogen from Waste Biomass. University of Leeds.

Lywood, W. J.; Twigg, M. V. EP Patent 0361648B1, 1993

Maluf, SS, and Assaf, EM. 2009. Ni catalysts with Mo promoter for methane steam reforming. Journal of Fuel. 88(9), pp 1547-1553.

Meshkani, F.; Rezaei, M. RSC Adv. 2015, 5, 9955−9964.

Mitchell, S, Thomas, JM and Perez-Ramirez, J. 2017. Single atom catalysis. Catalysis Science & Technology. 7, pp 4248-4249.

Murphy, DM, Manerbino, A, Parker, M, Blasi, J, Kee RJ, and Sullivan, NP. 2013. Methane steam reforming in a novel ceramic microchannel reactor. International Journal of Hydrogen Energy. 38, pp. 8741-8750.

Najfach, A.J. 2017. Effect of manganese and zeolite composition on zeolite-supported nickel catalysts for dry reforming of methane

NASA. 2017. The consequences of climate change. [Online]. [Accessed 3 October 2017]. Available from: https://climate.nasa.gov/effects/

Nayebzadeh, H, Saghatoleslami, N, Maskooki, A, and Vahid, BR. Effect of Calcination Temperature on Catalytic Activity of Synthesis SrO/S-ZrO2 by Solvent-free Method in Esterification of Oleic Acid. The Journal of Chemical and Biochemical Engineering Quarterly. 27(3), pp. 267-273.

Nguyen, LQ, Abella, LC, Gallardo, SM and Hinode, H. 2008. Effect of nickel loading on the activity of Ni/ZrO2 for methane steam reforming at low temperature. Reaction Kinetics, Mechanisms and Catalysis. 93(2), 227-232.

Nieva, MA, Villaverde, MM, Monzon, A, Garetto, TF and Marchi, AJ. 2014. Steam-methane reforming at low temperature on nickel-based catalysts. Chemical Engineering Journal. 235, pp 158-166.

Ramu, S, Lingaiah, N, Prabhavathi Devi, BLA, Prasad, RBN, Suryanarayana, I, and Sai Prasad, PS. Esterification of palmitic acid with methanol over tungsten oxide supported on zirconia solid acid catalysts: effect of method of preparation of the catalyst on its structural stability and reactivity. Applied Catalysis A: General. 276(1), pp. 163-168.

Ratnasam, y, C.; Wagner, J. P., Water Gas Shift Catalysis. Catalysis Reviews Science and Engineering 2009, 51 (3), 325-440.

Reddy, GK, Gunasekara, K, Boolchand, P, Smirniotis, PG. 2011. Cr- and Ce-doped ferrite catalysts for the high temperature water-gas shift reaction: TPR and Mossbauer spectroscopic study. The Journal of Physical Chemistry. 115(4), pp 920-930.

Reddy, G. K.; Boolchand, P.; Smirniotis, P. G. J. Catal. 2011, 282, 258−269

Reddy, G. K.; Kim, S. J.; Dong, J. H.; Smirniotis, P. G.; Jasinski, J. B. Appl. Catal., A 2012, 415-416, 101−110.

Rhodes, C, Hutchings, GJ, Ward, AM. 1995. Water-gas shift reaction: finding the mechanistic boundary. Catalysis Today. 23(1), pp 43-58.

Rhodes, C, Williams, BP, King, F and Hutchings, GJ. 2002. Promotion of Fe3O4/Cr2O3 high temperature water gas shift catalyst. Catalysis Communications. 3(8), pp 381-384.

Rodriguez, J. A, Grinter, D.C, Liu, Z, Palominoa, R.M and Senanayakea, S.D. 2017

Rodríguez-reinoso, F. 1998. The role of carbon materials in heterogeneous catalysis. Carbon. 56(3), pp 159-175.

Ronsse, F, Van Hecke, S, Dickinson, D and Prins, W. 2012. Production and characterization of slow pyrolysis biochar: influence of feedstock type and pyrolysis conditions. Global Change Biology: Bioenergy. 5(2), pp 104-115.

Rossignol, A, Gerard, F and Duprez, D. 1999. Effect of the preparation method on the properties of zirconia–ceria materials. Journal of Materials Chemistry. 9, pp 1615-1620.

Santer, BD, Taylor, KE, Wigley, TML, Johns, TC, Jones, PD, Karoly, DJ, Mitchell, JFP, Orot, AH, Penner, JE, Ramaswamy, V, Schwarzkopf, MD, Stouffer, R and Tett, S. 1996. A search for human influences on the thermal structure of the atmosphere. International Journal of Science. 382, pp 39-46.

Sehested, J. 2006. Four challenges for nickel steam-reforming catalysts. Catalysis Today. 111(1-2), pp 103-110.

Shinde, VM, and Madras, G. 2012. Water gas shift reaction over multi-component ceria catalysts. Applied Catalysis B: Environmental. 123, pp. 367-378.

Sun, J, Mei, D, Karim, AM, Datye, AK, and Wang, Y. 2013. Minimizing the Formation of Coke and Methane on Co Nanoparticles in Steam Reforming of Biomass‐Derived Oxygenates. ChemCatChem. 5(6), pp. 1299-1303.

Taylor, SH, Hutchings, GJ, and Mirzaei, AA. 2003. The preparation and activity of copper zinc oxide catalysts for ambient temperature carbon monoxide oxidation. Journal of Catalysis Today. 84, 113-119.

Trimmm DL. 1999. Catalysts for the control of coking during steam reforming. Journal of Catalysis Today. 49(1), pp. 3-10.

Twigg, M. V.; Spencer, M. S., Deactivation of supported copper metal catalysts for hydrogenation reactions. Applied Catalysis a-General 2001, 212 (1-2), 161-174.

United States Environmental Protection Agency (EPA). 2017. Global Greenhouse Gas Emissions Data. [Online]. [Accessed 8 October 2017]. Available from: https://www.epa.gov/ghgemissions/global-greenhouse-gas-emissions-data

Urasaki, K, Tokunaga, K, Sekine, Y, Matsukata, M, and, Kikuchi, E. 2008. Production of hydrogen by steam reforming of ethanol over cobalt and nickel catalysts supported on perovskite-type oxides. Catalysis Communications. 9(5), pp. 600-604.

Wei, Z and Sun, J, Li, Y, Datyec, AK and Wang, Y. 2012. Bimetallic catalysts for hydrogen generation. Chemical Society Reviews. 41, pp 7994–8008.

Welaya, YMA, El Gohary, MM and Ammar, NR. 2012. Steam and partial oxidation reforming options for hydrogen production from fossil fuels for PEM fuel cells. Alexandria Engineering Journal. 51, pp 69-75.

Wang, X, Gorte, RJ, Wagner, JP. 2002. Deactivation mechanisms for Pd/Ceria during the water-gas-shift reaction. Journal of catalyst 212, 225-230

Wongmaneenil, P, Jongsomjit, B, and Praserthdam, P. 2009. Journal of Catalyst Communications. 10, pp. 1079.

Wu, C., Wang, L., Williams, P.T., Shi, J. and Huang, J., 2011. Hydrogen production from biomass gasification with Ni/MCM-41 catalysts: Influence of Ni content. Applied Catalysis B: Environmental, 108, pp.6-13.

Wu, C., Wang, Z., Huang, J. and Williams, P.T., 2013. Pyrolysis/gasification of cellulose, hemicellulose and lignin for hydrogen production in the presence of various nickel-based catalysts. Fuel, 106, pp.697-706.

Wu, C, and Williams, PT. Investigation of coke formation on Ni-Mg-Al catalyst for hydrogen production from the catalytic steam pyrolysis-gasification of polypropylene. Applied Catalysis B: Environmental. 96(1), pp.198-207.

Xu, J, Chen, Tan, KF, Borgna, A, and Saeys, M. 2009. Effect of boron on the stability of Ni catalysts during steam methane reforming. Journal of Catalysis. 261(2), pp. 158-165.

Yanik, J., Steve Ebale, S, Kruse, A, Saglam, M, Yüksel, M. 2008. Biomass gasification in supercritical water: II. Effect of catalyst, International Journal of Hydrogen Energy. 33(17), pp. 4520-4526

Yu, J., Tian, F., and Li, C. 2007. Novel Water−Gas-Shift Reaction Catalyst from Iron-Loaded Victorian Brown Coal. Energy Fuels, 21 (2), pp 395–398

Yu, J, Tian, FJ, McKenzie, LJ and Li, CZ. 2006. Char-Supported Nano Iron Catalyst for WaterGas-Shift Reaction: Hydrogen Production from Coal/Biomass Gasification. Process Safety and Environmental Protection. 84(2), pp 125-130.

Zhang, RQ, Wang, YC and Brown, RC. 2007. Steam reforming of tar compounds over Ni/olivine catalysts doped with CeO2. Journal of Energy Conversion and Management. 48, pp 68-77.

Zhu, M and Wachs, IE. 2015. Iron-Based Catalysts for the High-Temperature Water–Gas Shift (HT-WGS) Reaction: A Review. ACS Catalysis. 6(2), pp. 722–732.

Zhu, M. And Wachs, I. E. 2016. Iron-Based Catalysts for the High-Temperature Water−Gas Shift (HTWGS) Reaction: A Review. ACS Catalysis, 6, pp. 722−732

Chapter 6: Effects of carbon dioxide adsorption by Calcium oxide for hydrogen production from a 3-stage reactor

6.0 Summary

In this chapter, a 3-stage fixed bed reactor involving biomass pyrolysis, a catalytic steam reforming reactor and a water gas shift reactor was utilised to determine the influence of calcium oxide addition to the 3rd stage water gas shift reactor to act as an adsorbent for CO_2 with the aim of improving hydrogen yield. The second stage catalytic steam reforming reactor contained Ni-alumina catalyst throughout the experiments.

The thermochemical process involved; pyrolysis followed by catalytic steam reforming and water-gas shift reaction. The most influential parameters investigated in the water gas shift were the temperature, the steam to biomass (S/B), the residence times and most importantly, the choice of catalyst. The effect of CaO in the water gas shift reaction was explicitly explored as a route for CO_2 capture in situ increasing hydrogen production. The Alumina (Al) promoted alkali earth oxides (CaO) catalysts were prepared by impregnation with different contents of CaO as detailed in chapter 3, and the effect of adding Fe to the CaO-alumina catalysts in different contents was also evaluated. A brief description of each section is given below.

In Section 6.1, the effect of adding reduced 10% nickel supported on alumina in the catalytic steam reforming stage with no catalyst at the water gas shift stage was investigated in order to determine the influence on hydrogen production.

Section 6.2 investigated the influence of adding CaO at states (reduced or unreduced) and different metal loadings to enhance water gas shift reaction performance. The impact of this on the CO/CO_2ratio, and CO_2 absorption was elucidated.

Section 6.3 The reacted catalysts were subjected to different characterisation techniques; Temperature Programmed Oxidation and X-ray diffraction (XRD) to investigate the type and extent of carbon depositions on the reacted catalysts.

6.1. Influence of addition of 10NiAl in the catalytic steam reforming stage.

In this section, the influence of the addition of reduced 10Ni-alumina in the catalytic steam reforming stage with no catalyst in the water gas shift stage was investigated. The results of total and product gas yields for H_2 (expressed both in mgg^{-1} and mmolg^{-1}), CO and CO_2, as well as the char residue yield and the mass balance, are shown in Table 6-1. The char yield was constant in both experiments (23wt% with no catalyst and 24wt% with reduced 10Ni-alumina catalyst); this performance is expected to be the same for all experiments because the process parameters at the pyrolysis stage are constant. When compared with the experiments made by Dong, et al. (2016) and Nahil, et al. (2013), the char residue yield obtained in the present study is significantly lesser, representing 36.3 and 33.5wt%, respectively. This difference could be attributed to the different process conditions, which include; higher heating rate, higher highest treatment temperature (HTT) and longer residence times at HTT.

Despite the preference for lower char yield which usually represents higher thermoconversion of the biomass into the volatiles as observed in this study, several studies, however, have contrary finding; that is, at lower process conditions (heating rate, lower HTT and shorter residence time at HTT), the char residue yield increased (Demirbras, 2007; Ronsse et al., 2014; Chen et al., 2014; Solar et al., 2016), this is partly as a result of different biomass samples used and perhaps the type of reactor used.

Table 6-1 Effect of addition of reduced 10Ni-alumina catalyst in the 2nd Stage in Mass Balance and Yields.

Catalyst in 2nd Stage	**No Catalyst**	**Reduced 10Ni-alumina**
Total Gas Yield (wt.%)	54.05%	70.56%
Hydrogen Yield (mgg^{-1} Biomass)	15.95	53.35
Mass Balance (wt.%)	91.47%	96.90%
Char Residue Yield (wt.%)	23.00%	24.00%
Gas Yield (mmolg^{-1} biomass)		
H_2	7.91	26.47
CO	10.53	10.86
CO_2	4.41	9.91

As seen in Table 6-1, the mass balances for the experiments are high (above 90%). This reveals a measure of the reliability of the obtained results; It is also observed that there was a significant improvement in the gas yield when the 10Ni-alumina catalyst was added to the catalytic steam reforming stage. Nevertheless, this rise in gas yield is a product of the addition of steam to the second stage (catalytic steam reforming reaction), since it releases the same quantity of product gases in both experiments. The hydrogen yields also significantly increased from 15.95 to 53.35 mgg^{-1} (that is, 7.91 to 26.47 $mmolg^{-1}$), upon the addition of the 10Ni-alumina catalyst to the catalytic steam reforming. This represents 23.4% increase which is consistent with other studies finding, that that the use of Ni-based catalysts in the thermochemical processes considerably optimises the yield of hydrogen (Dong et al., 2016; Wu et al., 2011, Peng, et al., 2017).

Without a catalyst in the catalytic steam reforming reaction, high selectivity towards CO is obtained while a small positive change in carbon monoxide yield is achieved when 10Ni-alumina is utilised, this shows the evidence of catalytic steam reforming reaction taking place. However, there is a significant increase in carbon dioxide and hydrogen yield upon addition of 10Ni-alumina, this rise is as a result of simultaneous catalytic steam reforming and water gas shift reaction taking place with the evidence of high selectivity towards hydrogen production (Wu et al., 2011).

Additionally, Figure 6-1 indicates the nitrogen-free gas composition when no catalyst was utilised at both the catalytic steam reforming and water gas shift stages, and when only reduced 10NiAl catalyst is used in the catalytic steam reforming stage. The concentration of the hydrogen produced was 29.17% when the whole thermochemical process was carried out uncatalyzed. This result almost doubled when it was catalysed representing 55.10% hydrogen concentration in the product gas.

Conversely, the CO yield reduced from 38.82 wt.% to 22.61 wt.%, this shows that the catalytic methane reforming was promoted, hence enhancing selectivity towards hydrogen and carbon dioxide, coupled with the fact that the carbon dioxide concentration also rose from 16.25% wt.% to 20.63 wt.%.

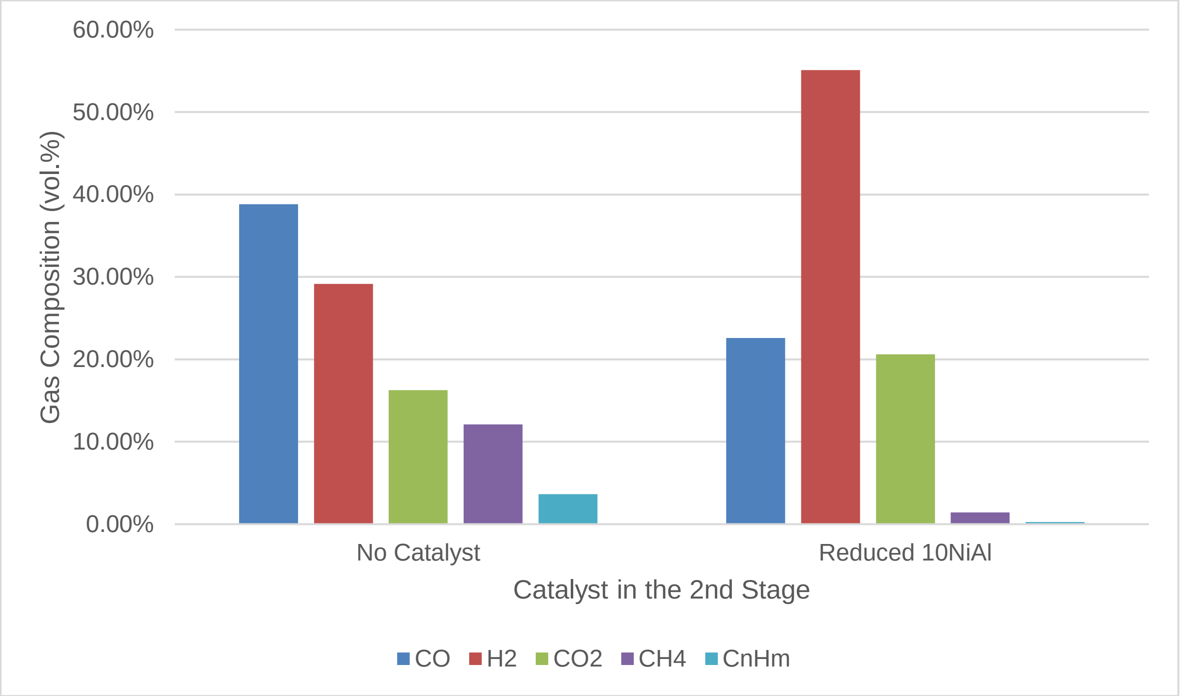

Figure 6-1 Effect of addition of 10Ni-alumina catalyst to the 2nd Stage in Gas composition (N_2 free)

More so, the production of methane (CH_4), hydrocarbons (C_nH_m)and some other product gases declined significantly, almost becoming negligible in the presence of the 10Ni-alumina catalyst. This suggests that a further reforming of the hydrocarbon gases is promoted with the catalyst.

The results shown in figure 6-3 are the hydrogen production molar ratios H_2/CO, H_2/CO_2 and H_2/C. The hydrogen to carbon monoxide ratio (H_2/CO) improved steeply from 0.75 to 2.44 upon the addition of the catalyst, since H_2 almost doubled and CO remained constant. This suggests that the catalyst promotes the catalytic reformation of the volatiles into carbon monoxide in the catalytic steam reforming stage and also a further catalytic activity in the water gas shift reaction. Also, the incorporation of a water gas shift stage, where steam is utilised at a lower temperature, positively influenced the H_2/CO ratio which explains the increases, in comparison to using only 2 stage- pyrolysis and catalytic steam reforming process with similar conditions (Dong, et al., 2016). In addition to this, the escalation of the H_2/CO_2 ratio from 1.80 to 2.67 also suggests that the water gas shift reaction is simultaneously promoted.

In a similar vein, the comparison of H_2/CO ratio with H_2/CO_2shows that the evidence of catalyst utilisation, with H_2/CO of 0.75 and H_2/CO_2 of 1.80 for uncatalyzed and catalysed processes respectively. However, the process is mainly driven by the catalytic steam reforming of the biomass rather than the water gas shift reaction.

It is also observed that the methane and other hydrocarbon compounds are not fully reacted, whereas the addition of the reduced 10NiAl catalyst leads to a higher catalytic conversion of the volatiles into carbon monoxide, which consequently converts to carbon dioxide following water gas shift reaction. (R.6-1).

$$CO+H_2O \leftrightarrows CO_2+H_2 \qquad \text{(R.6-1)}$$

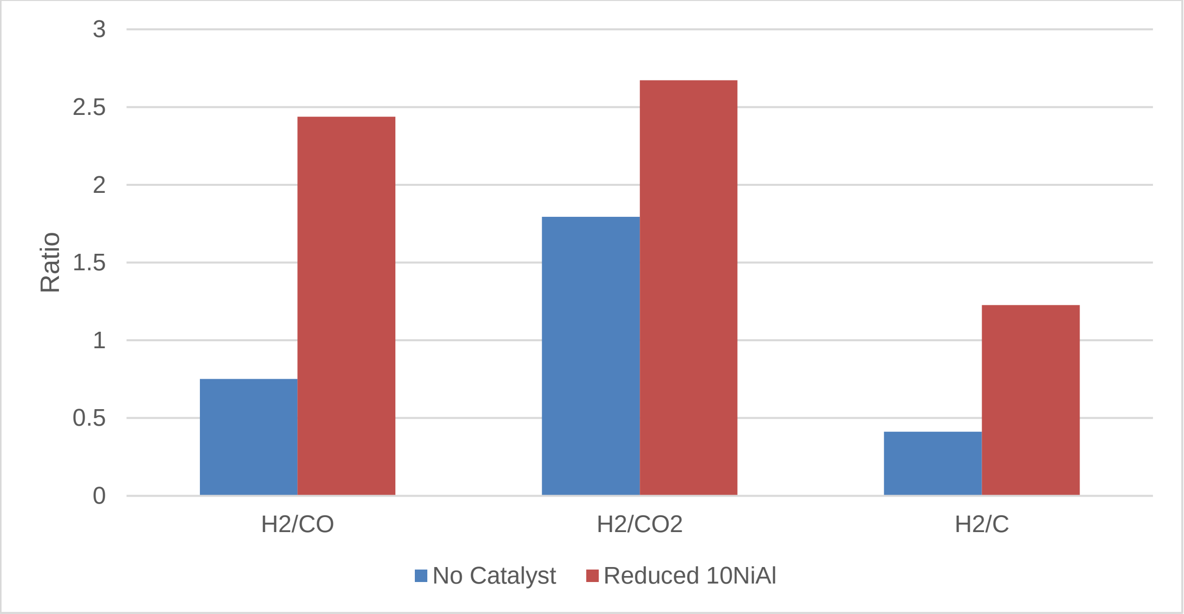

Figure 6-2 Effect of the addition of 10Ni-alumina catalyst to the 2nd Stage in H2 production molar ratios.

In general, the H_2/C ratio shows a substantial elevation; this implies that the overall performance in hydrogen production from the biomass is improved when the 10Ni-alumina catalyst is utilised in the catalytic steam reforming stage while other unwanted compounds are produced in minute quantities.

6.2. Influence of CaO sorbent/catalysts addition in the water gas shift stage.

The study of Bunma and Kuchonthara (2018) showed that high production of hydrogen is achievable with the use of a combined catalyst and sorbent (NiO-MgO-CaO/γ-Al2O3). The rise in hydrogen yield is a product of CO_2 absorption of the alkali earth catalysts, hence, promoting water-gas shift reaction. Nevertheless, the question remains, what are the best operating parameters for optimum hydrogen yield? Therefore, in this section, two parameters (reduction or non-reduction of catalysts during synthesis and different amount of the CaO) are investigated. As shown in section 6.1, 10Ni-alumina has excellent catalytic activity in enhancing hydrogen production via the catalytic steam reforming stage. in this section 10ni-alumina catalyst was retained in the catalytic steam reforming while CaO sorbents/catalysts were added to the water-gas shift reaction stage in different proportions and both reduced and not reduced in order to investigate the effect of CaO catalysts in hydrogen production and carbon dioxide reduction. The experiment with no catalyst in the third stage in section 6.1 was used as a reference.

Table 6-2 reveals the yields for the permanent and hydrocarbon gases, the char residue yield, the total gas yield, and the mass balance for the investigations where CaO-alumina sorbent/catalyst with different compositions were added in the water gas shift stage. All the results depict high reliability with mass balances above 93 wt.% for the experiments. As earlier found and discussed in section 6.1, the unchanged process conditions for the biomass pyrolysis yielded a relative constant char yield for the five different experiments, with a mean of 22.80%. However, the experimental results differ from one another with respect to the gas yields and the hydrogen yields.

A variety of empirical studies show that the chemical states of catalysts, that is either reduced or unreduced exert an influence on their catalytic activities (Tang et al., 2017, Joshu et al.; 2009, Ryzhikov et al., 2008, Cutrufello et al. 1999). In essence, a reduction of catalysts is made to obtain a phase that is catalytically active and to prevent them from being oxidised during product gases reactions. Cutrufello et al. 1999, studied the acid-base characteristics and catalytic activity of nanophase ceria-zirconia catalysts ($Ce\text{-}_xZr_xO_2$) and found that upon catalysts reduction treatment, the acid sites promoting catalytic activity weakened. However, Ju et al. 2019 and Tang et al. 2017 reported similar findings that the H_2 reduced catalysts do not have any significant advantage over the unreduced adsorbent. Since both studies used Nickel-based catalysts and calcinated at a temperature range from 350°C to 500°C, it is therefore difficult to infer that reduced and unreduced catalysts have similar activity strength.

Notably, when catalysts are not reduced, it is assumed that the catalysts are reduced in-situ by the pyrolysis gases containing the reducing gases; hydrogen and CO. (Xiong et al 2011)

In this study, firstly, upon the addition of unreduced 10CaO-alumina sorbent/catalyst to the water-gas shift, a total gas yield of 63.38 wt.% was generated which significantly increased to 82.73 wt.% when the catalyst with the same composition (10CaO-alumina) was used, but this time, the catalyst was reduced. The gas yield depicts a contrary trend as it declined from 72.83 wt.% to 59 wt.% when the 20CaO-alumina was added both when reduced and not reduced respectively. Similar results were observed in the hydrogen yield in mmolg^{-1} but with a higher difference between not reduced and reduced 10CaO-alumina, and a much lower difference between not reduced and reduced 20CaO-alumina.

Secondly, the experimental results showed that, upon the introduction of the CaO-alumina sorbent/catalyst to the water gas shift reaction stage, the hydrogen yield improved in comparison to when no catalyst was utilised. An optimum hydrogen yield, representing 51.51 mmolg^{-1}was obtained with the Reduced 10CaO-alumina catalyst. This is considerably higher compared with reports in which the process eliminates a third stage-water gas shift reaction (see Figure 6-2) (Dong, et al., 2016; Peng et al., 2017; Nahil et al., 2013).

This implies that upon the addition of the reduced 10CaO-alumina catalyst, the catalyst aids the reaction between the added steam and the CO produced in the catalytic steam reforming stage. This justifies the incorporation of an independent third stage exclusively for the water gas shift reaction having its catalyst so that both processes can be selective and promoted discretely. The results prove that the alkali earth oxide (CaO) can perform not only as a sorbent but also as a catalyst.

Table 6-2: Influence of CaO catalysts addition in the water gas shift stage on mass balance and yields

CaO Catalyst/Sorbent in 3rd Stage	**No Catalyst**	**10CaO-alumina**	**Reduced 10CaO-alumina**	**20CaO-alumina**	**Reduced 20CaO-alumina**
Total Gas Yield (wt.%)	70.56%	63.38%	82.73%	72.83%	59.00%
Hydrogen Yield (mgg^{-1} Biomass)	53.35	58.05	103.96	67.89	64.93
Mass Balance (wt.%)	96.90%	93.85%	101.80%	96.59%	96.15%
Char Residue Yield (wt.%)	24.00%	21.50%	22.50%	23.50%	22.50%
Gas Yield (mmolg^{-1} biomass)					
H_2	26.47	28.80	51.58	33.68	32.21
CO	10.86	14.53	21.02	13.68	13.25
CO_2	9.91	8.38	13.47	10.03	9.21

More so, when compared with the blank experiment (that is, when the water gas shift stage was uncatalyzed), all the experimental results depict an increase in the carbon monoxide yield, mainly when the reduced 10CaO-alumina catalyst was utilized, so this suggests that the catalyst allows the steam and the volatiles to be further catalytically reformed, and the water gas shift reaction to being promoted for carbon dioxide generation. A contrary and unpredictable trend is observed with respect to the CO_2 yield where the 10CaO-alumina and the reduced 20CaO-alumina catalysts produced lower yields than the experiment with no catalyst (9.91 mmolg^{-1}), with 8.38 and 9.21 mmolg^{-1} respectively.

However, the reduced 10CaO-alumina and the unreduced 20CaO-alumina catalysts indicated yields above the blank experiment, with 13.47 and 10.03 mmolg^{-1} respectively representing 35.9% and 1.21% rise respectively. Therefore, this implies that different compositions of CaO-alumina catalysts have different influence on the promotion of the water gas shift reaction. This is further discussed under the hydrogen production ratios below. Although there is no existing literature that investigated the influence of different CaO loadings in water gas shift reaction but the report of Panagiotopoulou and Kondarides (2011) indicated that the catalytic performance of alkaline metal metal-promoted catalysts (CaO-X) is dependent on the nature, loading of the promoter and the calcination temperature of the catalysts, 1-2 wt.% CaO produced 2-3 times H_2 compared to Ni-alumina catalyst. Similarly, Charisiou et al. (2016), 6.0 wt% CaO–Al_2O_3 catalysts reveal higher yields for X_{CH4}, X_{CO2}, Y_{H2} when matched with the Ni/Al catalyst for investigating temperature between 550 and 750 °C. Again, this study did not consider higher CaO loadings nor varied the alkaline metal loadings. A reliable explanation for the result obtained in this investigation would, therefore, imply that the addition of CaO under the parameters utilised in this study should not exceed 20wt% in order to optimise hydrogen production.

Figure 6-3 shows the composition of the product gases produced in the water gas shift process. Importantly, the reduced 10CaO-alumina catalyst produced the maximum H_2 content with 59.71 vol.%, as earlier stated in this section, the same catalyst generated the maximum hydrogen yield per grams of biomass. This suggests that the catalyst, together with the 10Ni-alumina catalyst in the 2nd stage enhances both the catalytic steam reforming and the water gas shift reactions, hence improves selectivity towards the hydrogen production as can be seen in the compositions of CO_2 and CO from the catalysts studied. In addition to this, the same catalyst yielded the least quantity of methane which can be regarded as negligible. One can, therefore, infer that CH_4 has almost completely reformed in the catalytic steam reforming stage into CO.

Also, the 20CaO-alumina catalyst depicts a high catalytic performance as it shows the least difference between its CO and CO_2 concentrations, and a significantly low amount of CH_4. This implies that the catalyst evidently promotes the water-gas shift reaction to a higher extent than the other catalysts investigated in this present study. It is also observed that an increase in the CaO content in the catalysts results in a decline in CO content from 27.14 to 23.58 vol.% in the not reduced 10CaO-alumina and 20CaO-alumina catalysts respectively, and from 24.34 to 23.79 vol.% in the reduced 10CaO-alumina and 20CaO-alumina catalysts respectively. Meanwhile, the CO_2 concentrations rose in the same pattern, suggesting that the water gas shift reaction is enhanced upon the addition of CaO to the sorbent/catalyst.

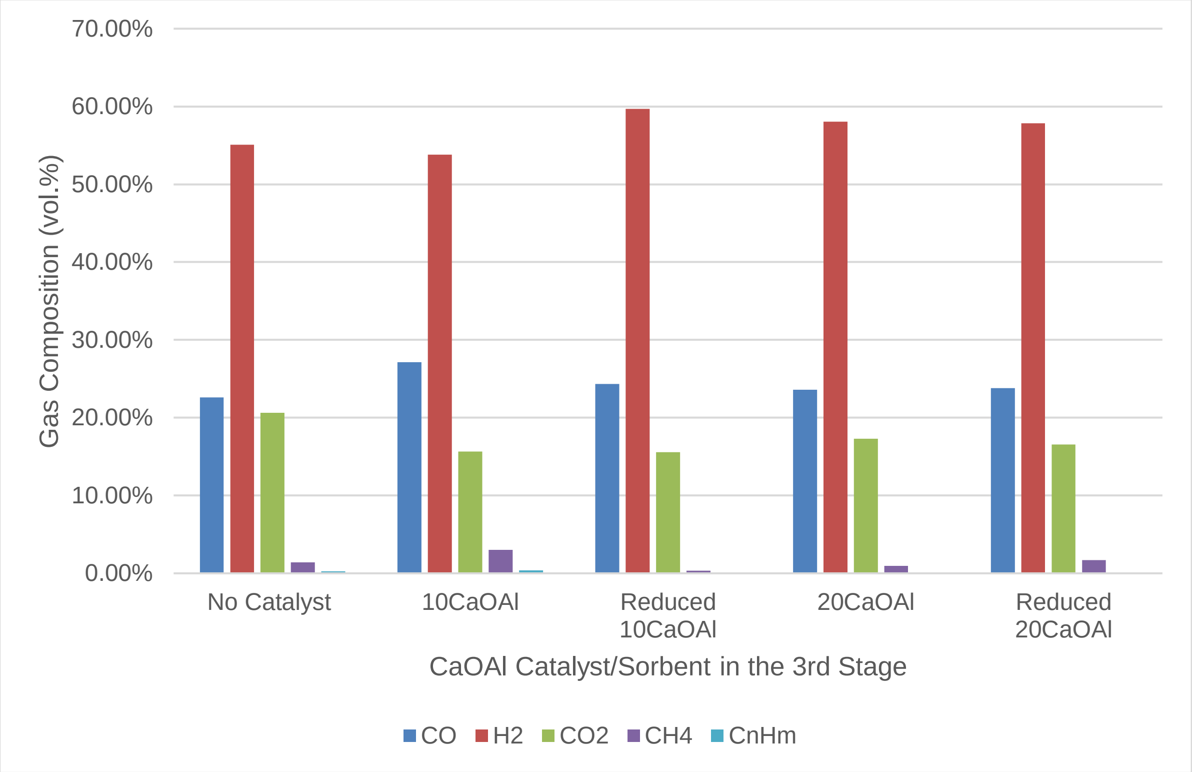

Figure 6-3: Effect of CaO catalysts addition in the third stage in gas composition (N2 free)

It is also observed that the 10CaO-alumina catalyst is the least effective catalyst with the least catalytic conversion of methane into carbon monoxide, as it produces its maximum CO content and the lowest hydrogen content. Additionally, the catalyst also produced the maximum difference between the CO and the CO_2 concentrations. This suggests that the catalytic performance of 10CaO-alumina catalyst in promoting the water gas shift reaction is weak. This reveals the significance of reducing the catalyst during preparation before use, while the reduced 10CaO-alumina produced the maximum hydrogen yield, the unreduced CaO-alumina significantly retarded the hydrogen production below the uncatalyzed system. Therefore, one crucial finding is that the unreduced 10CaO-alumina was catalytically selective towards CO and CH_4.

The H_2/CO, H_2/CO_2, CO/CO_2 and the H_2/C molar ratios are presented in Figure 6-5. From this figure, it is shown that the H_2/CO molar ratio is relatively the same for all catalysts investigated except for the 10CaO-alumina sorbent/catalyst which shows the highest ratio due to high CO and low H_2 production which reflects the least its performance in promoting the water-gas shift reaction for further CO consumption and CO_2 production.

Similarly, the results reveal a decline in the H_2/CO_2 molar ratio when the CaO content of the sorbent catalyst rises from 10 to 20 wt.% in both not reduced and reduced catalysts. Thus, this implies that the addition of CaO enhances the water gas shift reaction performance. This influence is also depicted in the CO/CO_2 ratio, which also shows a declining trend with CaO addition. Kumagai et al. (2015) studied the effect of CaO addition to Ni-Mg-Al based catalysts in order to promote the in-situ CO_2 absorption; this gave rise to a significant increase in the hydrogen production from the pyro-gasification of a biomass/ plastic mixture. Additionally, the rise in the H_2 production is primarily as a result of CO_2 adsorption by CaO which shifts the equilibrium of the water-shift reaction as illustrated in figure 6-4 below.

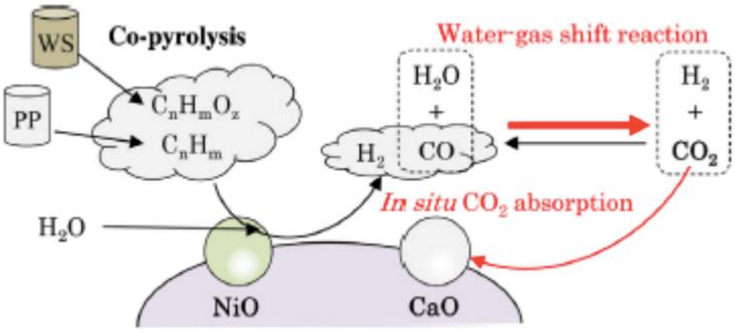

Figure 6-4: Pyrolysis and hydrogen production from biomass and plastic using Ni-Mg-Al-Ca catalysts. Source: Kumagai et al. (2015)

The results in this present work indicate the same increasing tendency but in different magnitude in H_2/CO mass ratios from 0.143 to 0.174 (gg^{-1}) where the 10CaO-alumina and 20CaO-alumina catalysts, respectively were added. This trend was also observed from 0.176 to 0.177 (gg^{-1}) when the reduced 10CaO-alumina and reduced 20CaO-alumina were added. This is consistent with what Nahil et al. (2013) suggested, that the water gas shift reaction is favoured when Cao is added, which is also expected to absorb CO_2.

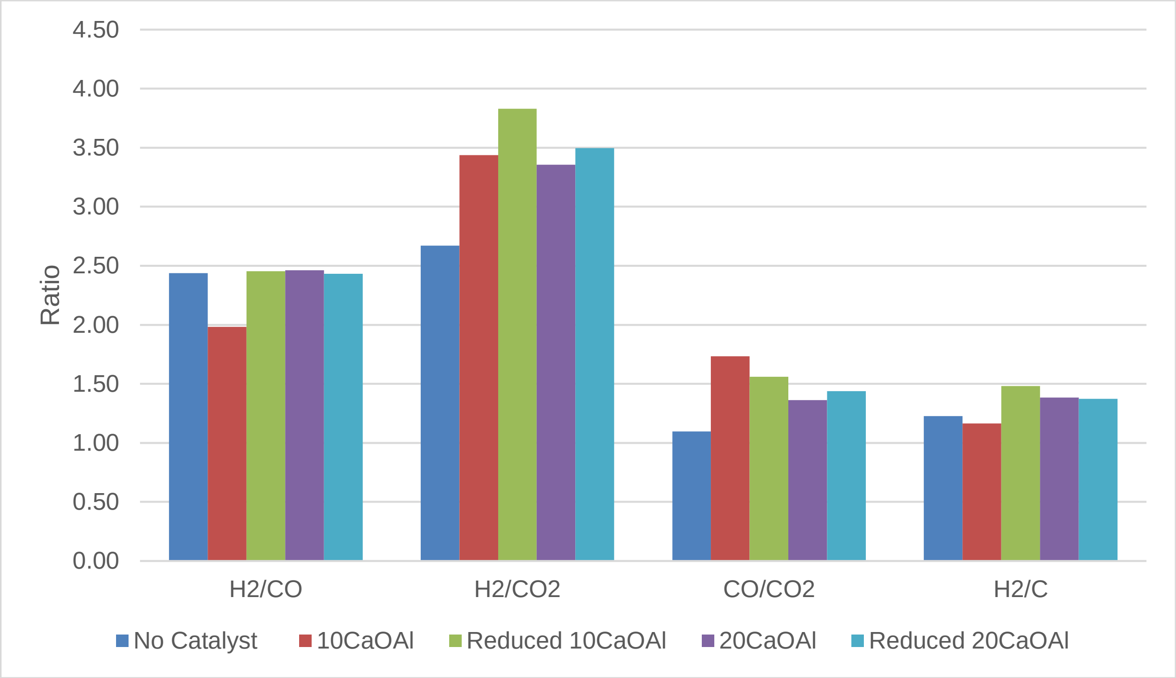

Figure 6-5 Effect of CaO-alumina catalyst addition in different compositions to the 3rd stage in the H_2/CO, H_2/CO_2, CO/CO_2 and H_2/C molar ratios.

In general, the overall hydrogen generation performance as shown by the H_2/C molar ratios was optimised when the Reduced 10CaO-alumina sorbent/catalyst was utilised in the water gas shift stage, representing a value of 1.48. According to Li, et al. (2014) the addition of CaO will have a positive effect in the water gas shift reaction, acting as both absorbent and catalyst, which is supported by the results obtained in this work, where the addition of CaO resulted in lesser CO/CO_2 molar ratio.

6.3. Influence of steam addition in the water gas shift stage.

The addition of extra steam increases the overall operational costs of hydrogen production; hence, the need to either minimise or eliminate is crucial (Junior et al. 2005; Araujo and Rangel 2009). Therefore, in this study, another investigation was carried out to analyse hydrogen production when no steam is added to both catalytic steam reforming and water gas shift reaction stages and to match it with the results obtained when steam is injected. The uncatalyzed experiment in the water gas shift stage just like the previous investigations is also used as a reference to evaluate how product gases yields and compositions change, even if there is a catalyst in the water gas shift reactor when no steam is injected to the process. Similar to previous investigations, the 10Ni-alumina catalyst was used for the water gas shift stage for all experiments while the reduced 10CaO-alumina sorbent/catalyst was used for the experiment with no steam because it had the best overall performance for hydrogen production in terms of CaO-alumina catalysts as shown in section 6.2.

The results for the char residue yield, the mass balances and the total gas yields together with the individual gas yields for H_2, CO and CO_2 in mmolg^{-1} are presented in Table 6-3 As discussed in the preceding sections, the char yield was constant in all the experiments due to the stable conditions for biomass pyrolysis. However, with respect to the experiment involving no steam injection, the remaining 77.50% (biomass conversion to volatiles) was expected to turn into gas, since no tar was obtained from any of the experiments. There is an increase in the gas yield when no steam is injected into the thermochemical process, this is primarily a function of no steam which can react in the catalytic steam reforming and water gas shift stages and what is generated at the bottom of the reactor is mainly the non-condensable gases produced by the reactions between the volatiles released only by the biomass.

More so, the hydrogen yields substantially reduced from 51.58 to 21.26 mmolg^{-1} since the reactor lacks steam (H_2O) to provide the H-atoms for further selectivity towards hydrogen production. Consequently, the pyrolysis of the volatiles released by the biomass is the predominant process, hence, generating mainly carbon monoxide. This reduction is normal because the H_2 that is produced comes principally from the biomass hydrogen content which is relatively low.

Concerning carbon dioxide, the experiment without steam injection produced the least yield as compared to the systems with various injection flowrates, the implication of this is that the water gas shift reaction is subsided or rarely promoted, again this can be explained to a result of starving the reactor with water. Hence, the CO could not be catalytically converted into CO_2. Additionally, the hydrogen yield is found to be lower when no steam is added than when no catalyst is added in the third stage in the presence of steam. This suggests that the steam injection plays a very crucial role in optimising hydrogen production by promoting catalytic activities in the catalytic steam reforming and water gas shift reactor.

Chen et al. (2010) studied the production of H_2 from CH_4 under the two-stage process; interaction of partial catalytic oxidation (CPOM), and water gas shift reaction. They reported that in addition to temperature, increasing steam addition (from 1 to 6 S/C ratio) strongly promoted H2 yield, the injected steam produced a cooling effect on the product stream and also alleviated the performance of CPOM. The reduction in CPOM performance resulted from the decline in the CH_4 conversion and the maximum temperature. One evidence from Chen et al. (2010) computational study, supported by Horn et al. (2007), was that the influence of the S/C ratio on the CH_4 conversion was slight.

More so, Udomsirichakorn et al. (2013) found out that, as the amount of steam (that is, steam/biomass - S/B ratio) was raised from 1.47 to 3.41, a consistent rise from 45.14% to 63.07% in the volumetric concentration of H_2 was obtained. On the other hand, the CO_2 yield diminished from 23.76% to 18.68%. In essence, the injection of more amount of steam (that is, higher S/B) a greater CO_2 absorption by CaO through a carbonation reaction (R6-3) , this inadeptly in effect reduces CO_2 partial pressure and then consequentially promotes water–gas shift reaction (R.6-4) to move in forward direction to produce more H_2. Another evidence of water gas reaction is the significant dip in CO concentration, which is in substantial agreement with the rise of H_2 concentration, over the same steam injection rate from 1.47 to 3.41 S/B ratio but beyond 3.41 S/B ratio, the concentration and yield of H_2 declined. This implies that 3.41S/B ratio was the optimum value for steam injection. Two studies; Han et al. (2011) and Manovic, and Anthony (2008) also acknowledged the enhancement of carbonation reaction by greater S/B ratios for increased H_2 production.

$$Carbonation:\ CaO + CO_2 \rightarrow CaCO_3 \qquad 6\text{-}2$$

$$Water\ gas\ shift:\ CO + H_2O \rightarrow CO_2 + H_2 \qquad 6\text{-}3$$

The reduced 10CaO-alumina with double steam injection produced the highest ratio of syn-gas ($H_2/CO>>3$), Charisiou et al. (2016) reported H_2/CO molar ratio ranging from 0.6 to 1 for Ni/CaO–Al indicating that the positive impact of CaO and steam addition, Abdollahifar et al. (2014) also reported similar findings but with MgO alumina. With a double steam injection, it depicts the strong capacity of the catalyst in dissociating CO followed by H_2 and CO_2 production, hence significantly promoting water gas shift reaction.

Table 6-3: Influence of steam addition and removal to the catalytic steam reforming and water gas shift reaction stages with no catalyst and reduced 10CaO-alumina catalyst in mass balance and yields.

CaO Catalyst/Sorbent in 3rd Stage	**No Catalyst**	**Reduced 10CaO-alumina**	**Reduced 10CaO-alumina**
Steam	**Double Steam**	**No Steam**	**Double Steam**
Total Gas Yield (wt.%)	70.56%	84.95%	82.73%
Hydrogen Yield (mgg^{-1} Biomass)	53.35	42.85	103.96
Mass Balance (wt.%)	96.90%	98.43%	101.80%

Char Residue Yield (wt.%)	24.00%	22.50%	22.50%
Gas Yield (mmolg^{-1} biomass)			
H_2	26.47	21.26	51.58
CO	10.86	19.04	21.02
CO_2	9.91	4.85	13.47
H_2/CO	2.4	1.1	2.5

Substantial differences are also observed in the gas composition based on the steam addition factor as shown in Figure 6-6, especially in the CO content. When the water gas shift stage is uncatalyzed compared to when no steam is injected into the reactor but in the presence of reduced 10CaO-alumina catalyst, the CO content is almost doubled from 22.61 to 41.91 vol.% respectively. Also, comparing the reduced 10CaO-alumina catalyst with no steam with the same catalyst but in the presence of steam, the CO content steeply reduced from 41.91 to 24.34 vol.%. Hence, this suggests that when no steam is added to the process, the pyrolysis of the volatiles is promoted to a higher extent than the water-gas shift reaction. Nevertheless, this gasification cannot be considered a steam reforming since only the gases released are used for the reactions, and they do not contain water. This promotion might be due to the presence of the 10Ni-alumina catalyst in the catalytic steam reforming stage which supports the reforming reaction.

6.0 Summary

In this chapter, a 3-stage fixed bed reactor involving biomass pyrolysis, a catalytic steam reforming reactor and a water gas shift reactor was utilised to determine the influence of calcium oxide addition to the 3rd stage water gas shift reactor to act as an adsorbent for CO2 with the aim of improving hydrogen yield. The second stage catalytic steam reforming reactor contained Ni-alumina catalyst throughout the experiments.

The thermochemical process involved; pyrolysis followed by catalytic steam reforming and water-gas shift reaction. The most influential parameters investigated in the water gas shift were the temperature, the steam to biomass (S/B), the residence times and most importantly, the choice of catalyst. The effect of CaO in the water gas shift reaction was explicitly explored as a route for CO2 capture in situ increasing hydrogen production. The Alumina (Al) promoted alkali earth oxides (CaO) catalysts were prepared by impregnation with different contents of CaO as detailed in chapter 3, and the effect of adding Fe to the CaO-alumina catalysts in different contents was also evaluated. A brief description of each section is given below.

In Section 6.1, the effect of adding reduced 10% nickel supported on alumina in the catalytic steam reforming stage with no catalyst at the water gas shift stage was investigated in order to determine the influence on hydrogen production.

Section 6.2 investigated the influence of adding CaO at states (reduced or unreduced) and different metal loadings to enhance water gas shift reaction performance. The impact of this on the CO/CO2ratio, and CO2 absorption was elucidated.

Section 6.3 The reacted catalysts were subjected to different characterisation techniques; Temperature Programmed Oxidation and X-ray diffraction (XRD) to investigate the type and extent of carbon depositions on the reacted catalysts.

6.1. Influence of addition of 10NiAl in the catalytic steam reforming stage.) Auto-thermal steam production is also a possibility because the auto-thermal process would need additional O_2 which could have been gotten from steam which would decline the stoichiometric H_2 yield or the experimental H_2 yield since some H_2 eventually oxidises to form water (Czernik and French, 2014).

In a similar vein, the experiment with no steam injections produces a gas yield of 46.78 vol.%, which comes mainly from the biomass moisture and volatiles content, which is significantly lower than the experiment with both steam and reduced 10CaO-alumina catalyst with 59.71 vol.%. Concurrently, the result for CO_2 was similar, being 10.67 and 15.59 vol.% for when there is no steam addition and when there is, respectively. It is implied then that the water gas shift reaction scarcely takes place with no steam. According to Zhang et al. (2004), with greater amounts of steam injected into the reactor system, the H_2 and CO_2 concentrations increases, while the CO concentration falls. In their study, with increasing steam injection (S/C from 2.8-6.5), hydrogen production also increases amounting about 30% rise, the producer gas (CO and CO_2) concentrations were also influenced; CO concentration declined by 50% while CO_2 yield rose by 50% from a steam/carbon ratio of 2.8–6.5. Another similarity between Zhang et al. (2004) is that reduced and unreduced catalysts were used (Z409 representing unreduced catalysts and RZ409 representing the reduced, both containing potassium, calcium and magnesium oxides). These empirical results confirm the positive effect of steam addition to enhance H_2 yield in water gas shift

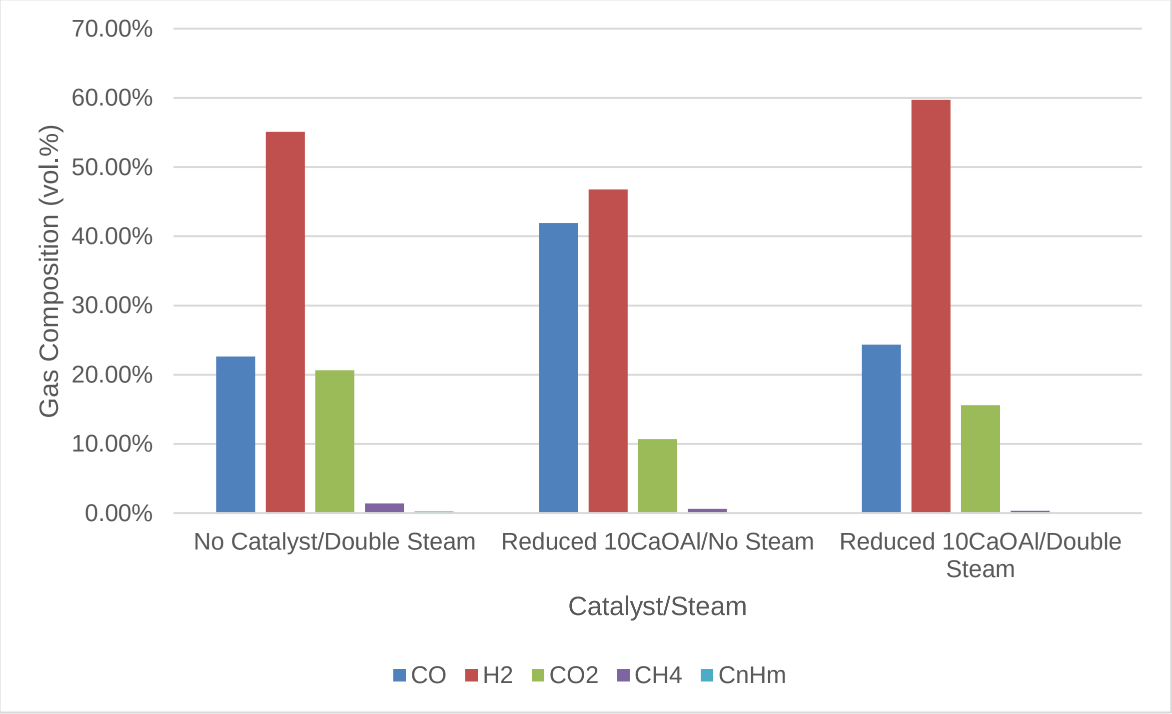

Figure 6-6 Effect of steam addition and removal to the catalytic steam reforming and water gas shift reaction stages with no catalyst and reduced 10CaO-alumina catalyst in gas composition (N_2 free)

(*Double steam means dual steam input into the experimental system*)

It is also noteworthy that upon the addition of the reduced 10CaO-alumina together with 10Ni-alumina catalyst in the catalytic steam reforming stage, even in the absence of steam, the catalytic reformation of the methane is enhanced as its contents are negligible (0.64 vol.% for $CH_{4)}$ and other hydrocarbon gases yields drop as well. However, with the addition of steam, using the same catalyst, the process achieves higher catalytic activity and selectivity towards hydrogen production.

More so, the H_2/CO, H_2/CO_2 and H_2/C molar ratios are shown in Figure 6-7. The injection of steam into both the absence and presence of the reduced 10CaO-alumina catalyst results in almost the same H_2/CO molar ratio, due to the high H_2 and moderate CO production, proving the execution of the steam reforming reaction.

Nevertheless, when no steam is injected, the H_2/CO ratio declines to 1.12, which implies that almost the same moles of hydrogen and carbon monoxide are produced, suggesting that a higher promotion of the reforming reaction takes place. Regarding the H/CO_2 ratio a contrary trend was obtained; with the highest ratio when there is no steam addition, due to the low CO_2 content, proving the previous statements that the absence of steam results in poor promotion of the water gas shift reaction. The low content in carbon dioxide could also be triggered by absorption from the catalyst, but since there is no measuring point between the two stages to know how much of the CO_2 enters and exits the water gas shift stage, there is not enough evidence of this absorption performance. With respect to the H_2/C molar ratio, the lowest is achieved from the experiment with no steam, which is 40% below the one with steam addition in the presence of the Reduced 10CaO-alumina catalyst, this is due to the low hydrogen yield and the production of the other gases, composed mainly of CO. This implies that the addition of steam has a significant influence in hydrogen production maximization, so it's crucial to include it in the process. The problem with this pyrolysis is that there is hydrogen consumption with the carbon dioxide in a reaction called reverse water-gas shift (R-water gas shift) (Oyama, et al., 2012):

$$CO_2 + H_2 \leftrightarrows CO + H_2O \tag{6-4}$$

According to Oyama et, al (2012), when the reactor is starved with steam, the hydrogen reacts with the CO_2 produced in the water gas shift reactor to form water and unidentate carbonate (CO) as shown in equation R.6-4, thereby favouring a backward reaction. Jacobs and Davis (2005) studied the kinetic mechanisms of reverse water-gas shift reaction over a Pt/ceria catalyst. They found that in the absence of H_2O, the activation energy barrier is raised and CO_2 is decomposed fast to CO, but when steam is added to the reversed water gas shift feed, RWGS proceed at a decidedly slower rate indicate the mechanism of forwarding shift reaction for water gas shift. Supporting this finding, Dagle et al. (2008) also reported that RWGS reaction rate constants are almost 20 times lower than that of methanol catalytic steam reforming, therefore accounting for the little concentration of CO produced in methanol steam reforming while no evidence of water gas shift reaction participation in methanol steam reforming was found. In other words, regarding CO, the water gas shift conversion is a reversible parallel-consecutive reaction (Van der Laan and Beenackers; 2000). One key finding of Dagle et al. (2008) was that RWGS is promoted by the type of catalyst rather than the absence of steam; the rate of RWGS on PdZn alloy exhibits the same reaction order with methanol conversion using metallic Pd, this explains the cause of small quantity of CO production in catalytic steam reforming of methanol coupled with methanol conversion on metallic Pd. Therefore, one deduction is that though lack of steam in the water gas shift reaction can lead to unwanted RWGS, the type of metal used can also contribute to it.

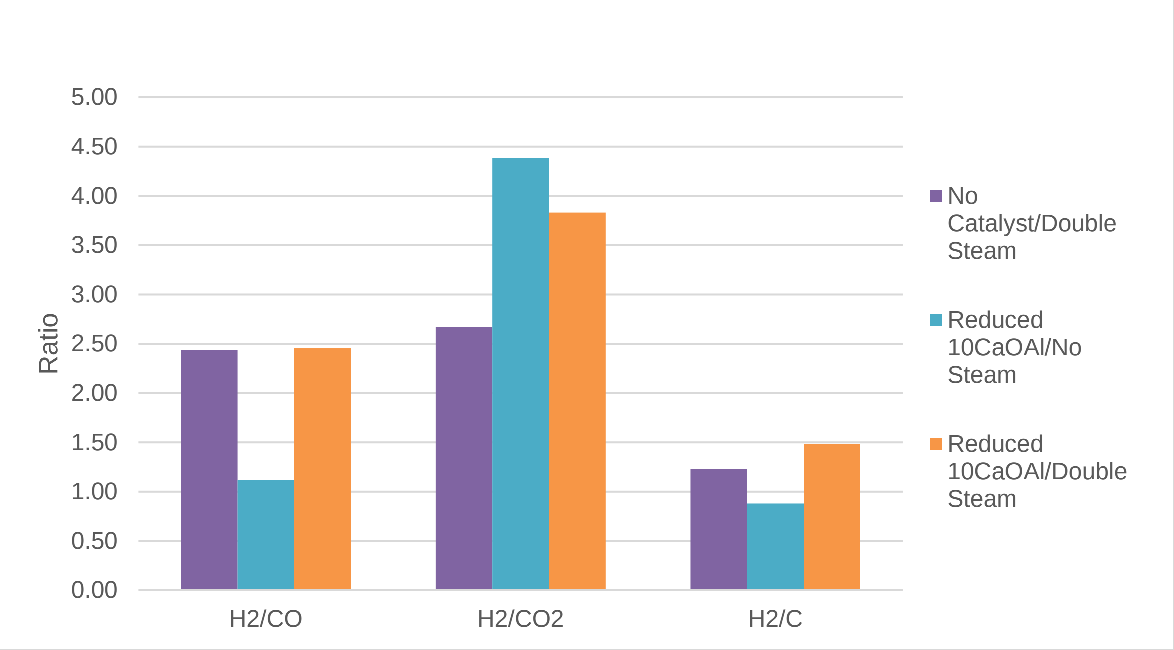

Figure 6-7: Effect of steam addition and removal to the catalytic steam reforming and water gas shift reaction stages with no catalyst and Reduced 10CaO-alumina catalyst in the H_2/CO, H_2/CO_2, and H_2/C molar ratios

6.4. Influence of Fe loading to CaO-alumina catalysts.

The effect of adding iron (Fe) to CaO-alumina catalysts (FeCaO-alumina catalysts) in different proportions on hydrogen generated was investigated as a sorbent in absorbing CO_2 produced in the thermochemical process. Iron (Fe) was chosen because several researchers have reported that it has an excellent catalytic activity in water-gas shift reaction when prepared on CaO catalyst supported on alumina, thereby promoting higher hydrogen yields (Pal, et al., 2018; Zu & Wachs, 2015) while the CaO portion acts as both catalyst and absorbent(Udomisirichakorn, et al., 2013). Similar to the previous experiments, 10Ni-alumina catalyst was utilised in the catalytic steam reforming stage and different catalysts with different Fe: CaO: Al ratios in 0.5g were used for the water-gas shift stage. The experimental results obtained using Reduced 10CaO-alumina were used as a reference. All the catalysts utilised required reduction processes since the Fe metal needed to be in its elemental state before it can be used as catalysts, so the “Reduced” term is omitted in this section.

The results obtained for the gas analysis from the different Fe loadings are presented in Table 6-4. Mass balances of almost 100% are observed for all the investigated catalysts, indicating that the mass losses are quite negligible and also implying that all the results are highly reliable. All the results obtained depict a high conversion of the biomass samples, considering that the product gases or volatiles and the moisture content from the biomass sample summed up 81.40 wt. % (see Table 6-4**Error! Reference source not found.**) and in all the experiments, a constant char residue yield of a pproximately 23 wt. % was obtained. This means that almost all the volatiles and moisture were liberated from the sample in the given pyrolysis conditions, which can then be reformed in the catalytic steam reforming stage.

The total gas yield declined upon the addition of Fe to the 10CaO-alumina catalyst, from 82.73 wt.% when there is no Fe to 66.87 wt.% when Fe is added at 10wt.% to the catalyst. There was also a minor reduction to 66.08 wt.% when the Fe loading was increased to 20 wt.% in the catalyst composition. This means that at higher Fe:CaO ratio, less of the added water turned into non-condensable gases since CaO helps the steam to react with both the volatiles and the carbon monoxide in the different stages and less liquid water is produced. Additionally, for cost implication, Fe at 10wt.% is reasonably the most suitable loading under the utilised process conditions for optimum total gas yield and H2 production since there is no substantial difference between what is obtained in 20wt.% Fe loading.

On the contrary, when a catalyst with ratio 1:2 for Fe and CaO respectively, (10 wt.% Fe, 20 wt.% CaO and 70% wt.% Al) the gas yield was 71.63 wt.%, still lower than the 10CaO-alumina catalyst due to the presence of Fe. A 40Fe40CaO-alumina (20 wt.% Al support) was also used, which resulted in the highest gas yield, as it contained more CaO to promote the catalytic steam reforming and water gas shift reactions, and it was observed that the Fe content does not have the same inhibition effect as with the other catalysts.

There is a decrease in the hydrogen yield upon the addition of the 10wt.% Fe to the 10CaO-alumina from 51.58 to 28.96 mmolg^{-1}, which is in line with the gas yield reduction. Nevertheless, upon further addition of 10 wt. % Fe, the H_2 yield rose slightly to 31.67 mmolg^{-1} despite the decrease in the gas yield. This implies that the Fe promotes hydrogen production by the water gas shift reaction, which is also supported by the increase in CO_2 from 7.12 to 9.16 mmolg^{-1}. Then, when there is 10 wt.% of Fe and 20 wt.% of CaO (1:2 Fe:CaO ratio), the hydrogen yield increases to 45.59 mmolg^{-1}. Likewise, the CO_2 yield remains almost the same for both experiments. It can be said then, that the CaO content has a higher impact than Fe content in water gas shift reaction performance and that it also demonstrates an absorption effect with CO_2 reduction. It is also suggested that, somehow, the Fe inhibits CaO capability of absorbing the carbon dioxide, for when the 40Fe40CaO, even though it produced the highest amount of H_2 among the catalysts, it also generated the highest CO_2 content, i.e. higher water gas shift reaction performance but lower CO_2 absorption capability. When looking at the CO yield, the trends stay in line with H_2 yield, and it thus implies that Fe addition to CaO-alumina catalysts does not have a considerable influence in the steam reforming reaction. Instead, this is mainly driven by the conditions in the catalytic steam reforming stage (such as temperature, steam flow rate, catalyst) that the catalytic steam reforming reaction presents a good and similar throughput in all the experiments, so Fe addition to CaO-alumina catalysts does not have a considerable influence in the steam reforming.

Both the CO_2 sorbent and catalyst behaviour showed that when CaO content is increased in the catalyst, Li et al (2014) observed similar result in the investigation involving the optimization mechanism of CaO on water gas shift reaction targeting hydrogen generation, upon adding CaO a higher H_2 concentration achieving a 75.5% CO conversion rate, and enhancement ratio of CaO of about 81%, the product gases representing the following volume per cent; 71% H_2, 22% CO and 7% CO_2 were obtained. CaO is an excellent absorbent as the rate of CO_2 absorption ranged from 87.41%–91.44%; this is also supported with a similar study by Udomisirichakorn et al., 2013.

Table 6-4: Effect of Fe addition to CaO catalysts in Mass Balance and Yields

CaO Catalyst/Sorbent in 3rd Stage	**Reduced 10CaO-alumina**	**Reduced 10Fe10CaO-alumina**	**Reduced 20Fe10CaO-alumina**	**Reduced 10Fe20CaO-alumina**	**Reduced 40Fe40CaO-alumina**
Catalyst Ratio (Fe:CaO:Al)	(0:1:9)	(1:1:8)	(2:1:7)	(1:2:7)	(2:2:1)
Total Gas Yield (wt.%)	82.73%	66.87%	66.08%	71.63%	97.32%
Hydrogen Yield (mgg^{-1} Biomass)	103.96	58.38	63.83	91.90	104.35
Mass Balance (wt.%)	101.80%	94.39%	95.38%	100.42%	106.32%
Char Residue Yield (wt.%)	22.50%	22.00%	22.00%	22.50%	22.50%
Gas Yield (mmolg^{-1} biomass)					
H_2	51.58	28.96	31.67	45.59	51.77
CO	21.02	13.48	14.90	21.79	24.57
CO_2	13.47	7.12	9.16	9.14	16.05

Figure 6-8 shows the product gases compositions obtained from different experiments upon the addition of iron (Fe) to the catalysts. It is observed that over 55 vol.% of hydrogen concentration was obtained from all the experiments. This implies that all catalysts investigated fairly promoted the thermochemical conversion of the volatiles and carbon monoxide into H_2. It is noteworthy that some catalysts have effective conversion tendencies with respect to better gas yield. However, the one which resulted in the highest H_2 content was the 10Fe20CaO-alumina catalyst in the water gas shift stage, with 59.30 vol.%. (Ignoring the 10CaO-alumina catalyst used as reference), even though this catalyst did not obtain the highest hydrogen yield. This suggests that, although, hydrogen conversion by catalytic steam reforming of volatiles and water gas shift reaction between CO and steam is highly promoted by 1:2 ratio of Fe:CaO, less steam used in the process is reacted, leading to a moderate gas yield. Natesakhawat et al. (2006) studied the influence of iron-based catalysts (Fe-Al) on water gas shift reaction; they observed that at higher aluminium (Al) contents, the water gas shift activity performance appreciated while at a higher iron amount, the CO conversion rate declined. Therefore, one can infer that only a small amount of Fe is required in the water gas shift catalyst for optimum hydrogen yield.

With respect to CO and CO_2 content, the same catalyst (10Fe20CaO-alumina) generates both the highest and lowest respectively, which suggests that the process using the combination of this and the 10Ni-alumina catalysts is driven mainly by catalytic steam reforming rather than the water gas shift reaction or that the CaO is absorbing some of the CO_2 contained in the catalyst and converted into $CaCO_3$. Further analysis of the reacted catalyst using XRD was carried out to confirm the presence of $CaCO_3$ in the residue.

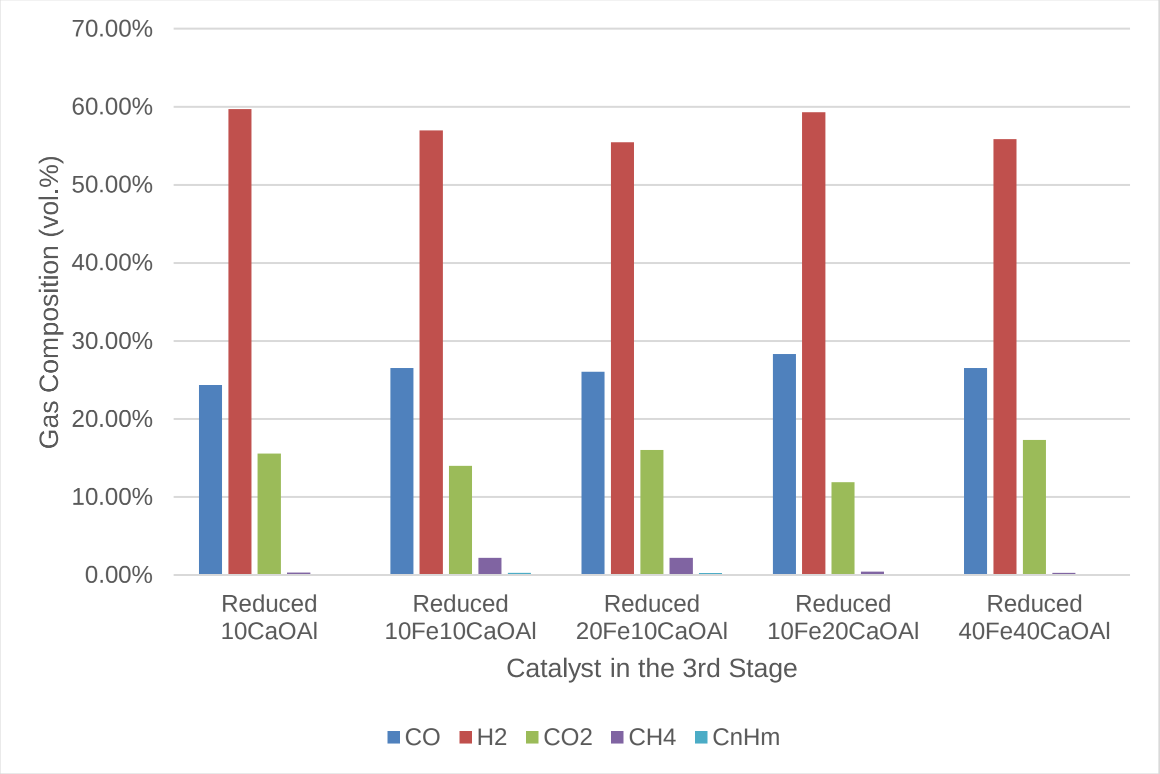

Figure 6-8: Effect of Fe addition to CaO catalysts in gas composition (N_2 free)

More so, an increasing trend in CO and CO_2 is obtained when the catalysts 10Fe10CaO-alumina and 20Fe10CaO-alumina were used. This suggests that upon the addition of Fe to the CaO-alumina-based catalysts, catalytic steam reforming and water gas shift are significantly promoted but inhibited the catalysts ability to absorb the CO_2. In addition to this, there is a relative decrease in the H_2 content while some methane (CH_4) is being produced, which could mean that the Fe addition causes the CO and the hydrogen to revert to water and methane, which can also explain the decrease in gas yield for both catalysts.

Importantly, it is also observed that 40Fe40CaO-alumina catalyst which generated the highest hydrogen yield has the second-lowest hydrogen content too, with 55.86 vol.%. This is probably due to its high gas yield, meaning that more of the steam injected is being reacted, added to a high conversion driven by both catalytic steam reforming and water gas shift reactions. This is supported as well by the CO and CO_2 content, which is relatively high for both, and the CH_4 content which is negligible. The high amount of carbon dioxide (16.05mmolg^{-1} biomass) in the gas implies that the Fe content in the catalyst inhibited its absorption capability. Currently, there is no available investigation that utilised FeCaO catalysts for water gas shift reaction. Hence, there is insufficient computational or empirical evidence to confirm this claim.

However, these suggestions can be supported when analysing the H_2/CO, H_2/CO_2, CO/CO_2 and H_2/C molar ratios, shown in Figure 6-9. There is hardly a change between the H_2/CO ratios which is around 2.10, 0.86 times the ratio using 10CaO-alumina catalyst with no Fe addition, so it is believed that the Fe content would cause further catalytic steam reforming reaction promotion to the 2nd stage and a slight enhancement of the water gas shift reaction.

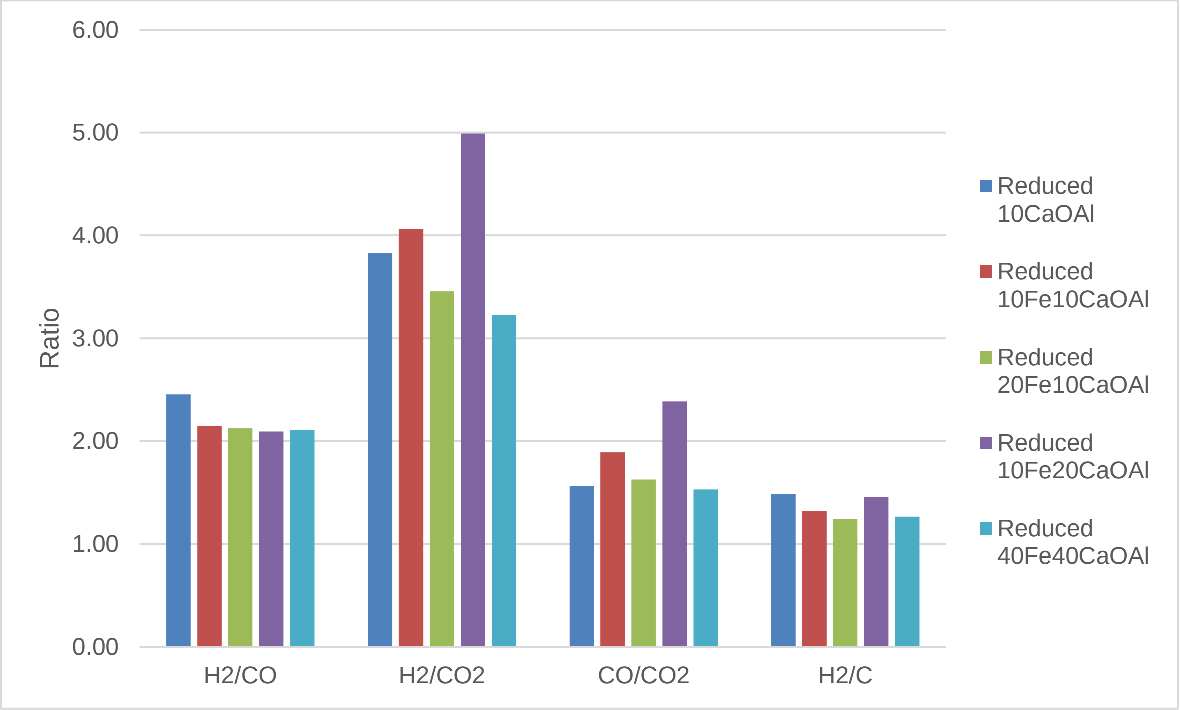

Figure 6-9 Effect of Fe addition to CaO catalysts in the H_2/CO, H_2/CO_2, $CO/CO_2$and H_2/C molar ratios

With respect to the H_2/CO_2 molar ratio, a different trend was observed. The addition of Fe with 10 wt.% metal loading, the molar ratio slightly rose from 3.83 to 4.06, and then it declined upon a rise in Fe content to 20 wt.%. One can infer that, that the higher the Fe content, the lesser capable the catalyst is to absorb the CO_2 and hence the gas will contain more of it in its composition.

Keeping the Fe content constant at 10 wt.% but increasing the CaO content to 20 wt.% resulted in a sharp increase in the H_2/CO_2 molar ratio to about 5.0. This is attributed to the high H_2 and low CO_2 production. This suggests that CO_2 absorption is taking place within the catalyst, which is supported by the CO/CO_2 molar ratio too. The 40Fe40CaO-alumina catalyst that produced the gas with the highest yield had low H_2/CO_2 and CO/CO_2 molar ratios of 3.22 and 1.53 respectively so it can be implied that water gas shift reaction was promoted while the CO_2 absorption barely occurred due to the content of Fe. The catalyst which showed the highest H_2/C molar ratio was the 10Fe20CaO-alumina as it produced a high amount of hydrogen while absorbing some of the CO_2 and producing a fair amount of CO.

6.5 Catalyst Characterization

The reacted alkali earth oxide (CaO) -based catalysts were characterised using different analytical methods to study and compare the influences of the reactions on the catalysts. In essence, all the reacted catalysts were characterised using temperature-programmed oxidation (TPO), and X-ray diffraction (XRD). The TPO profiles showed the weight losses of the evaluated reacted catalysts as a function of temperature or time, and these data were also taken for comparison. Following this analysis, the change in the amount of deposited coke, as well as the type of carbon over the spent catalysts, are determined.

6.5.1 Temperature Programmed Oxidation

The results for the temperature programme oxidation of alkali earth metal mixed oxide (CaO) catalysts at different steam injection conditions from 100-900^{0}C are shown in figure 6-9 to 6-10. As can be seen in figure 6-9, at 100^{0}C weight loss in the range of 0.77% to 2.15% was observed for all the reacted catalysts, this was principally due to moisture loss. A significant weight loss due to the oxidation of carbon occurred at about 300^{0}C in the range of 3% to 10%; this was attributed to amorphous carbons oxidation that was deposited on the reacted catalysts (Han et al. 2011). More so, at about 550^{0}C another substantial carbon oxidation in the range of 4.14% to 12.41% weight loss, the losses were suggested to be filamentous carbon deposited on the reacted catalysts. The losses from 700^{0}C representing 13.2% and 10.4% for Red10Fe20Cao Double Steam and reduced 40Fe40CaO-alumina double Steam catalysts indicated a characteristic of carbon deposits with different degrees of graphitisation (Zhang et al. 2016; Kukovitskii et al. 1997). The differences in the amount of weight losses of the alkali earth metal oxide catalysts indicated that there was a superior performance in the oxidative conversion of methane to CO and H_2 at a very low temperature among the reacted catalysts.

Of the catalysts tested, reduced10Fe10CaO catalyst with double steam injection showed the most significant resistance to weight loss, with about 95.54% of the original mass being retained at 800^{0}C indicating a favourable CO_2 adsorption, followed by reduced 20CaO double steam and 20CaO double steam catalysts with total losses of approximately 5 and 5.23%respectively at 800^{0}C. Similarly, pure calcium oxide catalyst (20CaO) has a low weight loss.

One important finding is that the presence of reduced higher alkaline earth oxide with higher Iron metal loading and double steam injection (reduced 40Fe40CaO-alumina double Steam) resulted in a substantial increase in weight loss or an apparent tendency for catalyst deactivation as seen in the oxidation reaction representing 13.2% weight loss. The most significant loss was observed in Reduced 10Fe20CaO double steam injection representing 13.2% which is equally an indication of susceptibility to coking. This indicated that a non-equilibrium Fe and CaO loadings affected the catalyst stability and resistance to carbon deposition.

The effect of steam injection is also evident, while reduced 10CaO double steam has a weight loss of about 7%, reduced 10CaO without steam loses higher by 7.12%. This result therefore agrees with literature which shows that an increase in the amount of steam or flowrate improves the activation, catalytic activity, resistance to coke formation, thermal cracking of the catalyst and hydrogen production in water gas shift and steam reforming reactions (Yoon et al. 2010; Wei et al. 2007, Srinakruang, et al., 2006). Despite this low resistance to weight loss by 10CaO due to steam effect, the performance was better than three other tested catalysts; reduced 20Fe10Cao double steam, reduced 40Fe40CaO-alumina double steam, and reduced 10Fe20CaO double steam. It is interesting to note that catalysts with a higher composition of the combination of Fe, CaO and Al; reduced 40Fe40CaO-alumina suffer significant weight loss of about 10.39% at 800^{0}C, one possible reason for this was the higher metal loadings. Likewise, high losses were seen in reduced 20Fe10CaO double steam and reduced 10Fe20CaO representing 9 and 13.2% respectively.

Comparing the composition and metal loading of catalysts, with reducing metal loading and catalyst composition and raising the amount of steam, the least reduced catalyst has the best performance, possibly as a result of elevated contact area (Choudhary et al. 1992). Beyond 20% metal loading, the catalyst became susceptible to higher weight loss.

However, reduced 10Fe20CaO took exception to this. Specifically, at the high-temperature condition of 800°C, the highest loss was found. As stated, the unequal metal compositions could facilitate this outcome. Li et al. (2008) reported a high amount of coke over the spent 0.2Ni-ZrO_2 catalysts around 400-600^{0}C indicating a whisker-like filamentous carbon (Quincoces et al. 2001), under the same temperature the TPO of CaO based catalysts (0.2Ni-0.2CaO-ZrO_2 and 0.2Ni-0.5CaO-ZrO_2) indicated a reduction in coke formation. Contrary to this, Quincoces et al. (2001) observed that upon the addition of 3% CaO to alumina (Al_2O_3), the catalyst did not significantly impede the whisker carbon formation at 600^0C, it stimulated the production of species that are hydrogenated at low temperature. One key finding from the TPO analysis is that the addition of CaO in small quantity slightly improve the coke deposit reduction and catalyst stability. Quincoces et al. (2001) further asserted that CaO support promoted the basicity of the catalysts which inadvertently increased CO2 adsorption, and also reduced the quantity of carbon deposit by promoting the inverse Boudouard reaction as shown in equation R.6-5. However, all the investigated spent catalyst depicts a broad peak which is an evidence of weakly bonded carbon deposit over the surface of the spent catalyst. Hence, further investigation is therefore required to unravel the cause of unequal metal compositions and to the role the optimum loading of CaO and Fe in eliminating carbon deposit.

$$Boudouard\ reaction: \qquad CO_2 + C \leftrightarrow 2CO. \quad R.6-5$$

The empirical results obtained in the study suggested that the reduced 10Fe20CaO double steam and reduced 40Fe40CaO-alumina double steam catalysts were the most affected by coking as their losses of mass means that a higher amount of carbon has been oxidised off the catalyst surface and as such were unfavourable to CO_2 adsorption. They could also be prone to pore plugging or attrition/crushing as a result of the growth of filamentous carbon.

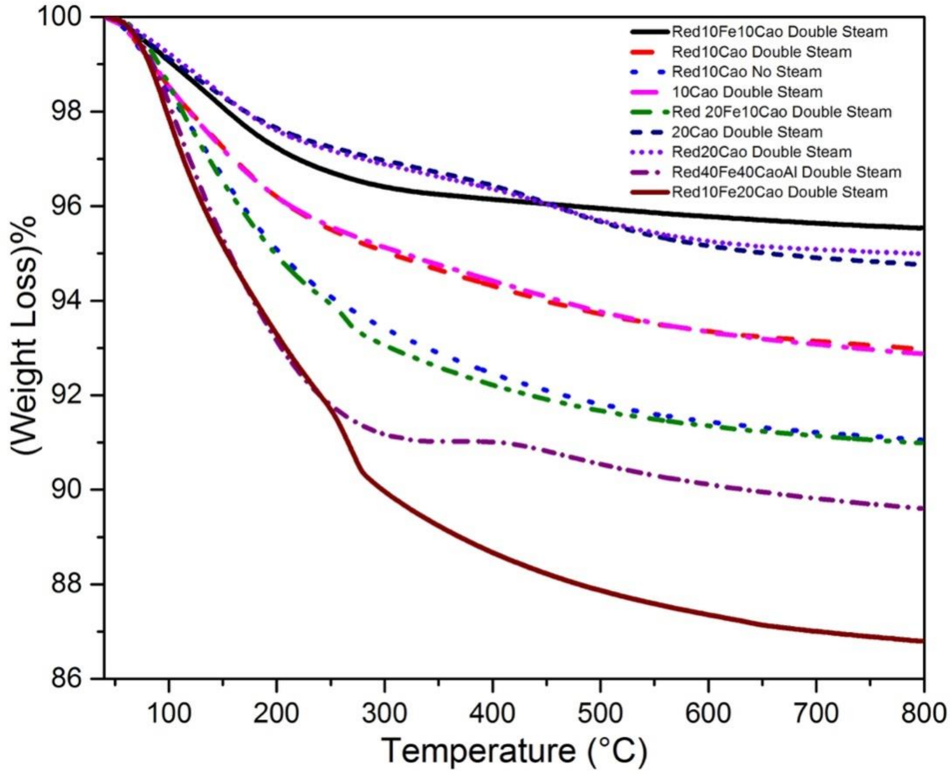

Figure 6-10: TPO result of reacted catalysts with different CaO contents

Additionally, as shown in figure 6-10, the thermal degradation TPO profiles illustrating the derivative of the weight variation based on temperature difference for reacted catalysts indicated that the carbonaceous species began to be oxidized at 250^0C and peaked at about 400^0C which is consistent with the filamentous carbon formation obtained by Goula et al. (1996), but their amounts were significantly affected by the support composition of CaO/Al_2O_3 ratio. In a similar study, Bartholomew et al. (1982) reported that the amorphous carbon formation could lead to catalyst deactivation when converted to graphitic carbon which has enormous potential to block the active site of metal.

The results indicated that the composition of reduced 10Fe10CaO has a positive effect on the carbon deposition. In essence, this catalyst above all others favoured the CO_2 adsorption which enhances the inverse of the Boudouard reaction (rx 6-1), reducing the quantity of carbon deposited (Quincoces et al. 2000).

$$CO_2 + C \leftrightarrow 2\,CO \quad \dots (6-3)$$

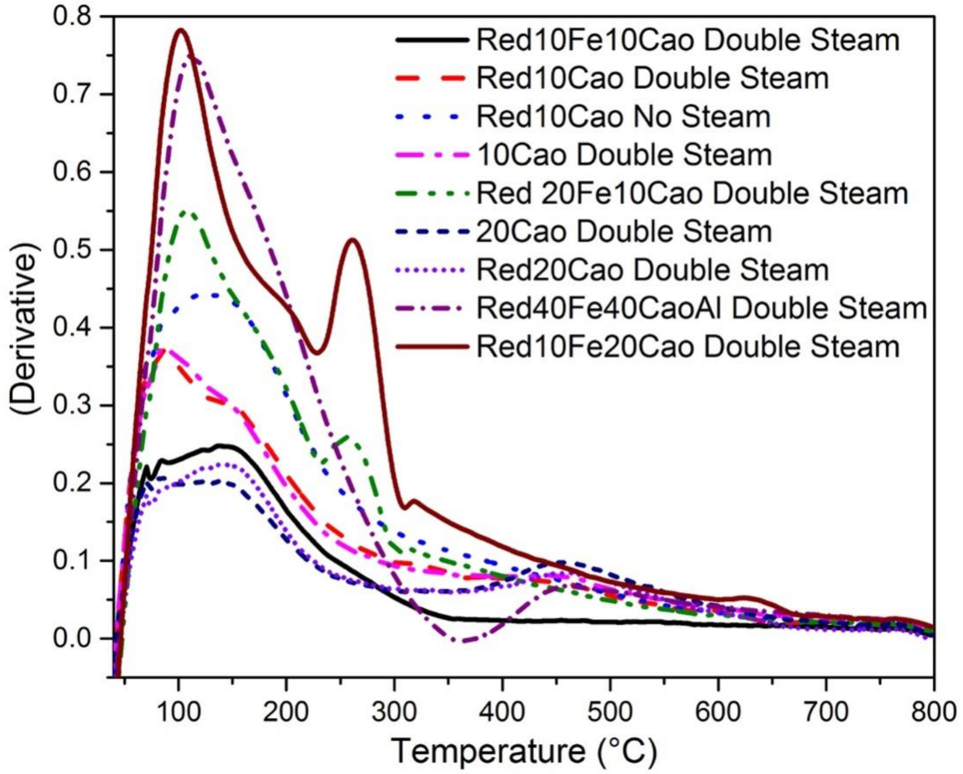

Figure 6-11: Derivative of weight variation as a function of temperature in TPO analysis

6.5.2 X-ray diffraction (XRD)

The X-ray diffraction (XRD) analysis was used to evaluate the crystallographic morphology of the reacted catalysts with the aid of a Bruker D8, using Cu α1radiation X-ray tube as revealed in figure 6-11, scanning from 20^0 to 80^0 (2q). The result of the XRD analysis of the reacted catalysts calcinated at 800^0C and 900^0C for 3 h was shown in table 6-5 and figure 6-11. It is evident from Table 6.6 and Figure 6-11 that Fe_2O_3, $CaFeO_2$, $Ca_2Fe_7O_{11}$ and Al_2O_3CaO phases were present in the reacted catalysts. This is indicated by the presence of diffraction peaks at 2ϑ values of 20.33^o, 29.5^o, 36.3^o, 49.69^o, 53.88^o, 64.26^o, 66.85^o, 72.47^o 74.88^o, and 75.9^o. The diffraction patterns obtained were in accordance with the standards of Joint Committee on Powder Diffraction Standard (JCDPS) for metal oxide catalysts. The formation of Al_2O_3CaO was due to the reaction between alumina and CaO with steam. As revealed in figure 6-11, the reacted metal oxide catalysts have narrow peaks which depicted good crystalline structure while the alumina with broad peaks depicted that the composition of this reacted catalyst was thoroughly dispersed indicating an amorphous carbon structure or poorly crystalline morphology (Ayas et al. 2016).

More so, as revealed in figure 6-11, the species and phase composition of calcium ferrites were influenced by the addition of iron to the $CaO-Al_2O_3$. When no alumina was added, no calcium ferrite species was present. This implies that even at high temperature, the $20CaO-Al_2O_3$ and $10CaO-Al_2O_3$ catalysts were not sintered nor oxidised, indicating high performance. Although the two catalysts have an equal amount of alumina, the $10CaO-Al_2O_3$ has a higher amount of CaO.

Upon the addition of Fe, the XRD pattern showed that no CaO was present, this depicts that the alkaline earth content has been oxidised into the two species of calcium ferrite observed ($CaFeO_2$, $CaFe_7O_{11}$) while the Fe is oxide to ferric oxide, otherwise known as hematite (Fe_2O_3). The alumina was present in all the XRD spectra of the investigated catalysts. When a low and equal amount of Fe and CaO-Al was used ($10Fe-10CaO-Al_2O_3$), hematite completely disappeared. Another finding from these spectra is that with the increase of Fe addition from 10 to 20, the amount of calcium ferrite species also increased but decreased upon further increase to 40. In essence, the fewer amount of phase composition of calcium ferrites ($CaFeO_2$ and $Ca_2Fe_7O_{11}$) were observed which showed that with higher Fe content, the catalyst was slightly resistant to oxidation. No observation influence of the increase in CaO was observed when Fe was added.

In general, the two compositions of calcium ferrites existed ($CaFeO_2$, $CaFe_7O_{11}$) simultaneously in the spent catalysts that incorporated Fe. Ferric oxide also produced in all the investigated Fe rich spent catalysts except in the $10Fe-10CaO-Al_2O_3$, which perhaps was a result of low content and an equal amount of Fe and Cao (10:10). Guo and Guo (2019) investigated the XRD pattern of Fe_2O_3-$CaO-Al_2O_3$ at various 990^oC and 1200^0C temperatures; in this research three compositions of calcium ferrites were present; $CaFe_2O_4$, $Ca_2Fe_{15.57}O_{25.56}$, and $Ca_{3.18}Fe_{15.48}Al_{1.34}O_{28}$. One key finding is that the amount of calcium ferrite species rose with the increase in alumina. Despite the fact that instead of pure iron that was used in this research, they used oxide of iron, one core consistency is the observation of calcium ferrite species which is an evidence of oxidation of the catalysts.

Similarly, the XRD analysis of $CaO–Al_2O_3$ calcined at 600^oC and 750^oC for 30-10min has been reported by Zhang et al. (2013) for CO_2 capture. The XRD pattern of catalyst derived from the $CaO–Al_2O_3$ calcined 750^oC for 10min showed the presence of active CaO and inert support material $Ca_{12}Al_{14}O_{33}$ which is quite similar to the XRD result of this study where inert substance $Ca_2Fe_7O_{11}$ was found in all the catalysts. The formation of the inert material is as a result of the high reaction activity of CaO with Al_2O_3 in the artificial sorbent above 700^0C (Zhang et al. 2013). Moreover, the presence of $CaFeO_2$ shows that the $FeCaO-Al_2O_3$ was reduced in the presence of Fe which was later oxidised to Fe_2O_3. Other studies also that investigated the XRD pattern of CaO based catalysts obtained similar findings (Anthony and Manovic,2009; Pacciani et al., 2008; Martavaltzi and Lemionidou, 2008; Li et al. 2006).

Table 6-5: Identified XRD Patterns List:

Visible	**Ref. Code**	**Score**	**Compound Name**	**Displacement [°2Th.]**	**Scale Factor**	**Chemical Formula**
*	00-033-0664	65	Iron Oxide	0.059	0.905	Fe_2O_3
*	00-021-0917	15	Calcium Iron Oxide	-0.646	0.218	$CaFeO_2$
*	00-036-0948	28	Calcium Iron Oxide	-0.143	0.205	$Ca_2Fe_7O_{11}$
*	01-084-9871	8	Aluminium Oxide	1.256	0.148	Al_2O_3

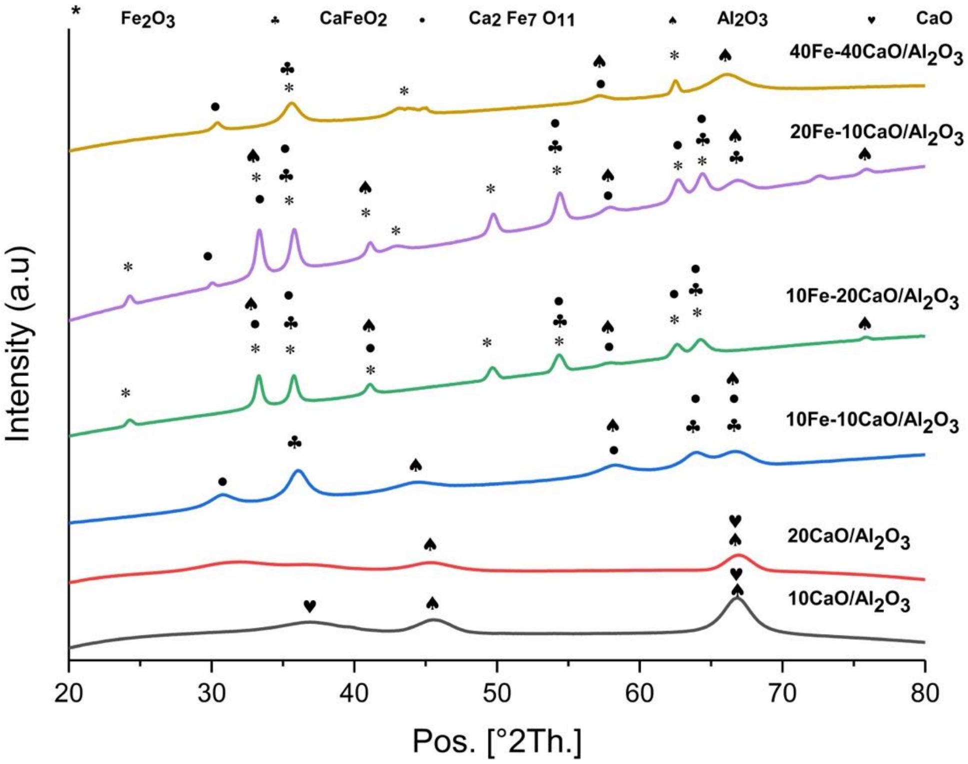

Figure 6-12: XRD pattern obtained from the reacted CaO based catalysts

6.6 Summary of the chapter

In this chapter a 3-stage fixed bed reactor involving pyrolysis, catalytic steam reforming (catalytic steam reforming) and water gas shift reaction (water gas shift) for biomass conversion. The catalytic steam reforming and water gas shift reactions, in particular, were examined with respect to the influence of 10Ni-alumina catalyst utilization in the catalytic steam reforming stage, the addition of reduced and not reduced CaO-alumina sorbent/catalysts with different CaO contents to the water gas shift reaction stage, steam injection and removal from the process and the FeCaO-alumina sorbent/catalysts in different Fe:Ca: Al mass ratios. From the results obtained, the following key findings were drawn:

1. The addition of 10Ni-alumina catalyst in the catalytic steam reforming reactor, compared with adding no catalyst, resulted in a considerable increase in gas and hydrogen yields representing 54.05 wt.% and 7.91 mmolg^{-1} to 70.56 wt.% and 26.47 mmolg^{-1}for uncatalyzed and catalysed systems respectively. The 10Ni-alumina catalyst in the catalytic steam reforming stage

promoted the reaction between the steam added to the process and the volatiles released by the biomass sample.

2. Without the injection of steam into the catalytic steam reforming and water gas shift reactors with a 10CaO-alumina catalyst in latter reactor produced low hydrogen content as there were no H atoms fed to the process. However, the catalyst showed evidence of catalysing the water gas shift reaction to a nonnegligible extent, utilising the gases released from the biomass sample only.

3. Upon the addition of 10Ni-alumina catalyst, the water gas shift reaction was also promoted, however in a lower extent. This was possible by reacting the steam with the same CO produced by the reforming of volatiles.

4. The 10Ni-alumina catalyst also promoted the reforming of methane (CH_4). Thereby improving the selectivity towards higher hydrogen production. Conversion back to $CH_4$was inhibited.

5. The water-gas shift reaction catalytic performance was found to be improved with the increase of CaO in the catalyst. This is evident in the change in CO/CO_2 molar ratios, which declined when the CaO content was increased from 10 wt.% to 20 wt.% from 1.73 to 1.36 for the not reduced catalysts and from 1.56 to 1.44 in the reduced ones.

6. Carbon dioxide (CO_2) absorption was not evident when only CaO is added and increased in the sorbent/catalyst, for the H/CO_2 and the CO/CO_2 molar ratios should increase (that is, more hydrogen production by catalytic steam reforming and water gas shift reactions over less CO_2 yield due to absorption by CaO) instead of the decrease.

7. The addition of iron metal (Fe) to CaO-alumina sorbent/catalysts promoted the water gas shift reaction by generating higher co_2 content. However, at the same time, it impedes the capability of the CaO to absorb the CO_2.

8. The addition of CaO to Fe catalysts at CaO:Fe ratios beyond 1 resulted in increased absorption of CO_2togetherwith a higher promotion of the WATER-GAS SHIFT reaction. This is supported by the H_2/CO_2 and CO/CO_2 molar ratios that are 4.06 and 1.89 respectively for the 10Fe10CaO-alumina sorbent/catalyst and increase to 4.99 and 2.38 respectively.

9. An optimal condition of 10 wt.% CaO-alumina catalysts was the best suitable for maximising hydrogen production because it produced the highest hydrogen yield of 51.58 $mmolg^{-1}$

biomass. It was found that the addition of Fe to FeCaO-alumina inhibited CO_2 absorption by the CaO, but at the same time, WATER-GAS SHIFT reaction was promoted.

10. In the use of iron and alkali earth oxide bimetallic catalysts, the optimal content of Fe and CaO in FeCaO-alumina catalysts for enhancing CO_2 absorption was found to be 10 wt.% Fe and 20 wt.% CaO. This catalyst produced the lowest CO_2 and the second-highest H_2 yields representing 9.14 and 45.59 mmolg^{-1} biomass, respectively**.** This was also supported by the TPO results since it has the lowest weight loss at 800^{0}C.

6.7 Reference

Abdollahifar, M., Haghighi, M., Babaluo, A.A.: Syngas production via dry reforming of methane over Ni/Al_2O_3–MgO nanocatalyst synthesized using ultrasound energy. J. Ind. Eng. Chem. 20, 1845–1851 (2014)

Bartholomew, C.H., Carbon Deposition in Steam Reforming and Methanation. Catalysis reviews, 1982. 24(1): p. 67-112.

Charisiou, N. D., Baklavaridis, A., Papadakis, V. G., & Goula, M. A. (2016). Synthesis gas production via the biogas reforming reaction over Ni/MgO–Al 2 O 3 and Ni/CaO–Al 2 O 3 catalysts. Waste and biomass valorization, 7(4), 725-736.

Chen, D., Zhou, J. & Zhang, Q., 2014. Effects of heating rate on slow pyrolysis behaviour, kinetic parameters and products properties of moso bamboo. Bioresource Technology, Volume 169, pp. 313-319.

Chen, W. H., Chiu, T. W., & Hung, C. I. (2010). Hydrogen production from methane under the interaction of catalytic partial oxidation, water gas shift reaction and heat recovery. international journal of hydrogen energy, 35(23), 12808-12820.

Cutrufello, M. Ferino, G. I Solinas, V. Primavera , A. Trovarelli , A. Auroux, A. and C. Picciau, Phys. Chem. Chem. Phys., 1999, 1 , 3369 -3375

Czernik, S., & French, R. (2014). Distributed production of hydrogen by auto-thermal reforming of fast pyrolysis bio-oil. International Journal of Hydrogen Energy, 39(2), 744-750.

Czernik, S., Elam, C. C., Evans, R. J., & Milne, T. A. (2006). Thermochemical Routes to Hydrogen from Biomass-A Review (No. NREL/CP-510-44207). National Renewable Energy Lab. (NREL), Golden, CO (United States).

Demirbas, A., 2007. Effect of Temperature on Pyrolysis Products from Biomass. Energy Sources, Part A, 29(4), pp. 329-336.

Dong, L. et al., 2016. Development of Fe-Promoted Ni−Al Catalysts for Hydrogen Production from Gasification of Wood Sawdust. Energy Fuels, Volume 31, pp. 2118-2127.

G.C. de Araújo, M. do Carmo Rangel. 2000. An environmental friendly dopant for the high-temperature shift catalysts. Catal Today, 62 (2–3), pp. 201-207

Guo, H and Guo, X., 2019. Effect of Alumina on Liquid Phase Formation in Sintering Process of Iron Ore Fines. Steel research international, 90(8)

Goula, M.A. Lemonidou, A.A. Efstathiou, A.M. Journal of Catalysis, 161 1996. 626.

Greenhalf, C.E., Nowakowski, D.J., Harms, A.B., Titiloye, J.O. and Bridgwater, A.V., Sequential pyrolysis of willow SRC at low and high heating rates – Implications for selective pyrolysis. Fuel, 2012. 93(0): p. 692-702.

Han, L. Wang, Q. Yang, Y. Yu, C. Fang, M. Luo, Z. (2011).Hydrogen production via CaO sorption enhanced anaerobic gasification of sawdust in a bubbling fluidized bed. Int J Hydrogen Energy, 36 (2011), pp. 4820-4829

Horn R., Williams, K.A. Degenstein, N.J. Bitsch-Larsen, A. Nogare, D.D. Tupy, S.A. et al. Methane catalytic partial oxidation on autothermal Rh and Pt foam catalysts: oxidation and reforming zones, transport effects, and approach to thermodynamic equilibrium. Journal of Catalysis, 249 (2007), pp. 380-393

Jacobs, G., & Davis, B. H. (2005). Reverse water-gas shift reaction: steady state isotope switching study of the reverse water-gas shift reaction using in situ DRIFTS and a Pt/ceria catalyst. Applied Catalysis A: General, 284(1-2), 31-38.

Joshi, A. Rammohan, A. Jiang, Y. and Ogunwumi, S. 2009. Journal Molecular Structure Theochem, 912, 73 -81

Ju, F., Wang, M., Wu, T. and Ling, H., 2019. The Role of NiO in Reactive Adsorption Desulfurization Over NiO/ZnO-Al2O3-SiO2 Adsorbent. Catalysts, 9(1), p.79.

Júnior, I.L. J.-M.M. Millet, M. Aouine, M. do Carmo Rangel. 2005. The role of vanadium on the properties of iron based catalysts for the water gas shift reaction. Applied Catalysis A Gen, 283 (1–2) (2005), pp. 91-98

Kukovitskii, E.F., et al., Carbon nanotubes of polyethylene. Chemical Physics Letters, 1997. 266(3–4): p. 323-328.

L. Han, Q. Wang, Y. Yang, C. Yu, M. Fang and Z. Luo, International Journal of Hydrogen Energy, 2011, 36, 4820- 4829.

Li, B., Wei, L., Wang, X. & Chen, H., 2014. The enhancing mechanism of calcium oxide on water gas shift reaction for hydrogen production. Energy, Volume 68, pp. 248-254.

Li, Z.S. Cai, N.S. Huang, Y.Y. 2006. Effect of preparation temperature on cyclic CO2 capture and multiple carbonation–calcination cycles for a new Ca-based CO2 sorbent. Ind Eng Chem Res, 45, pp. 1911-1917

Liu, S., Guan, L., Li, J., Zhao, N., Wei, W., & Sun, Y. (2008). CO2 reforming of CH4 over stabilized mesoporous Ni–CaO–ZrO2 composites. Fuel, 87(12), 2477-2481.

Manovic, V. Anthony, E.J. 2009. Long-term behaviour of CaO-based pellets supported by calcium aluminate cements in a long series of CO2 capture cycles Ind Eng Chem Res, 48, pp. 8906-8912

Manovic, V. Lu, D. E. Anthony, J. 2008. Steam hydration of sorbents from a dual fluidized bed CO2 looping cycle reactor. Fuel, 87, pp. 3344-3352

Martavaltzi, C.S. Lemionidou, A.A. 2008. Parametric study of the CaO–Ca12Al14O33 synthesis with respect to high CO2 sorption capacity and stability on multicycle operation. Ind Eng Chem Res, 47, pp. 9537-9543

Nahil, M. A. et al., 2013. Novel bi-functional Ni-Mg-Al-CaO catalyst for catalytic gasification of biomass for hydrogen production with in situ CO2 adsorption. RSC Advances, Volume 3, pp. 5583-5590.

Natesakhawat, S., Wang, X., Zhang, L., & Ozkan, U. S. (2006). Development of chromium-free iron-based catalysts for high-temperature water-gas shift reaction. Journal of Molecular Catalysis A: Chemical, 260(1-2), 82-94.

Oyama, S. T., Hacarlioglu, P., Gu, Y. & Lee, D., 2012. Dry reforming of methane has no future for hydrogen production: Comparison with steam reforming at high pressure in standard and membrane reactors. International Journal of Hydrogen Energy, Volume 37, pp. 10444-10450.

Oyama, S. T., Hacarlioglu, P., Gu, Y., & Lee, D. (2012). Dry reforming of methane has no future for hydrogen production: Comparison with steam reforming at high pressure in standard and membrane reactors. International journal of hydrogen energy, 37(13), 10444-10450.

Pacciani, R. Müller, C.R. Davidson, J.F. Dennis, J.S. Hayhurst, A.N. 2008. Synthetic Ca-based solid sorbents suitable for capturing CO2 in a fluidized bed Can J Chem Eng, 86, pp. 356-366

Pal, D., Chand, R., Upadhyay, S. & Mishra, P., 2018. Performance of water gas shift reaction catalysts: A review. Renewable and Sustainable Energy Reviews, Volume 93, pp. 549-565.

Panagiotopoulou, P., & Kondarides, D. I. (2011). Effects of promotion of TiO2 with alkaline earth metals on the chemisorptive properties and water–gas shift activity of supported platinum catalysts. Applied Catalysis B: Environmental, 101(3-4), 738-746.

Peng, W. et al., 2017. Hydrogen and syngas production by catalytic biomass gasification. Energy Conversion and Management, Volume 135, pp. 270-273.

Quincoces, C. E., S. Dicundo, A. M. Alvarez and M. G. Gonzalez. "Effect of addition of CaO on Ni/Al_2O_3 catalysts over CO2 reforming of methane." Materials letters 50, no. 1 (2001): 21-27.

Quincoces, C.E. Dicundo, S. Alvarez, A.M. Gonzalez. M.G. 2000. Effect of addition of CaO on NirAl_2O_3 catalysts over CO2 reforming of methane. Materials Letters 50, pp. 21–27

Ronsse, F., van Hecke, S., Dickinson, D. & Prins, W., 2014. Production and characterisation of slow pyrolysis biochar: influence of feedstock type and pyrolysis conditions. Bioenergy, Volume 5, pp. 104-115.

Solar, J. et al., 2016. Influence of temperature and residence time in the pyrolysis of woody biomass waste in a continuous screw reactor. Biomass and Bioenergy, Volume 95, pp. 416-423.

Srinakruang J, Sato K, Vitidsant T, Fujimoto K. Highly efficient sulfur and coking resistance catalysts for tar gasification with steam. Fuel 2006; 85:2419–26.

Udomisirichakorn, J., Basu, P., Salam, P. A. & Acharya, B., 2013. Effect of CaO on tar reforming to hydrogen-enriched gas with in-process CO2 capture in a bubbling fluidised bed biomass steam gasifier. International Journal of Hydrogen Energy, Volume 38, pp. 14495-14504.

Udomsirichakorn, J., Basu, P., Salam, P. A., & Acharya, B. (2013). Effect of CaO on tar reforming to hydrogen-enriched gas with in-process CO2 capture in a bubbling fluidised bed biomass steam gasifier. International journal of hydrogen energy, 38(34), 14495-14504.

Van der Laan, G. P., & Beenackers, A. A. (2000). Intrinsic kinetics of the gas-solid Fischer–Tropsch and water gas shift reactions over a precipitated iron catalyst. Applied Catalysis A: General, 193(1-2), 39-53.

Wang, W., Li, X., Zhang, Y., Zhang, R., Ge, H., Bi, J. and Tang, M., 2017. Strong metal–support interactions between Ni and ZnO particles and their effect on the methanation performance of Ni/ZnO. Catalysis Science & Technology, 7(19), pp.4413-4421.

Wei L, Xu S, Zhang L, Liu C, Zhu H, Liu S. Steam gasification of biomass for hydrogen-rich gas in a free-fall reactor. Int J Hydrogen Energy 2007; 32:24–31.

Wu, C. et al., 2011. Hydrogen production from biomass gasification with Ni/MCM-41 catalysts: Influence of Ni content. Applied Catalysis B: Environmental, Volume 108-109, pp. 6-13.

Xiong, W. M., Fu, Y., Zeng, F. X., & Guo, Q. X. (2011). An in situ reduction approach for bio-oil hydro processing. Fuel processing technology, 92(8), 1599-1605.

Yoon, SJ, Choi, Y, Lee, J. 2010. Hydrogen production from biomass tar by catalytic steam reforming. Energy Conversion and Management 51, pp 42–47

Yurdakul, M, Ayas, N. Bizkarra, K. El Doukkali, M. Cambra. J.F. 2016. Preparation of Ni-based catalysts to produce hydrogen from glycerol by steam reforming process. international journal of hydrogen energy 41 (2016)

Zhang, M, Peng, Y. Sun, Y. Li, P.Yu, J. 2013. Preparation of CaO–Al2O3 sorbent and CO2 capture performance at high temperature. Fuel, 111, pp 636-642

Zhang, R., Brown, R. C., Suby, A., & Cummer, K. (2004). Catalytic destruction of tar in biomass-derived producer gas. Energy Conversion and Management, 45(7-8), 995-1014.

Zhang, Y., et al., Carbon nanotubes and hydrogen production from the pyrolysis catalysis or catalytic-steam reforming of waste tyres. Journal of Analytical and Applied Pyrolysis, 2016.

Zhu, M. and Wachs, I. E., 2015. Iron-Based Catalysts for the High-Temperature Water−Gas Shift (HTWGS) Reaction: A Review. ACS Catalysis, Volume 6, pp. 722-732.

Chapter 7: Conclusions and Future Work

7.1 Investigation of Catalysts Influence on Hydrogen Production from Two and Three-Stage Catalytic Steam Reforming of Biomass

7.1.1 Conclusions

The key findings of the study include:

1. The nickel loading was instrumental in the production of hydrogen and carbon monoxide. 10% of nickel loading produced the highest amount of hydrogen at 20.90mmol/g while under the same conditions, the sand produced the lowest amount of hydrogen at 2.24mmol/g. 5% nickel loading produced the highest amount of carbon monoxide at 33.93mmol/g with the lowest amount produced by the 20% nickel loading at 8.41mmol/g
2. The 20 wt.% nickel dolomite catalyst produced the highest amount of syngas from the thermal processing of the biomass at 43 $mmolg^{-1}$ syngas which was 33% higher than the 20 wt.% nickel alumina catalyst at 29 $mmolg^{-1}$ syngas
3. Due to the increased nickel content in the nickel dolomite, the catalytic activity increased in relation to hydrogen production. Due to the increased nickel content in the nickel silica, the catalytic activity decreased in relation to hydrogen production.
4. Catalyst is undoubtedly required for catalysing the steam reforming stage of the hydrogen generation from biomass. The blank test indicated negligible non-catalytic steam reforming before the catalytic experiments. The results obtained show that without catalyst in the second stage of the thermochemical conversion, the production of hydrocarbons (C_nH_m) and Methane were favoured representing 19.2vol% and16.4vol%. Hence, the potential of hydrogen production from biomass is underutilised and a long cleaning process will be required to generate pure hydrogen fuel, this drives the production cost up.
5. It is also evident that the third stage is also not inconsequential in optimising the production of syngas, a 10NiAl catalyst with zero catalysts in the WGS stage yielded the higher level of the unwanted C1-C4 hydrocarbons and Methane gas (0.7vol% and 2.3vol% respectively) compared to a 10NIAl-5FeAl (0.5vol%CH_4 and 2.0vol% CmHn respectively).
6. Although, nickel supported on dolomite catalyst appears to be the most effective catalyst for optimising the production hydrogen (56.4vol% and 27.195mmol per gram of biomass and reduction in other permanent gases (18.1vol%CO and 23vol%CO_2), it is surpassed potentially by nickel supported on Alumina because of its poor mechanical intensity and friableness. The nickel alumina, on the other hand, as supported by several experimental studies can withstand

high temperature, actively destroy tars and are relatively cheap. This makes it the most suitable for fixed-bed pyrolytic, catalytic steam reforming and water gas shift process of producing hydrogen fuel.

7. There is no significant improvement in H_2 yield under the bimetallic catalysts relative to the single metal catalysts.
8. The best catalytic activity occurs over the 10Ni-Do among the 5 catalysts tested (Ni-Al, Ni-Si, Ni-Do, Ni-Ze and Ni-MCM4), having a total gas yield of 80.722 mmol per gram of feed, H_2 yield of 27.195mmol per gram of feed and H_2/CO molar ratio of 3.12. However, 10NiZe under the process conditions are undertaken in this study proved to be an excellent alternative catalyst to replace Ni-Al which is the conventional industrial catalyst due to its low selectivity to CH_4 and C1-C4 hydrocarbons (0.829 and 0.287wt% respectively).

7.2 Optimization of water gas shift reaction following pyrolysis-catalytic reforming for hydrogen production

The three-stage thermochemical process consisting of pyrolysis, catalytic steam reforming and water gas shift reaction has presented a reliable route for the generation of hydrogen from raw biomass, most especially wood pellets which were utilised in this investigation. Previous studies have well established the enormous potential of hydrogen to become a possible clean alternative fuel due to its high energy density and its reaction producing only water as a by-product. This eventually will help to mitigate both the diminishing reserves globally of fossil fuels and the increasing environmental pollution associated with their use.

However, the possibility of birthing the future sustainable hydrogen economy is contingent on certain factors which must be resolved; this includes the requirement of a new renewable feedstock (biomass) for production and not the current natural gas and coal. Integrating a renewable biomass feedstock into hydrogen production is again problematic unless an ancillary operating unit is provided in addition to the steam reforming and water-gas shift unit currently being used. This is known as pyrolysis and is required to turn the biomass into a gaseous feed.

It is also established from the literature that the temperature at which pyrolysis takes place, and the type of biomass also used greatly influence both the composition and yield of product gases. With respect to steam reforming and water gas shift reaction, a number of metals such as Fe, Ni, Al, Mn, and Zn among others can effectively catalyse the reaction. To optimise this conversion process, some process parameters, chiefly temperature, steam to carbon(S/C) ratio and steam flow rate were identified for probable manipulations. As the temperature is increased, the conversion of carbon monoxide also increased. Unlike temperature, the pressure of the system was reported to have little effect on performance. This was explained by the stoichiometry of the water-gas shift reaction equation.

More precisely, the findings from bench-scale three staged reactor system distinguished iron (Fe) as the best metal with the greatest affinity to catalysing the water-gas shift reaction. Fe-based catalyst produces the greatest yields of both gas and hydrogen, and a significantly low concentration of carbon on the reacted catalyst. All metals tested, apart from cobalt, catalysed the water-gas shift reaction. The poor performance of cobalt has been attributed to it catalysing the reverse water gas shift reaction. This assumption was supported by the fact that both the gas and hydrogen yields were less than the system with no catalyst present, although the high concentration of carbon dioxide did not support it. Despite literature suggesting that cobalt has the ability to catalyse the unwanted methanation reaction, the results presented in this report do not distinctly demonstrate this.

Another finding in this investigation is that manganese has greater selectivity towards dry reforming rather than the water-gas shift reaction. This assertion is made base on the high hydrogen yield shown when the catalyst was used despite the concentration of carbon monoxide remaining relatively low. When the reacted catalysts were analysed using TPO, it was shown that manganese suffered the most significant weight loss suggesting that it is the most susceptible to coking.

It is evident also that metal loading does not significantly affect catalyst performance (about 32 mmol H_2 g^{-1} biomass) until high weight fractions (100 wt% iron) where performance decreases (26.45mmol H_2 g^{-1} biomass). It has been suggested that the reduction in performance of the pure catalyst (at high loadings of 100 wt%) is due to the agglomeration of active particles within the catalyst resulting in a reduction in active surface area (that is, the lack of magnetite present in the catalyst which is the active phase of iron catalysts). A number of literature sources supported this. On the other hand, the consistency shown in the performance of catalyst with metal loadings ranging from 5 wt. % to 40 wt. % was not supported by previous studies which suggest it should have increased. One conclusion drawn from this is the necessity of catalysts supports to increase the active surface area, especially by dispersion. The TPO analysis also has shown that carbon deposition varies with metal loading as the pure iron catalyst was most susceptible to coking.

One last finding from the investigation of the effects of steam to carbon ratio (S/C) on the water-gas shift reaction is that, increasing the level of steam results in a decrease in the yield of hydrogen. This, however, contrasts with equilibrium and reaction theory; the reason is not yet apparent. Hence, further findings are required.

Summarily, the findings in this study show that catalyst composition, metal loading, and steam to carbon ration are relevant matrices in upscaling hydrogen production in a 3-stage thermochemical technique.

Maximisation of hydrogen production from biomass has been investigated following three-stage reactions viz a viz pyrolysis, catalytic steam reforming and water-gas shift reactions in a fixed bed reactor at 850°C. Above these metals Co, Cu, Mn, and Zn, Fe-catalyst yielded the highest volume of hydrogen (32.6 mmol H_2 g^{-1} biomass) and gas (92.38wt%) with the lowest concentration of CO in the product gases. Fe also showed the least coke deposit on the reacted catalysts which were analysed through Temperature programmed oxidation (TPO). Notably, while Mn and Zn indicated the best selectivity to dry reforming consequent to the low concentration of CO_2 in the process gases Co, on the other hand, indicated the best affinity to methanation. A relative increase in H_2 production was promoted by increasing the metal loading of the Iron alumina catalysts from 5wt% to 40wt% above which a dip in production performance was observed, and this suggests that the amalgamation of active particles. It was also found that the flow rate of steam into the third stage of the reactor has a significant influence on both the yield of hydrogen and other product gases. However, the observed inverse relationship between the flow rate of steam and H2 yield was a result of over-saturation of the reactor system with steam bridging the contact times for the reactants and the surface of the catalyst.

7.3 Effects of carbon dioxide adsorption by Calcium oxide for hydrogen production from a 3-stage reactor

In this chapter a 3-stage fixed bed reactor involving pyrolysis, catalytic steam reforming (catalytic steam reforming) and water gas shift reaction (water gas shift) for biomass conversion. The catalytic steam reforming and water gas shift reactions, in particular, were examined with respect to the influence of 10Ni-alumina catalyst utilization in the catalytic steam reforming stage, the addition of reduced and not reduced CaO-alumina sorbent/catalysts with different CaO contents to the water gas shift reaction stage, steam injection and removal from the process and the FeCaO-alumina sorbent/catalysts in different Fe:Ca:Al mass ratios. From the results obtained, the following key findings were drawn:

1. The addition of 10Ni-alumina catalyst in the catalytic steam reforming reactor, compared with adding no catalyst, resulted in a considerable increase in gas and hydrogen yields representing 54.05 wt.% and 7.91 mmolg^{-1} to 70.56 wt.% and 26.47 mmolg^{-1}for uncatalyzed and catalysed systems respectively. The 10Ni-alumina catalyst in the catalytic steam reforming stage promoted the reaction between the steam added to the process and the volatiles released by the biomass sample.

2. Without the injection of steam into the catalytic steam reforming and water gas shift reactors with a 10CaO-alumina catalyst in latter reactor produced low hydrogen content as there were no H atoms fed to the process. However, the catalyst showed evidence of catalysing the water gas shift reaction to a nonnegligible extent, utilising the gases released from the biomass sample only.

3. Upon the addition of 10Ni-alumina catalyst, the water gas shift reaction was also promoted, however in a lower extent. This was possible by reacting the steam with the same CO produced by the reforming of volatiles.

4. The 10Ni-alumina catalyst also excellently promoted the reforming of methane (CH_4). Thereby improving the selectivity towards higher hydrogen production. Conversion back to $CH_4$was inhibited.

5. The water-gas shift reaction catalytic performance was found to be improved with the increase of CaO in the catalyst. This is evident in the change in CO/CO_2 molar ratios, which declined when the CaO content was increased from 10 wt.% to 20 wt.% from 1.73 to 1.36 for the not reduced catalysts and from 1.56 to 1.44 in the reduced ones.

6. Carbon dioxide (CO_2) absorption was not obvious when only CaO is added and increased in the sorbent/catalyst, for the H/CO_2 and the CO/CO_2 molar ratios should increase (that is, more hydrogen production by catalytic steam reforming and water gas shift reactions over less CO_2 yield due to absorption by CaO) instead of the decrease.

7. The addition of iron metal (Fe) to CaO-alumina sorbent/catalysts promoted the water gas shift reaction by generating higher co_2 content. However, at the same time, it impedes the capability of the CaO to absorb the CO_2.

8. The addition of CaO to Fe catalysts at CaO:Fe ratios beyond 1 resulted in increased absorption of CO_2togetherwith a higher promotion of the water-gas shift reaction. This is supported by

the H_2/CO_2 and CO/CO_2 molar ratios that are 4.06 and 1.89 respectively for the 10Fe10CaO-alumina sorbent/catalyst and increase to 4.99 and 2.38 respectively.

9. An optimal condition of 10 wt.% CaO-alumina catalysts was the best suitable for maximising hydrogen production because it produced the highest hydrogen yield of 51.58 mmolg^{-1} biomass. It was found that the addition of Fe to FeCaO-alumina inhibited CO_2 absorption by the CaO, but at the same time, water-gas shift reaction was promoted.
10. In the use of iron and alkali earth oxide bimetallic catalysts, the optimal content of Fe and CaO in FeCaO-alumina catalysts for enhancing CO_2 absorption was found to be 10 wt.% Fe and 20 wt.% CaO. This catalyst produced the lowest CO_2 and the second-highest H_2 yields representing 9.14 and 45.59 mmolg^{-1} biomass, respectively**.** This was also supported by the TPO results since it has the lowest weight loss at 800^{0}C.

7.4 Future work

- This research examined the catalytic pyrolysis of biomass using the wet impregnation method for various metal loading. There is evidence in the literature, that the preparatory method for the catalyst has a significant impact on the effectiveness of the catalyst and its activity. It is recommended that a different catalyst preparation method is used primarily for the co-precipitation and sol gel method primarily. This might have significant impacts on the pyrolysis product yield and composition.

- This research was limited to biomass as the only feedstock. It is recommended that various feedstocks are investigated such as RDF, Plastics, other types of biomass and a mixture of biomass and plastics. This might significantly impact the pyrolysis yield and composition

- There are some parameters during this research work that could be investigated further; for example, the calcination temperature may also affect the catalyst properties and performance. The catalyst preparation temperature is crucial in determining the catalyst particle size since the crystal growth is susceptible to temperature.

- More catalyst characterisation techniques in addition to those described in this work, such as transmission electron microscopy (TEM), X-ray photoelectron spectroscopy (XPS), Raman spectroscopy and CO_2-temperature programmed desorption (CO_2-TPD) are also suggested to be applied to both fresh and reacted catalysts. These comprehensive catalyst characterisations could improve the understanding of the catalyst properties, which include surface properties and carbon deposition characteristics.

- The stability of the catalysts should be investigated; this should be done by using the catalyst in an experiment for more than 24 hrs at one time, this will help in evaluating the catalysts deactivation resistivity and suitability of the catalysts for continuous reaction in an industrial-scale process system.

7.5 Reflections

Overall the experimental process has been good, a few ups and down including the use of rare metal such as chromium. The hydrogen yield results from using chromium was disappointing and was not included in this piece of work. The development of the two-stage process was good considering it has been well established and a proven method by other researchers for quite some time now.

The development of the three-stage process was a novel method at the inception due to the fact that there was nothing like it and nothing to compare it with. In industry there is a similar process being used but on a lab scale there were no three stage fixed bed reactors around. The three-stage fixed bed reactor still has enormous potential, this is yet to be explored. For example, different type of catalyst for the steam reforming and water gas shift stages, different feedstock for the pyrolysis gases, dual steam input, single steam input and dry reforming.

Due to these reasons and more this research is worth pursuing with more research.